# The Development of an Artificial Imine Reductase Based on the Periplasmic Binding Protein Design

Rosalind Booth

Doctor of Philosophy

University of York

Chemistry

September 2022

# Abstract

Artificial metalloenzymes (ArMs) offer chemists an opportunity to perform challenging transition metal-catalysed transformations while benefiting from the advantages of natural enzyme catalysis. One such ArM is composed of a Cp*Ir(pyridinylmethylsulfonamide) catalyst attached to a type of iron-chelating molecule known as siderophore. The iron-coordinated siderophore binds tightly within a periplasmic binding protein (PBP), which provides the protein environment that surrounds the transition metal catalyst (Figure 1 (a)). The protein environment has been shown to be key to imparting enantioselectivity in transfer hydrogenation catalysis.

This thesis reports the synthesis of a series of Cp*Ir(pyridinylmethylsulfonamide)Cl complexes with the addition of electron-withdrawing or electron-donating groups to the pyridine group of the ligand. Trends in the catalytic transfer hydrogenation of imines by these catalysts provide insights into the potential catalytic mechanism and are supported by spectroscopic analysis. Methyl substituents on the pyridine ring were identified to contribute to an improvement in catalytic rate.

These improved catalysts were then incorporated into ArMs in combination with three PBPs. The position of the methyl substituent on the pyridine ring proved influential in the enantioselectivity of the resulting ArM. Overall, the best ArM displayed a 14-fold increase in catalytic rate compared with the first reported PBP ArM design (Figure 1 (b)), together with a higher enantioselectivity of 37.2% before genetic modification. The enantioselectivity of the catalytic reaction could further be improved by lowering the temperature. These results present an exciting opportunity for the continued development of the PBP artificial imine reductase and future developments towards new-to-nature chemistry.

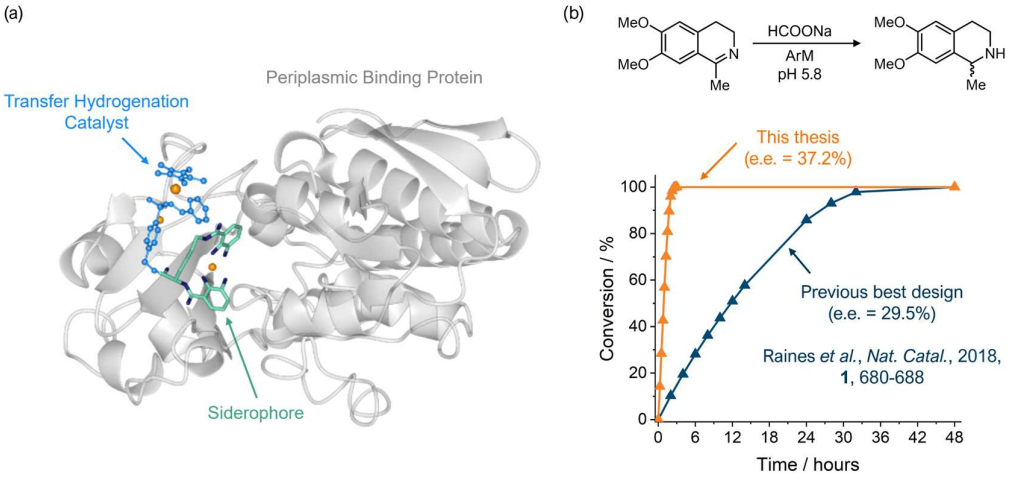


Figure 1 (a) Structure of the PBP artificial imine reductase and (b) summary of best performing ArM presented in this thesis compared to the previously reported best design

# Table of Contents

# Table of Figures and Tables

# Acknowledgements

To my supervisors Prof. Anne-Kathrin Duhme-Klair, Prof. Keith Wilson and Prof. Gideon Grogan my endless gratitude for your continued support and guidance throughout the project. I thank Anne for her excellent ideas that have hugely guided the work presented in this thesis. Keith's infinite knowledge of CeuE proteins and excellent proof-reading skills have been indispensable. My thanks to Gideon for his guidance in the field of enzyme biocatalysis and his help with substrate/protein modelling.

This project would not have been possible without the immense help of the technical and administration staff in the Department. In particular, my thanks to Heather for her time and help with the variable temperature NMR experiments with the iridium complexes. My thanks to Alex H for helping to run an extremely efficient NMR service, Karl for prompt mass spectrometry results, Graeme for elemental analysis, Adrian for measurements and analysis of crystal structures, Scott for help with the temperamental HPLC instruments and Emma for her general help and support in our lab.

Many thanks must also go to members of the research group, particularly the ArM team of Elena, Ben, Alex M, Nat and Kalum. I'm extremely grateful to Elena for providing me with a non-stop supply of proteins for my work and her swift responses to any questions I have had throughout the project; additionally to Alex for helping greatly with measuring the $K_d$ values of the proteins and for our many enzyme-based discussions. I am also grateful to my summer and MChem project student, and now fellow PhD candidate, Lukas for his input in the project, to past postdoc of the group Lisa who was responsible for the smooth running of the lab, and to other past AKDK members Conor, James and Thorsten for both your scientific discussions and your superb pub quiz knowledge.

I am extremely thankful to the EPSRC for funding me during my PhD and to the University of York for additional support through demonstrating opportunities and conference funding. I thank the Department for providing excellent facilities and additional training opportunities to develop my skills. I am additionally grateful to the Wild fund for funding an amazing opportunity in my placement abroad this summer, to Prof. Thomas Ward for kindly accommodating me in his lab and to Zhi Zou (Robin) for his excellent mentorship during my time in Basel.

I also wish to thank my previous colleagues and mentors Fraser and Clare who showed me how exciting research can be which led me to choose this PhD in the first place.

Last, but not least, I thank my friends and family who have stood by me during a far-from-straightforward four years; To my many PhD friends made before and since coming to York

who have supported me through the PhD journey; To my “non-PhD” friends for their patience in my missing so many events over the last few years; To my teammates and coaches of the university rowing club for strengthening my time management skills by not letting me say no to anything. And finally, to my family, who have been endlessly supportive; to my sister Julia for being my most positive supporter and closest confidant and to my parents who have been so encouraging throughout - I cannot thank you enough.

# Declaration

I declare that the research presented in this thesis is my own and, to the best of my knowledge, original work. I carried out this research at the University of York under the supervision of Prof. Anne-Kathrin Duhme-Klair, Prof. Keith Wilson and Prof. Gideon Grogan between October 2018 and September 2022. None of the work presented within this thesis has been submitted for any other qualification, or to any other university. I wish to recognise the contributions of those other than myself who have contributed to this this work as follows:

- Mass spectrometry measurements were performed by Mr. K. Heaton, Dr. R. Cercola and Mr. A. Lopez
- Elemental analysis was performed by Dr. G. McAllister and Dr. S. Hicks
- X-ray crystallography measurements and structure solutions were performed by Dr. A. Whitwood
- Variable temperature NMR measurements presented in Chapter 3 were carried out on the Brucker 500 MHz instrument by Ms. H. Fish
- A crystal of the complex Cp*Ir(**88**)Cl for X-ray structure analysis of the complex presented in Chapter 3 was prepared by Mr. L. Gečiauskas
- All the proteins used in my experiments in Chapter 4 were expressed and purified by Dr. E. Blagova
- Mr. L. Gečiauskas contributed to the development of the synthesis methods of compounds **102a**-**104a**
- Autodoc modelling of the substrate in the crystal structure of H227A *Cj*CeuE displayed in Figure 87 and 107 was prepared with the help of Prof. G. Grogan
- Dr. M. Miller helped develop of the chiral HPLC method

Rosalind Booth

# Chapter 1 Introduction

## 1.1 Background

Ever increasing regulatory and consumer pressure on manufacturing industries to be cleaner, greener and less environmentally damaging has prompted chemical industries to look towards developing methods that reduce hazardous materials and toxic waste.[1–3] Key targets such as replacing reactions where stoichiometric amounts of additives are consumed with catalytic methods are one such approach, with the field of biocatalysis drawing increasing attention.

Biocatalysis involves the use of enzymes or microbes to catalyse synthetic reactions[4] and offers a number of additional advantages over chemical catalysis such as functioning under very mild conditions at ambient temperatures and using water as a solvent at near neutral pH.[3,5,6] The avoidance of high temperature and pressure conditions reduces associated operational hazards and lowers energy consumption.[3,7,8] Biological catalysts generally require non-toxic cofactors and contribute few to no by-products, reducing the quantity of hazardous waste.[3,7,9] As catalysts they can exhibit exceptionally high chemo-, regio- and stereoselectivities which can help in shortening synthesis routes by avoiding the need for cycles of protecting and deprotecting of incompatible and reactive functional groups.[3,8–11] High enantioselectivity can boost yields and avoid additional chiral resolution processes.[2,3,6,8,12]

These benefits are particularly attractive to the pharmaceutical industry, where the trend for new small molecules with highly complex structures incorporating several chiral centres provides many opportunities for biocatalysis.[1,3,13] Requirements by the US Food and Drug Administration (FDA) and the European Committee for Proprietary Medicinal Products for chiral pharmaceutical products to provide full physiological characterisation of each enantiomer before it may go to market provides motivation for control of chirality during synthesis. Additionally, there are cost-saving benefits of producing the physiologically active isomer in high purity, allowing for lower dosages.[12–14] Furthermore, the high number of synthetic steps in the synthesis of pharmaceuticals assign the industry with some of the highest E-factors, a measure of the amount of waste produced in a particular synthesis,[15] commonly 25-100 kg of waste per 1 kg of product (Table 1).[3]

Consultation with industry leaders and academics have identified key aims and challenges for the field of biocatalysis including improving the performance and stability of enzymes under operating conditions, expanding the commercial availability of enzymes and activity towards non-natural substrates, and developing technologies for faster engineering of enzymes for

Table 1 Typical E-factors as a measure of waste production by industry as reported by Woodley.[3]

| Industry | E-factor (kg waste/kg product) |
|---|---|
| Bulk Chemicals | <0.1 |
| Fine Chemicals | 5 to 50 |
| Pharmaceutical processes | 25 to 100 |

specific reactions.[1–5,11,16–20] Other factors, such as enzyme inhibition at high substrate and product concentrations has also limited biocatalysis.[13,14] Poor solubility of substrates and products of interest in water and downstream processing to recover products are additional challenges.[3,6,21] However, enzymes can be engineered to be more tolerant of organic solvents.[1,5]

In recent years, substantial progress in enzyme discovery, enzyme engineering and process development has led to significant advances in this area with new technologies ensuring faster development of catalysts specially optimised for chosen reactions.[4,12,17–19,22] There are now several hundred reported synthetic pathways in which biocatalysts have been incorporated.[6,12,16] Further developments such as immobilisation of enzymes to improve stability and reusability, two-phase solvent systems and the identification of cascade reactions avoiding the isolation of intermediates are increasingly making biocatalysts more applicable to industrial processes.[2,3,7,12,13]

Natural enzymes have evolved over millions of years to carry out specific reactions required by living organisms. However, there exist a number of other synthetic transformations developed by chemists which have no equivalent in nature. There is significant value in creating biocatalysts for these new-to-nature transformations.[4,23] Strategies involving modification of proteins to incorporate non-natural chemical complexes have produced semisynthetic enzymes displaying catalytic activities different from the unmodified protein.[24–26] One approach is the use of non-natural metal complexes, including transition metal complexes, with the aim of accessing the broad reaction scope displayed by transition metal catalysts.[27,28] Such semisynthetic modified proteins are known as artificial metalloenzymes (ArMs).

## 1.2 Artificial Metalloenzymes

ArMs consist of a non-native metal or metal complex incorporated in a protein scaffold, to produce a catalyst that combines the broad reaction scope of organometallic catalysts with the selectivity and activity in mild conditions that enzymes demonstrate.[29,30] Non-native metals and metal complexes are capable of introducing reactivities that have no equivalent in nature

and can benefit from being integrated into the protein by protecting the catalytic metal centre from inactivation from agents such as thiols, water and oxygen.[30–34] The protein scaffold provides a well-defined secondary coordination sphere to the metal ion that would be very challenging to achieve with equivalent complexity by synthetic means.[35,36] The secondary coordination sphere has been shown to contribute significantly to the enantioselectivity observed in enzymes.[37,38] Incorporation into a protein improves the biocompatibility of the organometallic catalyst and protects these catalysts from the surrounding media as many are susceptible to deactivation by oxygen, water or biomolecules present in physiological solutions.[30,34] This opens up the use of these artificial enzymes in cascades with natural enzymes; particularly valuable if accessing a previously unachievable transformation, with the benefit of performing a multistep process which does not require the use of protecting groups or the isolation and purification of intermediates.[30,34] Protein based catalysts may also be easier to separate from solution for recovery and reuse.[4,31] The ability to incorporate organometallic catalysts into aqueous solutions presents a "greener" solution to catalysis since use of organometallic complexes are usually restricted to organic solvents.[35]

When selecting a protein scaffold for an ArM there are several considerations, such as whether the size of the protein pocket where the catalytic conjugate will be located is large enough to accommodate both the conjugate and the target substrates[39]. This generally restricts candidates to proteins with reported crystal structures, that are structurally well understood. A structurally characterised protein is also beneficial when approaching optimisation of the scaffold for catalysis.

There are a number of strategies for anchoring the metallic conjugate inside the protein scaffold including covalent, dative, supramolecular binding, or a combination of these[37,40]. Dative bonding strategies describe an approach where the protein scaffold is modified with coordinating amino acids that bind directly to the catalytic metal centre. Covalent designs incorporate a chemical moiety that covalently binds with the protein scaffold but is separated from the immediate coordination sphere of the catalytic metal centre. Supramolecular binding relies on a chemical group with high affinity for the target protein but does not involve covalent linkages between the protein and the catalytic conjugate.[33,37–39]

There is a range of desirable properties to consider when choosing the catalyst for an ArM. Importantly the complex must be soluble and moderately stable in water, allowing for the assembly of the ArM in aqueous solution, since most proteins cannot tolerate more than trace amounts of organic solvents. It is also desirable that the complex be stable in air as this makes handling and storage of the catalyst significantly easier, although it is not absolutely necessary.

There are three approaches to designing an ArM. The first is the repurposing an existing natural metalloenzyme by incorporating a non-natural organometallic conjugate into a defined binding site. The major drawback of this method is that the protein scaffold has evolved specifically for the binding of the target substrate of the natural enzymes, which may limit the type and variety of substrates the artificial enzyme will be able to accommodate. Examples of this type include ArMs reported by the Hartwig group constructed from cytochrome P450 where the naturally-occurring Fe-haem complex is replaced by a synthetic Ir(Me) complex coordinated by a haem-like porphyrin (Figure 2 (b)). In nature, cytochromes P450 catalyse C-H bond oxidation reactions and as scaffolds for ArMs they have been repurposed for other C-H bond insertion reactions, in particular the insertion of carbenes. The scaffold CYP119 from a thermophilic organism *Sulfolobus solfataricus* was the P450 selected for the ArM design, which proved highly evolvable in its optimisation.[41,42] In one set of experiments the turnover frequency (TOF) of catalysis, a measure of catalytic rate measured as the number of catalytic cycles achieved per individual ArM per minute, was improved 180-fold to a TOF rivalling natural enzymes (reaction shown in Figure 2 (a)). Enantioselectivity for the reaction product was also improved from initially displaying no selectivity to an e.e. of 94%.[41]

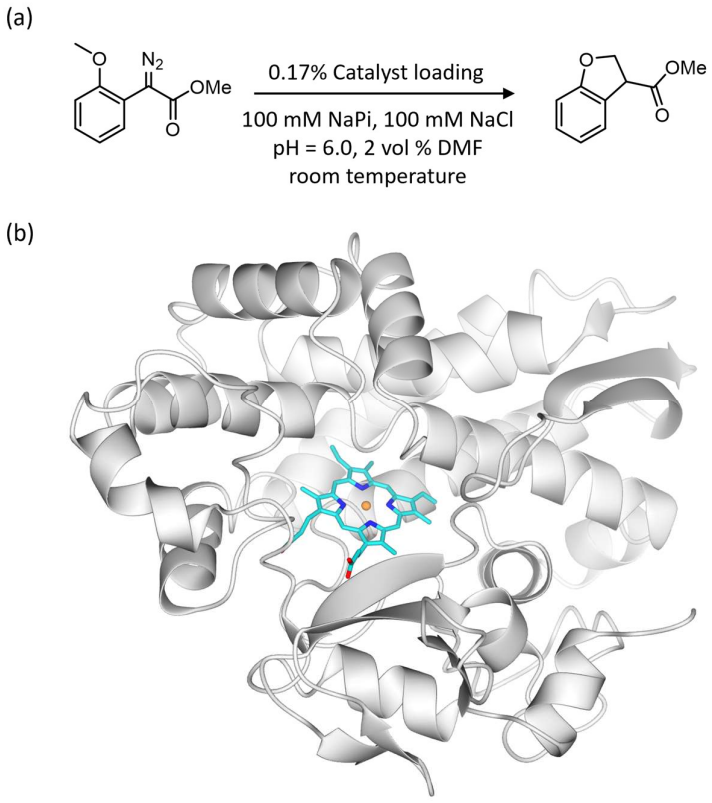


Figure 2 (a) Example carbene insertion reaction catalysed by Ir(Me)(porphyrin)-CYP119 ArM. (b) crystal structure of a Ir(Me)(porphyrin)-CYP119 ArM (PDB code: 1IO7) with apo CYP119 shown as grey ribbons, the haem-like porphyrin ligand as blue cylinders and Ir as an orange sphere. as blue cylinders and Ir as an orange sphere.

The second strategy takes the opposite approach where the enzyme scaffold is constructed from non-natural protein sequences known as *de novo* design. This potentially offers greater opportunities for diversification as a protein scaffold compared to starting from a natural protein that has already evolved for a specific purpose. While these scaffolds offer great potential, they require extensive engineering efforts to create a functional ArM. The groups of Hilvert and Jiménez-Osés reported such a design that catalysed a Diels-Alder reaction. The protein scaffold was composed of a short protein sequence of 97 amino acids that was designed to form a helical bundle (Figure 3 (b)). Two histidine residues (His61 and His65) and a cysteine (Cys35) coordinate a zinc(II) ion which, as a Lewis acid, can catalyse a Diels-Alder reaction. The Rosetta design computational algorithm[43] was used to identify mutations to the protein sequence that would stabilise the transition state to the desired product without altering protein stability. The final optimised ArM catalysed the selected reaction (Figure 3(a)) with complete selectivity for the endo product and total enantioselectivity.[44]

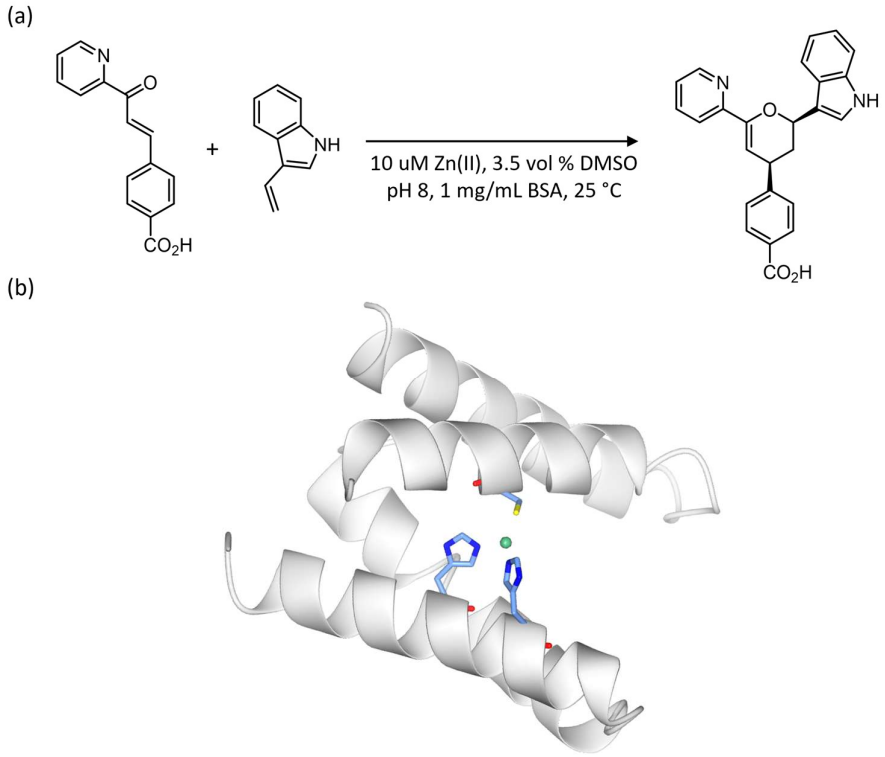


Figure 3 (a) Target Diels-Alder reaction for the preparation of a de novo design ArM. (b) Crystal structure of the *de novo* ArM (PDB code: 7BWW) with the protein scaffold displayed as grey ribbons and the Zn(II) ion as a green sphere. The coordinating residues Cys35, His61 and His65 are shown in blue.

The third strategy is the use of an abiotic cofactor with high affinity for a natural protein to act as a supramolecular anchoring system. This approach usually involves proteins with natural functions that are distinctly different from the reaction the ArM is designed to catalyse. This option presents better opportunities to design ArMs for non-natural reactions than using proteins with closely-related natural functions.[45] Spontaneous self-assembly of the protein scaffold and associated conjugate also make these designs attractive due to their operational simplicity.[46] An ArM based on the Lactococcal multidrug resistance Regulator (LmrR) protein scaffold developed by the Roelfes group has been developed to catalyse Friedel-Crafts alkylation of indoles. LmrR is a homodimer which forms a large hydrophobic cavity at the interface of the two subunits, that has been shown to bind planar metal complexes with aromatic ligands through π-stacking interactions with tryptophan residues present on either side of the cavity (Figure 4 (b)). A $Cu^{II}$(phen) complex (Figure 4 (c)) was demonstrated to bind in the hydrophobic cavity spontaneously and the resulting ArM was capable of catalysing Friedel-Crafts alkylation of indoles with excellent enantioselectivity (Figure 4 (a)).[38]

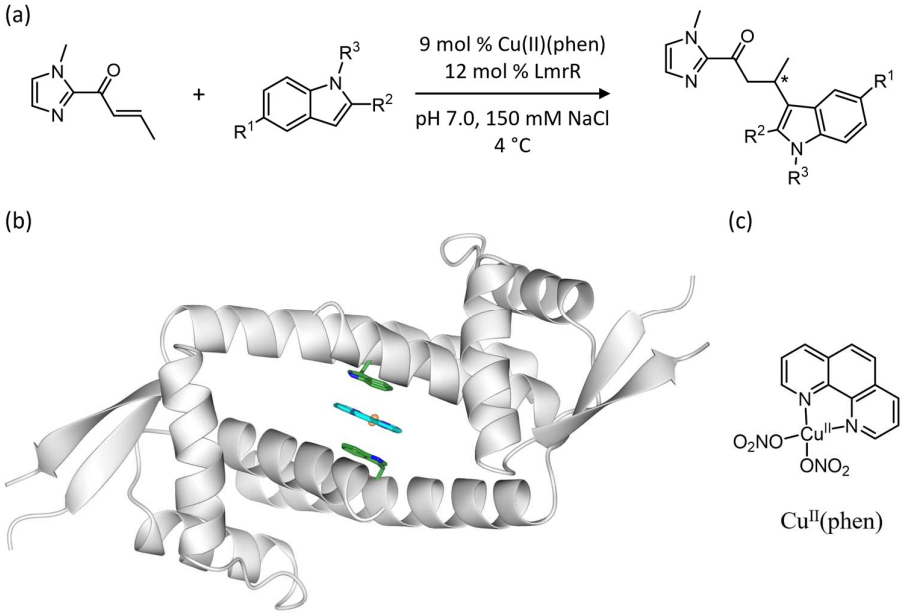


Figure 4 (a) Example Friedel-Crafts reaction catalysed by the ArM from $Cu^{II}$(phen)-LmrR. (b) Crystal structure of $Cu^{II}$(phen)-LmrR with π-stacking demonstrated between the tryptophan residues (green cylinders) and phen ligand (cyan cylinders) in the LmrR scaffold (grey ribbons) (PDB code: 6R1L). (c) Structure of $Cu^{II}$(phen) complex added to the LmrR protein scaffold to produce the ArM.

There are reports of more than 80 different protein scaffolds that have been employed in the construction of ArMs and these have been collected in an online database by the Ward group (https://amp.ward-lab.ch/). These ArMs catalyse a diverse range of transformations including reduction reactions, C-C bond formation, oxygen insertion and hydration chemistry.[23]

## 1.3 Enantiomeric Amines as a Synthetic Targets

Enantiomerically-pure amines are valuable intermediates in the pharmaceutical, agrochemical, and flavour and fragrance industries.[14,47,48] Chiral amines make up around 40% of all pharmaceuticals[49] and have increasing use in the agrochemical industry, hence there is demand to find large-scale, cost-effective synthesis strategies.[14,50] In 2007, the ACS Green Chemistry Institute Pharmaceutical Roundtable presented a list of key areas for development with the aim to make pharmaceutical synthesis procedures "greener". Among a list of aspirational target reactions, asymmetric hydrogenation of unfunctionalized olefins/enamines/imines ranked as one of the most important goals. The roundtable noted particular value in controlling the enantiomeric product produced.[51]

Traditional hydrogenation methods often have drawbacks in terms of low chemo- and enanotio-selectivity.[52] Methods of converting racemic mixtures to enantiomerically-pure chemicals by crystallisation with chiral carboxylic acids and Dutch resolution are well established in industry but until recently the direct synthesis of amines with high optical purity in industrial quantities was limited.[14] An increasingly intriguing approach is transfer hydrogenation using transition metal catalysts or organocatalysts to transfer a hydride ion from an organic donor such as isopropanol or formate, in addition to a proton, across an unsaturated bond.[29,48,52] The main advantages of this method are the mild conditions and use of affordable, non-toxic reagents.[52]

Noyori and co-workers first developed piano-stool transition metal complexes with diamine ligands for transfer hydrogenation. Complexes of Ru, Rh, Ir and, more recently, Os have been extensively explored as catalysts for transfer hydrogenation of aldehydes,[53] ketones and imines as well as other reactions including C-C bond formation.[54] Transfer hydrogenation of ketones has been particularly widely studied including the mechanism of the catalytic processes. It is widely agreed that the mechanism follows an outer-sphere process, where the substrate does not directly coordinate the catalytic metal centre at any point in the reaction.[55,56] Early studies suggested the reaction may proceed through a 6-membered transition state where donation of both a hydride and a proton occur in a concerted step[57,58] but more recent works have identified consecutive $H^+$ and $H^-$ transfer is more likely.[56] The equivalent mechanism for imine reduction is not as well understood but proposals have suggested the imine substrate is protonated before

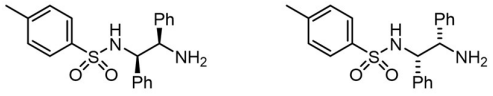


*R,R*-TsDPEN *S,S*-TsDPEN

Figure 5 Chemical structures of chiral TsDPEN ligands which, in combination with piano-stool Ru, Ir and Rh complexes, are able to catalyse transfer hydrogenation reactions enantioselectively.

hydride transfer from the catalytic hydride species.[59,60] The mechanism for the transfer hydrogenation of imines is discussed in greater detail in Chapter 3.

The discovery of the chiral 1,2-*N*-(*p*-tolylsulfonyl)-1,2-diphenylethylenediamine (TsDPEN) ligand (Figure 5) set a precedent for enantioselective small-molecule transfer hydrogenation catalysts.[61,62] Precatalysts of ($\eta^6$-arene)-Ru and ($\eta^5$-arene)-Rh and -Ir with the TsDPEN ligands have been shown to be capable of exceptionally high levels of enantioselectivity, typically in excess of 90% e.e. for many aromatic ketones.[63–69] For many years an absolute explanation for the source of enantioselectivity remained elusive, with suggestions that enantioselectivity of aromatic ketones arising from a CH-π interaction between the arene ligand of the catalyst and the aromatic ring of the ketone substrate.[47,70,71] However, this did not suitably account for some experimental results, in particular, the exchange in enantioselectivity between $C_6H_5$-aromatic and perfluoroaromatic ketones.[72] Recent studies have presented different approaches to explaining the enantioselectivity of these catalysts in more detail supported by Density Functional Theory (DFT) calculations.[56,72–75]

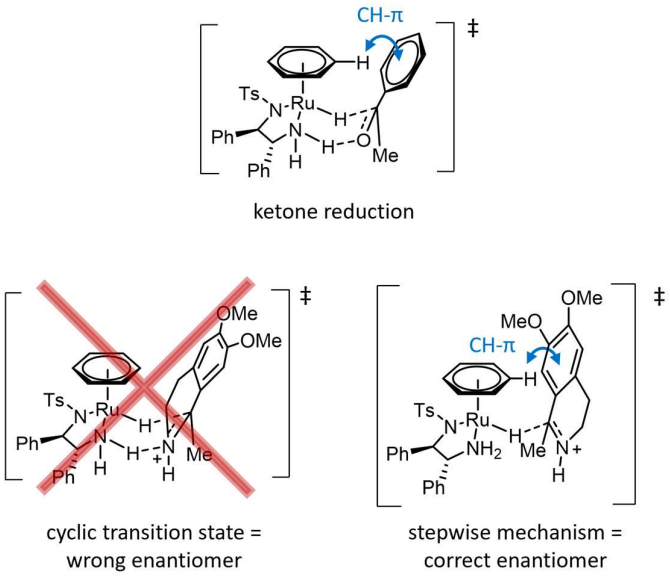


Figure 6 Proposed transition states for transfer hydrogenation of aromatic ketones and cyclic imines

Alternatively, enantiomerically pure amines can be accessed through enzyme-catalysed reduction of imines or reductive amination of ketones under very mild conditions.[14,76–78] Naturally-occurring imine reductases (IREDs) were first reported by Mitsukura *et al*. in 2010.[48] A growing number of IREDs have since been identified by the use of bioinformatics to scan large databases of enzyme sequences.[79] In comparison to the related transformation, reductive amination, imine reduction by IREDs have received comparatively little attention. This is probably because reductive amination is able to access a more synthetically useful

range of secondary and tertiary amines[60] while imine reduction is limited to the synthesis of mainly cyclic amines, since non-cyclic imines tend to have poor stability in water.

Several problems still stand in the way of IREDs becoming industrially significant catalysts, among them a poor understanding of the catalytic mechanism and hence the role of particular structural motifs to target in optimisation strategies.[79] The enantioselectivity of some IREDs has been demonstrated to reverse under different catalytic conditions and enzyme preparations indicating the complex nature of the mechanism.[80] Many IREDs also report substrate and product inhibition which presents additional complications with regards to industrial applications.[60] IREDs additionally require NADH/NADPH cofactors which are expensive and so require NADH/NADPH recycling methods to be implemented for any moderate to large scale reactions.[81,82]

## 1.4 Artificial Imine Reductases

With imine reduction being identified as an important target reaction for industry, several artificial metalloenzymes have been developed in parallel to natural IREDs[76]. Noyori-Ikariya-type transition metal piano-stool complexes were identified as superb candidates for the catalytic metal complexes following reports of high conversions, robust performance and broad reaction scope.[50,67,83–89] These organometallic catalysts benefit from using formate instead of more expensive phosphorylated cofactors. A number of imine substrates have been used to evaluate artificial imine reductases (ArtIREDs) (Figure 7).[90]

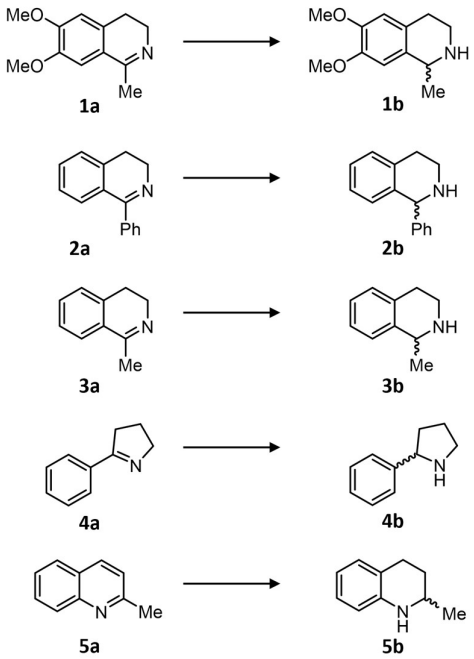


Figure 7 Structures of commonly used imine substrates **1a-5a** and their corresponding chiral amine products **1b-5b**.

### 1.4.1 The Streptavidin-Biotin Artificial Imine Reductase

The streptavidin ArtIRED design was developed from the first reported ArM pioneered by Wilson and Whitesides in 1978,[36] which exploited the high affinity of the protein avidin for biotin, a small water-soluble compound also known as vitamin B7. The biotin-avidin ArM was first designed to reduce a C=C bond of α-acetamidoacrylic acid to *N*-acetylalanine. This design inspired Ward and co-workers to develop an ArM using another protein of the avidin family, streptavidin, because it has a deeper binding pocket which more fully encapsulates the organometallic complex, while still having a similarly strong binding affinity for biotin[35]. The ArM is formed using a non-covalent anchoring strategy, with the organometallic catalyst linked to the convenient side-chain of the biotin molecule, causing spontaneous localisation of the catalyst inside the protein scaffold (Figure 8). The affinity between biotin and streptavidin is so strong that the binding of the biotin-anchored organometallic conjugate inside streptavidin is effectively irreversible.[29]

In the first reports, the catalytic metal complex was linked to the biotin anchor *via* a group extending from the arylsulfonamide bidentate ligand (Figure 8 (a)).[47] Analysis of the crystal structure of this ArM revealed a relatively low occupancy of the Ir atom of the metal complex in the protein pocket. This suggested the flexible linker between the fused 5-membered rings of biotin, which account for the strong binding of the conjugate, and the metal complex results in the catalytic complex being poorly localised.[91] It was proposed that localising the catalytic metal in a tight, well-defined secondary coordination sphere would result in higher enantioselectivities. Therefore, a second design was developed in an attempt to combat this with biotin attached instead to the arene ligand of the complex (Figure 8 (b)). This left additional coordination sites at the metal centre for dative interactions with the protein scaffold to improve localisation of the metal (Figure 9), and additionally provided extended freedom in the choice of coordinating ligands.[92]

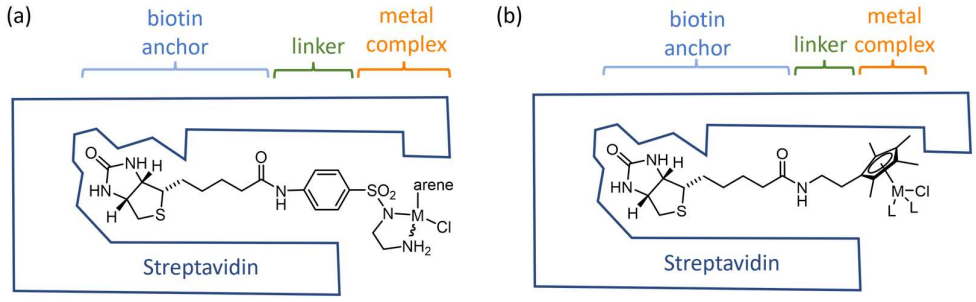


Figure 8 (a) Schematic figure for the design of the streptavidin ArM with the arylsulfonamide bidentate ligand linked to the biotin anchor. M-arene pairs: Ru-$\eta^6$-benzene, Ru-$\eta^6$-*p*-cymene, Rh-Cp*, Ir-Cp* (b) Schematic figure for the design of the streptavidin ArM with the metal complex linked to biotin by the arene ligand.

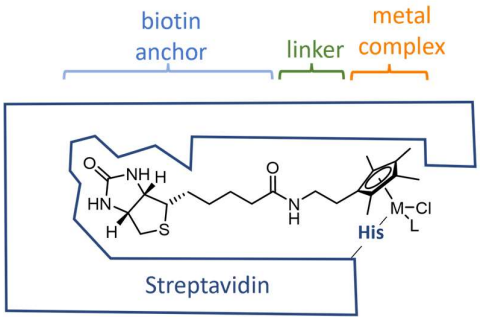


Figure 9 Schematic figure for the dually-anchored streptavidin ArM where, in addition to supramolecular anchoring of the biotin group, the catalytic metal complex is bound to the protein scaffold covalently *via* a histidine genetically engineered into the protein pocket.

A weakness in the streptavidin design is that the protein exists as a tetramer, with the protein pocket in which the catalytic complex is located being at the interface of two subunits. This presented problems during attempts to optimise the protein scaffold through genetic modification as making a change at one position in the amino acid sequence would be reflected at two locations in the protein pocket, reducing the effectiveness in the control of the secondary coordination shell of the catalytic metal complex. To overcome this, a dimeric streptavidin was engineered by linking two genetic sequences of streptavidin together with a short peptide sequence of 26 amino acids. The His127 residue contributes to stacking the Sav-A and Sav-B dimers together was also replaced by cysteine residues in Sav-B to promote the formation of a disulfide bond between dimers, while leaving His127 in Sav-A to ensure the specified assembly of the tetramer, with the two Sav-A units and the two Sav-B units arranged as shown in Figure 10 (b). This design allowed the Sav-A and Sav-B subunits to be modified independently.[93]

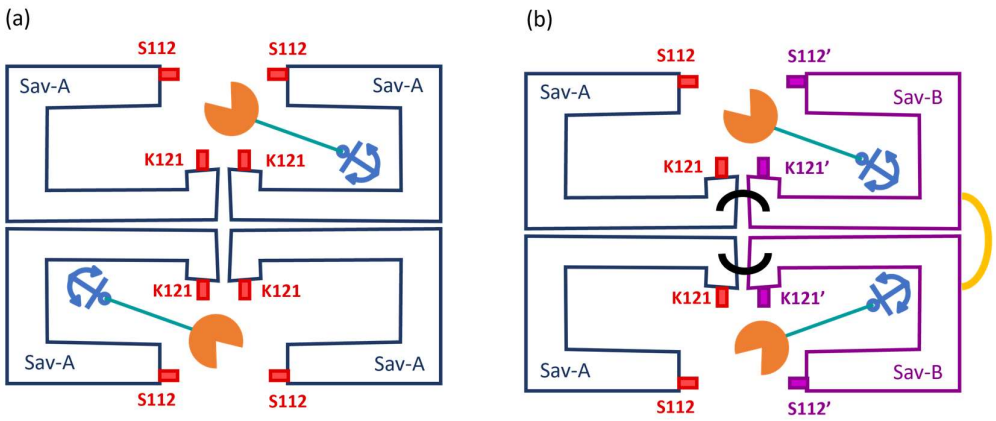


Figure 10 (a) Schematic figure demonstrating the tetrameric nature of the streptavidin (Sav) scaffold and (b) the engineered dimer or dimeric streptavidin scaffold with the 26 amino acid linker between two streptavidin monomers indicated by the black line and the disulfide bond between two Sav-B units indicated by the yellow line. The anchor represents the biotin anchoring unit of the conjugate linked to the catalytic metal complex (represented by the orange sector).

### 1.4.2 The Human Carbonic Anhydrase II Artificial Imine Reductase

The design of the human carbonic anhydrase II (hCAII) ArM demonstrates a dative-anchoring approach, where a zinc (II) ion located in a hydrophobic channel of the protein readily binds aryl sulfonamides. By attaching a *p*-arylsulfonamide group to the ligand of a pentmethylcyclopentyl iridium complex (Cp*Ir), a functional ArtIRED was formed (Figure 11 (a)).[40]

It has been proposed that improving the localisation of the catalytic complex within the protein scaffold will improve the catalytic performance of ArMs in terms of both enantioselectivity and turnover number (TONs), a measure of catalyst stability and activity given by the number of catalytic turnovers per individual ArM.[94] Following analysis of the crystal structure of the previous hCAII ArM, two amino acid positions located close to the catalytic complex were identified and chosen as positions to incorporate cysteine. Mutants of hCAII were prepared with cysteine exchanged for the natural amino acid in either of the two identified positions. A catalytic conjugate was designed with a nitro substituent on the bidentate ligand of the catalyst, positioned in close proximity to the newly incorporated cysteine residues. On binding of the catalytic conjugate through dative anchoring by the aryl sulfonamide group, it was expected that nucleophilic aromatic substitution would occur, with the electron-rich sulfur of cysteine displacing the nitro group of the pyridine ring. This transformation did not occur, however, and it was instead found that a sulfonamide bond had been formed between the conjugate and the cysteine residue (Figure 11 (b)). Regardless, this achieved the dual-anchoring strategy that had been proposed.[94]

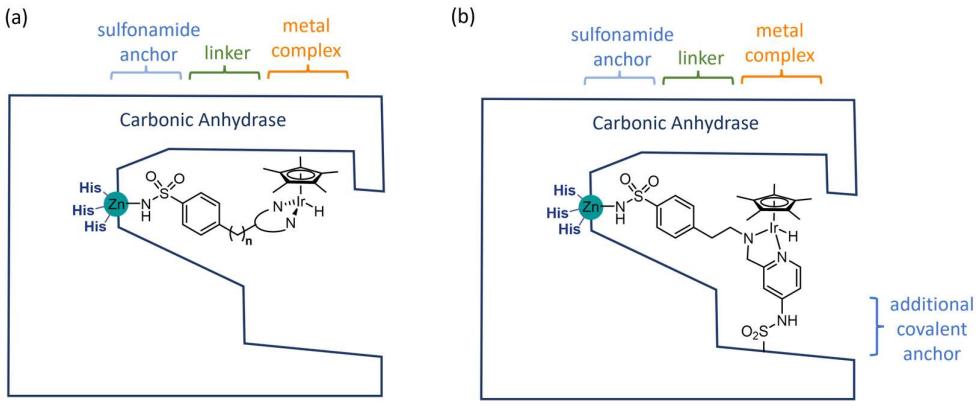


Figure 11 (a) Schematic representation of the hCAII ArM design with the arylsulfonamide group anchoring the catalytic conjugate in the protein scaffold. (b) A dual-anchoring approach to the hCAII ArM with an additional sulfonamide bond between the catalytic conjugate and the protein scaffold.

### 1.4.3 The Ribonuclease S Artificial Imine Reductase

The ribonuclease S ArM design is derived from the natural ribonuclease A from which a small α-helical peptide section is removed by digestion with subtilisin and replaced with a synthetic α-helical unit. The synthetic α-helical peptide can be designed to contain natural and non-natural amino acids capable of coordinating metal ions or small complexes. Early studies introduced Hg(II)[95] and Cu(II)[96] ions for different purposes but incorporating a Cp*Ir produced transfer hydrogenation activity (Figure 12).[97]

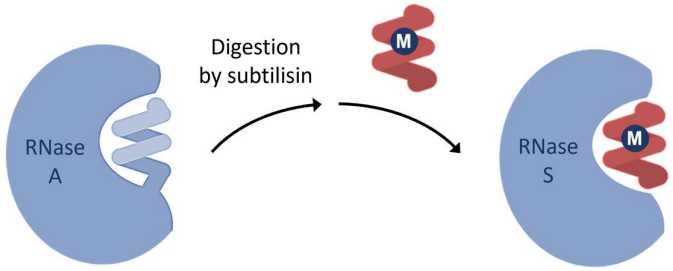


Figure 12 Schematic demonstrating the process of preparing the ribonuclease ArM. In the case of the ArtIRED, M=Cp*Ir.

This ArM has not been exposed to extensive modification attempts except for a brief genetic optimisation study targeting three amino acid residues that are in close proximity to the catalytic metal ion. The rational design approach was, however, unsuccessful and the mutant displayed no improvement in catalytic performance.[97]

### 1.4.4 Cytochrome $b_{562}$ ArtIRED

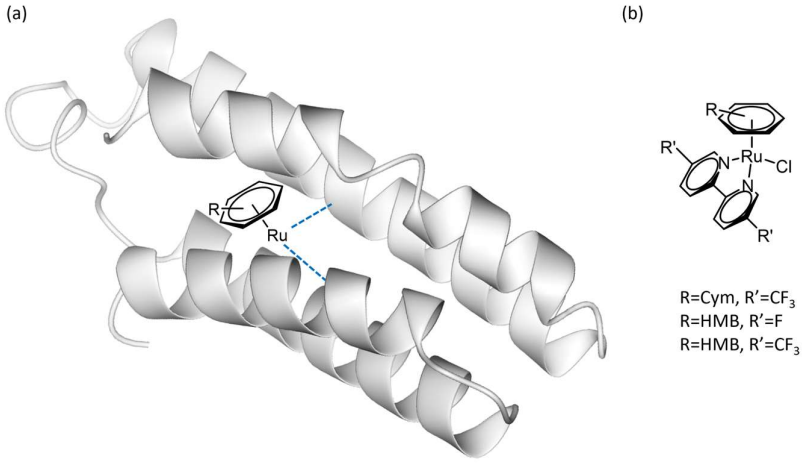


Figure 13 (a) Representation of the Cytochrome $b_{562}$ ArM design where the addition of complexes shown in (b) to apo cytochrome $b_{562}$ lead to dissociation of the bipyridine ligand replaced by Ru-protein interactions.

The design of the cytochrome $b_{562}$ ArM by the Boss and Barker groups was aimed at maximising coordination between the protein scaffold and an ($\eta^6$-arene)Ru fragment. The

reasoning behind this was to make use of genetic optimisation to evolve the primary coordination sphere, not just the secondary coordination sphere as is mostly targeted in optimisation reports of other ArtIREDs. Coordination of the ($\eta^6$-arene)Ru fragment inside Cytochrome $b_{562}$ was achieved by the addition of a $[Ru^{II}(\eta^6\text{-arene})(\text{bipyridine})Cl]^+$ precomplex (Figure 13 (b)) to the apo protein at pH 8.0 which triggered substitution of the bipyridine ligand for peptidic ligands within the protein scaffold (Figure 13 (b)). Substitution was established by mass spectrometry. Cytochrome $b_{562}$ is a four-helix bundle protein with suitable cofactor promiscuity and highly versatile structure. The ArM was shown to catalyse the transfer hydrogenation of imine substrate **6a** (Figure 14), which spontaneously forms fluorescent product umbelliferone, **6c**, which allows the reaction progress to be monitored in real time by fluorescence spectroscopy. An order of magnitude enhancement of the catalytic rate was observed for the ArM compared to $[Ru(Cym)Cl_2]_2$, the most closely related small-molecule catalyst.[98]

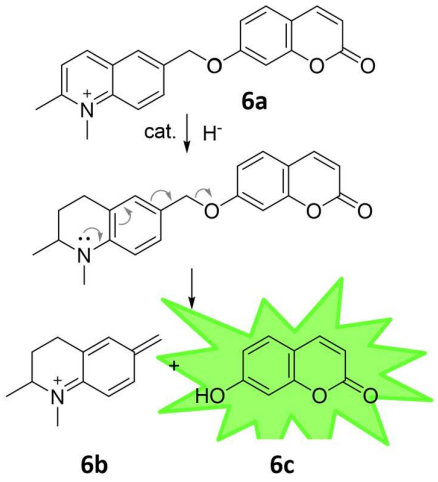


Figure 14 Scheme demonstrating the transfer hydrogenation of substrate **6a** which decomposed following reduction of the imine bond to produce products **6b** and the fluorescent umbelliferone, **6c**.

## 1.4.5 Alcohol Dehydrogenase ArtIRED

The design of an ArM using an alcohol dehydrogenase scaffold was informed by computational predictions used to select a small chemical fragment with a high affinity for the selected protein scaffold, a $NADP^+$-dependent alcohol dehydrogenase from *Thermoanaerobacter brockii* (*Tb*ADH). The high affinity of these fragments was to be used to anchor Cp*Ir(sulfonamide) catalyst conjugates inside the protein scaffold. A small group of conjugates was prepared and produced binding affinities with *Tb*ADH in the range 4.410 mM to 0.052 mM. Unfortunately, upon incorporation in the protein scaffold, only one of the conjugates displayed any level of activity for the transfer hydrogenation of imine **1a**, which remained extremely slow in comparison with the free conjugate. This ArM also lacked any

enantioselectivity demonstrating a need for significant further development of computational-assisted design in the preparation of ArMs.[99]

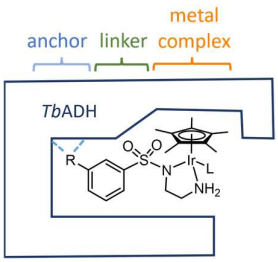


Figure 15 Schematic representation of the generalised design of the *Tb*ADH ArtIRED.

## 1.5 The Periplasmic Binding Protein Artificial Imine Reductase

The design of the artificial imine reductase developed by the Duhme-Klair group was inspired by the iron uptake pathways of microorganisms.[100] Iron is a crucial nutrient for bacterial survival and growth because of its redox chemistry, with applications in cell respiration, electron transport and superoxide metabolism.[101,102] Low aqueous solubility of Fe(III), the oxidation state in which iron exists in aerobic environments, is not sufficient to support bacterial growth hence microorganisms have adapted to be able to extract necessary amounts of iron from their surroundings.[101,102] One method is the production and secretion of siderophores, small iron-chelating organic molecules.[101,102] Over 500 examples of siderophores have been reported, most of which contain bidentate binding groups such as catechols, hydroxamates and α-hydrocarboxylates linked by linear or cyclic scaffolds.[101–104] While the most common denticity is hexadentate, examples of tetradentate, tridentate and bidentate siderophores have also been reported.[101,102] Once bound to iron, these ferrisiderophore complexes are taken up into bacteria *via* specific transporters in the outer membrane. In the case of gram-negative bacteria, transport of these complexes also has to occur through the inner membrane into the cytoplasm of the cell, one pathway of which uses proteins known as periplasmic binding proteins (PBPs) that recognise and direct these complexes to ABC transporters in the inner membrane.[101] There are three proposed mechanisms for releasing iron from the siderophore-complex inside the cell: hydrolysis of the siderophore, proton-assisted release and reduction of the metal.[101,102] Reduction of Fe(III) to Fe(II) results in a less thermodynamically stable and kinetically labile complex that readily dissociates, releasing Fe(II).[102,105]

It was expected that by linking an organometallic catalyst to a siderophore, this conjugate would be incorporated or bound by a periplasmic binding protein in the presence of Fe(III),

locating the organometallic catalyst within the protein scaffold. The PBP *Cj*CeuE, from *Campylobacter jejuni,* was selected because it is well characterised and shows significant ligand promiscuity.[105] A tetradentate siderophore, azotochelin from *Azotobacter vinelandii*, was used as it has several reported syntheses, is hydrolytically stable and has a strong binding affinity for *Cj*CeuE ($K_d = 4.9 \pm 0.4$ nM).[105] Structural studies of *Cj*CeuE complexed with Fe-azotochelin identified binding of the Fe-azotochelin in a shallow pocket with direct coordination of two amino acid side chains, His227 and Tyr288, to iron.[105]

A [Cp*Ir(pyridinylmethylsulfonamide)Cl] complex was identified as a superior catalyst to the more widely-used complex incorporating an aminoethylsulfonamide ligand, when under mildly acidic conditions. Linking this [Cp*Ir(pyridinylmethylsulfonamide)Cl] complex to azotochelin by the aryl sulfonamide group of the pyridinylmethylsulfonamide bidentate ligand produced a siderophore-catalyst conjugate (Figure 16 (a)) that was successfully inserted into the protein scaffold on addition of Fe(III) and the PBP. A crystal structure of the ArM showed that the His227 that normally coordinates to the iron ion of the Fe(III)-tetradentate siderophore complex was displaced by the addition of the organometallic catalyst and now was positioned in close proximity to Ir. The apparent coordination of histidine to the conjugate presents a dual-anchoring type ArM, with dative anchoring of the siderophore and direct coordination of the protein scaffold to the Ir metal ion (Figure 16 (b)).

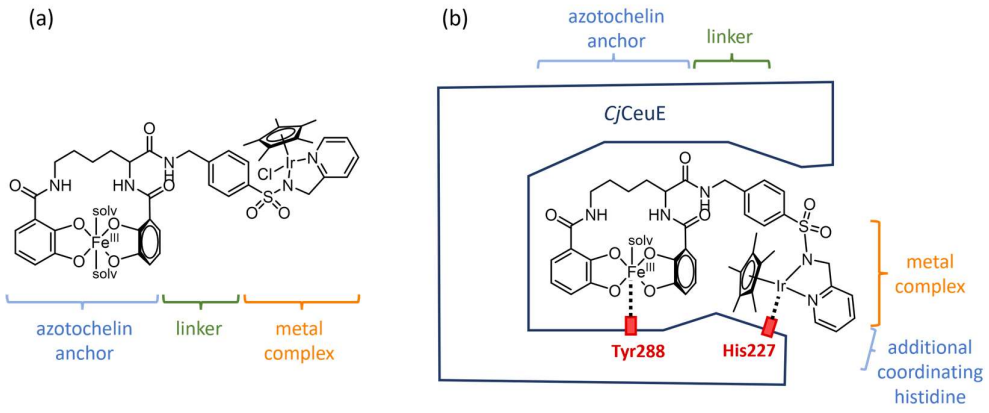


Figure 16 (a) Structure of the siderophore-catalyst conjugate for the PBP ArM design. (b) Schematic diagram of the PBP ArM showing coordination of Tyr288 at the Fe metal and coordination of His227 at the Ir metal.

The ArM catalysed transfer hydrogenation of **1a** using formate as a hydride source with an e.e. of 35% before any optimisation efforts. The activity of the Ir catalyst was around 20-fold lower once bound inside the *Cj*CeuE scaffold, suggesting that the His227 residue binds to iridium impeding binding of hydride to iridium. Replacement of His227 with non-coordinating

alanine did improve the activity of the ArM to just 3-fold lower than the free conjugate but with almost a complete loss of enantioselectivity.[100]

A feature that sets this ArM apart from many others is the reversibility of the binding of the conjugate with the protein scaffold, controlled by the oxidation state of the iron ion. Reducing Fe(III) to Fe(II) using sodium dithionite resulted in the dissociation of the iron from the azotochelin and consequently of the siderophore from the protein scaffold. Oxidation of Fe(II) to Fe(III) reversed the disassembly reproducing the ArM (Figure 17). The recycled ArM showed the same level of enantioselectivity, confirming reassembly had successfully occurred. The ability to control the release of the siderophore-catalyst conjugate from the protein scaffold by reduction of Fe(III) to Fe(II) is a significant advantage allowing recovery and recycling of both the costly protein as well as the organometallic siderophore-catalyst conjugate.[100]

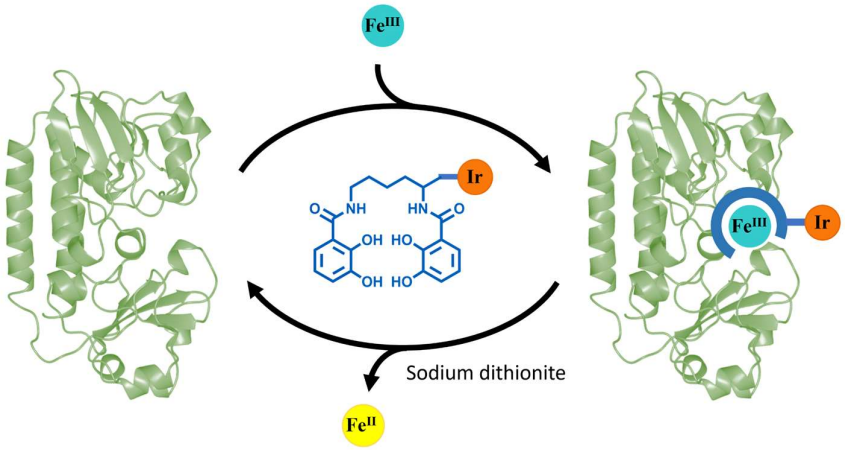


Figure 17 Schematic representation of the recycling and reassembly process for the PBP ArM.

# 1.6 Optimisation Strategies for Artificial Metalloenzymes

## 1.6.1 Dual Optimisation Strategies

A design feature of ArMs constructed from separate metal and protein components is that both components offer cooperative opportunities for optimisation.[27,34,35,106] Improving the chemical component can be approached by altering the catalytic metal or the first coordination sphere of the active metal complex, for example by tuning the electronic properties of coordinating ligands. It also allows alterations to be made to catalyst conjugates that affect the site where the catalytic metal ion is situated in the scaffold. Generally optimisation of the chemical component can account for far greater diversity than optimisation of the protein scaffold.[27,32,107]

Optimisation of protein scaffolds has benefited from enormous innovations in protein engineering technologies in recent years.[2] Engineering scaffolds by rational design, while successful in some cases, has proved challenging due to inadequate understanding of how subtle effects of protein structure and bonding relate to activity.[38,108] Instead, combinatorial approaches, such as directed evolution and computationally-assisted design, have become increasingly popular for optimising ArMs. There are limitations, however, as these approaches mostly require high-throughput screening methods to be developed as well as expression and purification of large protein libraries.[76] This introduction examines the optimisation studies and applications of ArtIREDs and represent a wide, but not comprehensive, range of approaches. A number of excellent additional reports covering progress in the wider field of ArM design are available on these topics.[23,34,109–112]

## 1.6.2 Optimisation of the Chemical Component

The majority of ArtIRED designs are composed of a Noyori-Ikariya-type piano-stool catalytic complexes attached to some kind of anchoring group with a high affinity for their protein scaffold. It was established in early ArtIRED designs that the $\eta^5$-Cp*Ir piano-stool complexes outperformed the isoelectronic $\eta^5$-Cp*Rh and $\eta^6$-(arene)Ru complexes, the latter of which had been the superior catalysts for transfer hydrogenation of ketones.[47,97]

A complementary step in the optimisation of the catalytic conjugate is to tune the electronic contribution of the bidentate ligands. The most extensive report of tuning the bidentate ligands in ArtIREDs is from Quinto *et al.*[92] which employed the arene-linked streptavidin ArM design (Figure 8 (b)) which gave more freedom for testing a broad range of bidentate ligands compared to the bidentate ligand-linked conjugate, which would have required considerably greater synthetic effort. Initially, eight commercially available ligands (Figure 18) were tested with the biotinylated arene-linked Cp*M conjugate in the absence of protein for the transfer hydrogenation of imine **1a** (M=Ir and Rh). Both in the absence of a protein scaffold and in

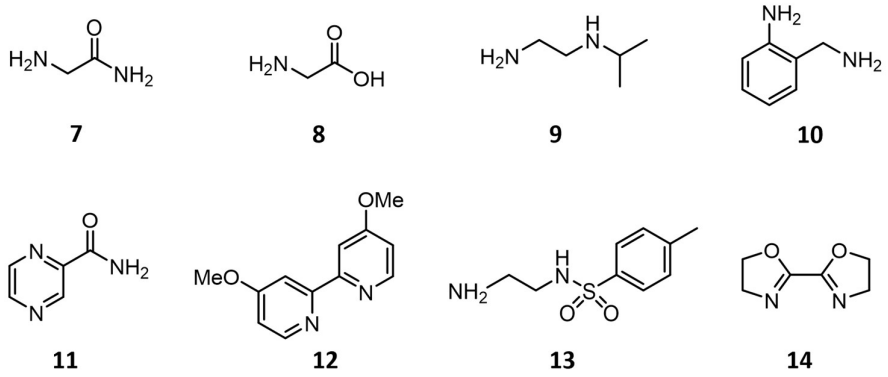


Figure 18 Chemical structures of eight commercially available bidentate ligands tested by Quinto *et al.*[92]

combination with streptavidin, the best activity was recorded for M=Ir conjugates containing ligand **7** and ligand **14**. While several of the M = Rh complexes displayed moderate activity in the absence of the protein scaffold, on incorporation into streptavidin almost all activity was lost. After identifying ligand **7**, an amino amide, as a promising candidate, a library of 28 commercially-available amino amides was also tested, with the best-performing ArM achieving 67% e.e. in an unmodified streptavidin scaffold.

A different approach to optimising the ArM through altering the chemical component is to consider how the length of the linker between the catalytic metal complex and the anchoring moiety influences the secondary coordination sphere the catalytic complex is exposed to. A series of conjugates for the hCAII ArM with increasing length of the linker were synthesised and the binding affinity for the hCAII measured (Figure 19). The conjugate with the shortest linker, **15**, had a very poor binding affinity which was reflected in poor catalytic activity of the corresponding ArM, due to most of the conjugate being washed from the protein during preparation of the ArM before catalysis testing. The conjugates with longer linker lengths bound with stronger affinity to the hCAII scaffold and produced catalytically active ArMs. The ArMs of conjugates **16** and **17** performed better in comparison to the ArMs of conjugates **18** and **19**, potentially due to the increased linker length of conjugates **18** and **19** positioning these conjugates in a less optimal part of the hydrophobic funnel so that the catalytic Ir centres experience a less-well defined secondary coordination sphere.[32]

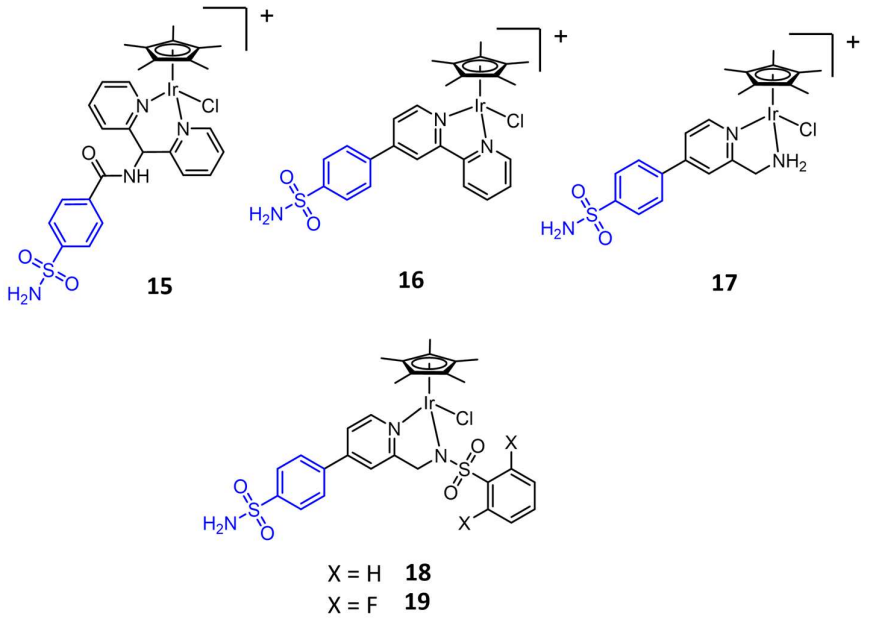


Figure 19 Chemical structures of a series of catalyst conjugates for the hCAII scaffold investigating the effect of increasing the length of the linker between the arylsulfonamide anchoring unit (in blue) and the catalytically-active metal complex.

## 1.6.3 Optimisation of the Protein Scaffold

### 1.6.3.a Site-Directed and Site-Saturation Mutagenesis

One of the most widely-employed approaches to optimising protein scaffolds is by rational design. This approach generally consists of identifying amino acid residues that are located in close proximity to the catalytic site that through exchanging for other amino acids would alter the secondary coordination sphere of the catalytic metal centre or the approach of the substrate.[113,114] Site-directed mutagenesis targets alterations of the protein sequence at specific amino acid positions. This may involve substituting non-coordinating amino acids for coordinating residues to give an additional site for anchoring the conjugate, often by direct coordination to the catalytic metal ion. An extension to this is the insertion of additional protein loops and bulky residues to extend the secondary coordination sphere or removing such groups to shape the catalytic site for better entry of substrates. In site-saturation mutagenesis, a single amino acid position is exchanged for all 19 other amino acids, or a subset of these. This is a powerful technique in the optimisation of protein scaffolds where it is not necessarily predictable which amino acid will have the most favourable attributes.

Examples where coordinating residues were introduced in the active site to help better localisation of the catalytic conjugate have already been highlighted in the dual-anchoring designs of the streptavidin and hCAII ArMs. Detailed structural knowledge of these scaffolds was important in the precise identification of amino acid residues in immediate proximity of the catalytic metal complex that presented an opportunity for modification. In streptavidin, residues H112 and K121 are the closest-lying residues in the protein pocket and are regularly targeted in genetic optimisation strategies of many different ArMs constructed from streptavidin.[35,114]

An approach to better localise the biotinylated conjugate linked *via* the bidentate ligand in the streptavidin scaffold attempted adding a sterically bulky "cap" around the edge of the biotin-binding vestibule.[115] A number of variants with short protein loops inserted in place of different amino acids around the vestibule were evaluated for changes to protein stability and tendency for the protein to aggregate. Mutants where no change to these characteristics occurred identified suitable positions for the insertion of larger protein motifs, which were selected from a pool of structurally well-defined, naturally occurring protein sequences. Unfortunately, the X-ray crystal structures of the resulting ArMs did not show any significant improvement in the localisation of the iridium catalytic centre. Some of the variants did show improved turnover numbers (TONs) perhaps reflecting the increased protection of the catalytic metal species from external deactivating factors.

Site-saturation mutagenesis has been used in many reports of ArM optimisation for example in the first optimisation studies for the streptavidin scaffold where a saturation mutagenesis library of S112X was screened. It was shown the enantioselectivity of the ArM for the (*R*)- or (*S*)-product of **1b** could be tuned from mutations at this site alone, with the S112K mutant proving selective for (*S*)-**1b** and S112A for (*R*)-**1b**.[47] This example is particularly interesting as it demonstrates the scope for tuning the enantioselectivity of the ArM, with the same scaffold able to direct to either enantiomer depending on small modifications.

Genetic modification of protein scaffolds does not always lead to improved performance, as demonstrated in the attempted optimisation of the streptavidin scaffold for the dual-anchored ArM with the biotinylated conjugate where the enantioselectivity of the scaffold could not be further improved from the unmodified scaffold by mutation of S112, K121 or L124.[92,116]

### 1.6.3.b Computational Modelling to Aid Scaffold Design

Computational modelling has been identified as a revolutionary tool in approaching enzyme optimisation.[106,117,118] Trial-and-error approaches, such as site-saturation mutagenesis and directed evolution, require the preparation of huge libraries of variants and extensive screening efforts to identify improvements. This is time-consuming and expensive.[118]

A computational modelling study calculated the energy of the transition states for the transfer hydrogenation of **1a** by ArMs of two streptavidin variants, one selective for the (*R*)-product, the other for the (*S*)-product.[119] The differences between the calculated transition state energies correlated well with the extent of enantioselectivity of both variants. This demonstrated the potential use of computational studies to aid our understanding of how the secondary coordination sphere contributes to catalysis and, using this information, might help in predicting beneficial modifications to the protein scaffold.

In a study lead by Baker and Ward, the Rosetta design algorithm was used to guide engineering efforts in the optimisation of the hCAII scaffold.[106] The project was aimed at improving localisation of the catalytic conjugate in the protein scaffold by increasing the hydrophobic nature of the pocket, improving the rigidity of the scaffold and providing more favourable interactions between the protein scaffold and the catalytic conjugate. The expectation was that a more well-defined, strongly coordinated conjugate would improve catalytic performance. A series of four hCAII variants suggested by the algorithm resulted in 46- to 64-fold improvement in conjugate binding affinity, and additionally led to ArMs with better activity and enantioselectivity. This included one of the best ArtIREDs reported to date for the reduction of **1a** to (*S*)-**1b** which achieved an e.e. of 96% and a 6-fold improvement in TON compared with the ArM with no modification to the hCAII scaffold.[23]

### 1.6.3.c Engineering of Multimeric Scaffolds to Overcome Duplicated Mutations

The fused tetrameric streptavidin scaffold was developed to overcome problems associated with two subunits of streptavidin creating the protein pocket that forms the catalytic active sites. This had meant that any modification to streptavidin was replicated twice in the protein pocket. The fused tetrameric scaffold is coded such that the replicated amino acid positions in the sequence can now be engineered independently leading to far greater control in engineering the pocket of the active site (Figure 10). The ArM was further finely-tuning by removing the ability of one streptavidin unit in each catalytic protein pocket to bind biotin, guaranteeing that the conjugate could only bind in the desired position and reducing the variation in catalytic results depending on the amount of biotinylated conjugate added. Overall, this design brought about significant improvements in enantioselectivity. Particularly notable are the selectivities achieved for (*R*)-**3b** (91% e.e.), (*R*)-**4b** (96% e.e.) and (*S*)-**5b** (91% e.e.) by different mutated scaffolds.[93]

### 1.6.3.d Directed Evolution

For many years it has proved challenging for researchers to employ rational design as a means to engineer better functioning proteins.[35,120] Our understanding of the effect of making small changes to the protein structure on performance of biocatalysts is not yet sufficient and hence success of engineering proteins by this route remains limited.[38] The development of directed evolution strategies has proven revolutionary in the engineering of naturally-occurring enzymes for characteristics such as stability in reaction conditions, catalytic performance (activity and selectivity) and substrate scope.[120] Directed evolution is a technique where repeated cycles of mutagenesis are used to create genetic diversity in the selected gene sequence by random mutagenesis and DNA recombination processes. Specialised high-throughput screening methods are then required to identify improved protein variants and their sequences analysed to inform future mutation cycles.[17] This method can result in huge libraries of variants that require screening which can prove time-consuming and materially costly.

Initially, directed evolution was thought to be out of reach of most ArMs optimisation strategies since expression, isolation and purification of each protein variant would be incredibly time-consuming and the synthetic effort to produce large quantities of the catalytic conjugate for testing each variant would be prohibitively expensive. It was recognised that avoiding the isolation and purification of the protein variants would be key to enabling directed evolution, but this would require catalysis screening in cell extracts or lysates which contain components such as thiols, for example glutathione, which are known to deactivate heavy metal catalysts such as the Noyori-Ikariya-type catalysts employed in streptavidin ArtIREDs.

It was established that treatment of cell extracts and lysates with oxidising agents such as diamine (DiAm) was effective in removing deactivating chemicals and ArMs could be formed successfully and showed catalytic activity.[121]This discovery paved the way for the first reported directed evolution study involving an ArM.[76] Random mutagenesis was restricted to a limited range of amino acids in the vicinity of the active site. Multiple rounds of mutagenesis revealed that enantioselectivity of the ArM was improved by an increased number of bulky residues surrounding the catalytic iridium site. It was proposed that this was due to increased interactions between the iridium complex and protein scaffold creating a better-defined secondary coordination sphere. Different evolutionary paths produced protein scaffolds that were selected for the (*R*)- or (*S*)- enantiomer of **2b**, with e.e.s on par with some of the best performing streptavidin ArMs and enhanced catalytic rates.

# 1.7 Additional Optimisation Strategies and Future Directions

## 1.7.1 Immobilisation

Immobilisation of enzymes has been influential in applications in biocatalysis as it can improve stability of the enzymes and increase tolerance to organic solvents. The heterogeneous quality creates an easier way to separate enzymes following competition of the catalytic reaction and reusability, as enzymes do not have to be recovered from solution. Immobilisation of streptavidin ArMs was achieved on organosilica coated nanoparticles which were demonstrated to allow recovery and reuse of the ArMs up to three times with only a small decrease in enantioselectivity each time for the transfer hydrogenation of **1a**.[81]

## 1.7.2 Encapsulation

Another approach to improving the stability of the streptavidin ArM to external factors was to encapsulate the ArM inside a larger protein, ferritin. This was accomplished by introducing the ArM in a solution containing ferritin at low pH (pH < 2), where ferritin will be denatured. In contrast, streptavidin is relatively stable at this low pH. On increasing the pH, ferritin refolds encapsulating the ArM. This additional layer of protein scaffold can provide significant interactions with the catalytic complex and substrate as demonstrated by the catalytic results for the transfer hydrogenation of substrate **1a**, where the (*S*)-amine was produced regardless of whether an (*R*)- or (*S*)-selective ArM was encapsulated. However, this effect was substrate specific to an extent, with no such alterations in enantioselectivities seen for substrate **2a**. Despite interesting results for enantioselectivities of the encapsulated ArMs, turnover-frequencies (TOFs) were poor and enantioselectivity reduced in some cases, although some

ArMs did appear to be stable under catalytic conditions for longer as indicated by improved TONs.[122]

### 1.7.3 Whole-Cell Catalysis

Whole-cell catalysis is an attractive goal since it removes the need for protein isolation and purification. Following the demonstration that treatment of cell extracts and lysates could enable formation of catalytically-active streptavidin ArMs, whole-cell catalysis seemed a logical target. Purified streptavidin for most ArM experiments is produced by overexpression in the cytoplasm of *E. coli.*, however, formation of the ArM and catalysis in the cytoplasm posed a number of challenges. Firstly, transport of compounds such as the biotinylated conjugate and substrate across the inner membrane might not be possible since the inner membrane is highly selective as to which chemicals can enter the cell. Secondly, the concentration of glutathione in the cytoplasm is very high, risking deactivation of the catalytic conjugate either before it can bind to streptavidin or once bound in the ArM. Instead, an approach to localise streptavidin in the periplasm of *E. coli* was devised by adding a transmembrane locating factor, OmpA, to the genetic sequence of streptavidin. Isolating the ArM in the periplasm is an attractive target as it contains a far lower concentration of glutathione together with being more easily accessed.[34,121] The OmpA locator acts to transport the attached protein across the membrane into the periplasm, before it is cleaved. Successful localisation of streptavidin in the periplasm was confirmed by SDS-PAGE. For catalysis testing, an imine substrate was selected that released a fluorescent compound following reduction to the amine so that the catalytic reaction could be followed by fluorescence spectroscopy (Figure 14).[123] A directed evolution study was then applied, with 450 clones screened, to prove this system was applicable in large-scale optimisation efforts.[124]

### 1.7.4 Enzyme Cascades

Enzyme cascades have been identified as desirable applications for naturally-occurring enzymes as well as ArMs. A considerable advantage is that a cascade removes the need to isolate intermediates in the reaction and is particularly valuable when some intermediates may be unstable. Streptavidin ArMs have been combined in cascades with natural enzymes either for the purpose of enantiomeric resolution, achieved by integrating an oxidase which converts the undesired amine product back to the imine substrate resulting in a single enantiomer of the amine being produced,[125] or for $NADP^+$/NADPH recycling where the product of interest of the cascade is produced by a downstream enzyme.[82,125,126]

In the first example, streptavidin ArMs were combined with monoamine oxidase (MAO), L-selective amino acid oxidase (LAAO) or D-selective amino acid oxidase (DAAO). The ArM catalyses the reduction of the imine substrate to the corresponding amine enantioselectivity, but since the ArM is not perfectly enantiospecific, some quantity of each enantiomeric product is produced. The unwanted amine product is then oxidised back to the imine substrate by a selective oxidase enzyme resulting in an accumulation of one enantiomer of the amine (Figure 20).[125]

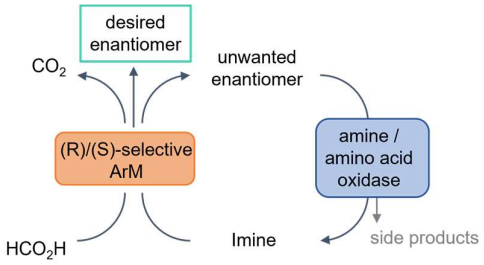


Figure 20 Simplified scheme for an enzyme cascade used for the enantiopure synthesis of a selected amine product.

For the second type of cascade, streptavidin ArMs designed for transfer hydrogenation of imines have also been shown to reduce $NADP^+$ to NADPH using formate, which can be incorporated as a cofactor regeneration system in more generic enzyme cascades where downstream enzymes complete the catalytic transformations of interest (Figure 21 (a)). Reactions such as hydroxylations[125] and reductions of α,β-unsaturated compounds[82] have been achieved using this method. In a more ambitious attempt, the ArM was employed for both NADPH regeneration and a catalytic step in a multi-step cascade with an alcohol dehydrogenase to reduce imine **4a** to amine **4b** (Figure 21 (b)).[126]

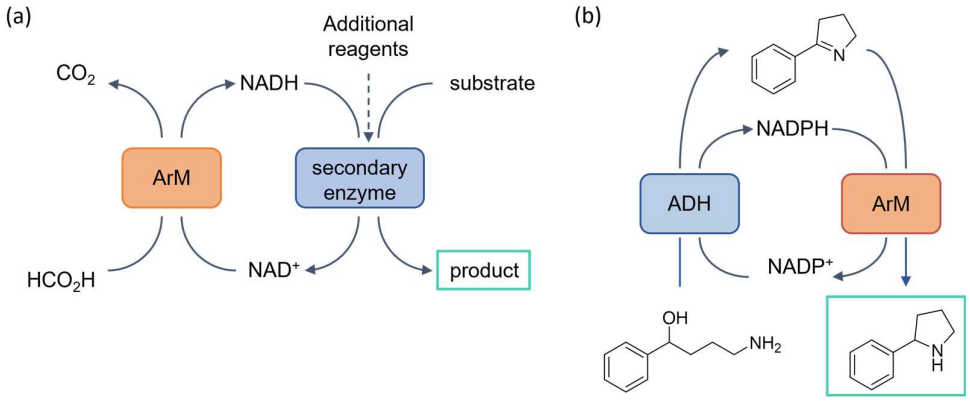


Figure 21 Simplified schemes for (a) a cascade using a streptavidin ArM in NADH cofactor regeneration and (b) NADH regeneration and imine reduction to produce amine **4b**.

## 1.7.5 Biomedical Applications

A potential biomedical application has been proposed for hCAII ArMs. Carbonic anhydrase is expressed on the surface of cells, and in the case of many cancer cells is overexpressed in much greater quantities. It was proposed that, if ArMs could be constructed from the surface-expressed proteins by addition of a catalytic conjugate designed to perform an uncaging transformation, they could be targeted at releasing drugs in the immediate proximity of the cancerous cell (Figure 22). Uncaging of drugs close to their site of action has been identified as a method to reduce side-effects of chemotherapy as many cancer drugs are not truly specific at attacking only cancer cells and can damage other cells in the body, contributing to side-effects. By delivering the drug to the body in a caged form that is significantly less toxic, and only transformed to the toxic form of at the site of action, attack of non-cancerous cells could be significantly reduced.

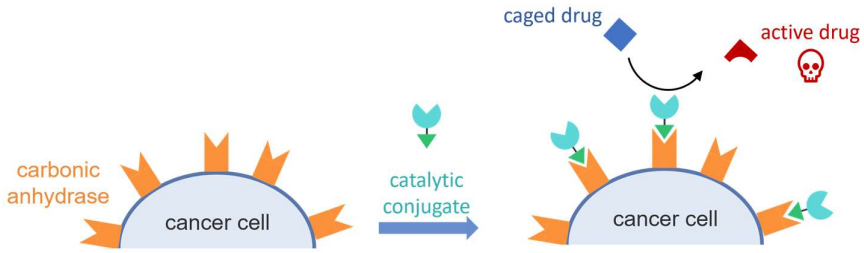


Figure 22 Schematic demonstrating the concept of harnessing hCAII ArMs for site-specific drug delivery for cancer cells

In an initial study to evaluate this proposal, hCAII was expressed on the surface of *E. coli* by fusing the genetic sequences of the protein to a truncated lipoprotein (Lpp) and outer membrane protein A (OmpA). Successful expression of functional hCAII on the cell surface was confirmed by staining with a fluorescent probe in combination with an anti-CAII antibody. A small series of different catalytic conjugates containing the arylsulfonamide anchoring group were added to a solution containing the *E. coli* cells, the cells were then thoroughly washed to remove any unbound conjugate and tested for catalytic activity. The imine substrate **19a** was used for activity testing as the reaction could be monitored by fluorescence spectroscopy as the fluorescent product umbelliferone is produced. All but one of the conjugates resulted in successful formation of ArMs and measurable catalytic activity.[32] This represents an exciting opportunity of ArMs beyond biocatalysis if the same results can be reproduced in eukaryotic cells.

## 1.7.6 Biocatalysis Applications

Whilst there have been a number of encouraging reports in the development of ArtIREDs, there remain few reports of achieving catalysis on an industrially-relevant scale.[93] Beyond this,

there remain limitations in the number of accessible amine products due to the poor stability of many non-cyclic imines in water. Competition from natural IREDs presents an additional challenge, since many of the techniques used to optimise ArtIREDs for catalysis applications are equally applicable to natural IREDs. However, there are some advantages for ArtIREDs over natural IREDs such as there are have been very rare reports of inhibition of ArtIREDs by substrates or products despite catalytic conditions often boasting high substrate concentrations in comparison to concentrations natural IREDs can tolerate.[127] Improved engineering of ArtIREDs also continue to improve catalytic performance relative to natural IREDs. Table 2 provides a short summary of the reported activity and selectivity for some best-performing ArtIREDs and reported natural IREDs on substrates **1a-5a**.[60,128–131]

## 1.8 Summary and Conclusions

ArMs offer exciting opportunities for the development of biocatalysts for transformations that have appeared beyond the scope of natural enzymes. The synthesis of chiral amines has been identified as a key target for biocatalysts in industry. While there have been exciting developments reported in the development of ArtIREDs there are a number of alternative catalysts such as small molecule Noyori-Ikariya-type complexes and natural IREDs. Nevertheless, imine reduction offers a good starting point for the evaluation of new ArM designs. Optimisation efforts can help our understanding of the interactions that contribute to enantioselectivity and rate enhancement. Improving genetic engineering technologies offer ever increasing opportunities to develop ArMs towards more challenging chemical transformations where suitable alternative catalysts do not exist. However, the knowledge gained from the development of ArMs for more modest catalytic transformations is very valuable for expanding the range of ArMs.

The design of ArMs offer two complimentary approaches to optimisation, through both the chemical and protein components. A number of strategies have previously been explored in the optimisation of ArtIREDs and were responsible for directing the work presented in this thesis.

## 1.9 Project Aims

The aim of this project was to develop the design of the PBP ArM to improve catalytic performance in terms of both catalytic activity and enantioselectivity. The reported PBP ArM[100] catalysed the transfer hydrogenation of imine **1a** with a very slow TOF of 0.3 $min^{-1}$. This is far from the activity of natural enzymes which can perform catalytic transformations in the range of hundreds of turnovers per minute. The enantioselectivity was reported to be 35% e.e. for (*R*)-**1b** before any optimisation attempts. It was hoped that the results of

Table 2 Comparing catalytic activities and selectivities of reported ArtIREDs and IREDs.

| Enzyme | substrate | | | | | | | | | | | |
|---|---|---|---|---|---|---|---|---|---|---|---|---|
| |  **1a** | | |  **2a** | | |  **3a** | | | 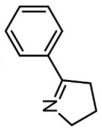 **4a** | | | 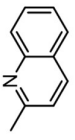 **5a** | | |
| | **Time / h** | **Conv. / %** | **e.e. / %** | **Time / h** | **Conv. / %** | **e.e. / %** | **Time / h** | **Conv. / %** | **e.e. / %** | **Time / h** | **Conv. / %** | **e.e. / %** | **Time / h** | **Conv. / %** | **e.e. / %** |
| Sav | 2 | quant. | 96 | 24 | 99 | 93 | n/r | 99 | 93 | 24 | 90 | 98 | n/r | 98 | 91 |
| | 48 | quant. | -78 | 48 | 99 | -78 | 18 | 100 | -25 | | | | | | |
| hCAII | 96 | 98 | -94 | | | | 98 | 74 | | | | | | | |
| | | | | | | 96 | 80 | -75 | | | | | | | |
| RNaseS | 16.5 | 25 | -39 | | | | | | | | | | | | |
| PBP | 24 | 100 | 35 | | | | | | | | | | | | |
| IRED | | | | 24 | 100 | 99 | 18 | 98 | 99 | 24 | >98 | -8 | | | |
| | 4 | >99 | -99 | 24 | 99 | -99 | 4 | >99 | -99 | | | | | | |

optimisation efforts would also help to develop a better understanding of this ArM design which could inform optimisation efforts of ArMs for other catalytic transformations in future.

Optimisation efforts focussed largely on developing the chemical component of the ArM. One of the ideas explored was a redesign of the siderophore-catalyst conjugate to shorten the link between the catalyst and the anchoring unit by attaching the siderophore at the $\eta^6$-arene ligand as opposed to the bidentate ligand (Chapter 2). This would additionally allow more freedom with the selection of ligands to occupy the remaining coordination sites of the piano-stool complex, allowing diversification beyond transfer hydrogenation catalysts. Another target was to improve the activity of the iridium catalyst through alterations to the sulfonamide bidentate ligand (Chapter 3). This was examined through a range of electron-donating and electron-withdrawing substituents added to the ligand. Two different PBPs from thermophilic organisms had been identified as alternatives to the original *Cj*CeuE scaffold. It was expected that combining these PBPs with siderophore-catalyst conjugates containing improved iridium catalysts from Chapter 3 could result in an improved ArtIRED of the PBP design (Chapter 4).

# Chapter 2 A New Design of Siderophore-Catalyst Conjugate for a Periplasmic Binding Protein ArM

## 2.1 Introduction and Aims

In the previously reported PBP ArM the iridium catalyst is moderately surface exposed meaning that the catalyst is not well buried in the protein scaffold. A larger protein encapsulation of the catalyst can have advantages in protecting the catalyst from destabilising factors such as oxygen and thiols.[100] The secondary coordination sphere that is provided by the protein scaffold determines the enantioselectivity of the ArM. If the catalyst is relatively surface exposed, the number of interactions that the secondary coordination sphere contributes is lower compared to a more buried catalyst site. It has previously been proposed that extending the secondary coordination sphere can contribute to ArM activity and enantioselectivity.[115] The length of the linker between the catalytic complex and the anchoring unit in supramolecular ArM assemblies determines the position which the catalyst occupies in the protein scaffold and hence the secondary coordination sphere. Altering the length of the linker in the conjugate could position the catalyst in a surrounding environment that imparts improved selectivity, or even selectivity for the opposite enantiomer.[91] In the PBP ArM the structure of the conjugate could be altered to decrease the length of the linker between the iridium catalyst and the siderophore anchor to bury the catalyst deeper within the protein pocket. However, another consideration is that the binding affinity of the conjugate may change: if the linker is too short and steric strain with the protein scaffold is high, the conjugate will not bind strongly and enantioselectivity could be entirely erased. Previous studies have shown an ArM can be optimised by finding the most suitable linker length.[32]

Rebelein *et al.*[32] reported a study optimising a carbonic anhydrase-based ArM by screening a number of cofactors with different lengths of linker between the anchoring sulfonamide group and the metal complex (Figure 23). They found the length of the linker had a marked effect on the dissociation constant ($K_d$) of the conjugate with the protein, with the shortest linker, **20**, giving a high dissociation constant which reflects the poor catalytic activity of the resulting ArM as the conjugate is effectively not bound by the protein. The conjugates with longer linkers gave similar binding constants but remarkably different catalytic activity in the resultant ArM. The intermediate length linker **21** located the catalytic complex in a more tightly-packed pocket in the protein and resulted in a more catalytically active ArM, with

double the conversion of the imine substrate after 16 hours compared with the ArM formed of the conjugate with the longest linker, **22**. In this particular report, the product of the catalytic reaction was not enantiomeric and, as such, it was not possible to reflect on any changes to enantioselectivity on altering the secondary coordination sphere.

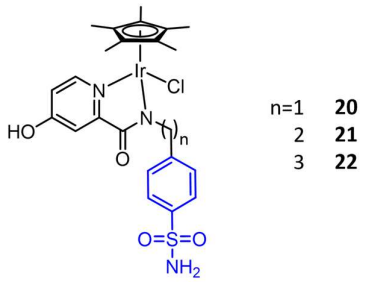


Figure 23 General structure for a range of catalytic conjugates trialled for ArMs of hCAII by Rebelein *et al.*[32] where the length of the linker between the catalytic metal complex (Cp*Ir) and the sulfonamide anchoring unit (in blue) is varied.

The design of the conjugate of the PBP ArM previously published (Figure 24) leaves limited options to shorten the linker between the anchoring azotochelin and the catalytic metal complex. Aryl sulfonamides are widely reported as optimal for Noyori-Ikariya-type catalyst activity[52] and the methylamine substituent was selected for the attachment to azotochelin over an amine group without a methylene spacer to improve the nucleophilicity of the amine and help in the amide coupling step between the arylsulfonamide ligand and azotochelin.[100]

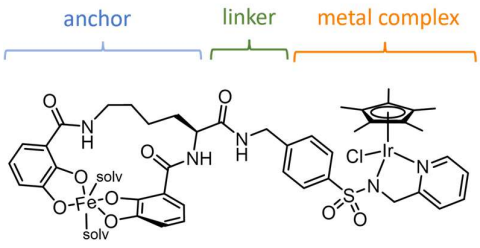


**23**

Figure 24 Structure of the conjugate reported by Raines *et al.*[100] for the PBP ArM.

An alternative approach would be to attach azotochelin to the arene ligand of the catalyst. This style of design has already been incorporated in the Streptavidin ArM, attaching the biotin anchoring unit to the cyclopentyl ligand of a rhodium or iridium piano-stool complex (Figure 25).[91,92] This design of conjugate was initially prompted by the low occupancy of the catalytic metal centre in X-ray structures of Streptavidin ArMs, reflecting the poor localisation of the metal atom in the binding pocket. To improve localisation and hence the influence of a more well-defined secondary coordination sphere, a histidine residue was incorporated in the binding pocket of the streptavidin scaffold to provide a covalent linkage directly to the

catalytic metal centre (Figure 25 (a)). The catalytic mechanism requires at least one labile ligand to the metal centre, which dissociates to make way for the activated hydride. If the protein scaffold with the introduced histidine was used in conjunction with the previously used Cp*Ir(aminoethylsulfonamide)-biotin conjugate, histidine would occupy the single labile site, reducing catalytic activity as the histidine-metal bond is stronger than the metal-labile ligand bond it would be replacing. In order to make way for this coordinating group, the previously used Cp*Ir(aminoethylsulfonamide)-biotin conjugate had to be redesigned with the biotin anchor attached to the arene ligand, leaving three remaining coordination sites which can be occupied by histidine, labile ligands such as chloride, or other ligands. The design of the conjugate relied on simulations modelling the proposed conjugate together with the X-ray crystal structure of streptavidin ArMs which suggested an ethylene spacer between the biotin anchor and the arene ligand was optimal for localization of the metal complex in close proximity to the sites selected for histidine incorporation at S112 or K121.[91]

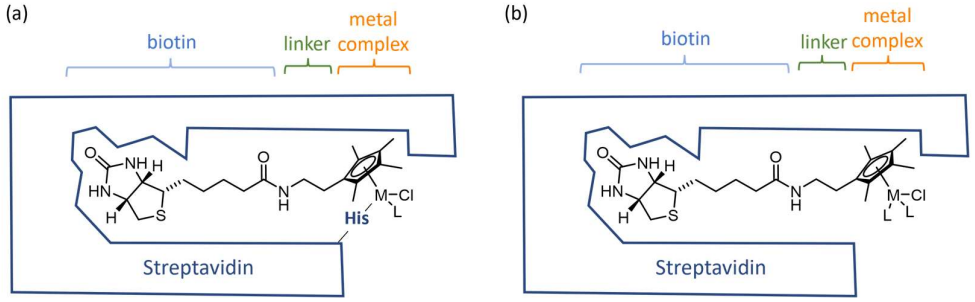


Figure 25 (a) Scheme indicating the ArM design reported by Zimbron *et al.*[91] containing a conjugate where the biotin anchoring unit is linked to the metal complex by the arene ligand in order to make way for a coordinating histidine residue incorporated into the protein scaffold and (b) scheme showing how the design of this conjugate in the absence of a coordinating histidine offers improved freedom in the choice of metal-coordinating ligands as reported by Quinto *et al.*[92]

Both Rh and Ir conjugates incorporated into WT streptavidin (with no coordinating histidine) produced ArMs with significantly lower catalytic activity and enantioselectivity than values reported for ArMs with the previously used Cp*Ir(aminoethylsulfonamide)-biotin conjugate. ArMs of the Ir conjugate did not improve on incorporating histidine into the protein scaffold. Some significant improvements were seen for the ArMs with the Rh conjugate, however, including opposite enantioselectivity depending on whether the histidine was included at the 112 (*S*-enantiomer) or 121 (*R*-enantiomer) position.[91]The three available coordination sites of the conjugate offer greater freedom to vary the primary coordination of the metal centre (Figure 25 (b)). This was demonstrated in a later work where a large number of bidentate ligands were screened with WT-streptavidin (without a coordinating histidine). This represented one of the most extensive chemical optimisation attempts.[92]

Similar arene-linked Cp*Rh- and (cyclohexane)Ru-complexes were incorporated into a protease-based ArM for ketone reduction (conjugates shown in Figure 26). There was some indication from MALDI-TOF measurements that the conjugate binds with the arene-ligand dissociated from the Ru complex, however, since the ArM still proves to be catalytically active, this is likely caused by the ionisation conditions associated with the mass spectrometric measurements.[132]

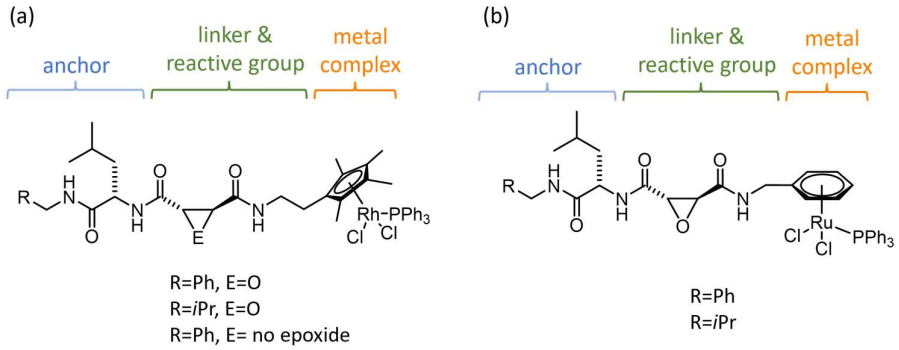


Figure 26 Structures of (a) the Cp*Rh-based conjugate and (b) the ($\eta^6$-arene)Ru-based conjugate for the protease ArM reported by Reiner *et al.*[132]

Several piano-stool complexes with functional attachments to the arene ligand have been reported for a number of catalysts, in particular for Ru, with a range of applications including catalysts for hydrogenation,[133] transfer hydrogenation[65,66,134–138] and C-C bond forming reactions.[139–141]

An interesting report by Movassaghi *et al.*[142] examined a ruthenium-based complex with an amino-acid substituent on a $\eta^6$-arene ligand, that was incorporated to improve water solubility in comparison to more widely-used hydrocarbon aromatic rings (Figure 27). The use of a L-phenylalanine-based arene ligand also provides a side chain with functional groups which allow further modification. Complexes shown in Figure 27 were prepared from the [($\eta^6$-arene)$RuCl_2$]$_2$ dimer, which was synthesised by refluxing the partially-reduced dually-

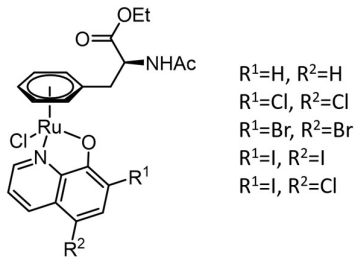


Figure 27 Structures of the ($\eta^6$-phenylalanine)Ru complexes reported by Movassaghi *et al.*[142] with a dually-protected phenylalanine as the arene ligand.

protected (ethyl ester and acetylamide) L-phenylalanine with $RuCl_3 \cdot xH_2O$ in ethanol overnight.

Reports of other $[(\eta^6\text{-arene})RuCl_2]_2$ dimers with amino-acid type substituents have revealed a number of challenges associated with their synthesis and stability when the carboxylic acid and amine groups are not protected. For example, $\alpha$-amino acids have the ability to coordinate metal ions so strategies to reduce the binding affinities of these groups is necessary. Adding a protecting group (usually an ester) to the carboxylic acid is essential in the case of phenylglycine-based arene ligands to avoid decarboxylation in acidic conditions (Figure 28 (a)).[143] This elimination is not observed for phenylalanine ligands, however, as it is a result of the highly electron-deficient nature of the carbon in α-position to the aromatic ring in phenylglycine. As such, a common approach to synthesising the relevant $[(\eta^6\text{-arene})RuCl_2]_2$ dimer consists of a two-step reaction where the carboxylic acid group is first esterified before reaction with $RuCl_3 \cdot xH_2O$ under acidic conditions to obtain the dimer with a protected carboxylic acid group and protonated amine group to avoid coordination of the amine (Figure 28 (b)).

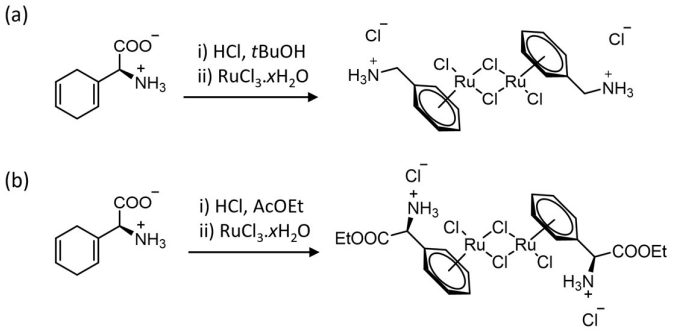


Figure 28 (a) Reaction of 2,5-dihydrophenylglycine with $RuCl_3 \cdot xH_2O$ under acidic conditions leads to decarboxylation at the $\alpha$-carbon. (b) Reaction scheme for the synthesis of $[(\eta^6\text{-phenylglycine})RuCl_2]_2$ in a single pot reaction involving the esterification of the carboxylic acid before reaction with $RuCl_3 \cdot xH_2O$ to avoid decarboxylation.

Without protection of the carboxylic acid group of phenylalanine, with the carboxylic acid at the $\beta$-carbon, a $\eta^6{:}\kappa^1$-complex is formed, **24**, with the amine group coordinating the Ru centre (Figure 29).

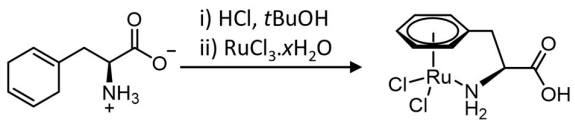


**24**

Figure 29 Scheme depicting the formation of complex **24** when 2,5-dihydrophenylalanine is reacted with $RuCl_3 \cdot xH_2O$ under acidic conditions

The [($\eta^6$-arene)$RuCl_2$]$_2$·2HCl dimeric complexes and complex **24** are poorly soluble in most organic solvents. Solvents such as DMSO and DMF dissolve these complexes, but are capable of coordinating to the metal centre and because of this can trigger a number of complications with regard to the stability of the complexes. It was found that for **24** in acidified solutions of DMSO, the $\kappa^1$-type coordination in complex **24** can be overcome, forming the protonated amine group with the coordination site that the amine had occupied being filled by a solvent molecule (Figure 30 (a)). Dissolving a similar [($\eta^6$-arene)$RuCl_2$]$_2$ dimeric complex, **25**, or related piano-stool complexes **24** and **26** in unacidified solutions of DMSO led to decomposition that is further accelerated by addition of triethylamine base (Figure 30 (b)). The addition of an acetyl group to the amine of **25** to avoid $\kappa^1$ coordination prevents decomposition. Exact decomposition products were not identified, although the most likely cause is ring slippage,[144] where the arene ligand dissociates leaving the ligand coordinated only *via* the amine group, and the vacated coordination sites replaced by other coordinating groups, such as solvent molecules.

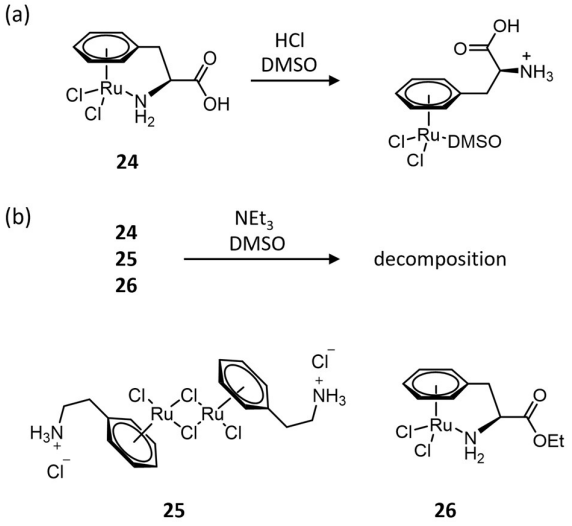


Figure 30 (a) Scheme of the reaction of complex **24** with a coordinating solvent, in this case DMSO, under acidic conditions and (b) Scheme demonstrating complexes such as **24**, **25** and **26** decompose in coordinating solvents such as DMSO, which is accelerated by addition of $NEt_3$.

Reacting [($\eta^6$-arene)$RuCl_2$]$_2$ dimeric complexes (with the carboxylic acid group esterified) with ethylenediamine ligands results in complexes that were more tolerant of basic conditions. This stability was proposed to arise from steric shielding of the metal centre by these ligands preventing solvent molecules displacing the arene ligand so easily (Figure 31).

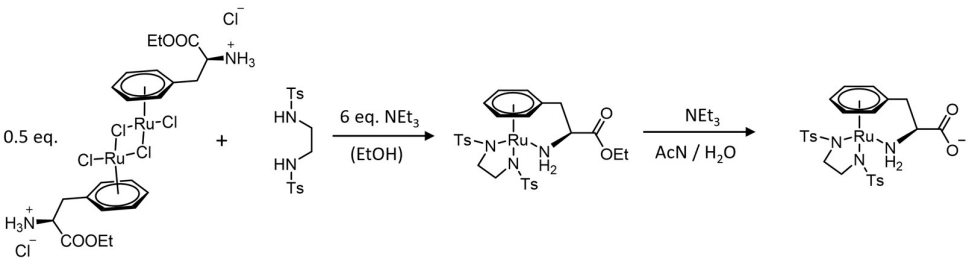


Figure 31 Scheme showing the synthesis of a ($\eta^6$-phenylalanine)Ru(ethylenediamine)-type complex which is more resistant to degradation under basic conditions than complexes without ethylenediamine-type coordinating ligands.

These reports inspired a new design for a conjugate with azotochelin linked *via* an arene ligand with an amino acid-type functional group (Figure 32). Attaching azotochelin to the arene ligand allows a greater degree of freedom for selecting the ligands occupying the other three coordination sites, allowing access to Ru and Os catalysts for different catalytic transformations. Phenylglycine was selected, as the shorter side chain length prevents destabilization caused by $\kappa^1$ coordination of the amine group to the metal centre during synthesis, and results in a shorter length of the linker between azotochelin and the catalytic complex. The carboxylic acid group must be esterified to prevent decarboxylation.

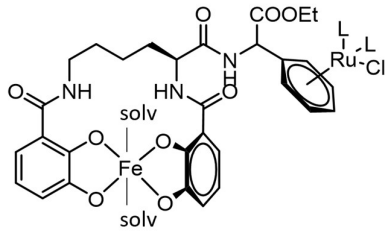


Figure 32 Proposed structure of a conjugate for a PBP ArM where azotochelin is linked to the metal complex by the $\eta^6$-arene ligand.

# 2.2 Synthesis and Catalysis Testing of Ruthenium Complexes

Initially, the suitability of using ruthenium catalysts in the design of the conjugate had to be investigated. Ru catalysts have been shown to be inferior to Ir-based catalysts for the transfer hydrogenation of imines but still show catalytic activity.[47,145] For the design of complexes for catalytic testing, a dually-protected phenylglycine arene ligand was selected to reduce complications from a coordinating amine group,[143] and two arylsulfonamide bidentate ligands, one with an ethylamine- and the other with a methylpyridine- attachment (Figure 33). Two very similar arylsulfonamide ligands had been investigated in the design of the previously

reported PBP ArM with isoelectronic Cp*Ir complexes, with the methylpyridine version proving superior.[100]

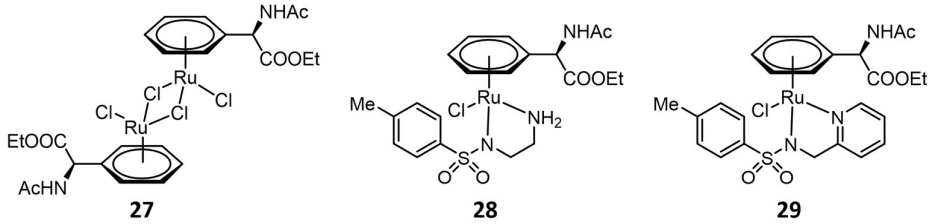


Figure 33 Chemical structures of the three Ru complexes synthesised and tested for catalytic activity for the transfer hydrogenation of a cyclic imine.

Complex **27**, from which complexes **28** and **29** were prepared, was synthesised in a three-step process from (*R*)-(-)-2-(2,5-dihydrophenyl)glycine, **30**, first by esterification of the carboxylic acid with ethanol followed by addition of an acetyl protecting group at the amine (Figure 34). It was important to carry out these steps in inert conditions as it was found that the presence of oxygen in the reaction accelerated aromatisation of the 2,5-dihydrophenyl, observed in mass spectrometry measurements as a larger error in the m/z measurements and unusual mass distribution patterns. This is also seen in the $^{1}$H NMR spectra as small additional peaks at 7-8 ppm, a small singlet at 4.5 ppm and a second triplet peak at 1.1 ppm (Figure 35 (a)) which match closely to the theoretically predicted spectrum for the aromatic by-product (Figure 35 (c)).

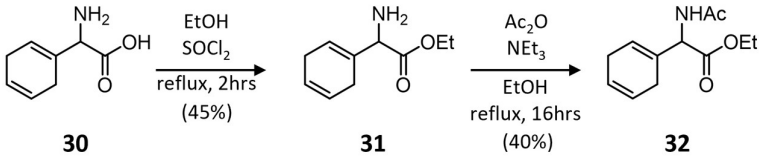


Figure 34 Scheme for the synthesis of the precursor to the dually-protected ($\eta^6$-phenylglycine) ligand.

While performing these reactions in oxygen-free conditions did help to reduce the amount of aromatised by-product, it proved impossible to isolate just the desired 2,5-dihydrophenyl product. This was because the 2,5-dihydrophenyl glycine starting material already contained traces of the aromatic alternative, as revealed by $^{1}$H NMR of the purchased starting material from two different suppliers. Separation of the desired product from the aromatic analogue was not pursued at this stage as the by-product is present in a small quantity and should be removed upon isolation of the Ru intermediate **27**.

The intermediate Ru dimer, **27**, was synthesised according to the literature procedure,[142] however, a yield of only 37% was obtained. Instead, a method taking inspiration from the preparation of $\eta^6$-arene-osmium complexes[50] using microwave radiation in place of an overnight reflux produced a far better yield of 70%.

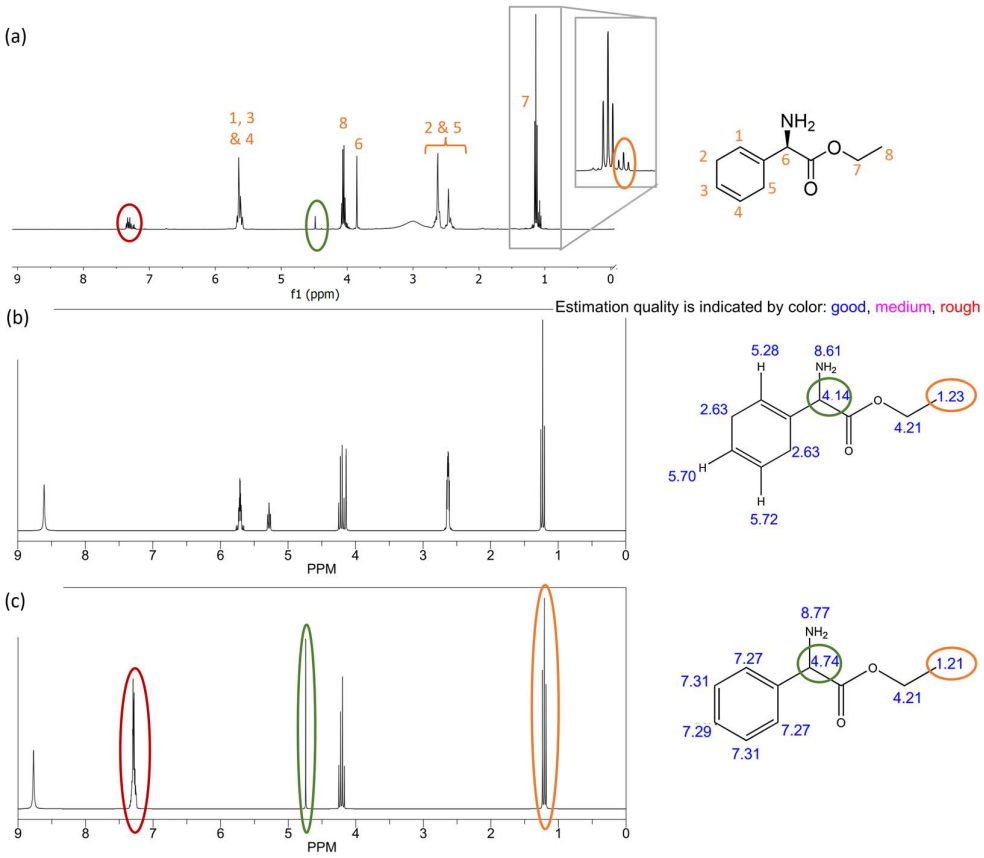


Figure 35 (a) Experimental $^1$H NMR spectrum (DMSO-$d_6$) for compound **31** and the theoretical spectra for the expected product (b) and the aromatised by-product (c).

Complexes **28** and **29** were then prepared from intermediate **27** by heating in isopropanol with the appropriate arylsulfonamide ligand under inert, anhydrous conditions. Both complexes were obtained in 70%+ yields. Complexes **27**-**29** were then briefly tested to confirm catalysis of the transfer hydrogenation of dehydrosalsolidine, **1a**, using sodium formate as a hydride donor (Figure 36). Conditions for the catalysis testing closely matched those used for testing the PBP ArM in previously published work, with 50 mM substrate, 0.125 mM catalyst, in buffer (0.6 M MES) at pH 6.0, 3 M sodium formate, 40 °C, with stirring.

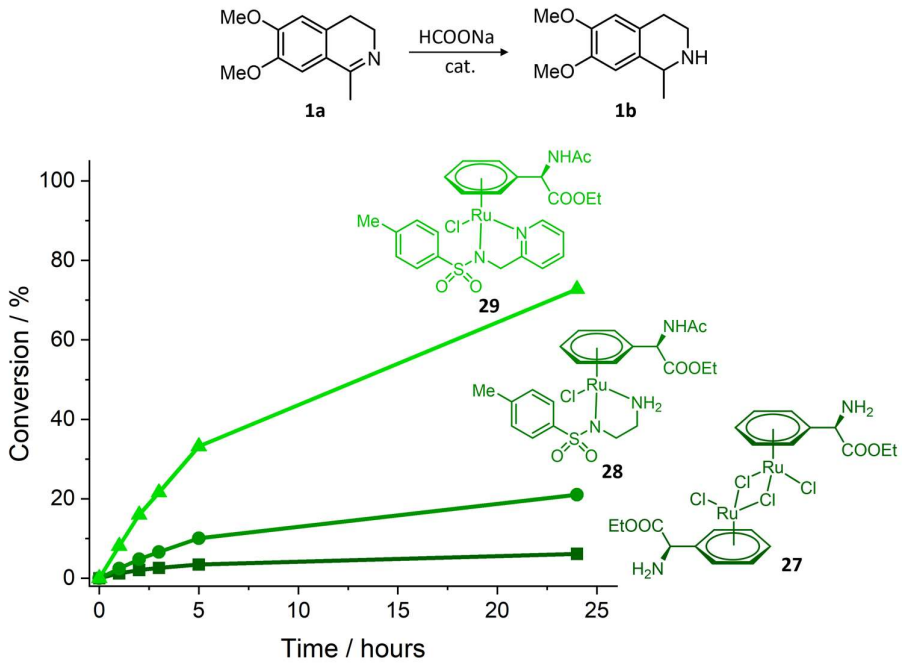


Figure 36 (top) The catalytic reaction scheme for the transfer hydrogenation of dehydrosalsolidine, **1a**, and (bottom) the catalytic activity of the Ru complexes plotted as conversion of the substrate to product against time.

The intermediate Ru dimer, **27**, showed very low catalytic ability, with a conversion after 24 hours of just 7%. The Ru complex with the aminoethylsulfonamide ligand (**28**) showed marginally enhanced activity, however, the Ru complex with the pyridinesulfonamide ligand (**29**) showed much improved activity, with 291 turnovers in 24 hours.

While, as expected, these pre-catalysts are considerably slower than the equivalent Cp*Ir-based complexes, the ($\eta^6$-arene)Ru(pyridinesulfonamide) catalyst shows sufficient activity for the purpose of testing our proposed conjugate.

## 2.3 Attempted Synthesis of the Arene-Linked Conjugate

When considering the various approaches to synthesising the proposed siderophore-catalyst conjugate linked *via* the arene ligand, there are four important steps: 1) forming the link between the azotochelin and arene ligand units, 2) the addition of ruthenium to the arene ligand, 3) removal of the protecting groups of azotochelin necessary for synthesis and 4) the addition of Fe(III) to azotochelin following removal of the protecting groups. In the synthesis of a number of catecholate Fe-siderophore complexes, protecting groups are required for synthesis prior to the addition of Fe(III) to prevent undesired side reactions. These protecting groups are generally left intact until immediately prior to addition of Fe(III), in other words, steps 3) and 4) are usually carried out in succession.

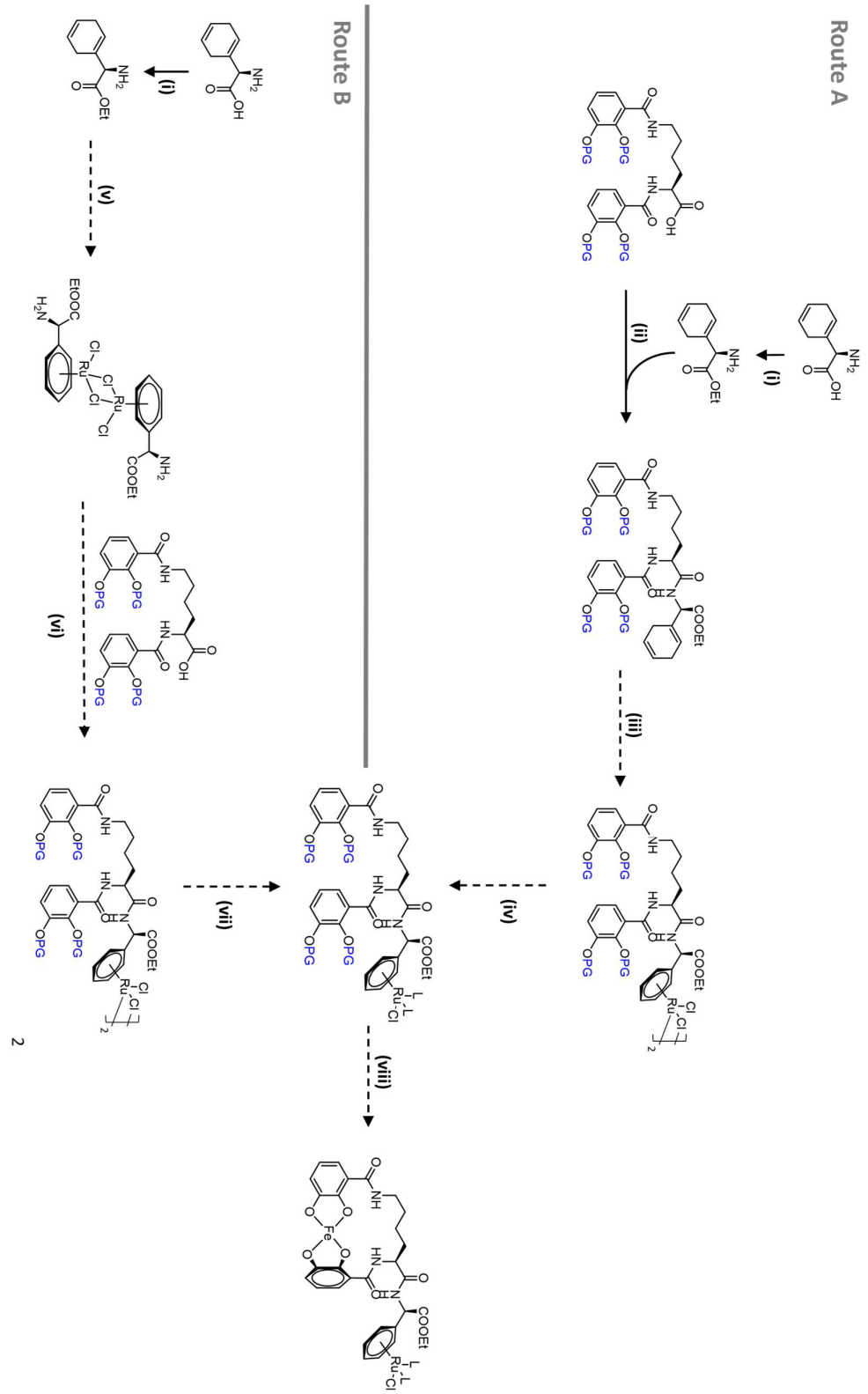


Figure 37 Scheme showing the simplified approaches to two possible synthetic approaches to the arene-linked siderophore-catalyst conjugate investigated in this chapter. Catechol protecting groups (PG) are indicated in blue.

The addition of Ru to $\eta^6$-arene ligand requires reflux or microwave radiation in alcohols. While the reported Fe-catecholate bond is strong,[101,102,104,146] reflux in ethanol could potentially displace Fe(III), therefore, step 2) would be better carried out prior to steps 3) and 4).

This leaves two basic approaches to the synthesis of the conjugate as shown in Figure 37. "Route A" requires the steps in the order 1), 2), 3) then 4), while "Route B" reverses the order of steps 1) and 2). An advantage of Route B over Route A is that it avoids an additional step involving the 2,5-dihydroxyphenyl group that is prone to aromatisation. Route B, however, is more challenging in the step of connecting azotochelin to the amine of the arene ligand since amide coupling conditions require bases, which are known to trigger decomposition of ($\eta^6$-phenylglycine) and ($\eta^6$-phenylalanine)-Ru complexes.[143]

What is obvious from both routes is that a catechol protecting group must be selected that is stable to the conditions in the early synthesis steps but is removed in conditions in which the Ru complex is unaffected. Benzyl protecting groups were used in the reported synthesis of the bidentate ligand-linked conjugate and these groups are removed by hydrogenation.[100] $\eta^6$-Arene Ru complexes have been reported to catalyse hydrogenation reactions and, as such, exposing them to hydrogenation conditions could result in a number of potential hydrogenation reactions of the siderophore-ligand backbone.[55] It was therefore decided that a different catechol protecting group should be employed.

### 2.3.1 Synthesis of *para*-Methoxybenzyl-Protected Azotochelin

Initially, acetyl protecting groups were selected as catechol protecting groups for the synthesis as they can be removed easily and selectively under mild conditions.[147] The synthesis of Ac-protected azotochelin ($Ac_4$-azotochelin, **36**) has been reported in the literature, providing confidence in exploring this route (Figure 38).[148] In contrast to the synthesis of Bn-protected azotochelin, the synthesis starts from 2,3-dihydroxybenzoic acid (**33**) in place of the aldehyde analogue. This is due to the reaction with acetic anhydride selectively protecting the catechol groups in the presence of a carboxylic acid group whereas benzyl chloride does not have the same selectively hence the carboxylic acid is revealed in a subsequent oxidation step. Not only does starting from 2,3-dihydroxybenzoic acid offer an advantage in reducing the number of synthesis steps, it is also cheaper.

In the first step of the synthesis, 2,3-dihydroxybenzoic acid (**33**) is reacted with acetic anhydride with a few drops of concentrated sulfuric acid as previously reported (Figure 38 (a)).[149] Activation of the carboxylic acid group by conversion to an acid chloride was achieved by refluxing a solution of **34** and thionyl chloride in diethyl ether/benzene.[150] This intermediate was recovered by evaporation of the solvents under reduced pressure before immediate reaction with L-lysine or L-lysine derivatives (as shown in Figure 38 (b)).

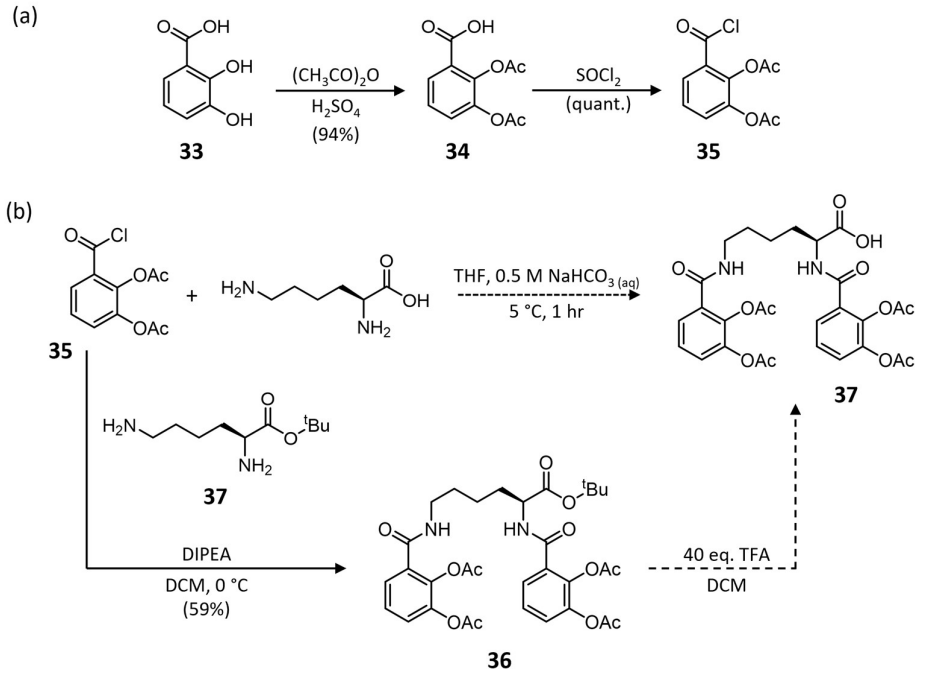


Figure 38 Reaction schemes for (a) synthesis of 2-(acetyloxy)-3-(carbonochloridoyl)phenyl acetate, **35**, and (b) $Ac_4$-azotochelin, **36.**

The final step in the literature procedure to produce $Ac_4$-azotochelin[148] is carried out by dissolving the acid chloride **35** in THF and combining with a solution of L-lysine in 0.5 M aqueous sodium hydrogen carbonate. The aqueous solution is necessary for dissolving L-lysine. Repeating these conditions returned only a very low conversion to product, with a significant quantity of **34** recovered. It was proposed that the water in the solution was responsible for reacting with the activated acid chloride, **35**, to return the less electrophilic carboxylic acid, preventing the reaction. Separation of the desired product (**36**) by recrystallisation or column chromatography was unsuccessful since the acetyl groups prove unstable on silica, C18 and alumina phases, with 2D TLC showing degradation. The amount of product could be somewhat enhanced during the aqueous work-up by controlling the pH of the aqueous layer, with compound **34** more soluble in the organic layer at pH 4 and product **36** then more effectively extracted at pH 2. While an improvement in the purity was seen, it could only ever be improved to around 60%.

An alternative method was devised to avoid the use of water as a solvent, thereby preventing the side reaction which recovers **34**. For this, a protecting group was added to the carboxylic acid of lysine to improve solubility in organic solvents (Figure 38 (b), **37**). A *tert*-butyl protecting group was selected because it allows good solubility in organic solvents and is removed in acidic conditions, to which acetyl groups are not susceptible. The commercially available compound 2-hydroxypropan-2-yl(2S)-2-amino-6-

{[(benzyloxy)carbonyl]amino}hexanoate was purchased and the benzyl ester removed with almost quantitative conversion (to produce **37**). The anhydrous conditions for the amide coupling step significantly helped to reduce the amount of unreacted starting material recovered. **38** was successfully produced with good purity as determined by $^{1}$H NMR (Figure 39). Analytical HPLC, as a more sensitive technique, did detect small amounts of starting material and side products, but purity was deemed to be acceptable for this stage of the synthesis. Fortunately, hydrolysis of the acetyl protecting groups was not observed under the conditions employed for HPLC. This suggests preparatory HPLC could be a suitable tool in the purification of these compounds, however, at the time of this work a preparatory HPLC was unfortunately not available in the department.

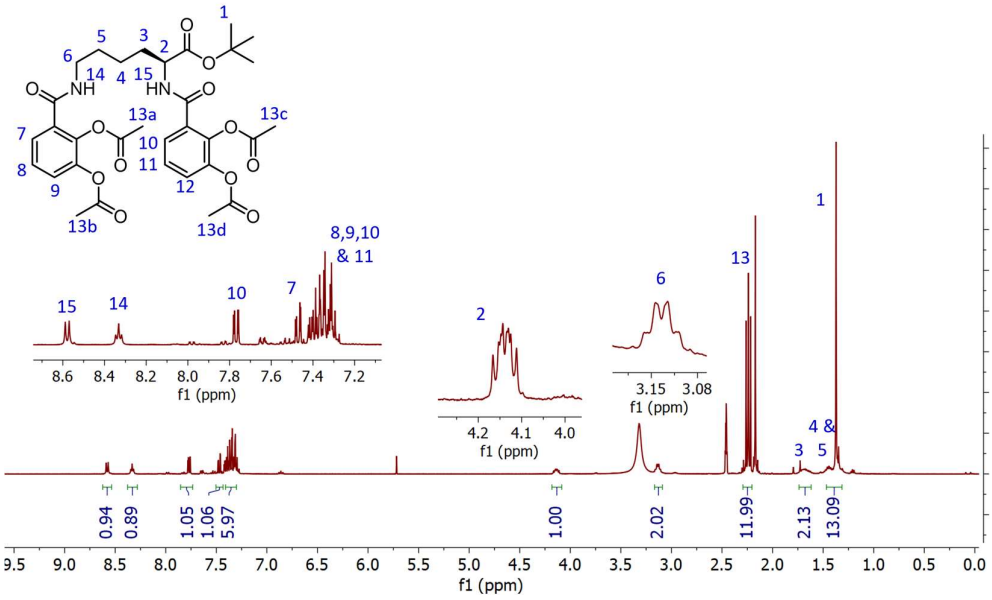


Figure 39 Assigned $^{1}$H NMR spectrum of compound **38.**

Following the successful synthesis of **38**, the next step was removal of the *tert*-butyl group protecting the carboxylic acid to produce **36**.[151] This was attempted with excess trifluoroacetic acid at room temperature. However, these conditions were too harsh and resulted in partial removal of the acetyl groups as observed by mass spectrometry.

While considering the next steps in the synthesis of the arene-linked conjugate, it was noted that activation of the carboxylic acid of the protected azotochelin was necessary for the amide coupling step used to link azotochelin and the amine substituent of the arene ligand. A report of synthesising an acid chloride in a single-pot reaction directly from *tert*-butyl protected carboxylic acids provided an interesting alternative to trying to recover **36**.[152–154] Compound **38** was dissolved in thionyl chloride and the solution heated to reflux (Figure 40). The reaction progress was monitored by mass spectrometry which revealed that after 30 minutes all the

starting material had been consumed. Analysis of the resulting mixture showed a large number of by-products. Further work was attempted to optimise conditions for this transformation, however, it was decided that exploring alternative catechol protecting groups might also be beneficial.

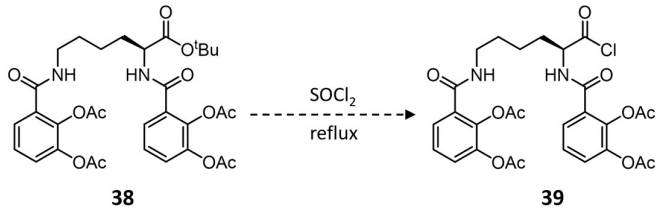


Figure 40 Scheme for the reaction to convert the tert-butyl protected carboxylic acid to an acid chloride in a single-step reaction.

*para*-Methoxybenzyl (PMB) was also identified as a suitable catecholate protecting group for azotochelin as previously reported (Figure 41).[155] The synthesis route starts from 2,3-dihydroxybenzoic acid, **33**. The addition of *para*-methoxybenzyl chloride under basic conditions results in the addition of PMB at the catechol sites and the carboxylic acid (**40**), however, the PMB at the carboxylic acid can be selectively removed in a 0.7 M solution of NaOH in water/dioxane (**41**). The following step requires widely-used amide coupling reagents to activate the carboxylic acid of the 2,3-bis[(4-methoxyphenyl)methoxy]benzoic acid, followed by addition of L-lysine methyl ester to produce Me-$PMB_4$-azotochelin (**42**). The tolerance of PMB protecting groups to bases allows the selective removal of the methyl ester to reveal the desired $PMB_4$-azotochelin (**43**). PMB protecting groups were more tolerant to purification methods, and most intermediates were purified using column chromatography.

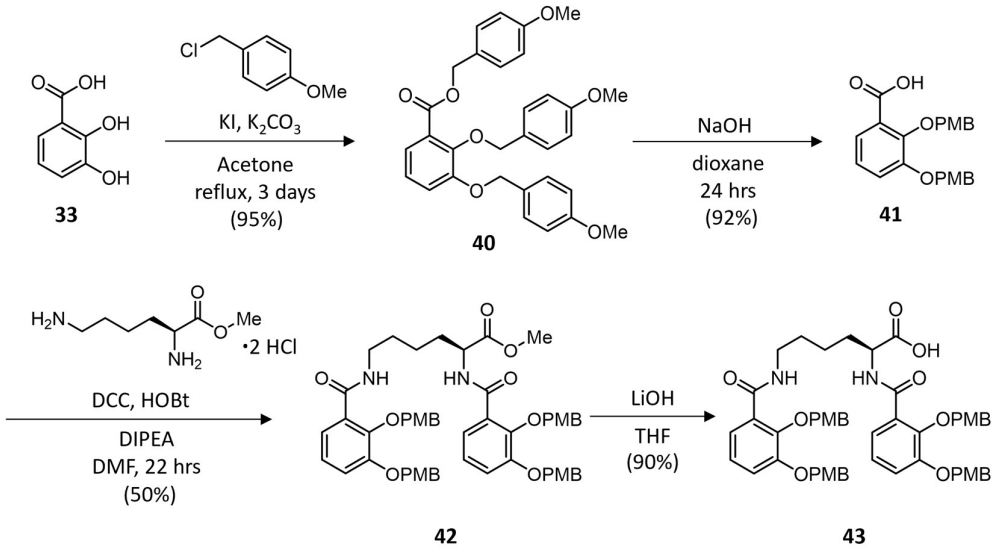


Figure 41 Synthesis scheme for $PMB_4$-azotochelin (**43**).

Synthesis of each of the compounds was confirmed by mass spectrometry, NMR spectroscopy and elemental analysis. $^1$H NMR spectra for each of the compounds **40**-**43** are shown in Figure 42. For the synthesis of **41** (Figure 42 (b)), the following changes in the $^1$H NMR demonstrate successful synthesis: A) the loss of one of the signals for the $CH_2$ of a PMB group, together with a peak lost in the region for the O-$CH_3$ protons of a PMB group. There is also the appropriate decrease in the integration values for the peaks in the aromatic region which matches the loss of 4 aromatic (marked Ar in Figure 42) C-H protons.

The $^1$H NMR of intermediate **42** (Figure 42 (c)) shows many more peaks in the range 1.0-5.0 ppm corresponding to protons of the lysine backbone. Of particular note are the two peaks that arise for the proton environment labelled 19 between 1.4-1.8 ppm in the spectrum, indicating the diastereotopic nature of the protons in this position, where the protons occupy an identical chemical environment but experience different magnetic interactions depending on their local position. The relative integration areas of each of the peaks confirm a ratio of two catechol groups to one lysine.

Successful synthesis of $PMB_4$-azotochelin (**43**, Figure 42 (d)) was then confirmed by the disappearance of the peak at 3.74 ppm (marked (B)) corresponding to the 3 protons of the methyl ester.

In order to confirm that PMB groups were suitable for use in either of the planned synthesis routes to the arene-linked conjugate, conditions to remove the PMB groups must be found in which the ruthenium complex remains intact. PMB groups can be removed by TFA so a simple ruthenium complex of the type ($\eta^6$-arene)Ru(ethylenediamine)Cl was prepared then exposed to a vast excess (over 100 equivalents) of TFA in a solution of methanol for one hour at room temperature. Thioanisole was added as it has been reported to promote cleavage of the PMB groups and suppress a potential side reaction from alkylation of aromatic rings by the PMB groups once they have been removed. The solvents were then evaporated and the $^1$H NMR spectra (in methanol-$d_4$) before and after the deprotection conditions were compared (Figure 43). Gratifyingly, no significant changes in the peaks related to the complex are observed following exposure to TFA/thioanisole, only some additional peaks related to thioanisole were now present.

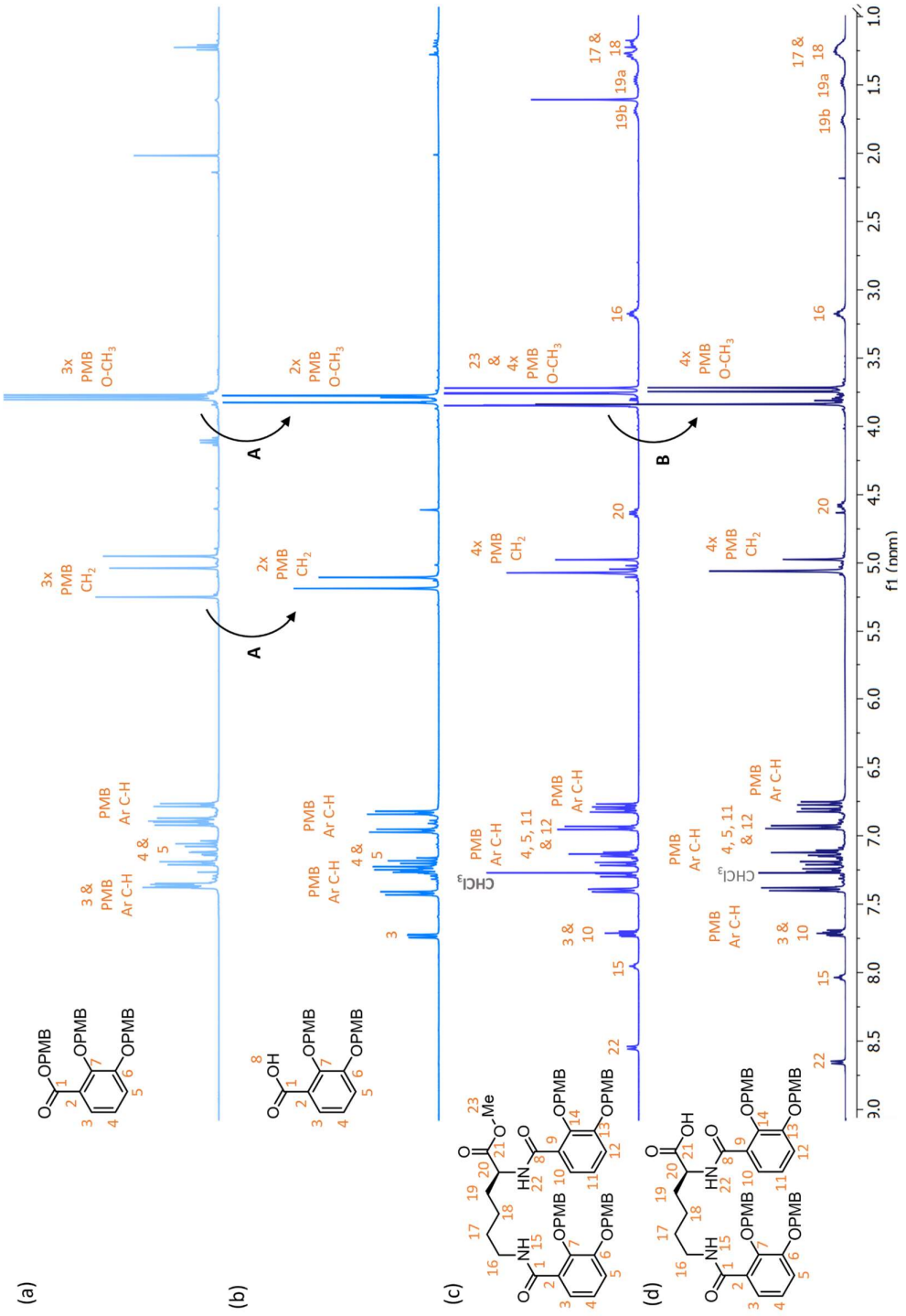


Figure 42 Assigned $^{1}$H NMR spectra of (a) compound **40**, (b) compound **41**, (c) compound **42**, and (d) $PMB_4$-azotochelin, **43**. The changes marked A indicate loss of signals corresponding to a third PMB group. The change marked B indicates loss of a peak for the methyl group.

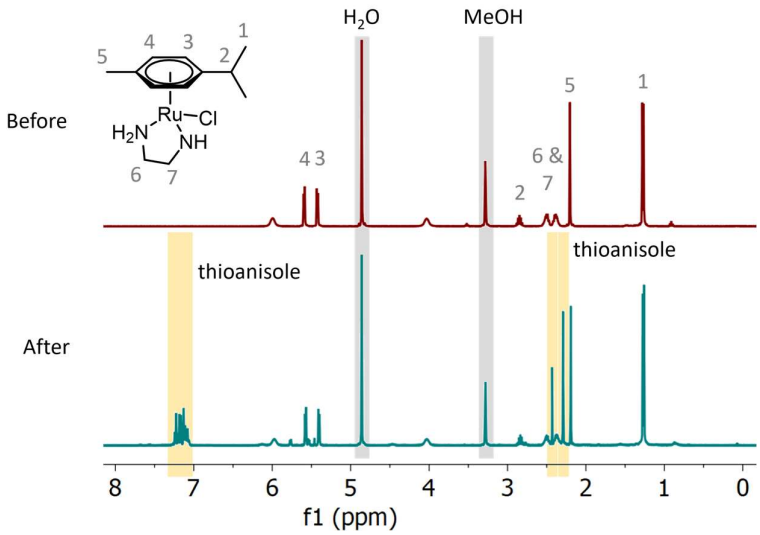


Figure 43 Assigned $^{1}$H NMR spectra for the (*p*-cymene)Ru(ethylenediamine)Cl before and after exposure to TFA/thioanisole. The peaks in the regions shaded grey relate to non-deuterated impurities in the NMR solvent used (methanol). The peaks in the region shaded yellow relate to thioanisole which was not removed following the reaction.

## Investigation of Synthesis Route A

Amide coupling of the 2,5-dihydroxyphenyl glycine derivative to $PMB_4$-azotochelin was accomplished using 1-[Bis(dimethylamino)methylene]-1H-1,2,3-triazolo[4,5-b]pyridinium 3-oxid hexafluorophosphate (HATU) as a coupling agent (Figure 44).

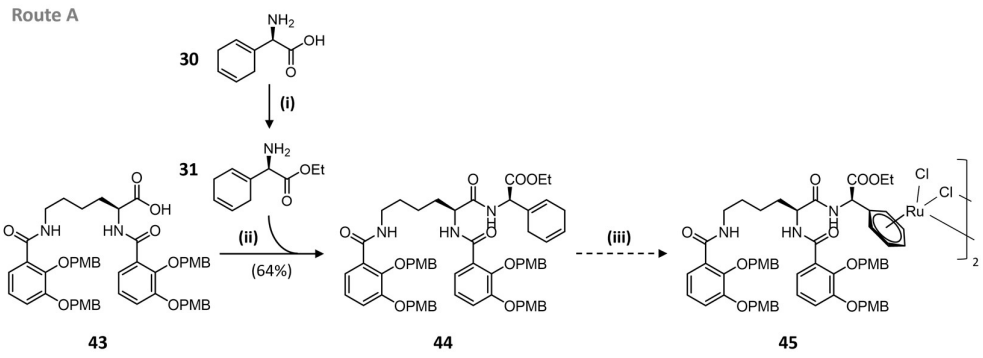


Figure 44 Simplified reaction scheme for the proposed synthesis of **45** by "Route A".

Synthesis of **44** was confirmed by mass spectrometry, NMR spectroscopy and elemental analysis. The $^{1}$H NMR of the product (Figure 45 (c)) shows an array of peaks that largely correspond to the spectra of the two starting compounds **31** and **43** (Figure 45(a) and (b)). The most distinctive changes in the spectra are the downfield shift of the proton labelled 24, from 3.96 ppm to around 5.0 ppm, as the environment changes from a neighbouring amine group to an amide group. This is accompanied by a small upfield shift of the proton labelled 20 from a

triplet doublet at 4.51 ppm to a multiplet at 4.54–4.41 ppm, again in line with changing from a neighbouring carboxylic acid group to an amide group.

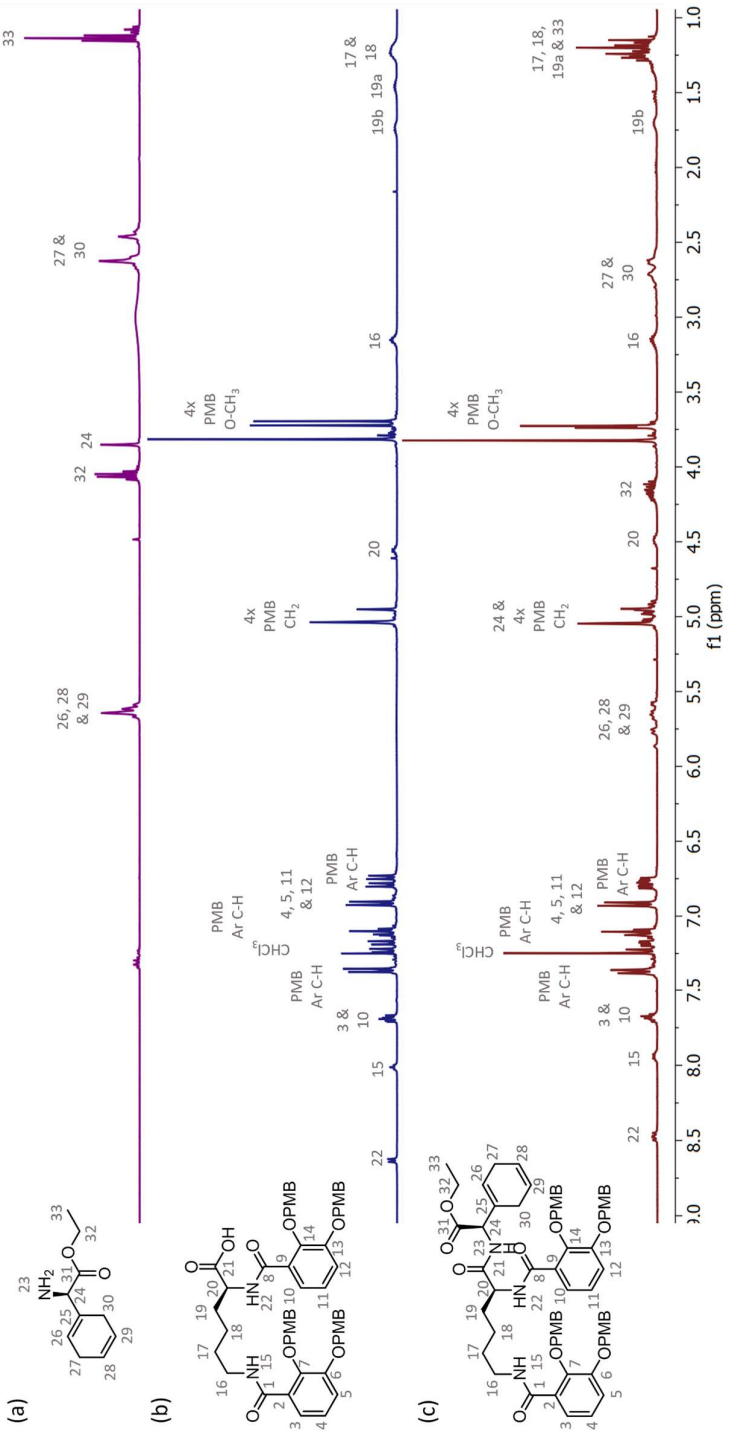


Figure 45 Assigned $^{1}$H NMR spectra of (a) compound **31**, (b) compound **43** and (c) compound **44** demonstrating the successful synthesis of compound **44** by the expected peaks as assigned from spectra of the two starting materials, **31** and **43.**

The following step to produce compound **45**, however, proved extremely challenging. Initially, microwave radiation of a solution of $RuCl_3 \cdot xH_2O$ and **44** (2:3 ratio) in ethanol, similar to conditions used in the synthesis of the [($\eta^6$-protected phenylglycine)$RuCl_2$]$_2$ dimer **27** were applied. A longer reaction time of 25 minutes compared to 20 minutes was used as it was expected the significant increase in size of the amine attachment would hamper the reaction. Instead of the expected colour change from a very dark, opaque solution to a bright red/orange solution as occurs for **27**, the solution after radiation was almost colourless, with a very slight orange tint, and a black precipitate had formed. The solution was filtered to remove the black precipitate and the solvent removed under vacuum. Neither mass spectrometry nor $^1$H NMR could provide evidence for the successful synthesis of **45**.

It was expected that the increased sterically bulky group neighbouring the 2,5-dihydroxyphenyl ring of the precursor of the arene ligand could be hindering the reaction. It was already known that the [($\eta^6$-protected phenylglycine)$RuCl_2$]$_2$ dimer **27** where the amine has an acetyl attachment was successfully synthesised using the microwave radiation method (150 °C/150 W/250 psi) for 20 minutes. An alternative ligand with a Boc attachment to the amine was prepared (Figure 46), and the ruthenium coupling reaction attempted in order to determine if increasing the steric bulk of the amine attachment did affect the reaction. It was found that a reaction time of 30 minutes was required in order to obtain a moderate yield of the ruthenium dimeric compound **47**. A small amount of a black precipitate was observed after radiation in this reaction, which had not been observed for the synthesis of the equivalent dimer with the acetylamide protecting group.

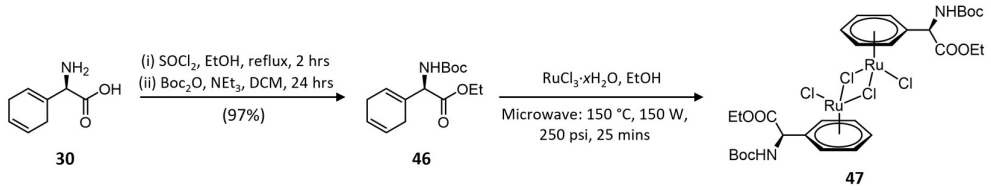


Figure 46 Reaction scheme for the preparation of a [($\eta^6$-phenylglycine)$RuCl_2$]$_2$ dimer with an ethyl ester/Boc-amide substituted attachment.

This result suggested that the hypothesis that the steric bulk of the azotochelin group may hinder the reaction was correct. Next the synthesis of **45** was attempted with an increased reaction time of 30 minutes, followed by another 20 minutes. After 30 minutes of radiation, a slightly stronger orange colour appeared than for the previous attempt, but still a large quantity of black precipitate formed. Radiation for a further 20 minutes caused no visible change in the reaction mixture. Once again the black precipitate was removed and the filtrate reduced to dryness. No useful conclusions could be made from mass spectrometry or NMR.

A further attempt, using reflux in place of microwave radiation, again resulted in the formation of black precipitate and no indication of **45**. The $^{1}$H NMR spectrum following the reaction, however, indicated PMB groups were being hydrolysed from **44**. On testing the pH of the solution, it was found to be acidic which explained the $^{1}$H NMR result as PMB groups can be removed in acidic conditions.

Analysis of the black precipitate was hindered by the fact it was very insoluble in most solvents. From simple benchtop tests using solutions of $RuCl_3 \cdot xH_2O$ in ethanol at a range of pH values, a black precipitate was formed in basic conditions. This precipitate was similarly insoluble in most solvents. This suggests that the black precipitate is ruthenium hydroxide which is readily formed from $RuCl_3 \cdot xH_2O$ in basic conditions and is also reported to have very poor solubility in most solvents.[156] The infra-red spectrum of the precipitate (Figure 47) likewise shows a broad absorption in the region 2900-3700 $cm^{-1}$.[156] The formation of ruthenium hydroxide removes Ru(III) from solution, hence explaining the poor reactivity in the reactions to synthesise **45**. The cause of this transformation is unknown, since it does not occur spontaneously but only on irradiation/heating of the $RuCl_3 \cdot xH_2O$ and **44** mixture. It is further puzzling that the pH of the solution after irradiation appears to be acidic, despite basic conditions being favourable to ruthenium hydroxide formation.

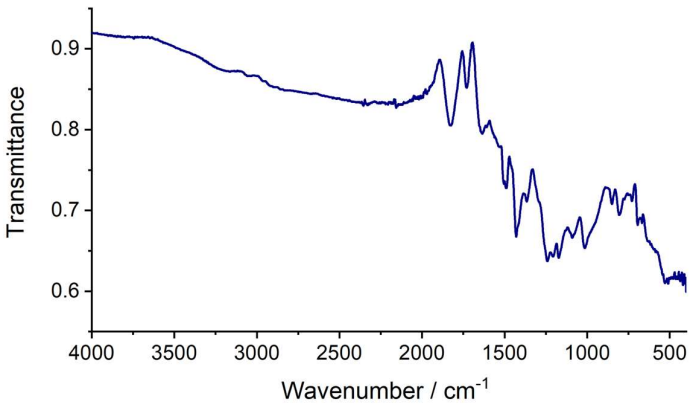


Figure 47 Infra-red spectrum of the black precipitate formed during microwave radiation of a solution of **44** and $RuCl_3 \cdot xH_2O$ in ethanol.

To combat the formation of ruthenium hydroxide in the reaction, the solution of $RuCl_3 \cdot xH_2O$ and ligand precursor was acidified prior to irradiation. An alternative to **44** was used, with benzyl protecting groups in place of the PMB group to avoid complications of protecting group removal in the acidic conditions. The solution was acidified to pH 4 before microwave irradiation for 30 minutes. Unfortunately, this produced no change from the previous reactions, with a large amount of black precipitate still forming. A pH of approximately 6 was measured in the solution after irradiation.

Overall, it was concluded that the bulky nature of the arene ligand precursor **44** might be a contributing factor to the poor reactivity in addition to other chemical changes that seem to take place upon irradiation. It was decided not to proceed with further investigation of this synthetic route due to the complications occurring in this reaction.

## 2.3.2 Investigation of Synthesis Route B

The first new step in the synthesis of the conjugate *via* route B is formation of the [($\eta^6$-arene)$RuCl_2$]$_2$ dimer **48** (Figure 48 (a)). Similar to the [($\eta^6$-protected phenylglycine)$RuCl_2$]$_2$ dimer **27**, upon microwave irradiation of $RuCl_3 \cdot xH_2O$ and **31** (1:6 ratio) a deep orange/red solution was recovered. Compound **48** could not be isolated from solution, however, by the addition of *n*-pentane or hexanes that had recovered **27**. The large excess of **31** used in the reaction meant that it is crucial to be able to precipitate the ruthenium compound from solution to prevent contamination with **31** which could react in further steps considerably complicating purification of the next compounds in the synthesis route.

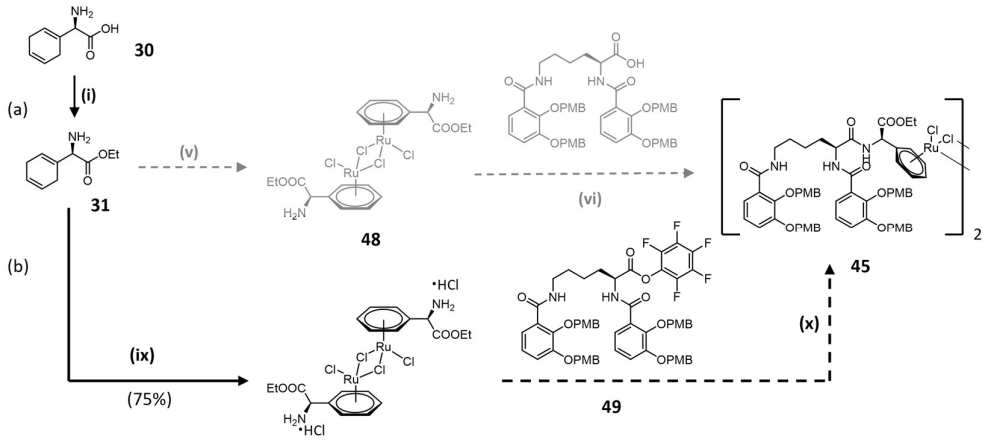


Figure 48 (a) Reaction scheme for coupling **48** to protected azotochelin. This approach proved unsuccessful following difficulty isolating complex **40x**. Instead (b) represent a possible alternative route from **48**·2HCl which is easily isolated.

A reported synthesis of the HCl salt of the complex **48** from (*R*)-(-)-2-(2,5-dihydrophenyl)glycine, **30**, and $RuCl_3 \cdot xH_2O$ in a single pot provided one option to recover the complex in acceptable purity.[157] Firstly, a solution of (*R*)-(-)-2-(2,5-dihydrophenyl)glycine, **30**, in ethyl acetate/aqueous HCl solution is stirred in solution for one hour before addition of $RuCl_3 \cdot xH_2O$ in ethanol and the mixture refluxed in an inert atmosphere for 16 hours (Figure 48 (b)). The product is formed as an orange precipitate. Successful synthesis was confirmed by mass spectrometry and NMR, with the assigned $^1$H NMR spectrum shown in Figure 49.

One drawback of the HCl salt of compound **48** is that it has very poor solubility in a number of solvents; of all solvents tested, DMF had the highest level of solvation. An initial amide coupling reaction to produce **45** was attempted using HATU as a coupling agent and DIPEA

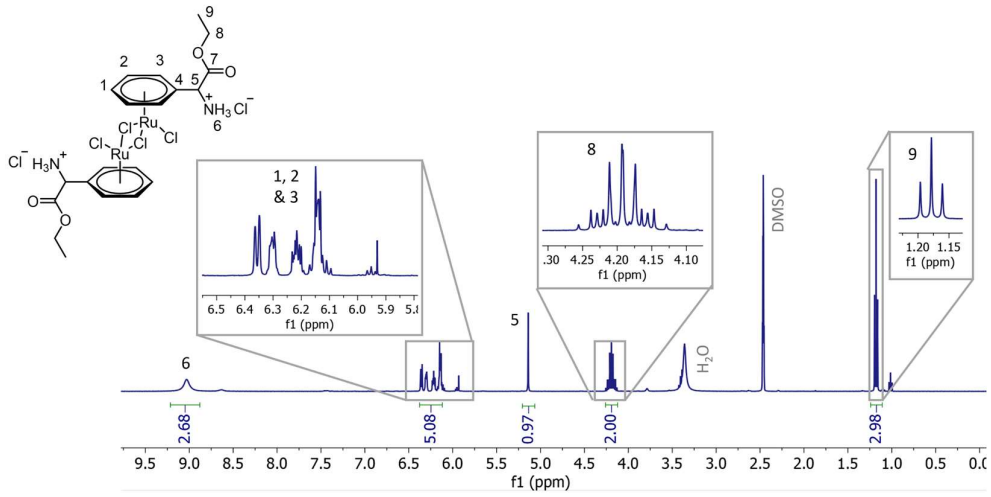


Figure 49 Assigned $^{1}$H NMR spectrum of the **48**·2HCl complex.

as a base in DMF. Upon addition of DIPEA, the reaction solution underwent an immediate colour change from pale yellow/orange to dark red. The solvent was removed by evaporation under vacuum and the remaining solid analysed. Mass spectrometry did not reveal any peaks corresponding to the expected product and the $^{1}$H NMR showed the aromatic C-H peaks corresponding to $\eta^{6}$-arene-Ru were missing. It was proposed that basic conditions were leading to the amine group coordinating ruthenium and degradation of the complex as previously reported for similar ($\eta^{6}$-phenylalanine)Ru-type complexes.[143]

A number of common laboratory bases were tested to see if degradation of the Ru complex could be avoided. Of all, *N*-methylmorpholine resulted in the slowest discolouration of the solution. Other factors such as reducing the temperature, decreasing the amount of base used and increasing the dilution of the reaction also reduced the rate of degradation.

Instead of using an *in situ* activating agent such as HATU, PMB$_4$-azotochelin was preactivated to place a pentafluorophenyl group at the carboxylic acid (Figure 50). This was advantageous as it simplified the amide coupling reaction conditions where previously activation of the carboxylic acid component and electrophilic attack by the amine all occurred in a single pot, exposing the ruthenium complex to additional reactive reagents. The pentafluorophenyl (PFP) PMB$_4$-azotochelin adduct (**49**) was prepared by dissolving dicyclohexylcarbodiimide (DCC, 1 eq.) and pentafluorophenol (3 eq.) in ethyl acetate and left stirring for 30 minutes.[158,159] The solution was then cooled to 0 °C before PMB$_4$-azotochelin (1 eq.) was added, followed by *N*-methylmorpholine (3 eq.). The solution was stirred for 7 hours at room temperature. 1,3-Dichyclohexyl urea (DCU) formed as a precipitate and was removed by filtration before the solvent was removed in vacuo to yield the PFP-PMB$_4$-azotochelin compound (**49**) as a white powder.

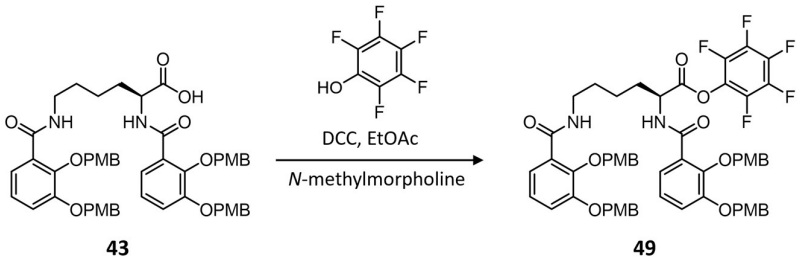


**43** **49**

Figure 50 Reaction scheme for the activation of $PMB_4$-azotochelin (**43**) with pentafluorophenol.

A number of different reaction conditions were tested for the reaction of the **48**·2HCl salt with PFP-$PMB_4$-azotochelin (**49**), including varying the temperature, base, equivalents of base added and dilution of solution, but none produced any evidence of a successful reaction. Different solvents in which the **48** HCl salt were only very sparingly soluble were also trialled with the hope that reducing the amount of Ru complex in solution could help the reaction progress before degradation of the complex, but this also proved unsuccessful.

Following a report that ($\eta^6$-phenylalanine)Ru-complexes were more tolerant to basic conditions following coordination of an ethylenediamine ligand,[143] the methylenepyridinesulfonamide ligand used in the synthesis of complex **28** was reacted with the **48**·2HCl compound (Figure 51).

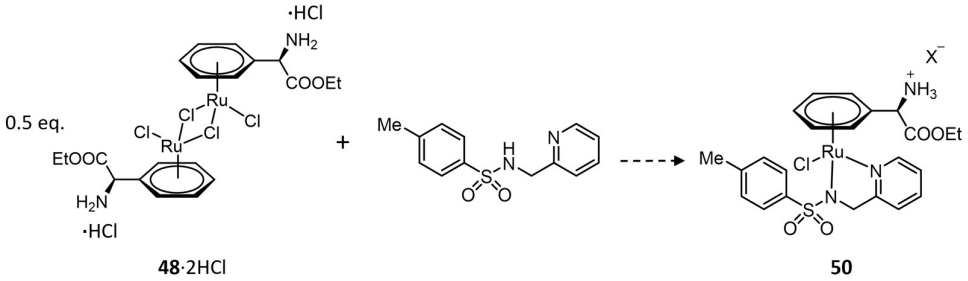


**48**·2HCl **50**

Figure 51 Reaction scheme for coordination of a methylenepyridinesulfonamide ligand to ($\eta^6$-phenylglycine)Ru complex **48**·2HCl.

Different reaction conditions were explored for the reaction reported in Figure 51, with successful synthesis of complex **50** reported by mass spectrometry for the conditions shown in the table below (Figure 52). In all these cases, however, the $^1$H NMR spectra showed distinctly broad and poorly resolved peaks indicating impurities and/or decomposition. The range of solvents used for the reaction was limited by the solubility of compound **48**·2HCl. Successful coordination of the pyridinylmethylsulfonamide ligand could be achieved with or without the addition of a base and both by heating or by reacting at room temperature. A hexafluorophosphate counterion in exchange for chloride was used in an attempt to promote precipitation of complex **50** from solution, however, this proved unsuccessful.

(a)

| | Solvent | Base | Heating | Time | counterion |
|---|---|---|---|---|---|
| **1** | EtOH | N-methylmorpholine (3 equivalents) | Reflux | 4 hours | $Cl^-$ |
| **2** | DMF/EtOH | No base | Reflux | 1 hour | $Cl^-$ |
| **3** | DMF | No base | No heating (sonicated) | 15 minutes | $Cl^-$ |

(b)

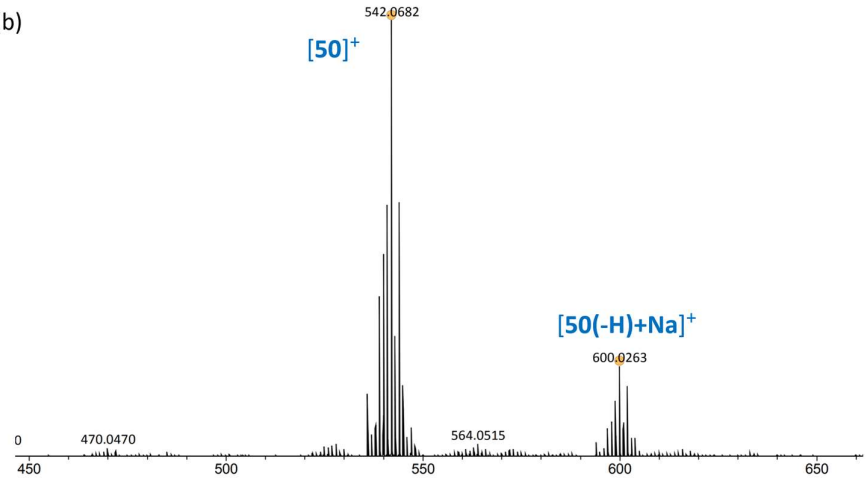


Figure 52 (a) Summary of reaction conditions that led to the successful formation of **50** (as measured by mass spectrometry). (b) The mass spectrum in the range m/z = 500-650 following reaction conditions 2 in the table above.

Unfortunately, further exploration of the synthesis of **50** was prevented by a lack of time.

## 2.4 Summary and Conclusions

A new design for a siderophore-catalyst conjugate for incorporation in a PBP ArM was suggested which connected the catalytic metal complex to azotochelin *via* an $\eta^6$-arene ligand of a Ru complex. Ruthenium complexes that were isoelectronic to Cp*Ir complexes reported in the development of the previously reported PBP ArM were synthesised and tested for their catalytic activity for the transfer hydrogenation of a cyclic imine substrate. Similarly to the Cp*Ir complexes, the best ($\eta^6$-arene)Ru catalyst incorporated a pyridinylmethylsulfonamide ligand. The catalytic activity of this complex, while significantly lower than that of the Cp*Ir analogue, was satisfactory for pursuing the new conjugate for the transfer hydrogenation of imines.

Two possible routes towards synthesising this conjugate were proposed and it was identified that different protecting groups of the catechols of azotochelin would be necessary as the previously used benzyl-groups were not compatible with either synthetic route. The use of

acetyl-groups was explored, but PMB-groups were ultimately chosen due to their better stability during purification.

The synthesis of the conjugate by "Route A" proved too challenging, with the very bulky nature of the azotochelin attachment on the precursory arene ligand being proposed to prevent coordination of ruthenium. A black precipitate that formed in place of the expected reaction was identified as ruthenium trihydroxide but the exact chemical changes that bring about its formation have not yet been identified.

The second synthetic approach, "Route B", provides a more promising approach for the future synthesis of the arene-linked conjugate. The main challenge remains the poor stability of these types of Ru complexes under basic conditions. Amide coupling reactions rely on bases to deprotonate the amine group to improve nucleophilicity, but bases accelerate decomposition of ($\eta^6$-phenylglycine/$\eta^6$-phenylalanine)Ru complexes. Reports that introducing a diamine ligand into the Ru complex improves tolerance of these Ru complexes to bases offers hope that amide coupling between the amine of the $\eta^6$-phenylglycine ligand and azotochelin may be possible. Unfortunately, due to time restraints, isolation of a ($\eta^6$-phenylglycine)Ru(pyridinylmethylsulfonamide) complex **50** in reasonable purity was not achieved, so this route has not yet been fully explored.

One drawback of having to incorporate a pyridinylmethylsulfonamide ligand to stabilise the Ru complex for amide coupling is that it removes the freedom of selecting a wider range of mono- and bi-dentate ligands, which was identified as a key attraction to pursuing the arene-linked siderophore-catalyst conjugate. A range of other desirable ligands may provide a similar stabilising effect, but this is yet to be explored.

# Chapter 3 Optimisation of a Cp*Ir(pyridinylmethylsulfonamide) Catalyst for Imine Reduction

## 3.1 Introduction and Aims

Noyori and co-workers developed piano-stool transition metal complexes with bidentate diamine ligands for transfer hydrogenation.[61,67] These catalysts provide a convenient option for the design of ArMs, as they are able to catalyse reactions in water and are stable when exposed to oxygen, and also tend to perform well at ambient temperature.[52,160]

Different mechanisms have been suggested for transfer hydrogenation using sulfonamide-containing Cp*Ir(*N*,*N*-bidentate ligand)Cl precatalysts, the most widely accepted of them shown in Figure 53. This mechanism was proposed following extensive analysis of experimental results of imine reduction catalysed by Ru($\eta^6$-arene)(TsDPEN) and Cp*Rh(TsDPEN) catalysts and was supported with DFT calculations.[145,161] This replaced the mechanism proposed in early studies which reasoned the mechanism proceeded *via* a 6-membered transition state that had previously been a key point of discussion in the rationalisation of the ketone reduction mechanism,[56,66,70,162–164] where a proton was transferred from a protonated amino group of the ligand with hydride from the catalyst centre in a

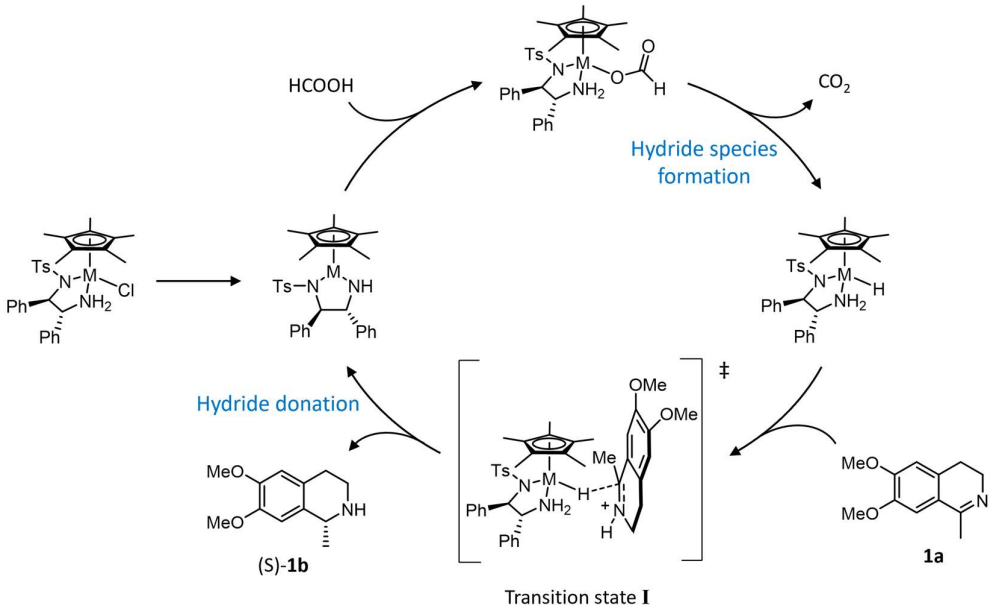


Figure 53 Mechanism for the transfer hydrogenation of imines by Noyori-Ikariya catalysts (M=Rh, Ir).

concerted step.[55,59,66] It has since been recognised that the transfer of the proton and hydride are likely to occur in a sequential rather than concerted manner. The presence of an N-H at one metal-coordinating nitrogen is crucial for transfer hydrogenation of ketones, however, not essential for transfer hydrogenation of imines.[164] A number of catalysts with $sp^2$ hybridised nitrogen metal-coordinating groups have been reported.[100,165] In many examples of imine reduction in water, acidic conditions result in protonation of the imine thus the catalytic mechanism involves only hydride transfer from the catalyst.[160,164,166] Further studies have shown that some activated metal-hydride complexes are incapable of catalysing the reaction of the unprotonated imine and only became active once the imine has been protonated, further supporting this idea of an ionic mechanism.[145]

A number of closely related transition metal piano-stool complexes have been investigated in the preparation of ArMs for the transfer hydrogenation of imines. Several piano-stool catalysts have been examined for different protein scaffolds, with Cp*Ir(aminoethylsulfonamide), **51** (Figure 54), the best suited in reports of streptavidin and ribonuclease S.[47,97] A [Cp*Ir(pyridinylmethylsulfonamide)Cl], **52**, complex was established as preferable to the more commonly used aminoethylsulfonamide ligand equivalent in the development of the PBP-based ArM.[100]

Cp*Ir(aminoethylsulfonamide) Cp*Ir(pyridinylmethylsulfonamide)

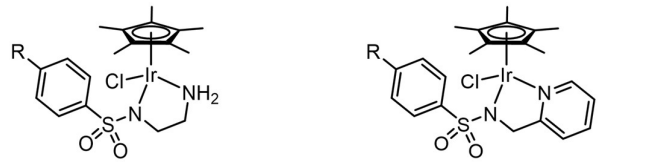


**51** **52**

Figure 54 Chemical structures of commonly-used Cp*Ir(aminoethylsulfonamide) precatalyst (**51**) and increasingly widely employed Cp*Ir(pyridinylmethylsulfonamide) precatalyst (**52**).

For another scaffold, human carbonic anhydrase II (hCAII), attempts to optimise the transition metal catalyst has been more extensive. In work by Monnard *et al.*[40] a series of complexes incorporating bis-pyridine (**53**), bipyridine (**54**), amino-pyridine (**55**) and sulfonamido-pyridine (**56** and **57**) ligands were investigated for imine reduction (Figure 55). Of these designs, complexes **53** and **54** were the least active. Complex **55** showed good activity in the absence of the protein scaffold, but upon incorporation displayed significantly lower activity. Complex **56** retained moderate activity upon incorporation into the protein but was inferior to complex **55** without the protein scaffold. The similar, but more electron poor Ir complex of **57** was less active than complex **56**.

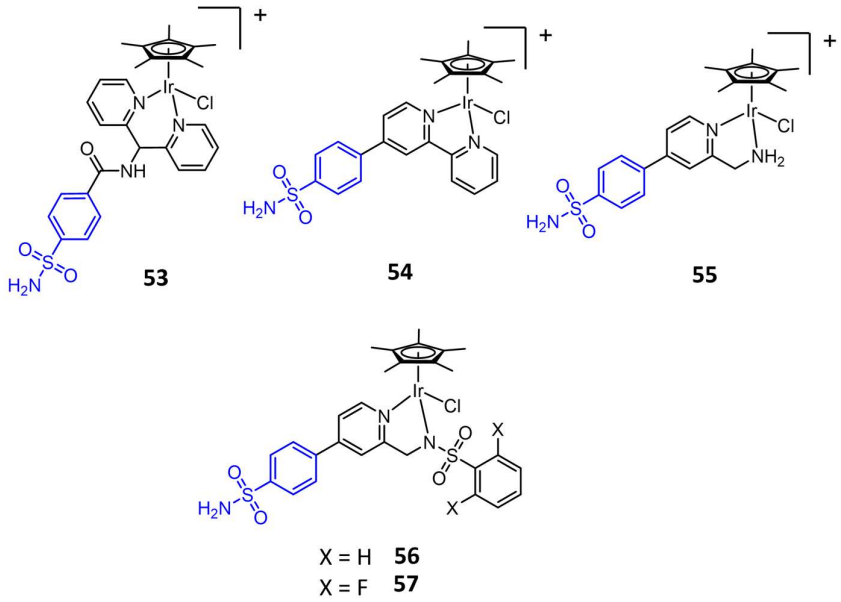


Figure 55 Ir-based precatalysts investigated by Monnard *et al.*[40] in the optimisation of the hCAII-based ArM.

A further investigation, this time targeted at finding the optimal length of the linker between the anchoring unit and the catalytic complex, considered a number of other alternatives (**58** to **62**, Figure 56) based on reports of several pyridinylmethylsulfonamide-based Ir complexes.[100,167–169] These complexes proved significantly superior to the previously used complex **53**. Complex **59** showed overall best performance in the ArM *in vivo* indicating a preference for the electron-donating OH group on the pyridine ring.[32]

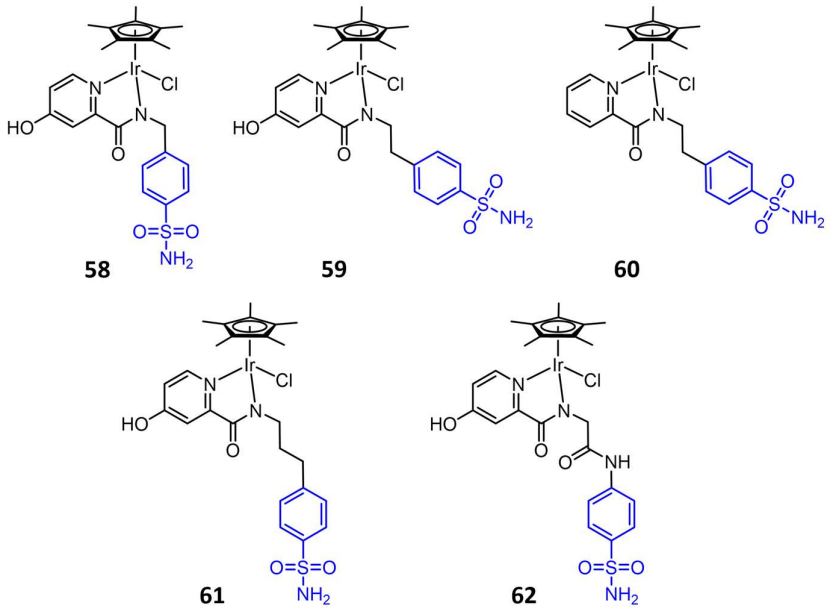


Figure 56 Ir-based precatalysts explored by Rebelein *et al.*[32] in further optimisation of the hCAII ArM.

The design of artificial metalloenzymes provides multiple approaches towards optimisation. Both the catalytic moiety and protein scaffold can be developed in parallel to produce the best results. Optimisation of the catalytic moiety can produce very significant improvements in the ArM.[27,107]

One approach to catalyst improvement is tuning the electronic contribution of the ligands. A number of investigations optimising Cp*Ir(N-heterocyclic bidentate) catalysts for different transfer hydrogenation reactions have been reported. One such report in 2010[160] examined the effect of adding electron-withdrawing substituents at the sulfonyl group of aminoethylsulfonamide ligands (Figure 57). These catalysts were targeted at transfer hydrogenation of ketones in water, using formic acid as the reductant. Reactions were carried out at very low pH, usually around pH 3.5. Results of this study showed adding strongly electron-withdrawing groups at the sulfonyl position improved the selectivity and activity of the catalysts, with precatalysts **64b** and **64c** performing best. This was in contradiction to a previous report with Ru(II)-based catalysts of the same ligand type, which found electron-donating groups to be beneficial in a 2-propanol/KOH supplemented system.[61]

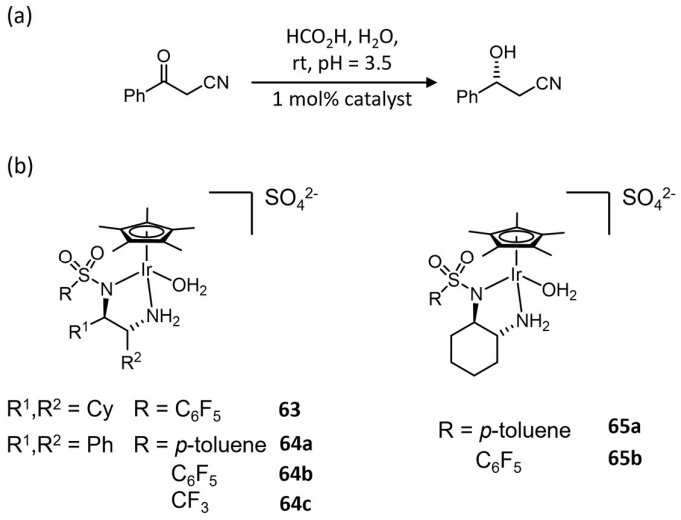


Figure 57 (a) Target ketone reduction reaction for screening catalysts in (b) in an approach to improve catalytic activity by Soltani *et al.*[160]

A 2016 report by Ruff *et al.*[52] investigated a series of Cp*Ir(pyridinylmethylsulfonamide) catalysts with substituents at the sulfonyl (Figure 58). The substituents covered a range of electron-donating and electron-withdrawing groups. The ligand backbone was constructed with an ethylene linker in place of the more common methylene linker. The catalytic reactions were carried out in isopropanol, which also acted as the hydride source. In contrast to Soltani *et al.*,[160] this study found electron-donating substituents at the sulfonyl group (complexes **66**, **68a**, **68b** and **68d**) were advantageous in improving catalyst performance. Complexes **67**, **68c**

and **68e**, bearing electron-withdrawing substituents, were notably poorer catalysts. A strong relationship was observed between the conversion of starting material after a fixed reaction time for each catalyst against the Hammett parameters of the substituents.

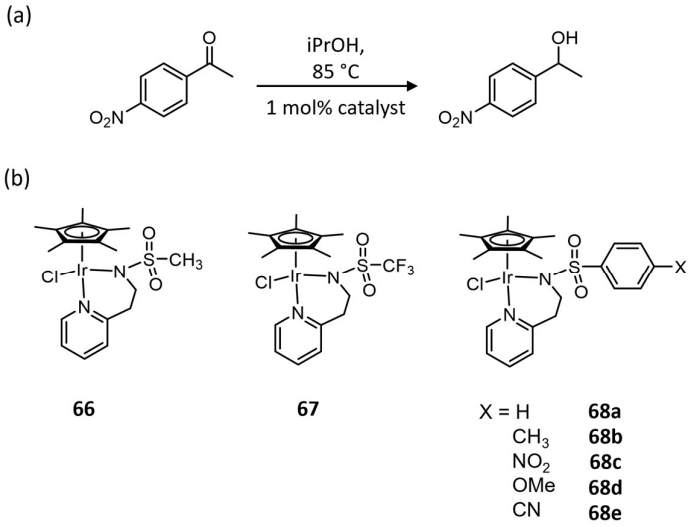


Figure 58 (a) Target ketone reduction reaction for screening Cp*Ir(pyridinylmethylsulfonamide) catalysts in (b) in an approach to improve catalytic activity by Ruff *et al.*[52]

Further investigations cover a number of Cp*Ir-coordinated *N*-heterocycles, in addition to pyridine. These ligands were not sulfonamide-based but revealed additional interesting trends in the development of Ir-based transfer hydrogenation catalysts. A series of *N*-heterocycle-containing complexes were reported in 2016[167] (Figure 59), which use NADH as the hydride source in the reduction of aldehydes in a butanol/water mixture. Of these complexes **69a**, **70** and **71** showed no or very low activity. Significantly better activity is seen for complexes **73a** – **73e**, but no distinctive trend was identified between electron-donating and electron-withdrawing groups in this group of ligands.

A more extensive, but similar series of Cp*Ir complexes were investigated for the dehydrogenation of formic acid in water (Figure 60). Although a different reaction to transfer hydrogenation of unsaturated C=X bonds, formation of a Ir-hydride species is an important step in both mechanisms. Catalytic reactions were carried out at 60 °C in highly acidic conditions which differ significantly from our reactions of interest. Formation of the hydride species varies greatly with pH so while the results of this study may not provide highly relevant results, any trends might still be applicable to the design of an Ir-based catalyst for transfer hydrogenation. The study found five-membered N-heterocycles such as imidazole, imidazoline and pyrazole outperformed 6-membered pyridine. In cases where ligands varied only in additional substituent groups (e.g. series **78a-c** and **79a-b**), it was found that electron-

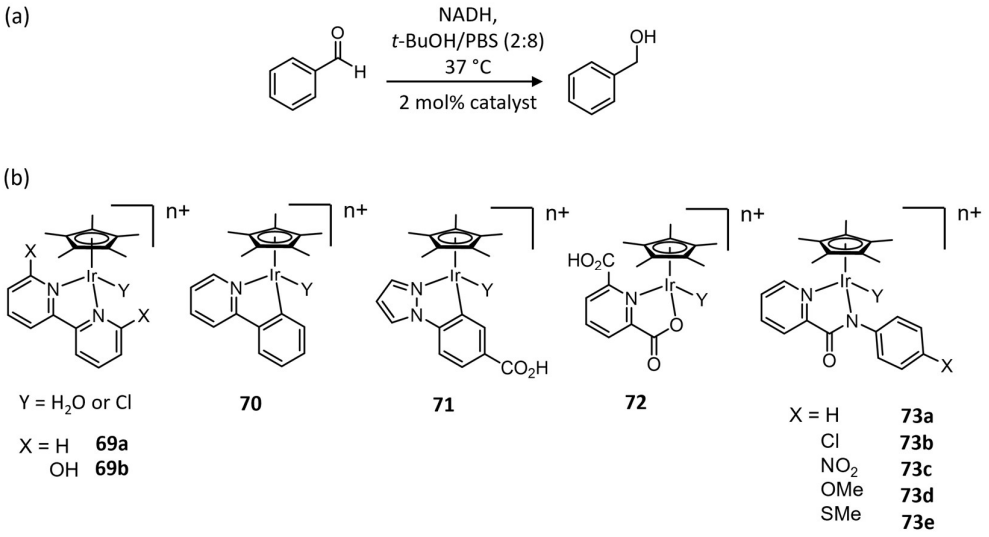


Figure 59 (a) Target aldehyde reduction reaction for screening catalysts in (b) in an approach to improve catalytic activity by Ngo *et al.*[167]

donating groups improved catalytic activity. These substituents also strongly influenced the optimal pH range of the catalyst.[169]

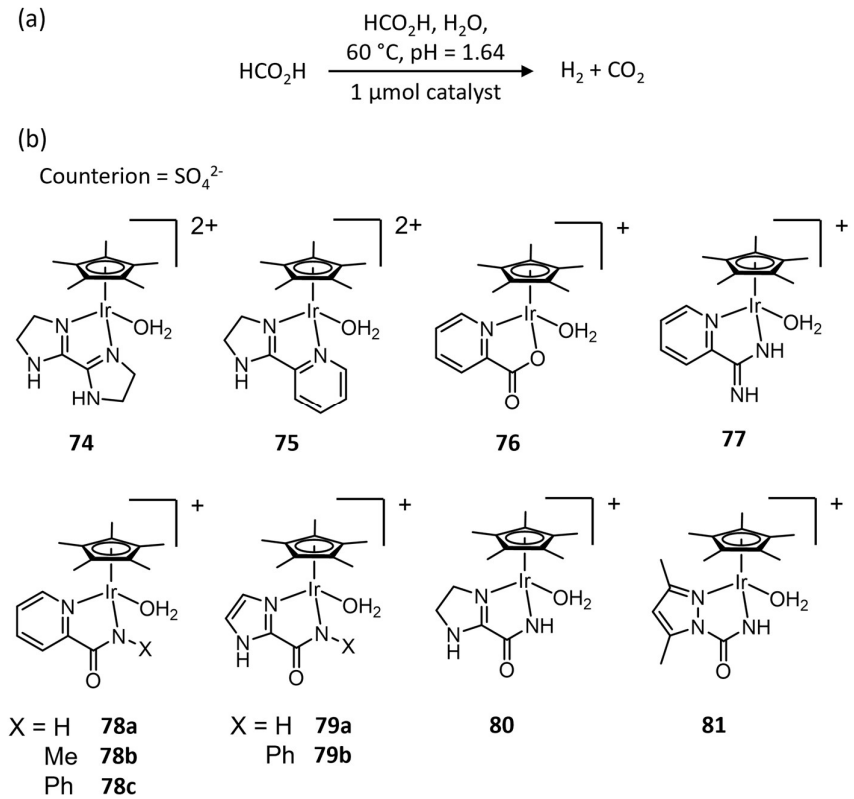


Figure 60 (a) Formic acid reduction reaction used for screening catalysts in (b) in an approach to improve catalytic activity by Kanega *et al.*[169]

Pitman *et al.*[170] carried out a detailed study of modified Cp*Ir(bipyridine) catalysts (Figure 61), to determine how substituent groups on pyridine influenced the "hydricity" of these catalysts. "Hydricity" is formally the free energy required to break a M-H bond and, hence, acts as a measure of the hydride donor ability of a metal complex.[171] The measurement of the free energy of hydride donation varies with both pH and the composition of the solution, but it was found that hydricity values correlate strongly with the Hammett parameters of substituents of the bipyridine rings, with electron-donating groups (as for complexes **85** and **86**) lowering the free energy required to break the Ir-hydride bond and electron-withdrawing groups (**82** and **83**) increasing the free energy required.

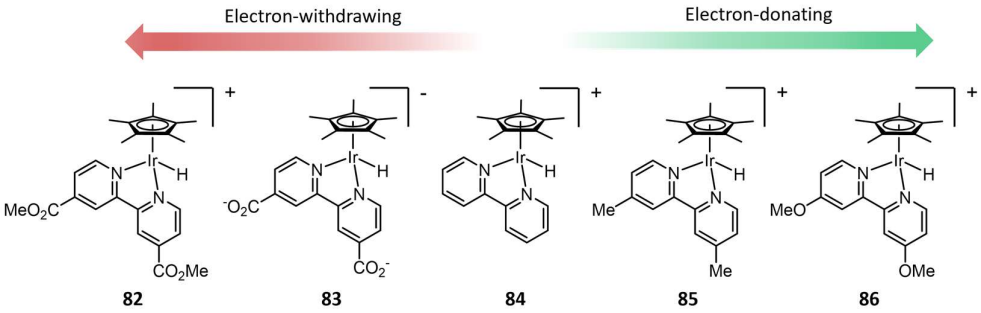


Figure 61 Range of Cp*Ir-based catalysts investigated by Pitman *et al.*[170] in a report quantifying the hydricity values of these complexes.

Of these studies, most reports supported the addition of substituents that increased the electron-density on the metal complex. The study by Soltani *et al.*,[160] however, which is closest to our own catalytic conditions for transfer hydrogenation with the PBP ArM, suggested the reverse trend was true. Pyridinylmethylsulfonamide ligands represent a primary point of interest since they produce highly active transfer hydrogenation catalysts and have already been used in our group's earlier work on the PBP ArM.[100] Limited studies have been applied to optimising aminoethylsulfonamide ligands towards imine reduction and investigations of the nearest reaction type, catalytic ketone reduction, have focussed on modifications at the sulfonyl site.

This leaves room for further investigation of Cp*Ir(pyridinylmethylsulfonamide) catalysts by the addition of substituents on the pyridine ring that will influence the different *N*-donor group coordinated to the metal. This is also the most suitable site for modification in the PBP ArM since the arylsulfonamide unit is involved in linking the catalyst to the anchoring group, hence is unsuitable for modification. The close proximity of the catalyst to parts of the protein scaffold mean that only a small substituent is suitable for incorporation into the ArM design, so substituents were limited to small, simple groups. From studying the crystal structure of the ArM, position 6 (Figure 62) on the pyridine ring was ruled out as a substitution site as it would introduce steric strain since it points towards the Cp* ligand. Site 5- provided the largest

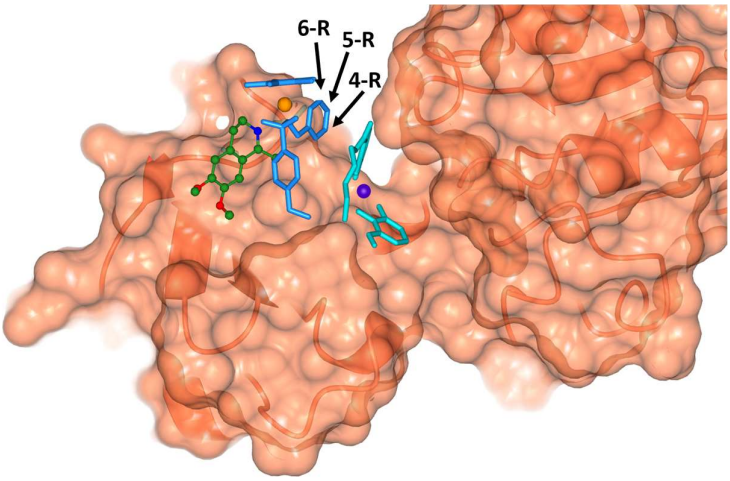


Figure 62 Crystal structure of the PBP ArM (PDB code: 5OD5) demonstrating the potential substitution sites of the pyridine ring.

number of commercially available substituted pyridine ring starting materials, hence was selected as the primary site for modification. The alternative 4-position was also selected for a methyl substituent. The selected ligands for the current investigation are shown in Figure 63.

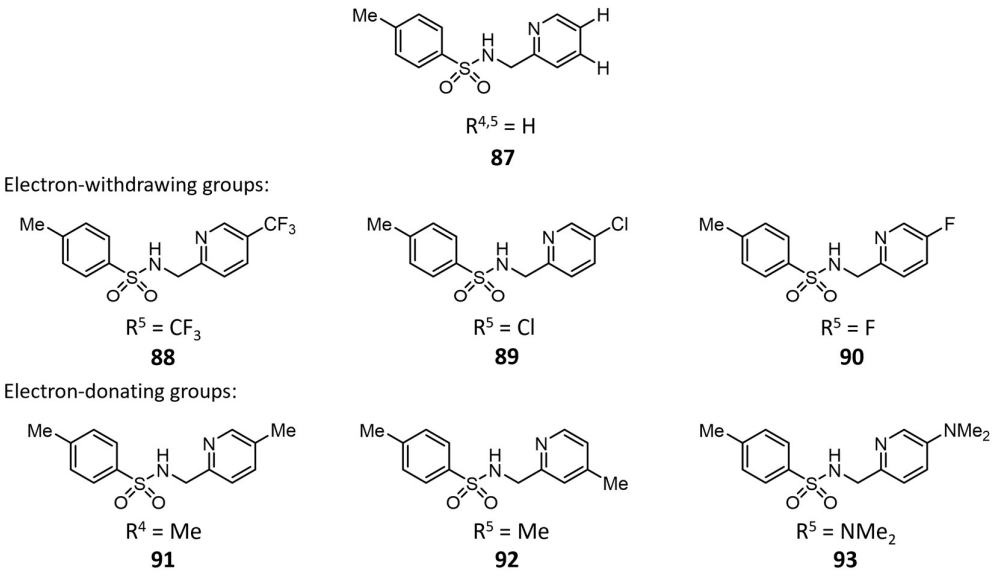


Figure 63 Chemical structures of the *N,N*-bidentate pyridinylmethylsulfonamide ligands investigated in this chapter.

## 3.2 Synthesis and Characterisation of Cp*Ir(pyridinylmethylsulfonamide)Cl Complexes

The sulfonamide ligands in Figure 63 were produced by reacting the corresponding (pyridin-2-yl)methylamine and 4-toluenesulfonyl chloride in the presence of 2 equivalents of an

appropriate base, either triethylamine or *N,N*-diisopropylethylamine (Figure 64).[52,100] A solution of 4-toluenesulfonyl chloride in DCM was added dropwise to a solution of the (pyridin-2-yl)methylamine in DCM at 5 °C to ensure mono-addition of the sulfonyl chloride at the amine only. All ligands were purified by a standard aqueous work-up and either column chromatography or recrystallisation.


Figure 64 General scheme for the one-step synthesis of the pyridinylmethylsulfonamide ligands from 4-toluenesulfonyl chloride and the appropriate (pyridin-2-yl)methylamine, in the presence of a base at 5 °C.

Successful synthesis of each compound was confirmed by ESI-HRMS, IR spectroscopy, NMR and elemental analysis. Examples for the characterisation analysis of ligand **89** are given in Figure 65 and Figure 66, but similar trends were found for all ligands **87-93**. In the IR spectrum (inset, Figure 65), there was a noticeable shift in the peaks representing the S=O stretching frequencies from 1371 $cm^{-1}$ to 1329 $cm^{-1}$ for the asymmetric stretch and from 1172 $cm^{-1}$ to 1158 $cm^{-1}$ for the symmetric stretch compared to 4-toluenesulfonyl chloride, indicating the successful formation of the sulfonamide bond. The HRMS spectrum (Figure 65) measured the $[M+H]^+$, $[M+Na]^+$ and $[M+K]^+$ ions at m/z 297.0466, 319.0284 and 335.0013 respectively.

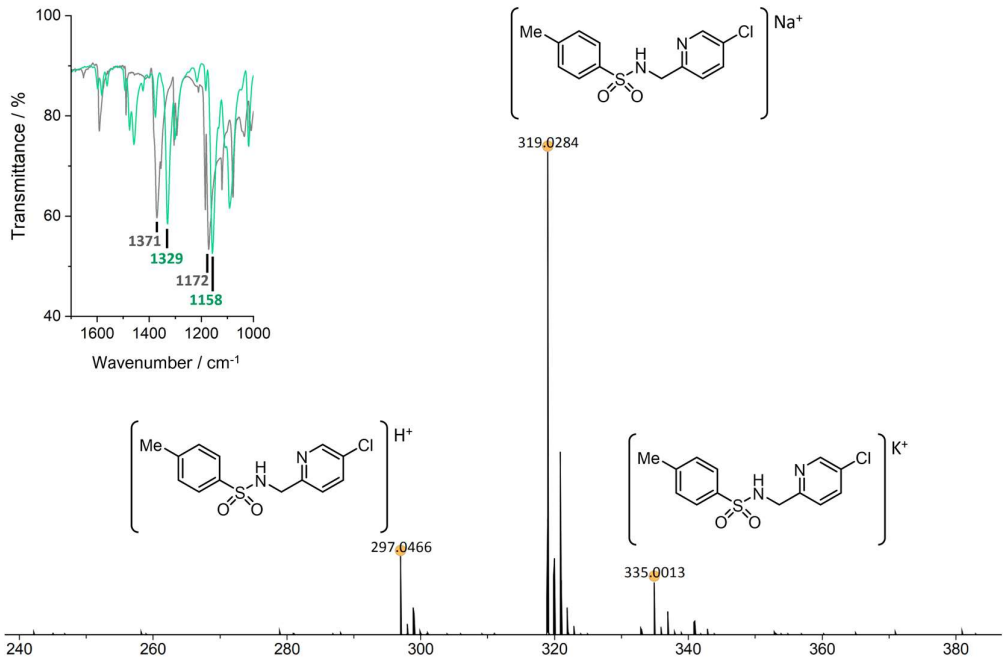


Figure 65 ESI-HRMS spectrum of compound **89** assigned with chemical structures and associated ionic charge contribution. Inset: the IR spectrum for the same compound in the region 1000-1700 cm-1, where grey trace is the transmittance signal of 4-toluenesulfonyl chloride and the green line is transmittance signal of compound **89**.

Analysis of the $^{1}$H NMR spectrum of ligand **89** (Figure 66) finds the triplet peak at 8.21 ppm assigned to proton 6, the NH of the sulfonamide; since this peak integrates to 1 equivalent proton, this indicates the successful formation of the sulfonamide bond as the starting material contained 2 protons at this position. The peaks of the $^{1}$H NMR are also close to the reported values of similar compounds in the literature.[100]

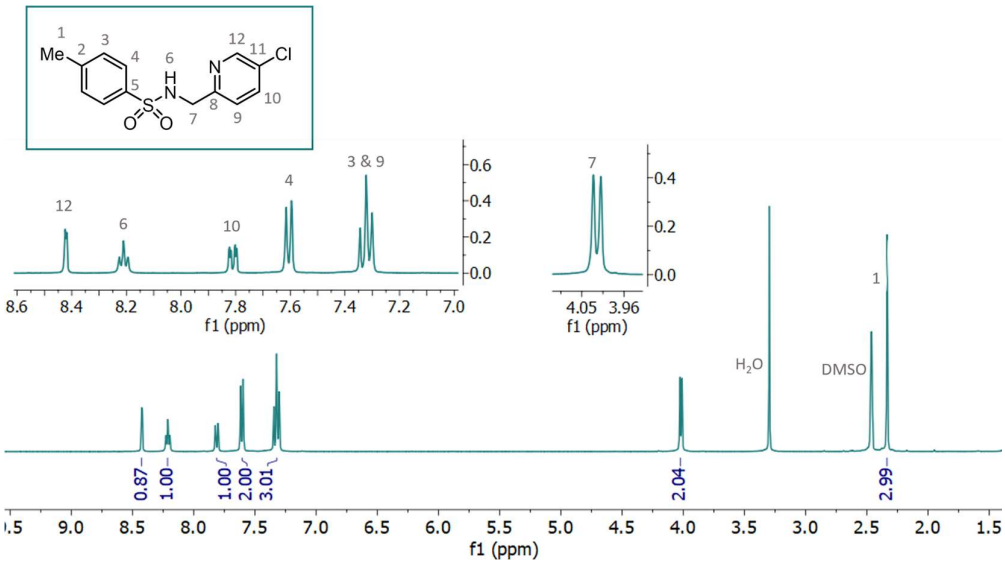


Figure 66 Assigned $^{1}$H NMR spectrum (solvent = DMSO-$d_6$) of compound **89**.

Ligands **87-92** were prepared from (pyridin-2-yl)methylamine starting compounds that were commercially available. The (pyridin-2yl)methylamine precursor to ligand **93** was not commercially available, but was synthesised following the literature method for a preparation of similar compounds[172] from (5-chloropyridin-2-yl)methylamine (Figure 67); (5-chloropyridin-2-yl)methylamine and an excess dimethylamine hydrochloride were dissolved in water, before the solution was basified with sodium hydroxide and this solution irradiated in a CEM Discover Reactor at 250 W. The length of time required for the reaction varied but was monitored by mass spectrometry and the appearance of the solution after microwaving for 20 minute time intervals. Initially, longer reaction time gives an increase in the intensity peaks for the product (m/z 152.1185 and 174.1004), and a decrease in those for the starting material (m/z = 143.0366). The appearance of a slight brown discolouration after 2-3 20 minute

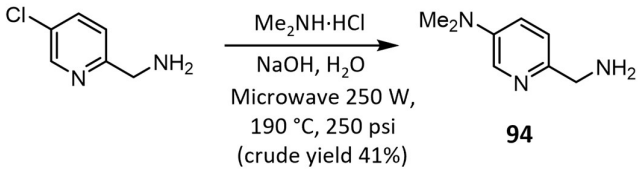


Figure 67 Scheme for the synthesis of the starting material for ligand **93**.

intervals corresponded to a decreased intensity of peaks for the product in HRMS-ESI spectrum (Figure 68), accompanied by the appearance of peaks at m/z= 135.0917, corresponding to $[C_8H_{11}N_2]^+$, with suggested structures for this side product indicated in Figure 68. Once this discolouration was observed, the reaction was halted.

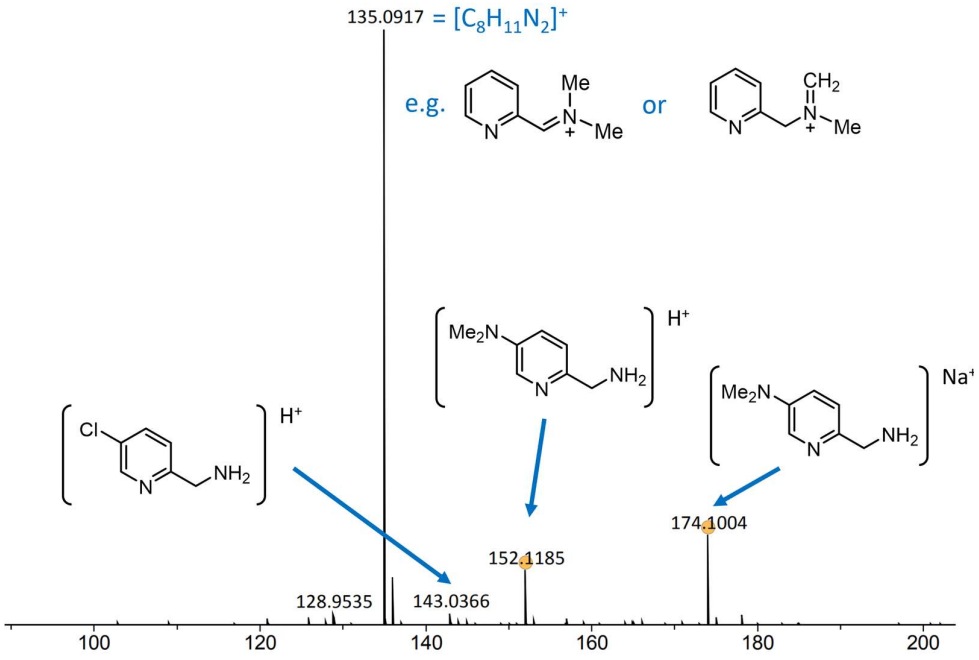


Figure 68 ESI-HRMS spectrum during the synthesis of compound **94** indicating the expected chemical structures for each peak, including remaining starting material (m/z = 143.0366), product (m/z= 152.1185 and 174.1004) and suggested structures of the by-product at m/z = 135.0917.

The water was then evaporated from the mixture. The remaining solids were sonicated in chloroform and the solution loaded onto a silica-gel column, before the product was eluted with a mixture of 8% methanol in chloroform with trace triethylamine. The crude mixture obtained from this step was a mixture of the (5-chloropyridin-2-yl)methylamine starting material and the desired [5-(dimethylamino)pyridin-2-yl]methylamine product. Methods to separate these two components by column chromatography were investigated but proved unsuccessful. Fortunately, the compounds produced in the next step of the reaction, **89** and **93**, could easily be separated by column chromatography so it was concluded purification following this first step was not necessary.

Ligands **87-92** were all crystallised from ethyl acetate and diethyl ether and X-ray crystal structures obtained (Figure 69). Ligand **93** was recovered in low yields so crystallisation was not attempted as other analytical methods were prioritised. It was found that despite identical conditions for recrystallisation of all the ligands, the molecules can form two different stacking

arrangements, either by intermolecular π-stacking giving linear molecular structures, or with intramolecular π-stacking where the two aromatic rings in the molecule stack parallel to each other. Comparison of the bond lengths of all structures revealed that, beyond the differences in stacking, there was very little variation in the structures.

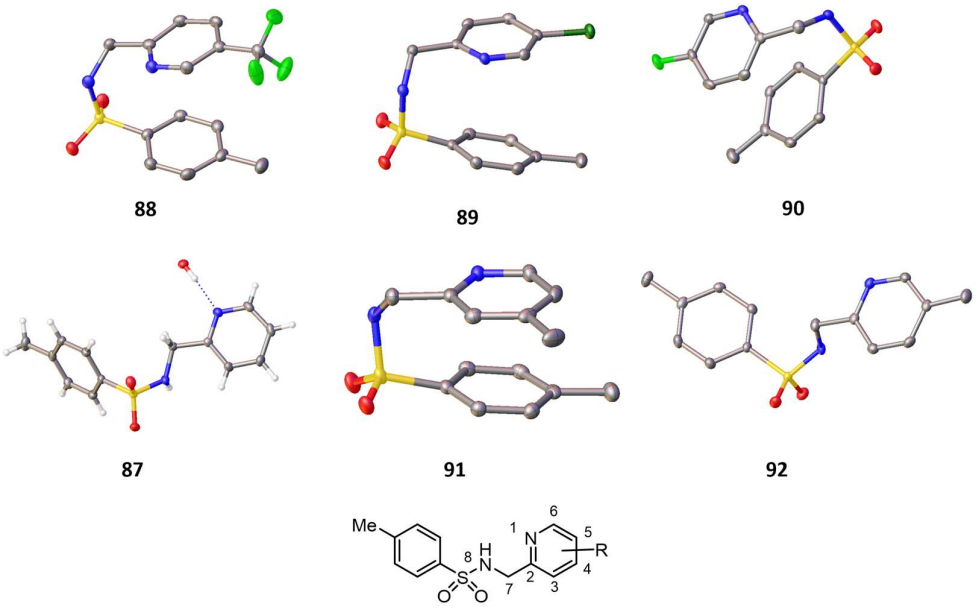


| Bond | 88 $R^5=CF_3$ | 89 $R^5$=Cl | 90 $R^5$=F | 87 $R^{4,5}$=H | 91 $R^4$=Me | 92 $R^5$=Me |
|---|---|---|---|---|---|---|
| R to 4 | - | - | - | - | 1.504 (2) | - |
| R to 5 | 1.489 (3) | 1.7457 (17) | 1.3556 (19) | - | - | 1.507 (2) |
| 1 to 2 | 1.339 (3) | 1.343 (2) | 1.344 (2) | 1.3386 (19) | 1.342 (2) | 1.334 (2) |
| 2 to 3 | 1.394 (3) | 1.388 (2) | 1.391 (2) | 1.381 (2) | 1.385 (2) | 1.391 (2) |
| 3 to 4 | 1.379 (3) | 1.385 (2) | 1.386 (2) | 1.388 (2) | 1.395 (2) | 1.386 (2) |
| 4 to 5 | 1.394 (3) | 1.382 (2) | 1.372 (2) | 1.381 (2) | 1.387 (2) | 1.389 (2) |
| 5 to 6 | 1.383 (3) | 1.386 (2) | 1.38 (2) | 1.374 (2) | 1.385 (2) | 1.388 (2) |
| 6 to 1 | 1.334 (3) | 1.337 (2) | 1.334 (2) | 1.345 (2) | 1.337 (2) | 1.344 (2) |
| 2 to 7 | 1.514 (3) | 1.514 (2) | 1.513 (2) | 1.5192 (19) | 1.517 (2) | 1.509 (2) |
| 7 to 8 | 1.463 (3) | 1.460 (2) | 1.470 (2) | 1.4610 (19) | 1.469 (2) | 1.467 (2) |
| 8 to S | 1.630 (2) | 1.6177 (15) | 1.6209 (14) | 1.6192 (13) | 1.6192 (14) | 1.6003 (15) |

Figure 69 Images of the crystal structures of ligands **87-92** and a table of bond lengths of interest (in Å).

The next step in the synthesis of the iridium complexes is coordination of the bidentate ligands to Cp*-bound Ir. The $[Cp^*IrCl_2]_2$ intermediate, **95**, necessary for this step was synthesised by the method reported in the literature.[173]

The complexes were prepared by dissolving two equivalents of the corresponding ligand and one equivalent of $[Cp^*IrCl_2]_2$, **95**, in dichloromethane before slow addition of 2 equivalents of NaOH, added as a 2 mol $dm^{-3}$ solution of NaOH dissolved in anhydrous methanol (Figure 70). These solutions were sonicated at room temperature for 20 minutes before a small volume of

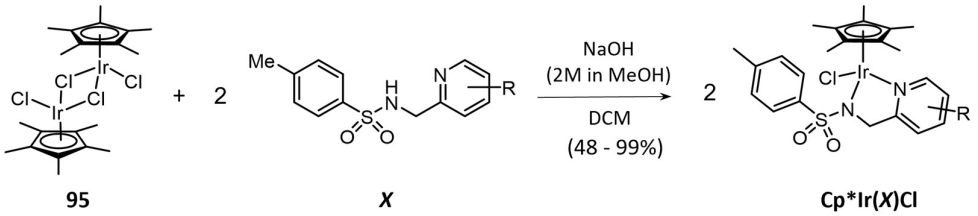


Figure 70 Scheme for the synthesis of Ir complexes with pyridinylmethylsulfonamide ligands.

water was added and the solution stirred vigorously for 30 seconds before the organic layer was transferred to a vial and the solution reduced in volume. Complexes with ligands **87**-**92** were isolated from the concentrated solution by adding diethyl ethyl ether gradually to promote the formation of crystals, which were then isolated by filtration. These complexes were obtained as bright orange crystals. This preparation method is adapted from that reported by Raines *et al.*[100] for the synthesis of a similar complex but changed to include an aqueous washing step as it was found to improve the ease with which the products would be crystallised.

The [5-(dimethylamino)pyridin-2-yl)methylsulfonamide ligand (**93**) derivative could not be crystallised from the dichloromethane solution and was instead evaporated to dryness. Although crystallisation is a desirable step in purification of the product, the $^{1}$H NMR spectrum

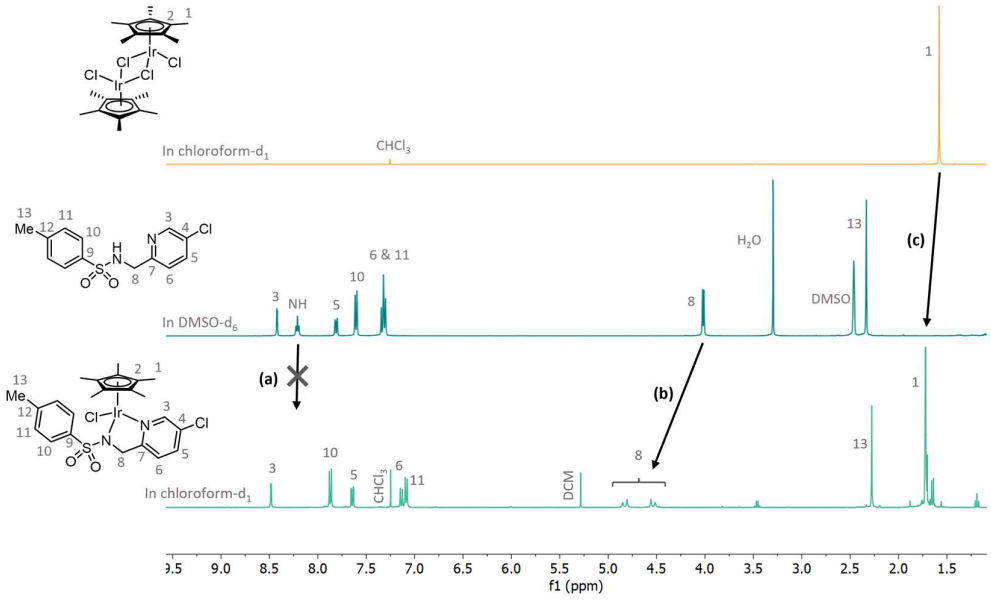


Figure 71 Assigned $^{1}$H NMR spectra of $[Cp^*IrCl_2]_2$, **95**, (orange), ligand **89** (teal) and Cp*Ir(**89**)Cl (green). Changes to indicate successful synthesis of the complex are (a) disappearance of the peak corresponding to the NH proton, (b) the downfield shift of the protons assigned 7 and splitting into two doublets as a result of the diastereotopic protons, (c) downfield shift of the protons of Cp*, assigned 1.

of this complex showed the presence of only a very small amount of impurities, so it was considered useable for the purposes of our experiments.

Successful synthesis of the complexes was confirmed by ESI-HRMS, NMR and elemental analysis. Distinct changes were observed in the $^{1}H$ NMR spectra compared to that of the starting materials (Figure 71): (a) The disappearance of the triplet around 8.2 ppm of the free ligand corresponding to the proton of the sulfonamide group that is lost on coordination to Ir, (b) a significant downfield shift of the peak around 4.2 ppm in the free ligand, corresponding to the $CH_2$ group, and splitting into two equal peaks in the region 5.2-4.6 ppm, (c) a downfield shift of the peak for Cp* protons from 1.59 ppm for $[Cp^*IrCl_2]_2$ to 1.72 ppm in the complexes.

The identification of two separate peaks corresponding to the $CH_2$ protons ((b) Figure 71) relate to the two distinct diastereotopic proton environments of these protons upon complex formation, as indicated by $H^a$ and $H^b$ in Figure 72. The chiral centre at the Ir means that while both protons occupy the same chemical environment, they occupy different spatial environments. This difference arises from proton $H^b$ (Figure 72) being in close proximity to protons of the Cp* ligand. The resonances of these neighbouring groups lead to a change in the chemical shift of proton $H^b$, while $H^a$ does not experience similar effects, being distant from the Cp* ring.

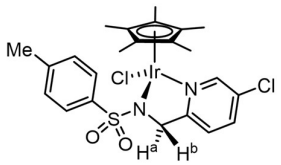


Figure 72 Structural diagram of the [Cp*Ir(**89**)Cl] complex indicating the two diastereotopic positions, $H^a$ and $H^b$, where protons are in identical chemical environments but are influenced by difference magnetic contributions due to their special positions.

For the complexes bearing an electron-withdrawing substituent on the pyridine ring, these two peaks in the NMR spectrum are well resolved into doublets, caused by $^{2}J$ coupling between the two diastereotopic protons, with $^{2}J$ coupling constants measured between 16.5-18.0 Hz in chloroform-d at 293 K. In contrast, the complexes of the unsubstituted pyridine or bearing electron-donating groups, show two broad, poorly resolved peaks in this region (Figure 73). Broadening of these peaks is due to the inversion of the stereo-centre of the complex on the NMR time-scale, as each diastereotopic proton will move into the other position.

Preparation of crystals for the Ir complexes with ligands **87-93** for X-ray diffraction proved challenging as the conditions used to isolate the complexes from solution following synthesis used DCM, which evaporated from the crystal structure following isolation leaving crystals of poor quality. A number of other solvent conditions for recrystallisation were attempted, but in most cases it was found that the complexes would revert to $[Cp^*IrCl_2]_2$. In some cases, X-ray data were successfully collected for crystals of the complexes where $R^{4,5}$ = H and $R^5$ = $CF_3$, but slippage of crystal layers meant that the resolution is lower than ideal. Nevertheless, the structures are reported in Figure 74, although the lower resolution means that it is difficult to gain much information from the measured bond lengths. Attempting careful crystallisation straight from the reaction mixture (as used in the isolation of the complexes) may be more successful in obtaining structurally better crystals compared to recrystallisation techniques, but this was not explored due to lack of appropriate starting materials.

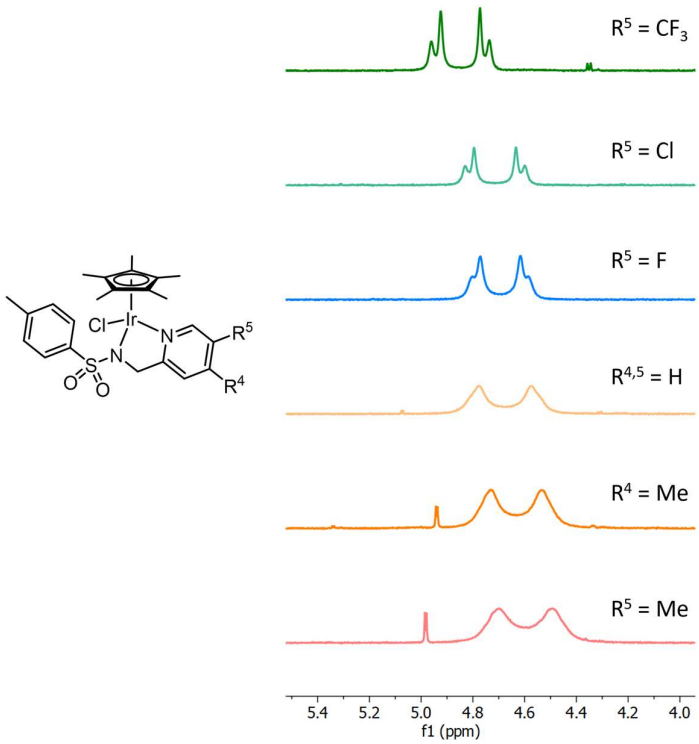


Figure 73 $^1$H NMR spectra in the 4.0-5.2 ppm region, indicating how the peak shape of the resonances assigned to the two diastereotopic protons are resolved depending on the pyridine ring substituent.

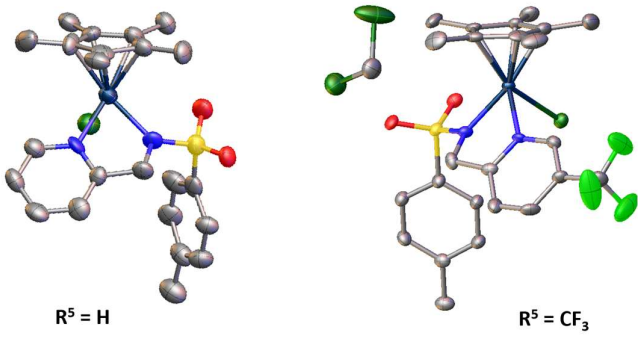


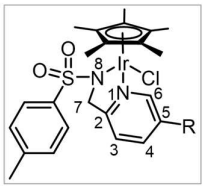


| Bond | H | $CF_3$ |
|---|---|---|
| 1 to 2 | 1.330 (17) | 1.358 (10) |
| 2 to 3 | 1.375 (19) | 1.393 (12) |
| 3 to 4 | 1.38 (2) | 1.372 (12) |
| 4 to 5 | 1.37 (2) | 1.396 (12) |
| 5 to 6 | 1.37 (2) | 1.373 (11) |
| 6 to 1 | 1.345 (18) | 1.336 (10) |
| 2 to 7 | 1.496 (19) | 1.500 (11) |
| 7 to 8 | 1.474 (17) | 1.456 (11) |
| 5 to R | | 1.495 (12) |
| 8 to Ir | 2.098 (11) | 2.091 (6) |
| 1 to Ir | 2.118 (11) | 2.100 (6) |
| Ir to Cl | 2.425 (4) | 2.4196 (18) |

Figure 74 X-ray crystal structures of two synthesised complexes, Cp*Ir(**87**)Cl and Cp*Ir(**88**)Cl, and the associated bond lengths reported in the table (in Å). DCM is trapped in the crystal of Cp*Ir(**88**)Cl as indicated above.

## 3.3 Measurement of the Activation Energies for Stereo-Inversion of the Iridium Chiral Centres by Nuclear Magnetic Resonance

The discovery that the resolution of the resonances associated with the $CH_2$ protons in the $^1H$ NMR spectra increased with the addition of EWGs relative to EDGs prompted investigations to obtain more information about the stereo-inversion of these complexes. The rate at which the chiral centre at iridium can invert can provide important information about the fluxionality of the complexes that might help in analysing their relative catalytic activity. Stereo-inversion can occur either by an intermolecular transformation, where dissociation of a ligand, likely the chloride ligand, occurs first before rebinding at the site in the opposite enantiomeric conformation, or by an intramolecular transformation, where the arrangement of ligands occurs without dissociation of any ligands, usually by passing through a transition state of a different geometry before relaxing back to the ground state geometry, in the other enantiomer.

The $^{1}$H NMR spectra of the complex Cp*Ir(**87**)Cl was recorded at room temperature in two different deuterated solvents which are both expected to have a weak coordinating effect, so should not competitively displace chloride ligand, chloroform-d and toluene-$d_8$. However, these solvents do differ in polarity. The spectrum in chloroform-d showed broad peaks in 4.2-4.9 ppm region, but clearly resolved doublets in toluene. This suggests that the mechanism of chiral exchange is probably intermolecular since the ability of the solvent to stabilise the dissociated ion ($Cl^-$) during exchange is crucial to the rate of exchange whereas there would be a much smaller solvent effect for an intramolecular mechanism. The more polar solvent (chloroform-d) is much more able to stabilise the dissociated chloride ion, hence chiral interchange proceeds more quickly and broad peaks are seen compared in with the non-polar solvent (toluene-$d_8$) where two well-resolved peaks are observed.

The trend in the rate of stereo-inversion with addition of electron-withdrawing or donating-groups on the pyridine ring therefore provides information about the strength of the Ir-Cl bond. This could be important to the investigation of our catalysts as the Ir-Cl bond strength provides indirect information on the Ir-hydride bond strength. Lower electron density on Ir would increase the Ir-Cl bond strength; hence we expect the addition of electron-withdrawing groups to increase Ir-Cl bond strength and reduce the rate of inversion at the Ir centre, leading to better resolved peaks in the $^{1}$H NMR spectrum. The converse is true for electron-donating groups. This is confirmed by the $^{1}$H NMR spectra reported in Figure 73.

Values for the activation energy of stereo-inversion and the thermodynamic parameters can be obtained from the line shape at 4.2-4.9 ppm using variable temperature $^{1}$H NMR experiments. Firstly, a suitable NMR solvent had to be found which gave a large enough temperature range to see all four regions of exchange as indicated in Figure 75, in which the complexes were soluble and that stabilised the stereo-inversion process in a measurable range. A solvent that was incapable of coordinating to Ir was preferred as this would ensure the measurements would correlate with the Ir-Cl bond strength. Chloroform-d gave good solubility and visible stereo-exchange but, with a boiling point of 61.2 °C, would not give the necessary temperature range to see all four exchange regions. Toluene-$d_8$ has a much higher boiling point of 110.6 °C but, as previously discussed, did not act to stabilise chloride dissociation but, even at temperatures approaching the boiling point, fast exchange was not achieved. Fortunately DMF-$d_7$ provided a solution, with a high boiling point (153 °C) and a temperature range in which all four exchange regions were visible for all complexes. DMF, however, is capable of coordinating Ir, so rather than measuring the Ir-Cl bond strength, it is more likely to be the dissociation of DMF solvent from Ir. Regardless of whether it is Ir-Cl dissociation or Ir-solvent dissociation we are able to measure, the data gathered still provided a suitable trend for the comparison between all the complexes.

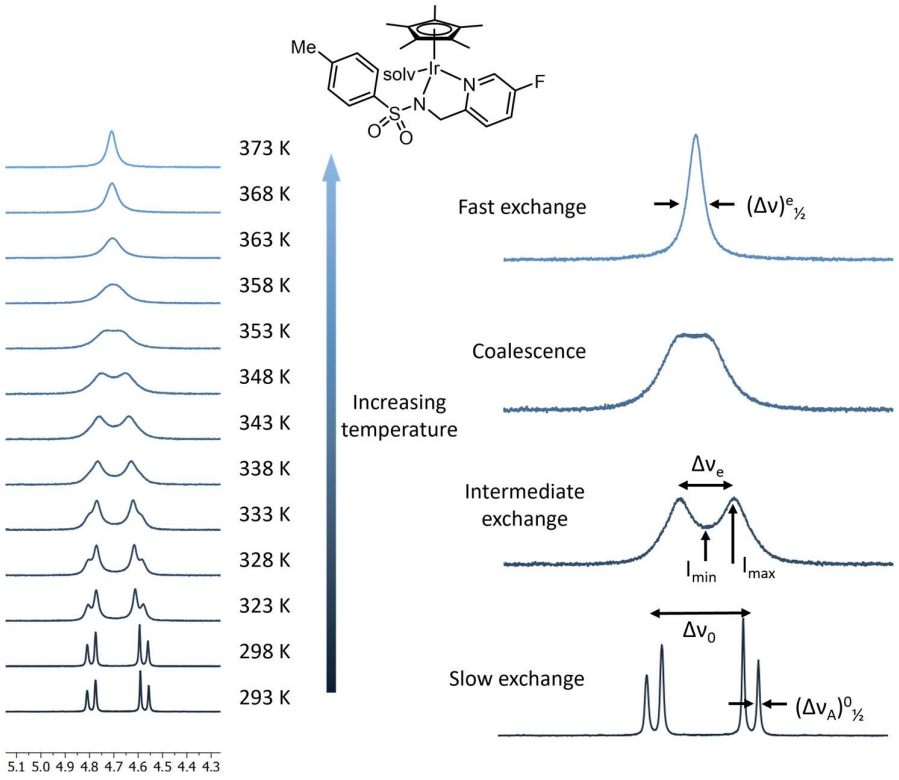


Figure 75 $^{1}$H NMR spectra (in DMF-$d_7$) for the iridium complex Cp*Ir(**90**)Cl in the temperature range 293 K to 373 K. To the left, the four regions of exchange are visualised, with indicators of how the parameters for calculating the rate of exchange are measured.

Using line shape analysis[174] derived from the Bloch equations[175] the function for line shape is given by

$$g(\nu) = \frac{K\tau(\nu_A - \nu_B)^2}{(^1/_2\,(\nu_A + \nu_B) - \nu)^2 + 4\pi^2\tau^2(\nu_A - \nu)^2(\nu_B - \nu)^2} \qquad (1)$$

for two uncoupled protons, where $g(\nu)$ is the intensity at frequency $\nu$. $\nu_A$ and $\nu_B$ are the frequencies of the two peaks at slow exchange representing the two distinct diastereotopic environments. $K$ is a normalisation constant, $\tau$ is $1/k$ with $k$ being the rate constant for the exchange. $\nu_A$, $\nu_B$ and $\tau$ are all temperature dependent variables.

Depending on the exchange region of the spectrum (as shown in Figure 75), certain approximations can be made to simplify Equation 1 as reported by Gasparro *et al.*[174] In the region of slow exchange, $\tau >> (\nu_A - \nu_B)^{-1}$, Equation 1 can be simplified to

$$g(\nu) = \frac{KT_{2A}{}'}{1 + 4\pi^2 T_{2A}{}'^2(\nu_A - \nu)^2} \qquad (2)$$

When considering just the line shape of the peak related to $H^a$, where $T_{2A}{}'$ is the spin-spin relaxation time of diasterotopic proton $H^a$ and

$$(\Delta\nu_A)^0_{1/2} = \frac{1}{\pi T_{2A}{}'} \tag{3}$$

At intermediate exchange, Equation 3 becomes

$$(\Delta\nu_A)^e_{1/2} = \frac{1}{\pi T_{2A}{}'} + \frac{1}{\pi\tau} \tag{4}$$

Knowing $\tau = 1/k$, Equation 4 can be rearranged to give

$$k = \frac{\pi}{\sqrt{2}}\left[(\Delta\nu_A)^e_{1/2} - (\Delta\nu_A)^0_{1/2}\right] \tag{5}$$

Because the peaks in the spectrum of this compound are coupled in the slow exchange region, i.e. are doublets, it would be inaccurate to try to measure $(\Delta\nu_A)^e_{1/2}$ since line broadening of the peaks is convoluted by increased line broadening of the doublets, in addition to the line broadening associated with the increased rate of stereo-inversion. Instead, the ratio method can be applied as long as there is significant overlap of the two peaks, then *k* is related to the intensities of the peaks and intermediate region, $I_{max}$ and $I_{min}$ (see Figure 75) by

$$k = \frac{\pi\Delta\nu_0}{\sqrt{2}}\,(r + (r^2 - r)^{1/2})^{-1/2} \tag{6}$$

Where

$$r = \frac{I_{max}}{I_{min}} \tag{7}$$

At the coalescence temperature, $I_{max} = I_{min}$ hence Equation 6 simplifies to

$$k = \frac{\pi\Delta\nu_0}{\sqrt{2}} \tag{8}$$

In the fast exchange region, $\tau << (\nu_A - \nu_B)^{-1}$ and Equation 1 simplifies to

$$g(\nu) = \frac{KT_2{}'}{1 + 4\pi^2 T_2{}'^2(\nu_A + \nu_B - 2\nu)^2} \tag{9}$$

Where

$$\frac{1}{T_2{}'} = \frac{1}{2}\left(\frac{1}{T_{2A}{}'} + \frac{1}{T_{2B}{}'}\right) \tag{10}$$

where $T_{2B}{}'$ is the spin-spin relaxation time of diasterotopic proton $H^b$. In the region of fast exchange where there is still some line broadening i.e. the fast exchange limit has not yet been reached, the rate of exchange can be approximated to

$$k = \frac{\pi \Delta \nu_0{}^2}{\sqrt{2}} \frac{1}{\left[(\Delta \nu_{1/2})^e - (\Delta \nu_A)^0_{1/2}\right]} \tag{11}$$

$(\Delta \nu_{1/2})^e$ is unperturbed by coupling between the two positions because at higher stereo-inversion rates, no coupling effect is seen. A best estimate for $(\Delta \nu_A)^0_{1/2}$ has been made based on the ½ height line widths of the doublet peaks of the best resolved complexes at slow exchange. This is sufficient since Equation 11 is not a very accurate approximation and often produces large errors in the calculated *k* value. Overall, a moderate degree of error is produced in using Equations 6 and 11 when compared to fitting values using the full line shape function, Equation 1. For the purposes of this experiment, however, qualitative analysis is sufficient in allowing comparison between our complexes, but it should be noted the values reported here are not highly accurate.

Using the Arrhenius equation, it is possible to use our approximated values for *k* at temperatures *T* to obtain values for the activation energy for exchange ($E_a$) using the expression

$$ln(k) = -\frac{E_a}{R}\left(\frac{1}{T}\right) + ln(A) \tag{12}$$

By plotting ln(*k*) against (1/*T*) and employing a linear line fitting, $-E_a/R$ is given by the gradient. R is the gas constant (8.3145 J $mol^{-1}$ $K^{-1}$) and *A* is a preexponential constant.

Thermodynamic parameters can also be calculated using the Eyring equation for a first order reaction and Gibbs Free Energy expression ($\Delta_r G^{\ddagger} = \Delta_r H^{\ddagger} - T\,\Delta_r S^{\ddagger}$) which produces the equation

$$k = \left(\frac{k_B T}{h}\right) e^{\left(\frac{-\Delta_r H^{\ddagger}}{RT}\right)} e^{\left(\frac{\Delta_r S^{\ddagger}}{R}\right)} \tag{13}$$

Where $k_B$ is the Boltzmann constant ($1.380649 \times 10^{-23}$ J $K^{-1}$), h is Planck's constant ($6.62607 \times 10^{-34}$ J s). Rearrangement of Equation 13 results in the expression

$$ln\left(\frac{k}{T}\right) = -\frac{\Delta_r H^{\ddagger}}{R}\left(\frac{1}{T}\right) + \frac{\Delta_r S^{\ddagger}}{R} + ln\left(\frac{k_B}{h}\right) \tag{14}$$

Hence plotting ln(k/T) against 1/T will produce a straight line with a slope of $-\frac{\Delta_r H^{\ddagger}}{R}$ and intercept of $\frac{\Delta_r S^{\ddagger}}{R} + ln\left(\frac{k_B}{h}\right)$.

Graphs were plotted from the approximated values for *k* obtained from the variable temperature $^{1}$H NMR experiments using Equations 12 (Figure 76(a)) and 14 (Figure 76 (b)), and the associated parameters were calculated from the linear least-squares line fittings (Table 3).

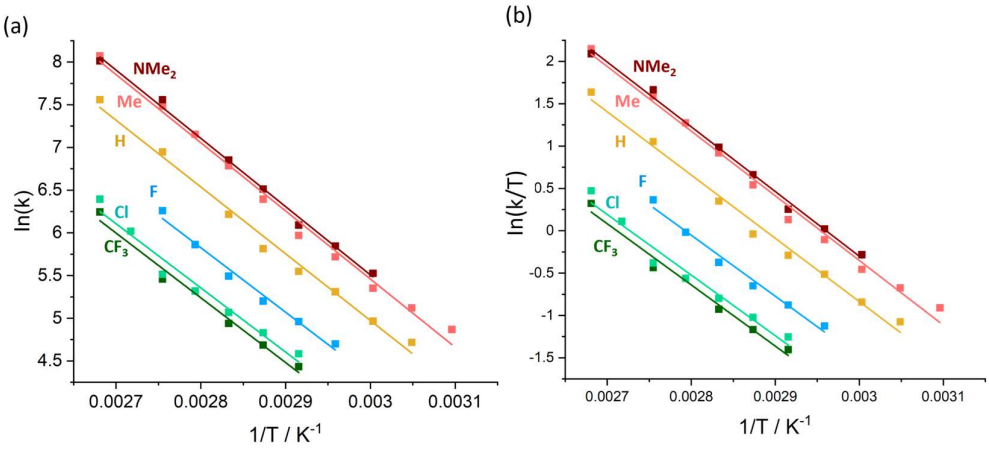


Figure 76 (a) plot of ln(k) vs 1/T. $E_a$ is determined from the gradient and (b) plot of ln(k/T) vs 1/T to determine $\Delta_rH^{\ddagger}$ and $\Delta_rS^{\ddagger}$ for complexes with substituent R at the 5- position (i.e. $NMe_2$ = Cp*Ir(**93**)Cl, Me = Cp*Ir(**91**)Cl etc).

Table 3 Table reporting the thermodynamic values for each complex by pyridine substituent.

| Group | Compound | $\Delta V_c$ | $E_a$ | $\Delta H^{\ddagger}$ | $\Delta S^{\ddagger}$ | $\Delta G^{\ddagger}$ (at T=298 K) | $\Delta G^{\ddagger}$ (at T=313 K) |
|---|---|---|---|---|---|---|---|
| | | kcal mol$^{-1}$ | kJ mol$^{-1}$ | kJ mol$^{-1}$ | J mol$^{-1}$ K$^{-1}$ | kJ mol$^{-1}$ | kJ mol$^{-1}$ |
| **$CF_3$** | Cp*Ir(**88**)Cl | 13.7 | 63.062 | 60.088 | -34.61 | 70.403 | 70.922 |
| **Cl** | Cp*Ir(**89**)Cl | 7 | 62.515 | 59.541 | -35.18 | 70.025 | 70.553 |
| **F** | Cp*Ir(**90**)Cl | 5.1 | 62.800 | 59.888 | -30.30 | 68.916 | 69.371 |
| **H** | Cp*Ir(**87**)Cl | 0 | 65.029 | 62.124 | -18.12 | 67.525 | 67.797 |
| **4-Me** | Cp*Ir(**91**)Cl | -3.3 | 63.510 | 60.630 | -20.63 | 66.779 | 67.088 |
| **5-Me** | Cp*Ir(**92**)Cl | -3.3 | 66.380 | 63.502 | -9.96 | 66.469 | 66.619 |
| **$NMe_2$** | Cp*Ir(**93**)Cl | -12.3 | 66.501 | 63.573 | -9.33 | 66.353 | 66.494 |

As expected from the spectra at room temperature, the rate constants for stereo-inversion increase with the electron-donating ability of the pyridine substituent. The rate constant, *k*, increases 6-fold between the complex with the strongest electron-withdrawing group, $CF_3$, compared to that of the strongest electron-donating group $NMe_2$ at temperatures where *k* was measurable for all complexes.

The activation energy, $E_a$, and enthalpy change of activation, $\Delta_rH^{\ddagger}$, are similar across all complexes as shown by the closely matching gradients of line in plots (a) and (b) in Figure 76. The entropy change of activation, $\Delta_rS^{\ddagger}$, is negative in all cases as would be expected since

dissociation of a ligand to form two charged species will result in increased solvation of the now charged Ir complexes and chloride ion thus increasing the order of the system. More negative values for $\Delta_rS^{\ddagger}$ occur as the electron-withdrawing nature of the substituent increases, reflecting the increasingly electron-deficient nature of the iridium metal ion. As the charge density of the iridium increases, the solvation effect will become larger, resulting in a more negative $\Delta_rS^{\ddagger}$. The trend in $\Delta_rG^{\ddagger}$ reflects the expected trend that increasing electron-withdrawing groups raise the Gibbs free energy demand for stereo-inversion of the complex. The contribution of $\Delta_rS^{\ddagger}$ is particularly significant. The trend in $\Delta_rG^{\ddagger}$ is nicely demonstrated in Figure 77 where $\Delta_rG^{\ddagger}$ at T=298 K is plotted against $\Delta V_c$, a theoretical alternative to experimentally-derived Hammett paramneters.[176] The $\Delta V_c$ parameter used to quantify substituent effects is formally the difference in the calculated molecular electrostatic potential at the nucleus of the *para* carbon of substituted benzene and a carbon atom in benzene. The calculated parameters correlate closely with experimentally-derived Hammett parameters and have been demonstrated to adequately predict the cumulative effect of multiple substituents. They also apply well to many other organic π-conjugated systems besides 6-membered aromatic rings.[176]

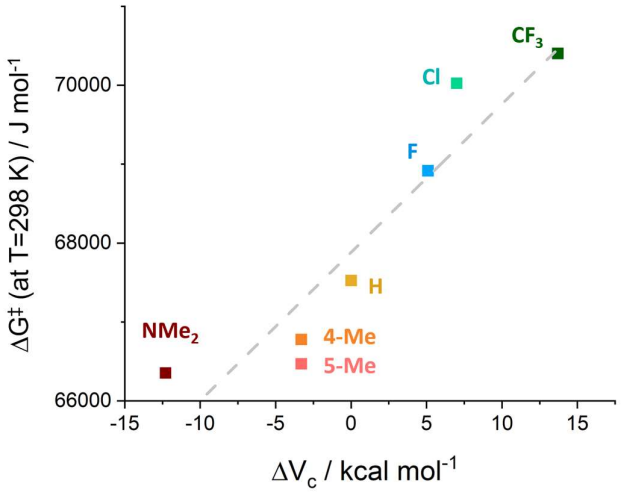


Figure 77 Plot of $\Delta_rG^{\ddagger}$ for each of the Ir complexes against the theoretical measurement of the electron-donating or withdrawing- ability of the pyridine substituent ($\Delta V_c$).

## 3.4 Catalytic Activity of Cp*Ir(pyridinylmethylsulfonamide) Catalysts

The complexes were tested for their catalytic potential on the imine reduction test reaction, the transfer hydrogenation of dehydrosalsolidine, **1a**, to (*R*)/(*S*)-salsolidine, **1b**, (Figure 78(a)). Reactions were carried out in pH 5.8 buffered solutions to closely mimic the conditions used

to test the artificial metalloenzyme.[100] All tests were carried out at 40 °C with a catalyst loading of 0.25% (50 mM substrate, 0.125 mM catalyst, pH 5.8 0.6 M MES buffer, 40 °C, stirring). Samples were taken from the reaction solution at selected time points and quenched in a solution of glutathione, which deactivates the catalyst, halting the reaction. The quenched samples were then analysed by HPLC, using the peak areas of the signals for the substrate and product to calculate conversion (Figure 78).

Additional control reactions were carried out to rule out any other contributions to the reaction progress. It was confirmed that over the course of the catalyst test there was no conversion of the starting material to the product in the absence of catalyst and, once quenched, the solutions were stable for a several weeks.

The $[Cp^*IrCl_2]_2$, **95**, intermediate showed very little catalytic activity with a conversion of just 6% after 60 minutes. The rate of catalysis was significantly enhanced by addition of the sulfonamide ligands (Figure 79).

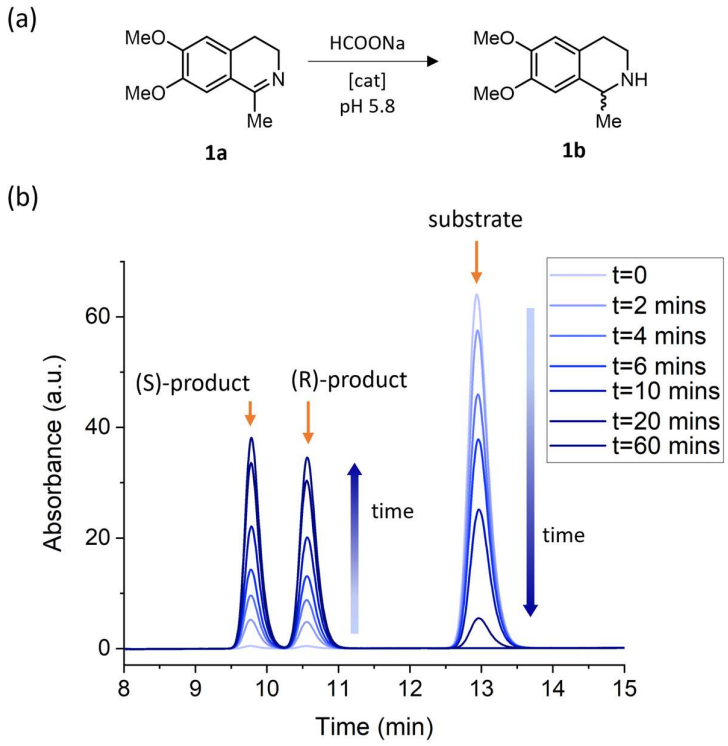


Figure 78 Typical (chiral) HPLC trace for monitoring the progress of the reaction.

The rate of reaction showed a distinct trend across the catalysts, with catalysts bearing electron-donating groups (Figure 79 (b)) catalysing imine reduction better than unsubstituted pyridine and electron-withdrawing groups (Figure 79 (a)). The strongest electron-withdrawing substituted pyridine, with the trifluoromethyl group (Figure 79, $R^5 = CF_3$), significantly reduced the catalytic ability of the complex. The methyl-substituted pyridine complexes

proved the best catalysts despite the dimethylamino-substituent being a more strongly electron-donating group (Figure 79 (b)). This could be for a number of reasons, including the additional steric bulk of the $NMe_2$ group making approach of the substrate more challenging, or that the step in the mechanism which is rate-determining for the pyridine catalyst is improved by the addition of the electron-donating groups to an extent that a different mechanistic step becomes rate-determining.

To contextualise this in terms of the catalytic mechanism (reported in Figure 53), the mechanism relies on two key steps: the formation of the Ir-hydride species by abstracting hydride from formate and the donation of hydride to the substrate (breaking of the Ir-hydride bond). These two steps are potentially rate limiting.[145]

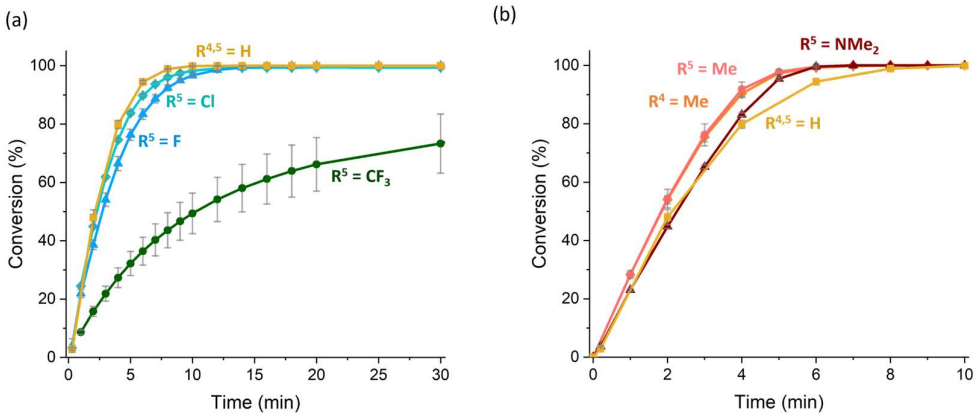


Figure 79 Plots of conversion of substrate to product against time, with (a) displaying Ir catalysts with electron-withdrawing substituents and (b) Ir catalysts with electron-donating substituents, relative to the catalyst with the unsubstituted pyridine ligand $R^{4,5}$=H (yellow).

Under the reaction conditions of the catalysis experiments reported in this chapter, formate is in large excess so the rate of formation of the Ir-hydride species is not limited by the concentration of formate. This step does not involve the substrate, the measurable variable used to monitor the progress of the reaction, hence, if formation of the Ir-hydride species was rate-determining, the reactions would proceed with zero-order kinetics, with respect to the concentration of substrate. In contrast, if donation of hydride to the substrate is rate-determining, the reactions will proceed with first-order kinetics with respect to the concentration of the substrate. This is because a 1:1 ratio of the Ir-hydride species and substrate is required in this step.

To determine the kinetics of the reactions, ln(concentration of substrate) (ln[S]) was plotted against time (Figure 80). If the data points result in a straight line, the reaction follows first-order kinetics and the first-order rate constant can be calculated from the gradient of the slope

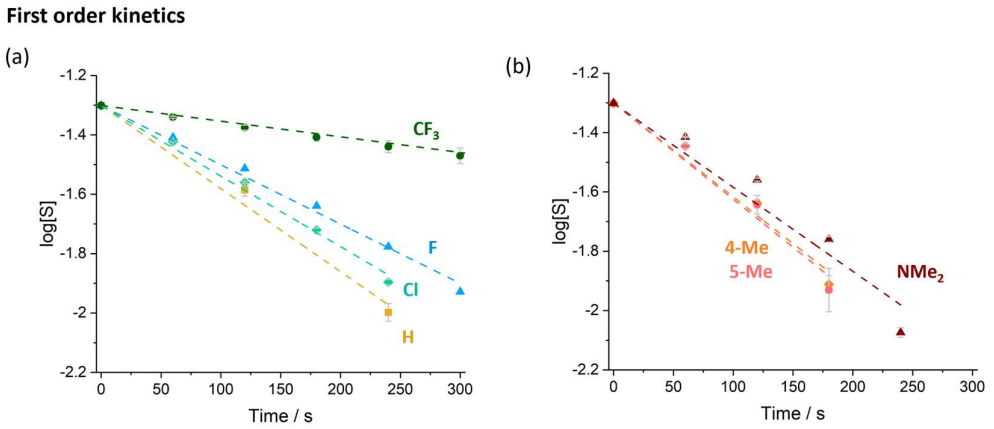


Figure 80 First order kinetics plots of log(concentration of substrate) against time for (a) catalysts with electron-withdrawing substituents on the pyridine ring and (b) catalysts with electron-donating substituents on the pyridine ring. The rate constant for each catalyst is calculated from the gradient of a straight-line fit. (a) demonstrates that catalysts with electron-withdrawing groups gave a good fit for a linear line while (b) data points of catalysts with electron-donating groups on the pyridine ring appear to be non-linear and produce poor line fits. Error bars display the standard deviation of log[S] from three repeats.

(gradient = -k). If this were the case, then the rate limiting step would be donation of the hydride to the substrate. The concentration of substrate ([S]) was also plotted against time (Figure 81). If the data points result in a straight line in this case, the reaction follows zero-order kinetics and the rate constant again obtained from the gradient (gradient = -k). If this is the case, then formation of the Ir-hydride species would be the rate-limiting step.

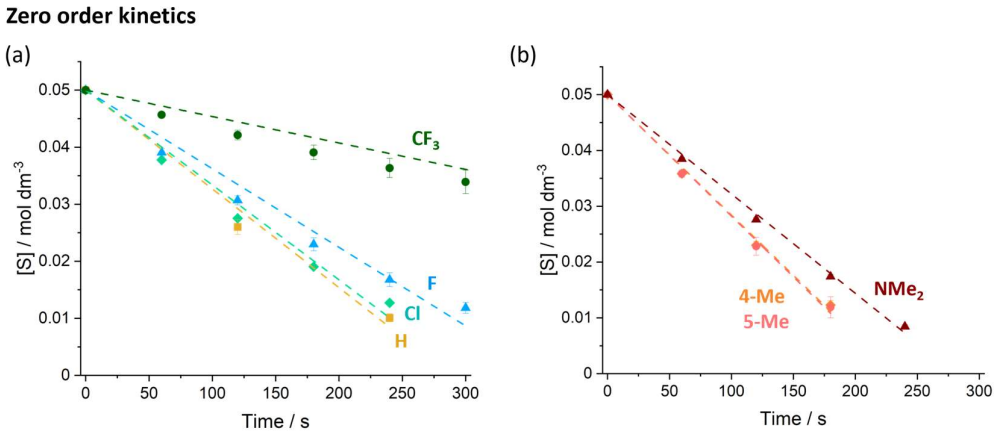


Figure 81 Zero order kinetics plots of concentration of substrate ([S]) against time with the rate constant calculated from the gradient of a straight-line fit, provided the kinetics of the reaction are zero-order with respect to the concentration of the substrate. Plot (c) demonstrates poor linearity of the data points for catalysts with electron-withdrawing groups while (d) demonstrates a good fit for catalysts with electron-donating groups. Error bars display the standard deviation of log[S] from three repeats.

As the electron-density of the Ir centre is increased with electron-donating groups, the Ir-hydride bond becomes weaker. This means the formation of the Ir-hydride species will have a lower thermodynamic pay-off and will be slower than for more electron-poor Ir catalysts. For the hydride donation step, however, the weaker Ir-hydride bond will lead to a faster hydride donation step for electron-rich Ir catalysts over electron-poor iridium catalysts.

The results of Figure 80 and Figure 81 show an interesting result in that some of the catalysts, namely those for the unsubstituted pyridine and electron-withdrawing substituents, agree closely with the first-order kinetics plots. The data points for the catalysts with electron-donating substituents, however, show a much better fit in the zero-order kinetic plots. This suggests that for the unsubstituted ligand the rate-determining step in the mechanism is the hydride donation step. Adding electron-withdrawing substituents onto the pyridine ring results in a stronger Ir-hydride bond, hence the rate of catalysis is reduced because the rate of the hydride donation step will be slower. Adding electron-donating groups has the opposite effect, with the Ir-hydride bond being easier to break, hence this step of the mechanism proceeds at a faster rate. It appears, however, that Ir-hydride formation and hydride donation occur at reasonably similar rates and the addition of electron-donating groups increases the rate of hydride donation to an extent that the formation of the Ir-hydride bond becomes the rate-determining step instead. Furthermore, electron-donating groups will reduce the rate of formation of the Ir-hydride species, which may also contribute to this change in the rate-determining step. This is probably why the substituent that should have the strongest electron-donating ability, $NMe_2$, produces a catalyst that is slower than the less electron-dense Me substituted catalysts. From the catalysts tested, the methyl-substituted catalysts achieve the best catalytic rate and show zero-order kinetics, suggesting the catalyst cannot be improved further by more strongly electron-donating groups.

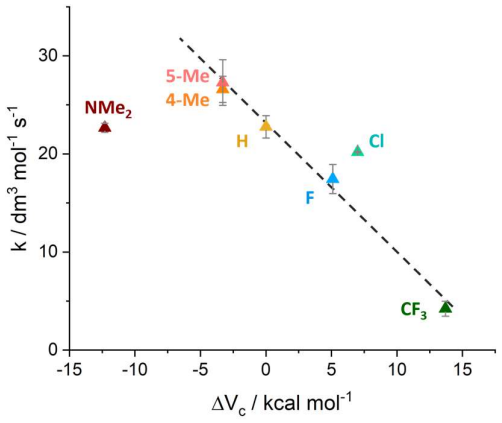


Figure 82 Hammett-type plot of the calculated first-order rate constants for each catalyst against $\Delta V_c$, a theoretical measure of the electron donating-/withdrawing- ability of substituent groups.

A Hammett plot (Figure 82) was made using the first-order rate constants from the best linear fit for each of the catalysts since the first- and zero-order rate constants are not directly comparable, having different units. The majority of the catalysts showed a better fit for first-order kinetics which is why these rate constants were chosen but a plot of the zero-order constants gave an almost identical plot. This showed a strong correlation between the theoretical measure of electron-donating ability of the substituents, $\Delta V_c$, and the rate constants for catalysis. The major outlier is $NMe_2$ which, as discussed, may have overextended optimisation of the rate of hydride-transfer to the detriment of the rate of Ir-hydride formation. The chlorine-substituted catalyst shows higher catalytic rate than expected. It is yet to be rationalised why this is so.

Another Hammett-type correlation can also be constructed by plotting the rate constants against the free energy of stereo-inversion of the complexes, $\Delta_rG^{\ddagger}$, as measured by NMR studies (Figure 83). $\Delta_rG^{\ddagger}$ is largely composed of the term for the energy to break the Ir-solvent bond hence the Ir-solvent bond strength. This value can be interpreted as an indirect measure of Ir-hydride bond strength. This gives another linear trend which would agree with the theoretical explanation that as Ir-hydride bond strength increases (by addition of electron-withdrawing substituents), the rate of reaction decreases where breaking the Ir-hydride bond, as in hydride donation, is the rate-determining step.

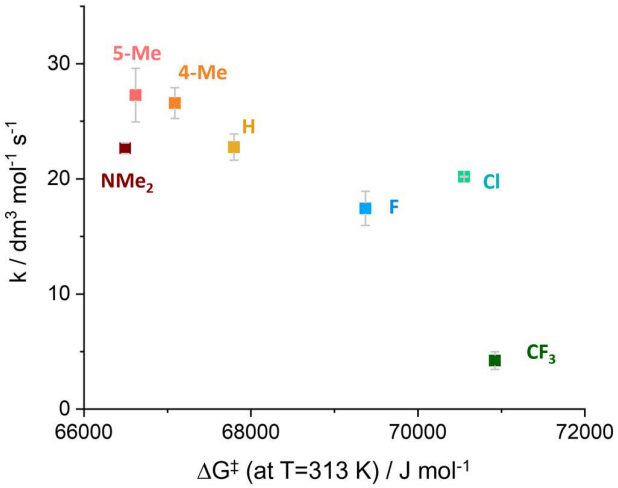


Figure 83 Plot of the calculated first-order rate constants for each catalyst against the $\Delta_rG^{\ddagger}$, the Gibbs free energy for inversion of the catalytic complexes, derived experimentally from variable temperature $^1$H NMR studies.

## 3.5 Summary and Conclusions

In efforts to optimise the selected Cp*Ir(pyridinylmethylsulfonamide) catalyst, we investigated the effect of adding electron-withdrawing and electron-donating substituents onto the pyridine ring of the sulfonamide ligand. Examination of the proposed mechanism for catalysis, and previous studies of similar transfer hydrogenation catalysts, suggested the ligands with more electron-donating groups might improve the performance of the catalyst, through electronic effects causing weakening of the Ir-hydride bond. A contradictory report suggested the reverse was true in catalysis reaction conditions most similar to our own.

A series of selected Cp*Ir(pyridinesulfonamide) complexes was synthesised for investigating this proposal. These complexes proved to be soluble and stable in water and could be synthesised in air, making them attractive catalysts for our artificial metalloenzyme. Analysis using variable temperature $^{1}$H NMR to investigate chiral exchange at the Ir centre demonstrated the effect of the pyridine ring substituents on the strength of the Ir-Cl bonds, and indirectly the strength of the Ir-hydride bonds. Electron-donating groups decreased the Ir-hydride bond strength, whereas electron-withdrawing groups had the opposite effect.

Testing the catalytic performance of these complexes revealed that the more electron-rich methyl-substituted catalysts improve upon the rate of catalysis while electron-withdrawing substituents had an adverse effect. Further analysis of the rate constants of catalysis, together with an understanding of the catalytic mechanism, revealed an explanation why using a more strongly electron-donating substituent then Me in $NMe_2$ decreased the rate of catalysis. This is explained by the catalytic mechanism where the two major steps in the mechanism, formation of the Ir-hydride bond and hydride donation to the substrate, proceed at a reasonably similar rate. While the rate-determining step for the unsubstituted Cp*Ir(pyridinylmethylsulfonamide) catalyst is hydride donation, further increasing the electron-density of the Ir centre leads to a decreased rate in the formation of the Ir-hydride species so that, despite an improvement in the rate of hydride donation, the reaction rate can only be marginally improved before the rate of formation of the Ir-hydride species becomes rate-determining. The methyl-substituted catalysts appear to reach a fine balance between increasing the hydride donating ability of the catalyst before Ir-hydride formation is significantly reduced.

This finding suggests that incorporating these improved methyl-substituted catalysts in ArMs may lead to improved activity from more optimal electronic tuning of the bidentate ligand.

# Chapter 4 Preparation and Evaluation of ArtIREDs

## 4.1 Introduction and Aims

In the example of the first siderophore-PBP ArM design published by Raines *et al.*,[100] the structure was assembled from the "apo" protein and a separately-synthesised conjugate, containing the Fe-siderophore anchoring group and the catalyst. The reported synthesis (Figure 84) involved the synthesis of the bidentate ligand containing a cyano group (**96**), from which the amine group used for linking the catalyst to the siderophore was revealed by reduction with $LiBH_4$. The siderophore, azotochelin, was selected for the ArM design because the synthesis is well-known[177] and because it contains a suitable functional group in the form of a carboxylic acid, to which the bidentate ligand of the Ir catalyst can be attached.

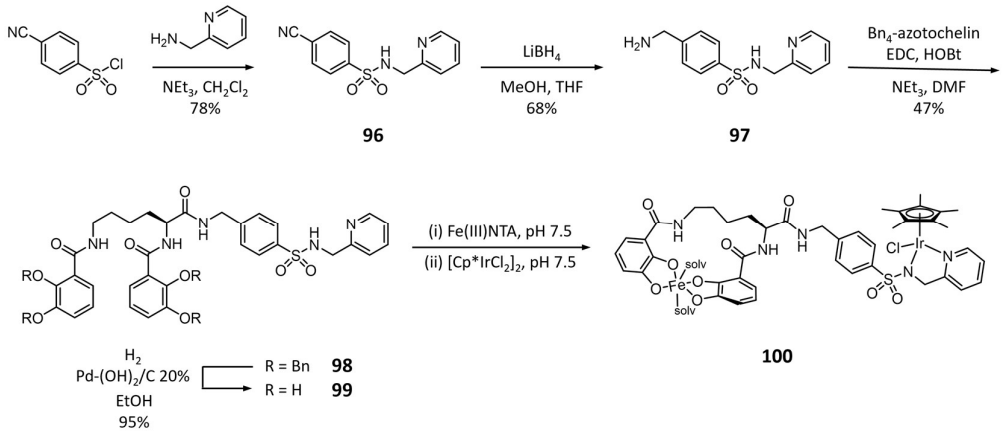


Figure 84 Scheme depicting the synthesis of the conjugate as reported by Raines *et al.*[100]

The periplasmic binding protein (PBP), *Cj*CeuE, used in this design originates from *Campylobacter jejuni*, in which it has an important role within the Fe(III) uptake pathway.[178,179] PBPs are required for gathering Fe(III)-siderophore complexes and delivering them to the appropriate inner membrane transporter.[102] *Campylobacter jejuni* does not synthesise any siderophores itself, but is capable of scavenging a number of structurally-different siderophores produced by competing organisms.[180] These include tetradentate catechol siderophores such as bis(2,3-dihydroxybenzoyl-L-Ser), a tetradentate hydrolysis product of enterobactin ($K_d$ = 10.1 ± 3.8 nmol $dm^{-3}$),[181] and azotochelin ($K_d$ = 6.9 ± 0.7 nmol $dm^{-3}$),[182] which are captured by *Cj*CeuE.

A number of other structurally-similar PBPs have been discovered, including two from the thermophilic organisms *Parageobacillus stearothermophilus* and *Geobacillus thermoglucosidasius,* which have been produced in our group by Dr. Elena Blagova. Proteins from thermophilic organisms are regularly a target of biocatalyst engineers, as thermostability is an important characteristic in industrial applications and thermophilic proteins have been shown to be more tolerant to introducing multiple mutations in optimisation efforts.[108,117,183,184] Thermostable proteins generally show higher stability[41,185,186] and occasionally increased tolerance to organic solvents[4,5,187,188]. Additionally, the structural changes in these thermophilic proteins could affect the enantioselectivity of the ArM, since small alterations in the protein can have significant effects on ArM catalysis.[27,76] The thermophilic PBPs have been shown to bind azotochelin with similar affinity to *Cj*CeuE (Pth $K_d$ = 5.3 ± 1.7 nmol dm$^{-3}$ and Gst $K_d$ = 3.5 ± 0.7 nmol dm$^{-3}$)[182] which made them a suitable alternative protein scaffolds for use in the ArM.

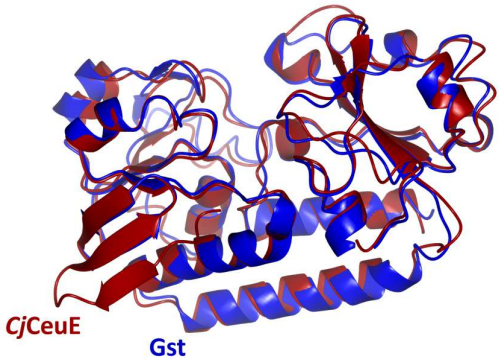


Figure 85 Superimposed crystal structures of *Cj*CeuE (red; PDB code 5OAH) and Gst (blue; unpublished X-ray crystal structure) bound to Fe-azotochelin (not shown). Superimposed structures show a high degree of similarity. . Crystals were prepared by Dr. Elena Blagova and the structures resolved by Prof. Keith S. Wilson and Prof. Eleanor Dodson.[100]

All three PBPs are structurally very similar (Figure 85) despite moderate differences in the amino acid sequences (Figure 86). Both thermophilic proteins are around 50% identical to *Cj*CeuE but bear a stronger similarity to each other with 68% sequence identity. The region of most interest regarding the design of our ArM is the flexible loop between positions 213-232 relative to the *Cj*CeuE sequence, as indicated in Figure 86. This loop contains His227 in *Cj*CeuE, which is conserved across all three proteins, and has a key role in coordinating Fe(III) in the PBPs native role. Both thermophilic proteins have a number of alterations in the amino acid sequence of this loop including the insertion of an additional amino acid for Gst.

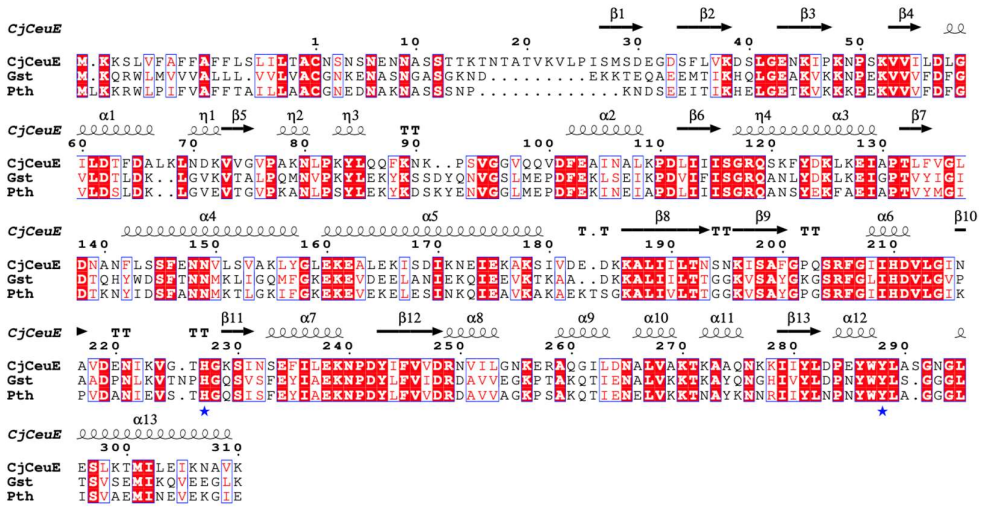


Figure 86 Amino acid sequences of periplasmic binding proteins of *Campylobacter jejuni* (*Cj*CeuE), *Geobacillus stearothermophilus* (Gst) and *Parageobacillus thermoglucosidasius* (Pth). Red shaded areas indicate fully conserved regions, areas of red text in boxes with a blue outline indicates alteration of the protein sequence for like amino acids (moderately conserved regions), regions of black text indicate exchange for un-like amino acids in one or more of the sequences. The region of particular interest is the flexible loop from position 210 to 240.

It was demonstrated in the reported crystal structure of the previously published PBP ArM (PDB code 5OD5) that His227 coordinates the Ir centre instead of Fe(III), displacing the chloride ion of the unbound conjugate (**100**).[100] It was proposed that this contributed to a 20-fold reduced catalytic rate of the ArM compared to the unbound cofactor as His227 occupied the coordination site needed to activate the hydride for the transfer hydrogenation reaction. Replacing histidine with alanine, an amino acid that is not capable of coordinating iridium, in order to remove competition for the coordination site, resulted in an ArM with an improved catalytic rate but almost a complete loss of enantioselectivity.[100] Thus, His227 was determined to be a crucial factor in the enantioselectivity of the previously reported PBP ArM.

Detailed analysis of crystal structures of the reported PBP ArM, and other structures of *Cj*CeuE, give some indication of how His227 may influence enantioselectivity. Although when forming the ArM the conjugate is added as a mixture of enantiomers, the Ir stereocentre can readily invert to coordinate the histidine residue, resulting in a single enantiomer bound in the protein. It is proposed this single configuration should contribute to the enantioselectivity of the catalytic reaction.

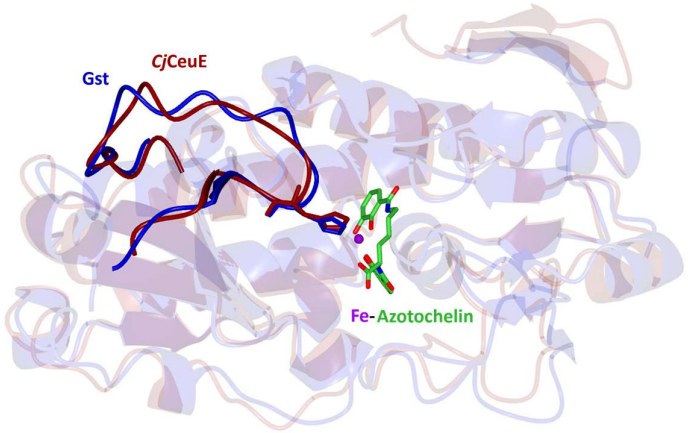


Figure 87 Superimposed crystal structures of *Cj*CeuE (red ribbons; PDB code 5OAH) and Gst (blue ribbons; unpublished) bound to Fe-azotochelin (green cylinders). The flexible loops between positions 213-232 (relative to the *Cj*CeuE sequence) is displayed as solid-colour ribbons separate from the rest of the structures semi-transparent ribbons. The position of His227 is indicated for each structure as cylinders extending from the ribbon structure (colour scheme same as protein ribbons).

In Figure 88, a composite image has been created from the conjugate as bound in the reported PBP ArM (pale blue cylinders; PBD code 5OD5) with the apo structure of H227A *Cj*CeuE (dark orange surface and ribbons; PBD code 5MBQ), which suggests the position that the flexible loop may occupy when His227 is not coordinating the Ir metal. The substrate, imine **1a** (green ball and stick structure), has been modelled into one potential binding site using calculation by Autodock. Analysing the position of the iridium (orange sphere) relative to the surrounding protein structure shows one small, shallow pocket to the left-hand side of the Ir atom marked by a black dotted line in Figure 88 (c), in which the substrate model is shown. To the other side of the iridium centre is a much larger pocket, marked by the black dashed line. The larger pocket may not control which face of the substrate approaches Ir, hence either enantiomer might be produced at this position in catalysis. Due to the much smaller size of the other pocket, and potential steric clash with the conjugate, the substrate may potentially be restricted in approaching Ir from the face indicated in Figure 88 as predicted by Autodock. In the case of the transfer hydrogenation reaction, the pocket from which the substrate will approach will be determined by the coordination position of the hydride coordinated to Ir. If the hydride is formed quickly following dissociation of His227, before stereo-rearrangement can take place, the hydride may be available in the smaller binding pocket. If the Ir stereo-centre inverts following dissociation of His227 before hydride binding, the substrate may approach from the larger pocket. It might be speculated that the moderate enantioselectivity during catalysis arises from a combination of these two options i.e., stereo-rearrangement can occur on the reaction time-scale but some enantio-preference arises from a proportion of the

reaction being catalysed by approach of the substrate from the smaller, selective pocket, but more experimental investigations would be required to support this theory.

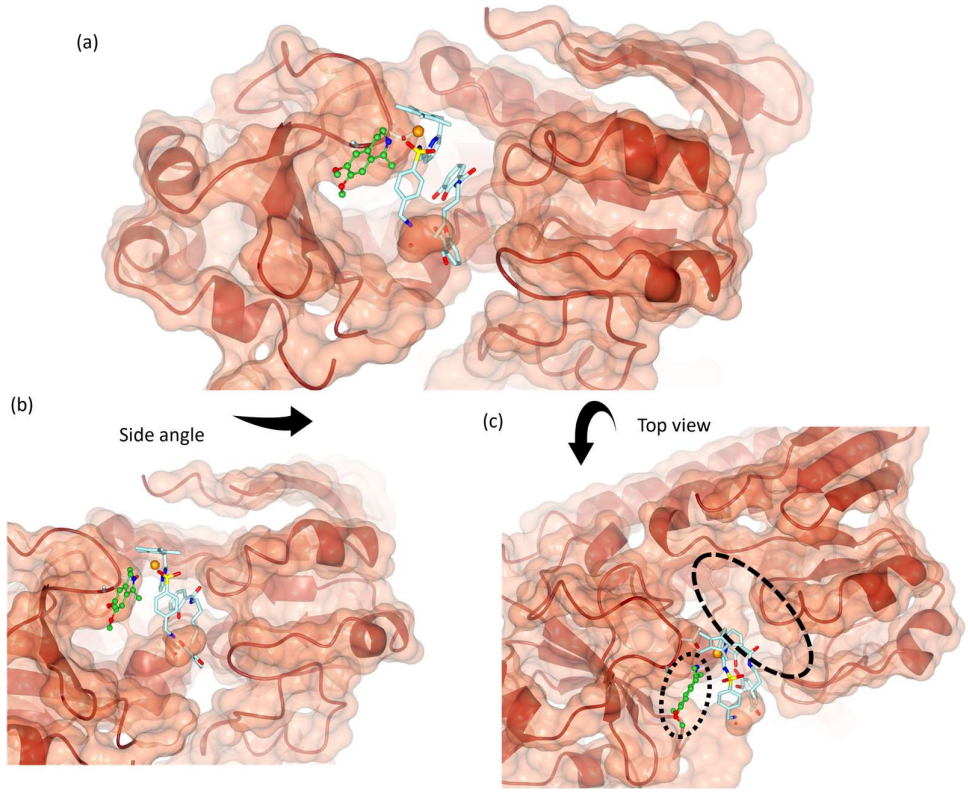


Figure 88 Composite image combining the catalytic conjugate (pale blue cylinders), apo H227A *Cj*CeuE (dark orange surface and ribbons) and model of the substrate (green ball and stick structure). The relative conjugate positions are taken from the crystal structure of the reported ArM (PDB code 5OD5), H227A *Cj*CeuE from the crystal structure of the apo form of the protein (PDB code 5MBQ) and the substrate modelled into the smaller binding pocket using Autodock. Three views of the sites surrounding the Ir catalyst have been shown as (a), (b) and (c). In (c) the black dotted line indicates the position of the smaller protein pocket and the black dashed line indicate the position of the larger protein pocket.

While the structural differences in the three proteins present one point of interest, another is the increased stability of the thermophilic proteins, which would permit operation at higher temperatures to help improve the rate of catalysis. The previously reported PBP ArM catalysed transfer hydrogenation of imine **1a** occurs relatively slowly so the option to heat the reaction above 40 °C would be useful. Another characteristic to examine would be the ArMs' tolerance to organic solvents, with regards to developing ArMs for other catalytic transformations where the substrates are not water soluble.

Another approach to improving the ArM is to optimise the catalytic conjugate. As demonstrated in Chapter 3, the addition of methyl-substituents onto the pyridine ring of the bidentate ligand positively improved catalysis. This prompted investigation as to whether a similar trend would be observed on incorporating these catalysts in our ArM (Figure 89).

While the ring position of the methyl-substituent had no effect on the catalytic rate of our iridium complexes, a more significant difference might be seen for the ArMs, where additional effects come into play; these include steric crowding or other interactions with the protein scaffold which could change the binding affinity of the conjugate or on the position and flexibility of the His227-containing loop. These changes might contribute to different levels of enantioselectivity and the catalytic rate. The positioning of the conjugate within the protein is in very close proximity to the His227-containing loop, so it was important to select small non-bulky substituents that would not completely disrupt the His227-Ir interaction.

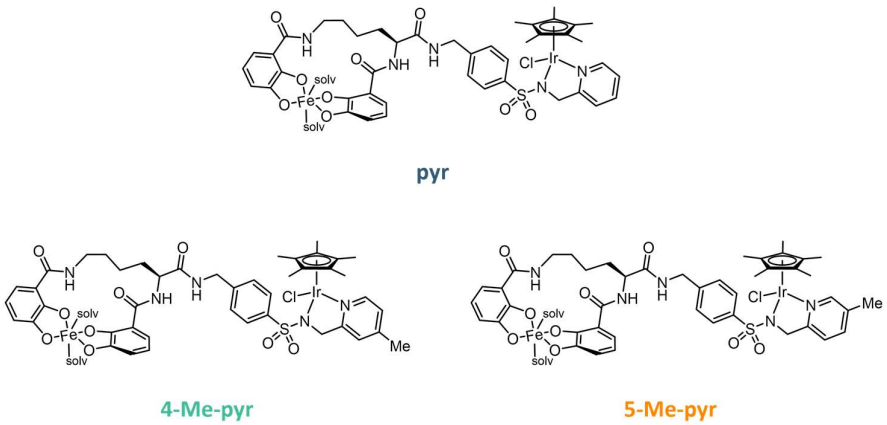


Figure 89 The structures of the three prospective conjugates for testing as part of the ArM design.

## 4.2 Synthesis and Characterisation of Siderophore-Catalyst Conjugates

In the reported PBP ArM, the conjugate containing the siderophore and organometallic catalyst was formed by an amide link between the siderophore and sulfonamide ligand.[100] This conjugate was prepared from the aryl sulfonamide ligand with an amine group at the *para*-position of the aryl group (Figure 84; **97**), allowing an amide formation to link this amine group with the carboxylic acid of the siderophore, azotochelin. To form the aryl sulfonamide with the amine group, it was necessary to start from the cyano-substituted aryl ring to avoid side reactions during the sulfonamide coupling (Figure 84; **96**). The amine group was then revealed by reduction of the cyano group with $LiBH_4$ (Figure 84; **97**).

However, when the reduction of the cyano group with $LiBH_4$ was attempted on a similar heteroaromatic ring, it resulted in an impure mixture of products also containing the compound in which the heteroaromatic ring was partially reduced (Figure 90). The reduced

heteroaromatic ring is also capable of binding to iridium hence it was necessary to find an alternative method to produce the desired amine group in good purity, without reduction of the heteroaromatic ring.

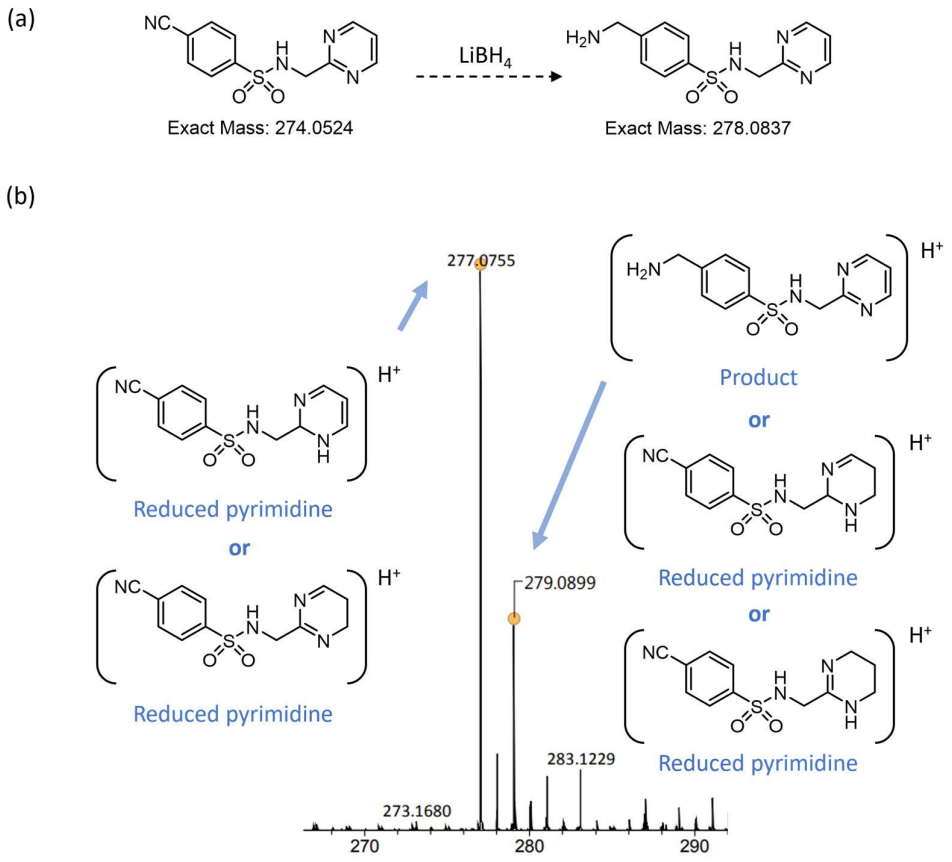


Figure 90 (a) Scheme for the expected reaction on reduction of the cyano-containing compound with $LiBH_4$ (b) the mass spectrum following the reaction with the peak at 277.0755 indicating the presence of compounds with reduced pyrimidine ring but the cyano group still intact.

A number of additional chemical reducing conditions were investigated; $NaBH_4$ was selected as a weaker reducing agent but proved impractically slow for the reduction of the cyano group, with only 12% conversion to product after 20 hours. Literature methods had suggested that $NaBH_4$ in combination with Co(II) could be used to successfully reduce cyano groups[189]. Analysis of a trial reaction using these conditions showed partial success for the reduction of the cyano group, however, the product is capable of coordinating to Co(II) which proved very challenging to remove, even with excess $EDTA^{4-}$.

While our group has also developed a method using a careful balance of Raney nickel and hydrogen for reduction of the cyano group,[190] concern remained that more electron-rich heteroaromatic rings may be more susceptible to reduction by some chemical reduction methods.

A route incorporating a Gabriel synthesis has instead been investigated. This route (Figure 91), although an additional synthetic step longer and with a reportedly lower yield than the alternative cyano-reduction route,[190] produced the desired amine product as a white powder with good purity as determined by $^{1}$H NMR and elemental analysis. This offers an advantage over the cyano-reduction route where the amine product is recovered as a colourless oil, as the solvent is difficult to remove in entirety, which in part contributed to the reported better yield. Recovering the amine as a solid allows for better analytical analysis of the compounds.

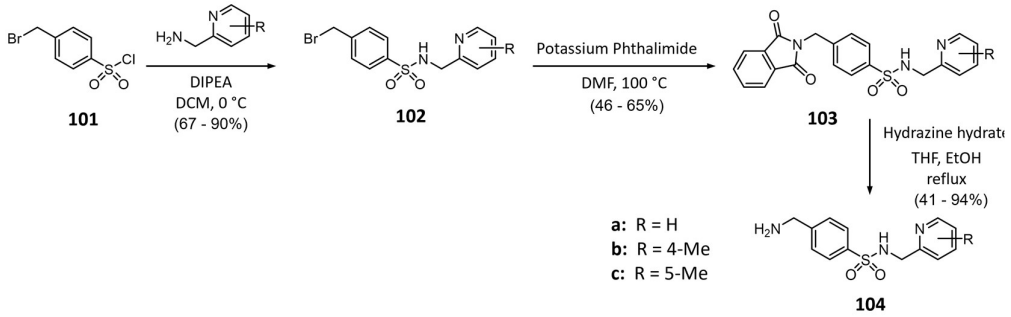


Figure 91 Scheme for the synthesis of the aryl sulfonamide ligand with the methylamine substituent suitable for linking the ligand bidentate ligand to azotochelin.

This route begins from the methylbromo-substituted aryl-sulfonyl chloride (**101**) and the selected methylamine-substituted pyridine. The sulfonamide coupling was achieved by adding 1 equivalent of methylamine-substituted pyridine to 1.2 equivalents of **101** at 0 °C, which prevented a potential nucleophilic substitution reaction of the amine with the bromo-group of **101**. The resulting intermediate **102** was isolated and purified by a standard aqueous work-up, followed by column chromatography (1:1 ethyl acetate: petroleum ether 40-60 °C). Yields between 65-90% were achieved. Example characterisation in the following figures and discussion examine the synthesis of the 4-Me-substituted pyridine compounds (R=4-Me) but methods, observations and characterisation data are very similar for all equivalent compounds of R=H and R= 5-Me.

Analysis of the product by ESI-HRMS and $^{1}$H NMR revealed that, while substitution of the amine for the bromo-group was prevented during the reaction, the presence of chloride ions either in the solvent (dichloromethane) or during the aqueous work-up, can displace the bromo-group. This was initially identified by the presence of two additional peaks in the ESI-HRMS spectrum at m/z = 311.0619 and 333.0437 which lack the distinctive pattern of approximately 1:1 peak height at m and m+2 caused by the two isotopes $^{79}$Br and $^{81}$Br with relative abundance 51:49 respectively (Figure 92). The masses correspond to the chloro-exchanged $[M+H]^+$ and $[M+Na]^+$ ions. This was confirmed by $^{1}$H NMR (Figure 93) where the peak representing the $CH_2$ protons of the methylbromo- substituent at 4.71 ppm has a small neighbouring peak at 4.78 ppm with integrated peak areas that must be added to achieve the

relative number of protons equal to 2. The peak is more downfield than the peak for the bromo-substituted product, as would be expected for chloro-substitution. It was decided that further purification to remove the chloro-substituted by-product would not be necessary as the by-product was expected to have similar reactivity in the next step of the synthesis, albeit at a slower rate. Even if the reactivity of the by-product was significantly reduced, it was present in relatively small quantities so judged not to seriously impact yields compared to the potential yield lost from additional purification efforts as this stage.

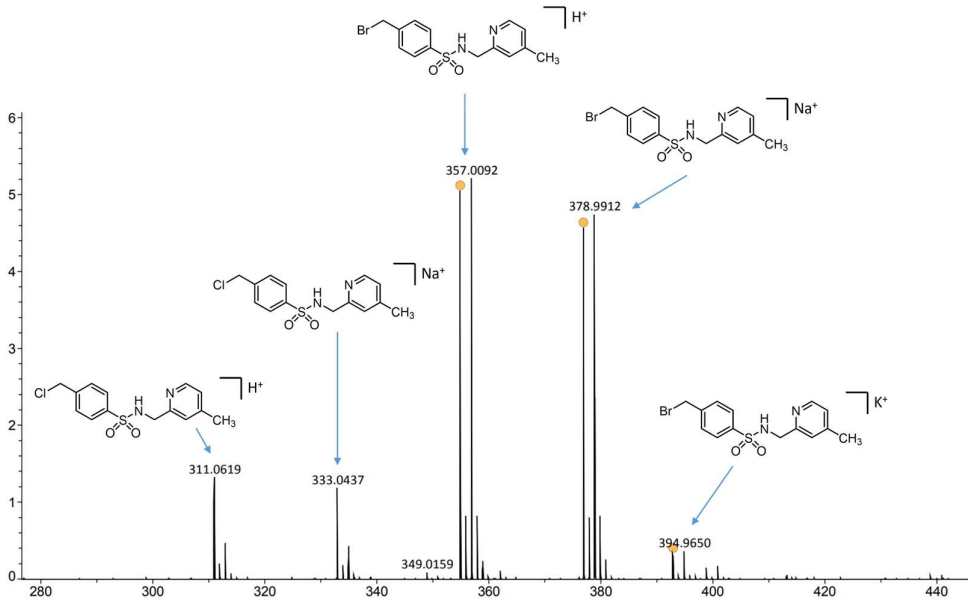


Figure 92 ESI-HRMS spectrum of the intermediate **102b** formed in step one of the Gabriel synthesis routes. It identifies that the bromo-group is partially substituted for chloro- in conditions used for this step.

Aside from these additional observations, characterisation of the intermediate **102b** confirmed successful synthesis by the m/z peaks in the ESI-HRMS spectrum at 357.0092, 378.9912 and 394.9650 agreeing nicely with the expected $[M+H]^+$, $[M+Na]^+$ and $[M+K]^+$ ions. There is a shift in the IR ATIR stretching frequencies of the S=O from 1371 $cm^{-1}$ to 1323 $cm^{-1}$ (asymmetric stretch) and 1172 $cm^{-1}$ to 1154 $cm^{-1}$ (symmetric stretch) on the formation of the sulfonamide group from the sulfonyl chloride. Assignment of the NMR spectra is also in line with similar previously reported compounds,[191] with well resolved peaks of protons of the pyridine ring giving coupling constants of expected magnitude to confirm the exact positions

of the methylsulfonamide- and methyl-substituents. A strong roofing effect is seen between the protons on the aromatic arylsulfonamide group (10 & 11).

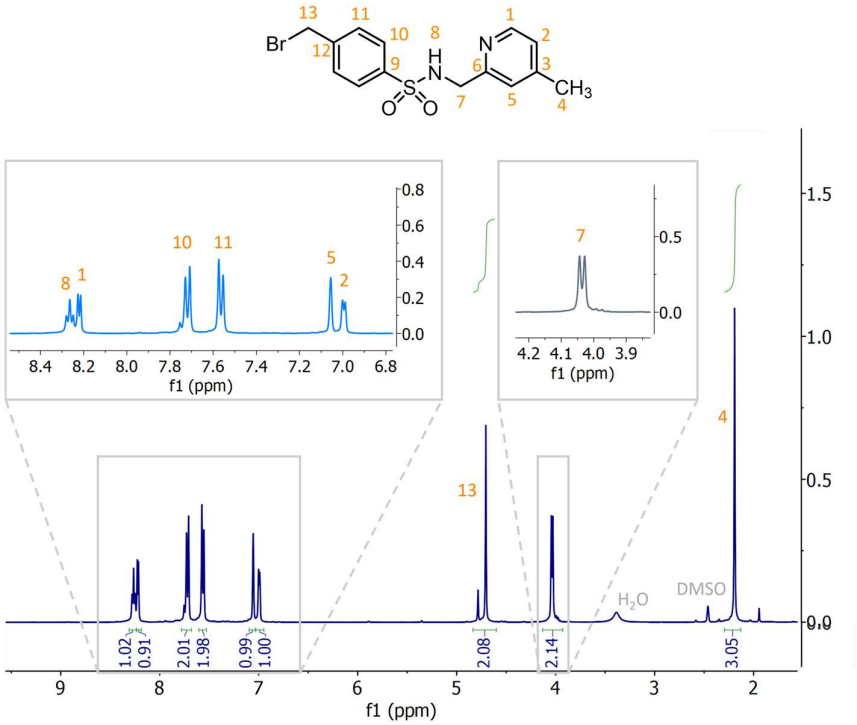


Figure 93 Assigned $^{1}$H NMR spectrum of **102b** (in DMSO-$d_6$). Peaks of the pyridine ring are resolved as multiplets. Two peaks appear in the region of 4.7 ppm corresponding to the proton assigned 13 indicating the exchange of the bromo- group for chloro-. The larger of the peaks is assigned to the desired bromo-substituted intermediate, while the smaller peak is assigned to the chloro-substituted by-product.

The second step in the synthesis requires heating **102** at 100 °C with excess potassium phthalimide salt in DMF. Following the reaction, DMF is removed, and the product extracted with DCM before purification by column chromatography. Synthesis was confirmed using a number of characterisation techniques including ESI-HRMS, ATIR and NMR. The best identifying changes occur in the $^{1}$H NMR spectrum (Figure 94), most notably the appearance of highly characteristic multiplets for the phthalimide group in the 7.8-8.0 ppm region of the spectrum. There is also a small downfield shift for the methylene protons neighbouring the site which is exchanged (13) from 4.71 ppm to 4.80 ppm.

The final step in the Gabriel synthesis is the removal of the phthalimide group with hydrazine to reveal an amine group. This was achieved using a 10-fold excess of hydrazine hydrate in a solution of THF/EtOH. The reaction was heated to reflux for 3 hours. After around 1 hour, formation of phthalhydrazide as a white precipitate could be observed. After cooling, the phthalhydrazide by-product could be removed by filtration and the product isolated as a white

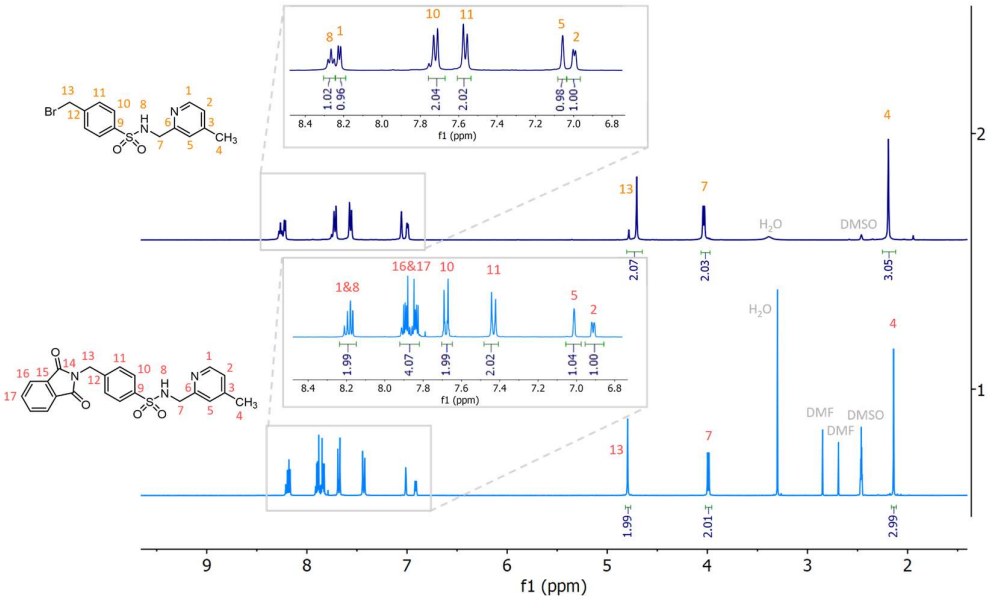


Figure 94 Assigned $^{1}$H NMR spectra (in DMSO-$d_6$) of the intermediates **102b** (dark blue) and **103b** (light blue) of the Gabriel synthesis route. Notable changes include the appearance of the characteristic phthalimide aromatic protons in 7.8-8.0 ppm region accompanying a downfield shift of the protons assigned 13 and an upfield shift of the protons assigned 11.

solid. Further purification was not necessary as analysis by NMR and elemental analysis revealed the good purity of the product, without any signs of reduction of the pyridine ring.

Characterisation including ESI-HRMS, ATIR, NMR and elemental analysis confirmed the synthesis of the expected product **104b**. Changes in the $^{1}$H NMR spectrum (Figure 95) were particularly indicative of this, including the complete disappearance of the characteristic phthalimide peaks in the region 7.8-8.0 ppm and a sizable upfield shift of the peak for the methylene protons (13) from 4.80 ppm in the phthalimide intermediate to 3.74 ppm in the amine product reflecting the change from neighbouring a moderately electron-withdrawing group to a weakly electron-donating group.

All three methylamine-substituted aryl sulfonamides **104a-104c** were successfully produced by this method.

For the synthesis of the whole conjugate (Figure 96), **104a-104c** were coupled to $Bn_4$-azotochelin using HATU as a coupling agent, under basic conditions. Following an acidic and a basic aqueous work-up, the product was purified by column chromatography (initially 100% EtOAc with increasing gradient 0-10% MeOH).

The intermediate **105a** was characterised by ESI-HRMS, IR, NMR, and elemental analysis. The $^{1}$H NMR spectrum (Figure 97; chloroform-$d_1$) was assigned with help from the spectra of the methylamine-substituted aryl sulfonamides (**104a-104c**) and $Bn_4$-azotochelin already

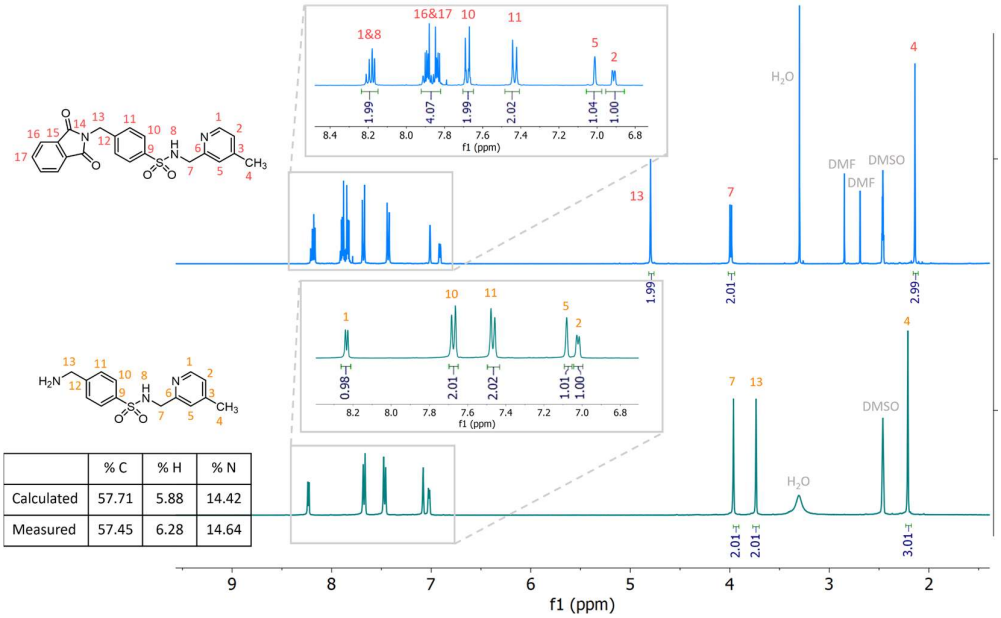


Figure 95 Assigned $^{1}$H NMR spectra of **103b** (light blue) and **104b** (teal) of the Gabriel synthesis route. Notable changes are the disappearance of the typical phthalimide protons in the region 7.8-8.0 ppm as well as a large upfield shift in the signal for the protons assigned 13.

characterised. The aromatic region of the spectrum is very convoluted due to the number of proton signals in these environments, making assignment of peaks difficult except for a few well resolved peaks in the region above 7.5 ppm. Integration of these peaks does correspond to the expected number of protons. Four singlets, each integrating to 2 protons, around 5.0 ppm represent the methylene protons of the four benzyl protecting R groups. The protons at position 12 are resolved as two separate multiplets due to their diastereotopic nature. Overall,

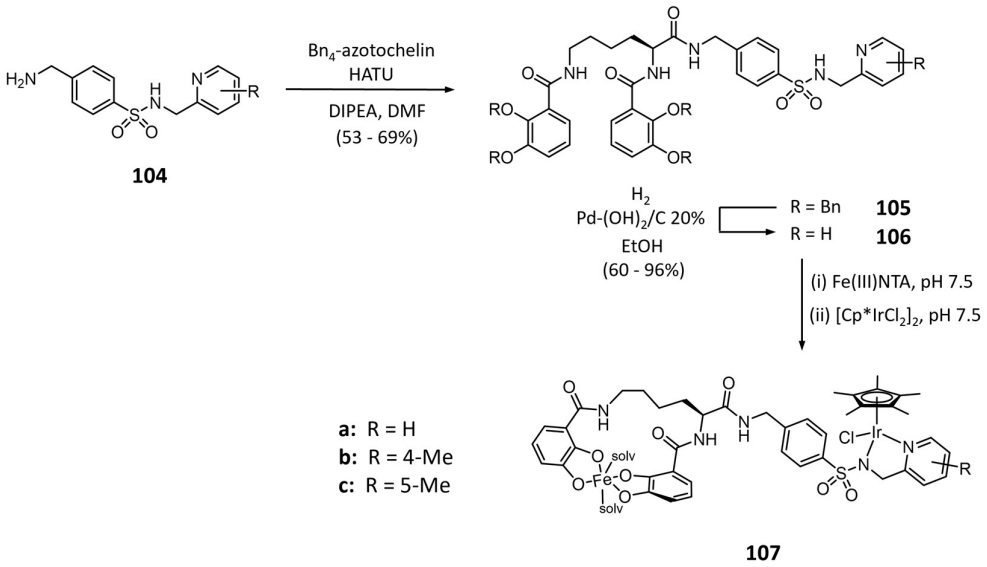


Figure 96 Scheme for the second part of the synthesis of the conjugates.

analysing the characterisation data confirmed the successful synthesis of all three benzyl-protected conjugates **105a-105c**.

In addition to the assigned peaks in the $^{1}$H NMR spectrum, an extra peak at 2.79 ppm indicates the presence of tetramethyl urea (TMU), a by-product of the HATU coupling agent. It was deemed unnecessary to take extra steps to remove TMU at this point of the synthesis since it was not expected to interfere in the next step.

The benzyl groups protecting the catechol groups were removed by hydrogenation using palladium hydroxide on carbon as a catalyst, with a small amount of ammonia added to help protect against reduction of the pyridine ring. It was necessary to treat glassware with 6 M HCl for some hours before hydrogenation to remove trace quantities of Fe(III) and other metal ions, which might coordinate the catechol coordination sites. The product was obtained by removing the solvent (ethanol) after filtration with a Whatman glass microfiber filter to remove the $Pd(OH)_2/C$. The product then had to be stored dry to prevent degradation. Even so, it was necessary to use the compound within a few weeks of synthesis.

Successful synthesis of compounds **106a-106c** was again confirmed by ESI-HRMS, IR, NMR, and elemental analysis. The $^{1}$H NMR spectrum (methanol-$d_4$) is particularly indicative of the successful removal of the benzyl catechol protecting groups by the reduction in the number of peaks in the aromatic region of the spectrum, to leave well-resolved peaks assigned in Figure 97 that integrate to the expected number of protons. The four singlets around 5.0 ppm shown in the spectrum of compound **105a** (dark blue) also disappear in the spectrum of compound **106a** (red), confirming removal of the benzyl groups. Peaks arising from heteroatom-bound protons are not visualised due to the selection of deuterated methanol as the NMR solvent.

Some additional peaks are present in the spectrum, including those marked MeOH and $H_2O$ which occur as contaminants from the deuterated solvent. Some ethanol also remained and proved difficult to remove in entirety. All compounds were stored in a vacuum desiccator before use in the ArMs to minimise remaining solvent. The peak at 2.79 ppm still remains as the solubility of TMU is relatively high in the solvents used for the reaction and purification of our product. It may be possible to reduce the amount of TMU in the sample by additional washing steps with solvents in which the desired product is not soluble but TMU is more so. It was decided, however, that additional and potentially challenging steps to remove TMU would not be needed as, although a tall peak, the peak only integrates to give a molar ratio of around 0.1, for all three compounds **106a-106c**. It is also thought TMU would not interfere in the binding of metals to conjugates **107a-107c**, or the conjugate with the protein, so the compound was used without further purification to remove TMU.

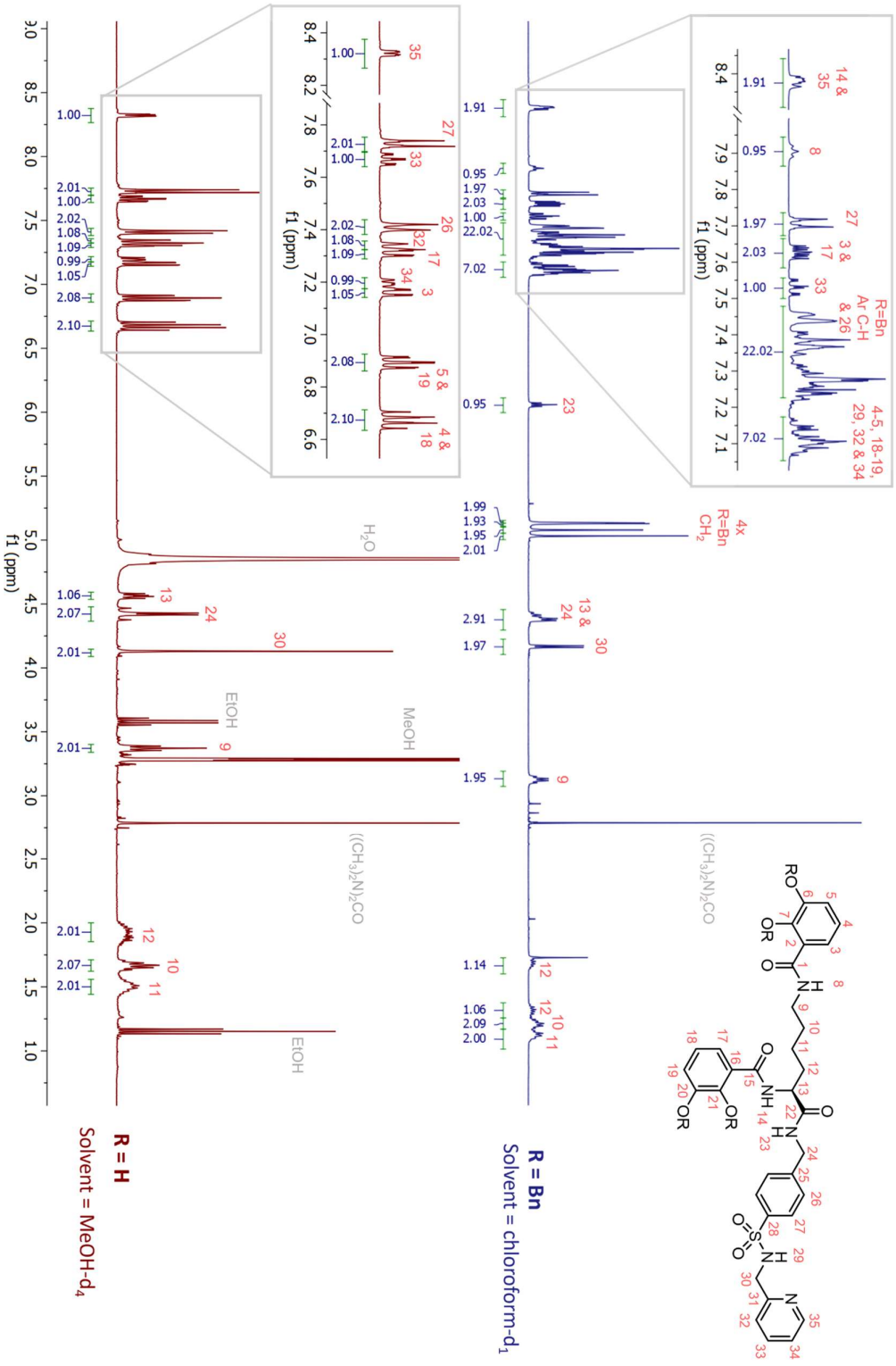


Figure 97 Assigned $^{1}$H NMR spectra of compound **105a** (dark blue) and compound **106a** (red).

The final steps in the synthesis of the conjugates were to coordinate Fe(III) and Cp*Ir selectively. First, a solution of Fe(III)-NTA (prepared as previously described[181]) was added, with Fe(III) coordination being strongly favoured at the catechol sites. A solution of $[Cp^*IrCl_2]_2$ was then added which resulted in Cp*Ir unit binding in the sulfonamide/pyridine bidentate site, leading to the formation of the complete conjugate **107a-107c**.

The final compound could not be analysed by NMR due to the paramagnetic state of Fe(III), and HRMS was challenging due to the multiple potential ions that could be formed. Instead metal complexation was confirmed by UV-vis spectroscopy (Figure 98), with characteristic absorption maxima at 326 nm and 535 nm.

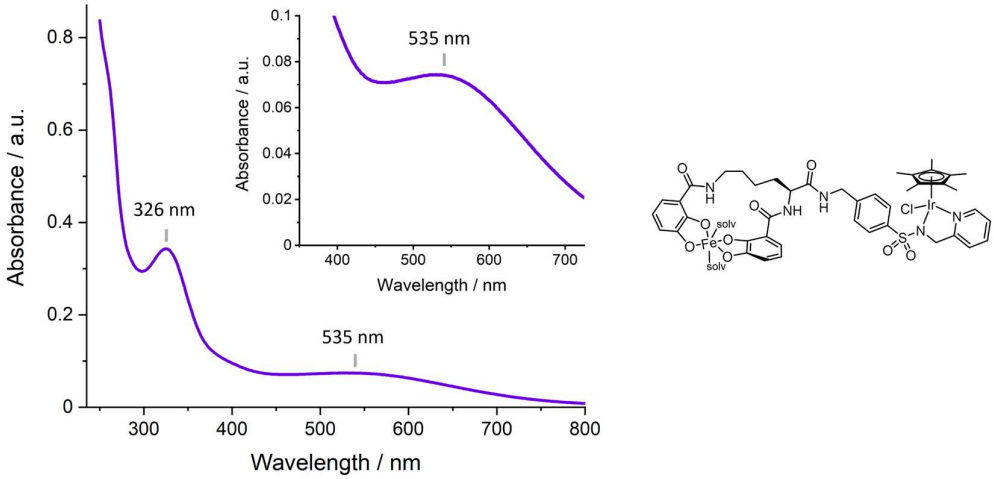


Figure 98 UV-vis spectrum between 250-800 nm for the conjugate **107a**. Two maxima at 326 nm and 535 nm are indicated. The inset spectrum shows more clearly the second maximum at 535 nm.

## 4.2.1 Catalytic Activity Testing of the Siderophore-Catalyst Conjugates

Conjugates **107a-107c** were assessed for their ability to catalyse the transfer hydrogenation of imine **1a** to (*R*,*S*)-salsolidine, **1b**. The catalytic conditions were similar to those reported in the test of the iridium catalysts in Chapter 3, namely 50 mmol $dm^{-3}$ substrate, 0.125 mmol $dm^{-3}$ conjugate, 3 mol $dm^{-3}$ sodium formate at pH 5.8 (0.6 mol $dm^{-3}$ MES), 40 °C with stirring.

First, control experiments were used to establish that the substrate does not convert to the product under the above conditions in the absence of the conjugate or catalyst over a period of 72 hours. The conjugate minus the Cp*Ir- component was also examined for catalytic activity. This control though showed a conversion of 3% in 24 hours (Appendix 1). The activity was attributed to trace amounts of palladium leached from the $Pd(OH)_2/C$ used to catalyse the

removal of benzyl groups in preparation of the conjugate. This background level of activity is negligible, however, when compared to the rate of catalysis for all conjugates and ArMs.

All three conjugates showed very similar levels of activity for catalysing the reaction (Figure 99). This is in contrast to the trend observed in Chapter 3. They all catalyse the reaction slower than their equivalent iridium catalysts reported in Chapter 3, with all conjugates completing the reaction within 30 minutes, compared to 10 minutes and 7 minutes for the pyridine and methyl-substituted pyridine alternatives, respectively. This was attributed to the significantly bulkier and flexible component added in the conjugate, which limits the accessibility of the catalytic site. A very similar degree of reduced catalytic efficiency was observed for the pyridine conjugate previously.[100]

None of the three conjugates displayed any enantioselectivity, as expected.

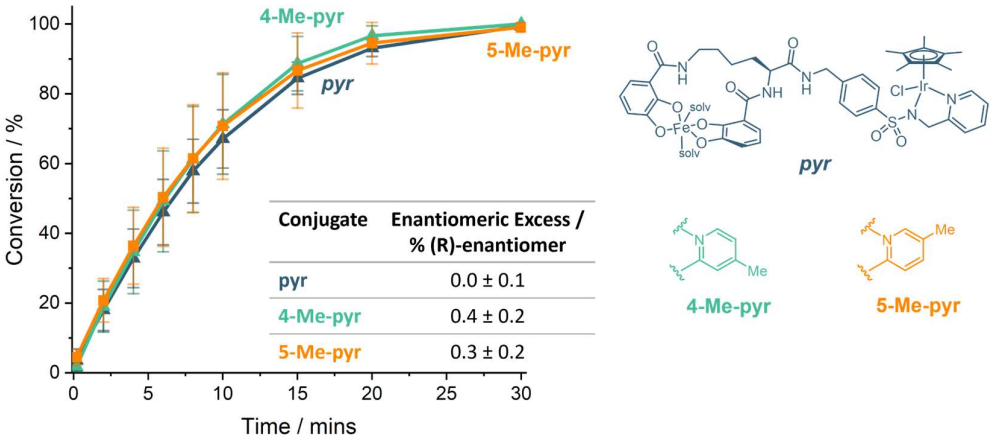


Figure 99 Plot showing the conversion of imine **1a** to (*R,S*)-salsolidine, **1b**, by conjugates pyr (**107a**), 4-Me-pyr (**107b**) and 5-Me-pyr (**107c**). Table reports the enantiomeric excess of the reaction for each conjugate, confirming that none of the conjugates is enantioselective. Conditions: 50 mmol $dm^{-3}$ substrate, 0.125 mmol $dm^{-3}$ conjugate, 0.6 mol $dm^{-3}$ MES pH 6.0, 3 mol $dm^{-3}$ sodium formate, stirring, 40 °C. Reaction data is displayed as the average (data points) and standard deviation (error bars) from three repeats. Enantiomeric excess data is reported as the average enantiomeric excess measured at 100% conversion of substrate and standard deviation from three repeats.

## 4.3 Preparation of the Artificial Metalloenzymes

All three proteins - *Cj*CeuE, Gst and Pth - were prepared and purified by Dr. Elena Blagova and supplied as concentrated protein stock.

The concentrated protein stocks were diluted to approximately 30-40 µmol $dm^{-3}$ and the concentration measured using the absorption at 280 nm in UV-vis spectroscopy. The concentration was calculated using the Beer-Lambert law, using extinction coefficients measured by Dr Alex Miller for each of the three proteins (*Cj*CeuE = 18,585 $dm^3$ $mol^{-1}$ $cm^{-1}$,

Pth = 29,196 $dm^3$ $mol^{-1}$ $cm^{-1}$, Gst = 34,239 $dm^3$ $mol^{-1}$ $cm^{-1}$).[182] The artificial enzymes were then assembled from a selected conjugate and protein combination by adding the conjugate stock solution to protein solution give a 1:1 ratio of conjugate to protein. Conjugates were added to the protein in a 1:1 ratio to reduce the chance of non-specific binding since we expect binding of the conjugate at the Fe-siderophore binding site to be thermodynamically the most favourable. The solutions were then left standing for 3 hours at 4 °C to allow time for the conjugate binding to reach equilibrium. Analysis by UV-vis spectra (Figure 100) was used to monitor the binding of the conjugate in the protein, with a distinctive shift in the maxima at 326 nm ($\lambda_1$) to longer wavelengths and slight changes of the second maxima at ($\lambda_2$) on binding compared to the unbound cofactor.

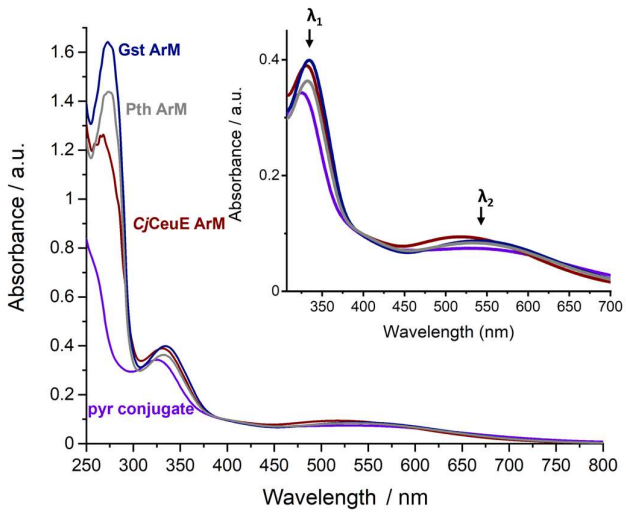


| | $\lambda_1$ / nm | $\lambda_2$ / nm |
|---|---|---|
| **pyr conjugate** | 326 | 535 |
| **CeuE ArM** | 331 | 520 |
| **Gst ArM** | 334 | 536 |
| **Pth ArM** | 333 | 541 |

Figure 100 UV-vis spectra comparing the change in $\lambda_1$ and $\lambda_2$ from the free conjugate (purple) in solution to the protein-encapsulated conjugate of the ArMs, with the *Cj*CeuE ArM (dark red), Pth ArM (grey) and Gst ArM (dark blue).

After incubating the protein with the cofactor for 3 hours, the ArMs were concentrated using spin concentrators with a 10 kDa cut-off to approximately 1-2 mmol $dm^{-3}$. The solution was washed with a further 2 mL buffer to ensure any unbound cofactor had been removed as unbound cofactor will pass through the 10 kDa filter, while the ArMs will remain in the concentrated fraction. The solution that passed through the cut-off filter was measured by UV-vis spectroscopy to check if the conjugate had not bound to the protein. For all ArMs, no

absorption peaks were seen in this solution. The concentrated ArM solutions were transferred to clean falcon tubes and stored at 4 °C overnight in preparation for catalytic testing.

A drawback for this method of ArM preparation was that the measurement of the volume of the concentrated sample of ArM is relatively inaccurate and hence the final concentration of ArM calculated has a high degree of error which introduces significant error into the catalytic testing experiments. This is discussed in more detail in the following subsection.

### 4.3.1 Catalytic Activity Testing of the Artificial Metalloenzymes

Analogous conditions to those for activity testing of the free conjugates were used for the ArMs. The reason pH 5.8 was selected for all activity testing is that it was previously determined to be optimal for the reported PBP ArM.[100]

From the three different conjugates prepared (with pyridine ligand, 4-Me substituted pyridine ligand and 5-Me substituted pyridine ligand) and the 3 periplasmic binding proteins (*Cj*CeuE, Gst and Pth), nine different ArMs were prepared, including the design originally published in Nat. Catal. 2018.[100] In the rest of this chapter, the following terminology will be used to name the ArM being discussed: "ligand type"_"siderophore"_"protein scaffold" (Figure 101).

Terminology:

"ligand type"_"siderophore"_"protein scaffold"

| ligand type | siderophore | protein scaffold |
|---|---|---|
| **pyr** = pyridine (**107a**) | **azoto** = azotochelin | **CjCeuE** |
| **4-Me-pyr** = 4-Me-substituted pyridine (**107b**) | | **Gst** |
| **5-Me-pyr** = 5-Me-substituted pyridine (**107c**) | | **Pth** |

Figure 101 Explanation of the terminology used in identifying the ArM in the discussion.

Control experiments to demonstrate the apo protein does not catalyse the reduction of imine **1a** in the absence of the conjugate had previously been carried out.[100]

The ArMs composed of the *Cj*CeuE protein scaffold were the starting point for catalytic activity testing (Figure 102) since the pyr_azoto_*Cj*CeuE ArM has already been reported.[100] The data recorded in these experiments agreed reasonably closely with those reported, with an enantiomeric excess of 29.5% for the (*R*)-enantiomer compared to 31-35%, respectively. The catalytic rate, as recorded by turnover frequency (TOF), was 0.28 $min^{-1}$ compared to 0.30 $min^{-1}$ reported in the literature. Slight differences in catalytic rate can arise from a number of factors including small differences in pH. This could be a possible explanation in the differences reported here since the pH of the buffer used for these experiments was adjusted to achieve

pH 5.8 at 40 °C using an online buffer calculating tool (https://www.liverpool.ac.uk/pfg/Tools/BuffferCalc/Buffer.html), whereas the previous work prepared the buffer to pH 6.0 at room temperature, which was less carefully controlled. Even a very small difference in pH can have a significant change in the rate of these ArM catalysed reactions.

The addition of a methyl-substituent onto the pyridine ring of the conjugates made a significant difference to the catalytic activity of the ArMs, particularly depending on its position. The (4-Me-pyr)_azoto_*Cj*CeuE ArM catalysed the reaction at a similar rate to the pyr_azoto_*Cj*CeuE ArM, but with much improved enantioselectivity, increasing to an enantiomeric excess of 47.7%. The (5-Me-pyr)_azoto_*Cj*CeuE ArM proved a very poor catalyst, however, with a much-reduced catalytic rate, achieving only 73% conversion to product after 48 hours and a lower enantiomeric excess of 9.5%. Some precipitate was observed during the catalytic tests of (5-Me-pyr)_azoto_*Cj*CeuE ArM that was not apparent for the other two ArMs and perhaps contributed to the poor catalytic activity. The 5-Me-pyr conjugate could be causing some conformational change on binding in the protein scaffold making it less soluble in solution or more inclined to aggregate.

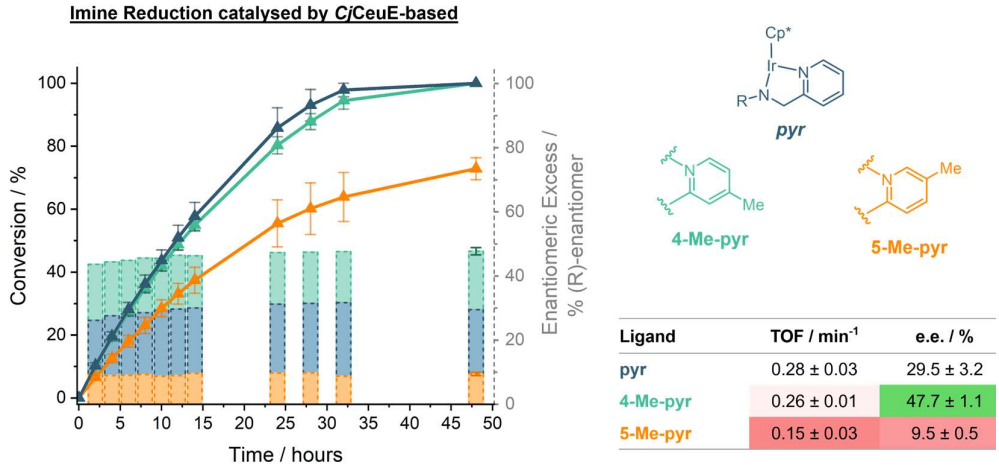


| Ligand | TOF / min$^{-1}$ | e.e. / % |
|---|---|---|
| pyr | 0.28 ± 0.03 | 29.5 ± 3.2 |
| 4-Me-pyr | 0.26 ± 0.01 | 47.7 ± 1.1 |
| 5-Me-pyr | 0.15 ± 0.03 | 9.5 ± 0.5 |

Figure 102 Plot of conversion (points & solid lines) of imine **1a** to (*R,S*)-Salsolidine catalysed by *Cj*CeuE-based ArMs. The enantiomeric excess during the reaction is displayed as an inset bar chart, corresponding to the right-hand y-axis. The dark blue line/bar represents the pyr_azoto-*Cj*CeuE ArM catalysed reaction, the teal line/bar represents the (4-Me-pyr)_azoto-*Cj*CeuE catalysed reaction and the orange line/bar represents the (5-Me-pyr)_azoto-*Cj*CeuE catalysed reaction. Conditions: 50 mmol dm$^{-3}$ substrate, 0.125 mmol dm$^{-3}$ ArM, 0.6 mol dm$^{-3}$ MES pH 6.0, 3 mol dm$^{-3}$ sodium formate, stirring, 40 °C. Reaction data is displayed as the average (data points) and standard deviation (error bars) from three repeats. Enantiomeric excess data is reported as the average enantiomeric excess measured at 100% conversion of substrate and standard deviation from three repeats.

The activity of the Pth and Gst ArMs were remarkably different from those of *Cj*CeuE. All ArMs for Pth and Gst were notably faster for the transfer hydrogenation of imine **1a**, and

whereas the 4-Me-pyr ligand was the most enantioselective choice of ligand for *Cj*CeuE ArMs, 5-Me-pyr was the best performing in Gst and Pth ArMs.

The ArMs of Pth (Figure 103) display TOFs at least 7-fold faster than their equivalent *Cj*CeuE-based ArM. In the case of pyr_azoto_Pth, this improved catalytic rate comes at the cost of enantioselectivity compared to pyr_azoto_*Cj*CeuE, falling from 29.5% e.e. to 23.4% e.e. The inclusion of a methyl substituent on the pyridine ring of the conjugate produces ArMs with faster rates of catalysis than the unsubstituted pyridine conjugate, as was the expected trend following the result of the iridium catalysts in Chapter 3. Adding the methyl in the 4-position resulted in decreased enantioselectivity (e.e. 16.7%) compared to the unsubstituted ring (e.e. 23.4%), however, placing the methyl at the 5-position led to an improvement in enantioselectivity (e.e. 34.9%).

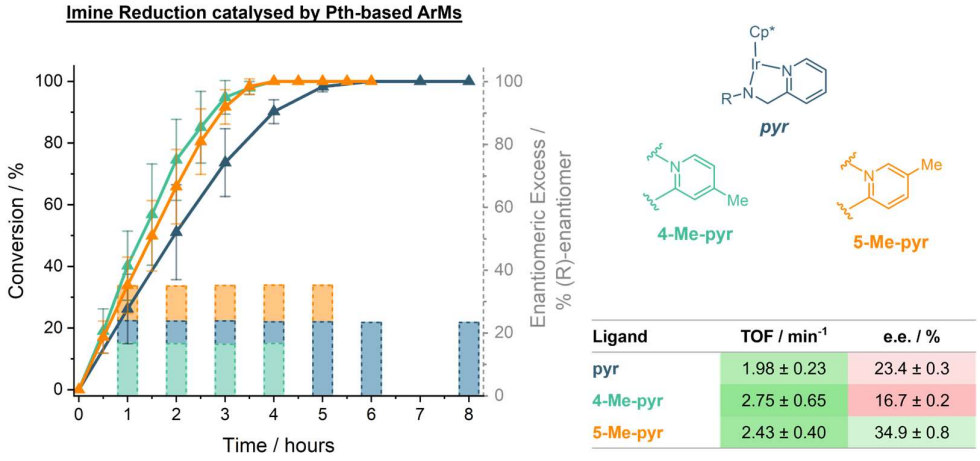


| Ligand | TOF / $min^{-1}$ | e.e. / % |
|---|---|---|
| pyr | 1.98 ± 0.23 | 23.4 ± 0.3 |
| 4-Me-pyr | 2.75 ± 0.65 | 16.7 ± 0.2 |
| 5-Me-pyr | 2.43 ± 0.40 | 34.9 ± 0.8 |

Figure 103 Plot of conversion (points & solid lines) of imine **1a** to (*R,S*)-Salsolidine catalysed by Pth-based ArMs. The enantiomeric excess during the reaction is displayed as an inset bar chart, corresponding to the right-hand y-axis. The dark blue line/bar represents the pyr_azoto-Pth ArM catalysed reaction, the teal line/bar represents the (4-Me-pyr)_azoto-Pth catalysed reaction and the orange line/bar represents the (5-Me-pyr)_azoto-Pth catalysed reaction. Conditions: 50 mmol $dm^{-3}$ substrate, 0.125 mmol $dm^{-3}$ ArM, 0.6 mol $dm^{-3}$ MES pH 6.0, 3 mol $dm^{-3}$ sodium formate, stirring, 40 °C. Reaction data is displayed as the average (data points) and standard deviation (error bars) from three repeats. Enantiomeric excess data is reported as the average enantiomeric excess measured at 100% conversion of substrate and standard deviation from three repeats.

The Gst-based ArMs were even faster than Pth-based ArMs, with pyr_azoto_Gst, giving a more than 9-fold improvement in turnover frequency compared to the equivalent ArM of *Cj*CeuE (Figure 104). The pyr_azoto_Gst ArM has lower enantioselectivity than the pyr_azoto_*Cj*CeuE counterpart. Incorporating a methyl substituent on the pyridine ring further improves catalytic rate, more so for (5-Me-pyr)_azoto_Gst. In both cases of methyl-substituted conjugates, the enantioselectivity of the ArM improves relative to the unsubstituted-pyridine ArM, particularly for (5-Me-pyr)_azoto_Gst which catalysed the reaction with an enantiomeric excess of 37.2%.

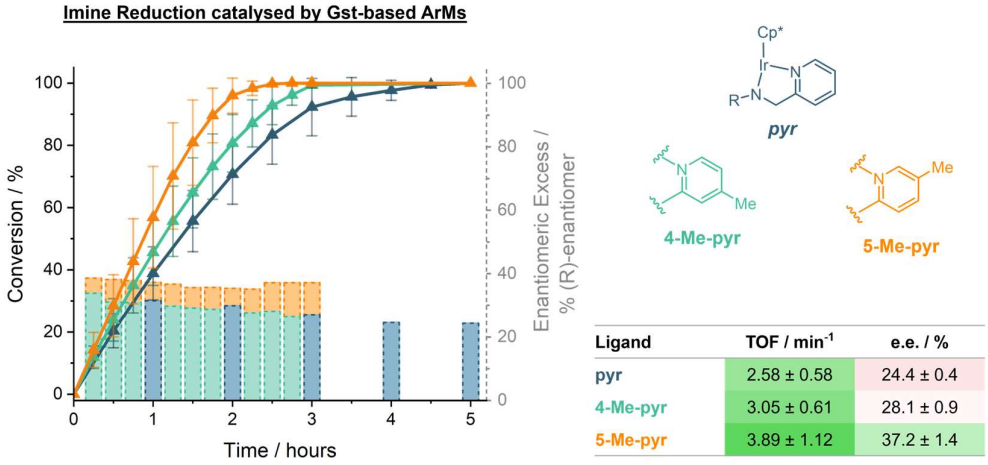


| Ligand | TOF / $min^{-1}$ | e.e. / % |
|---|---|---|
| pyr | 2.58 ± 0.58 | 24.4 ± 0.4 |
| 4-Me-pyr | 3.05 ± 0.61 | 28.1 ± 0.9 |
| 5-Me-pyr | 3.89 ± 1.12 | 37.2 ± 1.4 |

Figure 104 Plot of conversion (points & solid lines) of imine **1a** to (*R,S*)-Salsolidine catalysed by Gst-based ArMs. The enantiomeric excess during the reaction is displayed as an inset bar chart, corresponding to the right-hand y-axis. The dark blue line/bar represents the pyr_azoto-Gst ArM catalysed reaction, the teal line/bar represents the (4-Me-pyr)_azoto-Gst catalysed reaction and the orange line/bar represents the (5-Me-pyr)_azoto-Gst catalysed reaction. Conditions: 50 mmol $dm^{-3}$ substrate, 0.125 mmol $dm^{-3}$ ArM, 0.6 mol $dm^{-3}$ MES pH 6.0, 3 mol $dm^{-3}$ sodium formate, stirring, 40 °C. Reaction data is displayed as the average (data points) and standard deviation (error bars) from three repeats. Enantiomeric excess data is reported as the average enantiomeric excess measured at 100% conversion of substrate and standard deviation from three repeats.

The degree of error introduced in preparing the ArM for catalysis testing (in the measurement of the volume of the concentrated ArM solution) is particularly noticeable in the results of ArMs with faster catalytic rates. There is need for a new method to be developed which reduces the degree of error in this part of the experiment. However, there are constraints since measurement of the protein concentration of the concentrated protein stock by nanodrop is very inaccurate and the concentration must be remeasured before preparation of the ArM to ensure a 1:1 ratio of conjugate is added. To do this, the concentrated stock must be diluted to 30-40 µmol $dm^{-3}$ which is the measurable range for the cuvettes of 1 cm path length. Cuvettes with smaller path lengths could potentially be used which would allow an increased concentration in the range of 150-200 µmol $dm^{-3}$. This more concentrated solution should pose no problem for conjugate binding, regardless, the ArM solution would still have to be concentrated before use in catalytic testing experiments. This is because the solution when binding the conjugate in the protein is usually controlled to pH 7.5 while catalytic testing is conducted at pH 5.8. The addition of a small volume of concentrated ArM stock at pH 7.5 into a large volume of pH 5.8 buffered solution ensures the pH 5.8 remains stable. Attempting to bind the conjugate at lower pH would be a concern as His227, an important residue in binding siderophores, may be partially doubly protonated at pH 5.8 (free histidine has a p$K_a$ of 6.0). Histidine aids binding of the siderophore by coordinating to Fe(III), or potentially the Ir in the

ArM.[100] If protonated, forming this interaction will be less energetically favourable and the conjugate might bind more slowly, and/or with lower affinity.

It is true, however, that if the affinity of the conjugate for the protein is lower at pH 5.8 than pH 7.5, the equilibrium that determines what proportion of protein is occupied with the conjugate should still be reached, regardless of the pH at which the ArM was formed. Lowering the pH to 5.8 following ArM formation at pH 7.5 could, therefore, result in leaching some conjugate from the protein, contributing to lower enantioselectivity than truly representative during catalysis testing experiments. It is encouraging, however, that the e.e. remains almost constant throughout the catalysis testing experiments for all ArMs, which would not be the case if there was noticeable unbound conjugate in solution. If there was a significant proportion of unbound cofactor in solution, the e.e. would be expected to decrease throughout the experiment due to the faster catalytic rate of the unbound, unselective cofactor in relation to bound cofactor in the ArM.

An adjustment to the catalysis testing method to reduce error could be to dilute the concentrated ArM sample with a small volume of pH 5.8 buffer (for example, approximately 1:1 concentrated ArM:pH 5.8 buffer) before remeasuring the volume to calculate the concentration of the ArM solution. A larger volume should reduce the degree of error in measuring the volume and hence reduce the error in the final concentration of ArM used in the experiment.

Table 4 Table summarising the catalytic activity of each of the nine ArMs investigated in this chapter.

| | *Cj*CeuE | | Pth | | Gst | |
|---|---|---|---|---|---|---|
| | TOF /min$^{-1}$ | ee / % R | TOF / min$^{-1}$ | ee / % R | TOF / min$^{-1}$ | ee / % R |
| pyr | 0.28 ± 0.03 | 29.5 ± 3.2 | 1.98 ± 0.23 | 23.4 ± 0.3 | 2.58 ± 0.58 | 24.4 ± 0.4 |
| 4-Me-pyr | 0.26 ± 0.01 | 47.7 ± 1.1 | 2.75 ± 0.65 | 16.7 ± 0.2 | 3.05 ± 0.61 | 28.1 ± 0.9 |
| 5-Me-pyr | 0.15 ± 0.03 | 9.5 ± 0.5 | 2.43 ± 0.40 | 34.9 ± 0.8 | 3.89 ± 1.12 | 37.2 ± 1.4 |

Of all the ArMs, (4-Me-pyr)_azoto_*Cj*CeuE catalysed the reaction with highest enantioselectivity but the vastly improved TOF of the Gst- and Pth-based ArMs make them far more attractive to pursue (Table 4). Of these, both the fastest and most enantioselective ArM was (5-Me-pyr)_azoto_Gst, with a TOF of 3.89 min$^{-1}$ and an e.e. of 37.2%. This represents an almost 14-fold improvement in TOF (Figure 105) in addition to improved enantioselectivity compared to the previously published PBP ArM. To put in another context, the already reported pyr_azoto_*Cj*CeuE ArM completes the reaction (50 mmol dm$^{-3}$ substrate, 400 turnovers) in under two days whereas the best identified new ArM completes the reaction

in a more practical 2.5 hours. The degree to which the TOF is reduced on binding the cofactor decreases from 20-fold reported by Raines *et al.*[100] to 8.5-fold.

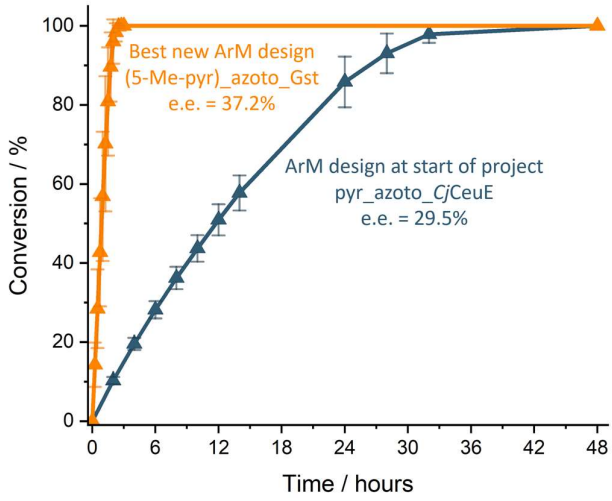


Figure 105 Plot comparing the catalysed conversion of imine **1a** to (*R,S*)-Salsolidine by the design of previously reported PBP ArM[100](dark blue) to the overall best performing new design ArM (5-Me-pyr)_azoto_Gst (orange). Conditions: 50 mmol $dm^{-3}$ substrate, 0.125 mmol $dm^{-3}$ ArM, 0.6 mol $dm^{-3}$ MES pH 6.0, 3 mol $dm^{-3}$ sodium formate, stirring, 40 °C.

The difference in catalytic activity across the ArMs will depend on a number of contributing factors. It is proposed that the major improvement in catalytic rate between the ArMs of the thermophilic proteins and *Cj*CeuE is largely due to the sequence of the flexible loop. This region for both thermophilic proteins is more rigid, with the replacement of a number of amino acids with bulkier residues with larger side-chains compared to *Cj*CeuE. The differing distribution of charged residues could also alter the flexibility of the loop. This theory is also supported by the experimental crystal structures for apo and azotochelin-bound proteins where *Cj*CeuE is observed with the flexible loop in the "open" position in the apo protein and the "closed" position on binding azotochelin, whereas both Gst and Pth are found to be in the "closed" position for both apo structures and azotochelin-bound structures.

Lower flexibility in the loop could either have led to strengthening of the His227-Ir interaction if the position of His227 was held more rigidly in the optimal position or weakening of the His227-Ir interaction if the position of His227 is now less optimal. The results of the catalytic testing suggest this second hypothesis is correct since a weaker interaction will result in a faster catalytic rate. This would further explain the reduced enantiomeric excess for the ArMs with the unsubstituted pyridine ligand as the enantioselectivity for the two ArMs of the thermophilic proteins show lower e.e. than the *Cj*CeuE ArM. This can be rationalised by a

weaker His227-Ir interaction imparting less stereo-control of the Ir centre, leading to more frequent inversion of the Ir centre and a higher proportion of transfer hydrogenation occurring at the larger, unselective pocket for the substrate. This is also in line with the observation that the H227A mutant erases almost all enantioselectivity as the interaction that causes the Ir complex to adopt a single configuration, which is responsible for the enantioselectivity, is removed.

The positioning of methyl groups on the pyridine ring brings additional conjugate-protein interactions, which have an further influence on catalytic performance. In the case of the *Cj*CeuE ArMs, positioning the methyl group in the 4-position is favoured compared to the 5-position (Figure 106). The most significant interactions involved are most probably steric, between the conjugate and the His227-containing loop. Positioning the methyl group at a site which causes an increase in steric interaction on inversion of the Ir centre would produce an ArM with higher enantioselectivity since inversion of Ir becomes less favourable. The reverse would be true if the methyl group occupies a position where steric interactions are eased on inversion of the Ir centre. For ArMs of *Cj*CeuE, the change in the positioning of a relatively small substituent must be sufficient in the difference between these two possibilities. Similar themes apply to the ArMs of Gst and Pth, although this time positioning the methyl at the 5-position results in the most positive outcome.

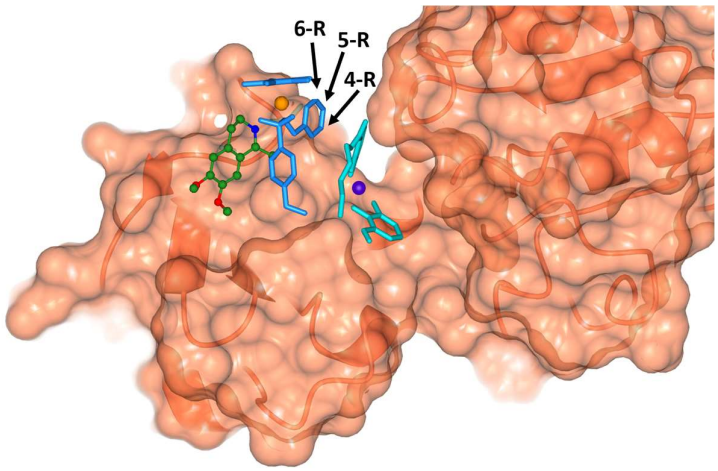


Figure 106 Crystal structure of the original PBP ArM[100] (PDB code: 5OD5) indicating the 4- and 5- substitution positions on the pyridine ring.

## 4.3.2 Variable Temperature Catalysis by the Artificial Metalloenzymes of Thermophilic Proteins

One of the reasons behind investigating the thermophilic proteins for the ArMs was that they offer additional stability at high temperatures. This was an important advantage since the

previously reported ArM with *Cj*CeuE had a very slow catalytic rate; it seemed advantageous to be able to access higher temperatures to help improve the catalytic rate. A thermal shift assay determined the temperature of denaturation ($T_m$) of the thermophilic apo proteins to be over 20 °C higher than *Cj*CeuE ($T_m$(*Cj*CeuE) = 60.4 °C, $T_m$(Pth) = 82.5 °C, $T_m$(Gst) = 80.9 °C).[192]

In addition, constructing the ArMs from the thermophilic proteins had already given hugely improved reactions rates, even before increasing the temperature above 40 °C. This prompted us to consider investigating both higher temperatures, as planned, but also lower temperatures since it has been demonstrated that enantioselectivity of some enzyme-catalysed reactions can be improved by reducing the temperature the reaction is carried out at.[40,193,194] Intuitively, this can be explained by lower kinetic energies of the protein structure resulting in a more rigid and highly organised environment able to influence enantioselectivity to a greater degree, but this is not always the case.[193,194] The much improved catalytic rate of the ArMs of the thermophilic proteins offers the opportunity to explore lower temperatures, something that was not feasible with the much slower *Cj*CeuE-based ArMs.

Since the conjugate with the 5-Me pyridine substituent performed best in terms of enantioselectivity for both Gst and Pth proteins, this conjugate was selected for the variable temperature experiments. The temperature of the reactions was controlled by oil baths surrounding conducting metal heating blocks in which the reaction flasks were placed. The temperatures were monitored at regular intervals throughout the reactions with the help of thermometers. 60 °C and 40 °C were achieved by using the heating setting on stirring hotplates. 20 °C was maintained using the room temperature of the lab, which is temperature controlled. Regular monitoring of the 20 °C oil bath showed a very consistent temperature of 20 °C despite the method being “uncontrolled”. An oil bath was maintained at 5 °C with the heating block placed in a jacketed water bath connected to a water circulator cooling the water to 5 °C. All reactions were stirred at a sufficient speed to neglect the rate of diffusion.

Both ArMs showed the expected trend, with higher enantioselectivity at lower temperature and the enantioselectivity decreasing as the temperature is increased (Figure 107). The (5-Me-pyr)_azoto_Gst ArM showed a much more pronounced change in enantioselectivity across the temperature gradient, while (5-Me-pyr)_azoto_Pth ArM shows only a very small change in enantioselectivity with temperature. The measurement at 5 °C appears to fall below the expected trend for the (5-Me-pyr)_azoto_Pth ArM but this may be due to the higher degree of error in calculating the integrated peak area of small peaks in the HPLC trace, since the conversion of the reaction is only 18% at 48 hours.

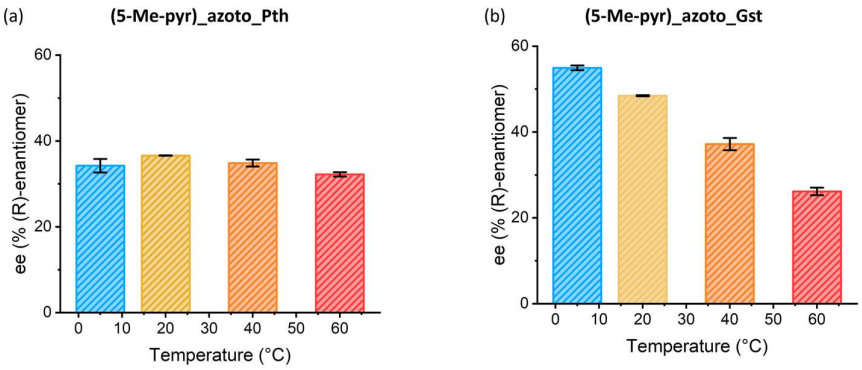


| ArM | | 5 °C | 20 °C | 40 °C | 60 °C |
|---|---|---|---|---|---|
| (5-Me-pyr)_azoto_Pth | e.e. / % (R)-enantiomer | 34.2 ± 1.6* | 36.6 ± 0.1 | 34.9 ± 0.8 | 32.2 ± 0.5 |
| | Time to reach 100% conversion / hours | **18% after 48 hours | <24[1] | 4 | 0.667 |
| (5-Me-pyr)_azoto_Gst | e.e. / % (R)-enantiomer | 55.0 ± 0.6 | 48.4 ± 0.1 | 37.2 ± 1.4 | 26.2 ± 0.9 |
| | Time to reach 100% conversion / hours | **79% after 48 hours | 7 | 2.75 | 0.333 |

Figure 107 Bar charts showing the enantiomeric excess of the catalysed transfer hydrogenation of imine **1a** against temperature of (a) (5-Me-pyr)_azoto_Pth and (b) (5-Me-pyr)_azoto_Gst. Temperatures: 5 °C (blue), 20 °C (yellow), 40 °C (orange) and 60 °C (red). Table reporting the enantiomeric excess and the time taken for the reaction to reach completion as measured for each ArM and temperature. *note this figure is less accurate than the other sets of conditions due to the higher error in integrating smaller peaks in the HPLC trace. [1] completed well within 24 hours, reached 82% in 12 hours. ** Reaction did not reach completion within 48 hours therefore conversion at 48 hours is reported instead. Conditions: 50 mmol $dm^{-3}$ substrate, 0.125 mmol $dm^{-3}$ ArM, 0.6 mol $dm^{-3}$ MES pH 6.0, 3 mol $dm^{-3}$ sodium formate, stirring.

An e.e. of 55% achieved with (5-Me-pyr)_azoto_Gst at 5 °C is the highest e.e. recorded for the PBP ArM design, however, the reaction is impractically slow with a conversion of only 79% after 48 hours. A more encouraging result is that an e.e. of 48.4% can be achieved with the same ArM at room temperature with 100% conversion within 7 hours, significantly slower than at 40 °C, but more practical in a number of applications where heating the reaction may be challenging. The rate of catalysis was very high for both ArMs at 60 °C, but with reduced enantioselectivity, making it unattractive since the main aim of designing ArMs is to induce high levels of enantioselectivity.

The difference in behaviour between (5-Me-pyr)_azoto_Pth and (5-Me-pyr)_azoto_Gst is difficult to rationalise with certainty. The theory that both proteins possess relatively rigid loops containing the coordinating histidine would agree with the trend in enantioselectivity with changing temperature. At higher temperatures, more energy is supplied for His227-Ir bond dissociation, together with a higher rate of inversion at the Ir centre, so would lead to reduced enantioselectivity. By this explanation, the enantioselectivity would decrease as the

temperature increases, as demonstrated. The minimal change in enantioselectivity for (5-Me-pyr)_azoto_Pth at different temperatures indicates that temperature has a very low effect on increasing His227-Ir dissociation and/or inversion of the Ir stereo-centre. Conversely, the (5-Me-pyr)_azoto_Gst ArM shows a more pronounced trend, closer to what might be expected.

The protonation state of this histidine could be a factor to consider in explaining this difference in behaviour since this will influence the strength of the interaction between histidine and the iridium metal centre. The protonation state depends on the $pK_a$ of the histidine residue which will be influenced by neighbouring residues, so may differ slightly between the two proteins due to their different amino acid composition. Measuring the $pK_a$ of histidine residues experimentally remains challenging[195] and use of models to calculate theoretical values have only recently been described and are not yet widely used.[196] Alternatively, the isoelectric point (PI value) of the entire protein can give some indication as to the charged nature of the protein. The PI value of a protein can be calculated by the online tool ProtParam[197] which calculates a PI of 5.51for Pth and 5.69 for Gst. These values suggest that at pH 6.0, both proteins will be uncharged and are very close in value suggesting a strong similarity in the nature of the charged residues in both proteins. Further measurements relating more specifically to the $pK_a$ values of the histidine residues of interest would therefore be needed before any conclusion on this theory could be provided.

## 4.4 Summary and Conclusions

In summary, a number of new PBP ArMs were prepared from three PBPs (including two thermophilic proteins) together with a previously reported conjugate,[100] plus two modified conjugates that investigation in Chapter 3 had indicated had higher activity. A new synthetic route for these conjugates was established, incorporating a Gabriel synthesis. Activity testing of the free conjugates showed no significant improvement in catalytic activity, however, when incorporated into the ArMs, showed distinctly different characteristics. The previously studied PBP ArM produced the most enantioselective ArM at 40 °C, achieving an e.e. of 47.7% for (*R*)-salsolidine with the 4-Me-pyridine conjugate. The higher rigidity of the thermophilic proteins Gst and Pth gave a significant improvement in the catalytic rate of the ArMs, with almost 14-fold improvement in TOF of the fastest ArM, (5-Me-pyr)_azoto_Gst, compared to the previously reported PBP ArM design. This Gst-based ArM also gave an improvement in enantioselectivity with an e.e. of 37.2% up from 29.5% for the previously reported PBP ArM design. The enantioselectivity of this ArM can be increased still further by lowering the temperature, with an e.e. of 55% at 5 °C the highest recorded for a PBP ArM so far.

There is a distinct difference in the characteristics of *Cj*CeuE compared to the two thermophilic proteins. *Cj*CeuE is best improved by the 4-Me-pyridine conjugate, while Gst and Pth are

better enhanced by the use of the 5-Me-pyridine conjugate. This observation is also reflected in other investigations by our research group where an ArM designed for ketone reduction shows opposite enantioselectivity dependent on whether the protein scaffold is *Cj*CeuE or one of the thermophilic variants.[190]

The much faster catalytic rate of the ArMs of the thermophilic proteins make them more attractive to pursue for a number of uses such as flow reactors, particularly in instances where heating the reaction to 40 °C is challenging. The (5-Me-pyr)_azoto_Gst ArM design offers the best starting point for further exploration, being able to catalyse our standard reaction at 20 °C with an e.e. of 48.4% and at an acceptable rate of reaction. Such an e.e. is very respectable for an unmodified protein scaffold, and expectations are this could be significantly improved with genetic optimisation. The thermophilic proteins also represent the most attractive starting points for genetic optimisation efforts, having the benefit that thermophilic proteins are more tolerant of multiple genetic mutations.

# Chapter 5 Conclusions and Future Work

## 5.1 Summary and Conclusions

This project followed on from the report of the first PBP ArM published in 2018[100] where the high affinity between siderophores and PBPs was used for the protein and anchor components of an ArM design. A Noyori-Ikariya-type iridium catalyst was synthetically attached to a siderophore resulting in an ArM capable of catalysing the transfer hydrogenation of cyclic imines enantioselectively, using formate as a hydride source. The aim of the work presented in this thesis was to improve upon that ArM and enhance our understanding of the characteristics of this ArM design for use towards further applications.

Artificial metalloenzymes offer a dual strategy to improving the performance, since both the chemical component and biological scaffold can be optimised. The investigations presented in this thesis have primarily targeted the chemical unit, that is the transition metal catalyst and the attachment of the catalyst to the siderophore anchor. By improving the electronic contributions of the iridium-coordinating bidentate ligand with the addition of electron-donating groups, the rate of catalysis was enhanced. Both this altered electronic contribution and the additional steric properties from introducing substituents to the conjugate provided a series of ArMs differing substantially in catalytic performance in terms of both catalytic rate and enantioselectivity. This series of ArMs was constructed from three closely-related PBPs: *Cj*CeuE, the PBP used in the original reported ArM, and two thermophilic analogues, Gst and Pth. ArMs constructed from the thermophilic analogues display dramatically improved catalytic rates compared to their *Cj*CeuE equivalents. These two proteins also displayed a preference for the 5-methyl-pyridine conjugate over the 4-methyl-pyridine alternative that was favoured by the *Cj*CeuE scaffold.

The combination of the *Cj*CeuE scaffold with the 4-methyl-pyridine conjugate produced the most enantioselective ArM of this design reported so far, with an e.e. of 47.7% at 40 °C. However, the most significant improvement was the ArM constructed of the 5-methyl-pyridine conjugate with Gst, which also had an improved enantioselectivity compared to the reported PBP ArM design in addition to a 14-fold increase in turnover frequency. This reduced the time taken for the ArM to catalyse a reaction under our standard test conditions (limited to 400 turnovers) from more than 32 hours to less than 2.5 hours. The enantioselectivity of this ArM was further optimised by reducing the reaction temperature, which resulted in an e.e. of 48.4% at 20 °C and an acceptable reaction rate (400-limited turnovers in under 7 hours). The more versatile nature of this ArM could prove advantageous in applications where controlling the temperature at 40 °C is more difficult, such as in some flow systems, or for inclusion in enzymatic cascades with other enzymes with poorer thermostability.

In the process of optimising the iridium-based catalysts, a clear trend between the electron-donating ability of the substituent on the pyridine ring and catalytic activity was established, with electron-donating substituents providing the greatest improvement in performance. Analysing the catalytic rate while considering the mechanism indicated the strength of the Ir-hydride bond is key in determining whether the rate-determining step of the catalytic cycle is formation of the Ir-hydride species or hydride donation to the substrate, where the latter step is decisive in the case of the catalyst with the unsubstituted pyridine group. The trend in Ir-hydride bonds strength across the series of catalysts was deduced from variable temperature NMR experiments investigating the stereochemical inversion of the precatalysts in DMF. These experiments confirmed a trend that as the electron-donating ability of the substituent increased, the Ir-hydride bond strength decreased. Decreasing the strength of the Ir-hydride bond gave an improvement in the rate of hydride donation but to the detriment of Ir-hydride formation to an extent that, for the catalysts with the most strongly electron-donating groups, Ir-hydride formation became the rate-determining step.

Although the synthesis of a new siderophore-catalyst conjugate linked *via* the arene ligand was not successfully achieved in the course of the work in this thesis, this proposed design remains of interest. There continues to be alternative approaches towards the synthesis of this compound that have not yet been fully exhausted.

Overall, this project has succeeded in evolving the PBP ArM design, with new combinations of catalytic conjugate and PBPs that vastly outperform the previously reported design. Incorporating the best performing of the improved Ir catalysts into the ArM proved that steric contributions, in addition to electronic effects, contribute to the catalytic performance. The enantioselectively gained by introducing the Ir catalyst into a PBP scaffold, before any genetic optimisation efforts have been attempted, offers a very promising starting point for the further development of this PBP ArM design for biocatalysis. In many cases, genetic optimisation of the protein scaffold of ArMs can dramatically improve enantioselectivity.

## 5.2 Future Work

### 5.2.1 Arene-linked Siderophore-Catalyst Conjugate

Despite challenges isolating the ($\eta^6$-phenylglycine)Ru(pyridinylmethylsulfonamide)Cl·HCl complex (**50**) in early attempts, approaches to synthesising this complex have not been exhaustively explored and this route still presents an opportunity to access the arene-linked siderophore-catalyst conjugate.

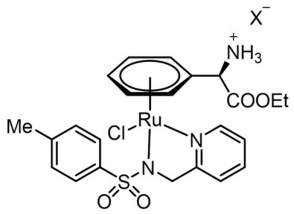


**50**

Figure 108 Structure of the ($\eta^6$-phenylglycine)Ru(pyridinylmethylsulfonamide)Cl·HCl complex.

Alternatively, a different type of arene-linking group could be employed. There are a number of piano-stool complexes reported with similar amine group attachments to the arene ligand, but without the additional carboxylic acid moiety of the phenylglycine and phenylalanine ligands. These complexes have been reported in a number of works ranging from other arene-ligand linked conjugates of the ArMs[91,92,132] to tethered arene piano-stool complexes[65,138]. It may be possible to construct the arene-linked siderophore-catalyst conjugate using approaches presented in these works, however, one reason these designs were not originally pursued is that the polar carboxylic acid group of phenylglycine and phenylalanine ligands were expected to improve solubility of these complexes in aqueous media and provide stabilising non-covalent interactions with the protein scaffold.

### 5.2.2 Further Optimisation of the Chemical Component of the ArM

The varied effect on the enantioselectivity of the ArM from the addition of small substituents on the pyridine ring of the conjugate suggest very close proximity of the pyridine ring to the protein scaffold. As such, the addition of much bulkier substituents would potentially risk significant steric repulsion and a weaker binding affinity of the conjugate to the PBP. It therefore does not seem desirable to attempt the addition of more bulky substituents onto the pyridine ring of the conjugate.

Instead, the addition of a bulky group at the methylene position of the bidentate ligand would be an interesting adaptation to test the theory that the enantioselectivity of the ArM arises from directing the substrate to approach from the smaller pocket in the conjugate binding site (Figure 109 (a)). On binding the conjugate in the protein scaffold, the iridium adopts one stereochemical configuration. If a bulky substituent was added in the stereochemistry indicated in Figure 109 (b) this would disfavour the approach of the substrate from the face of Ir in the large, unselective pocket in the structure, and would hopefully lead to an increase in the enantioselectivity of the ArM, perhaps to the detriment of the TOF. The chirality of the ligand could also help to enhance the stereopreference of the catalyst, as is seen for TsDPEN ligands, however, this would have to be investigated further.

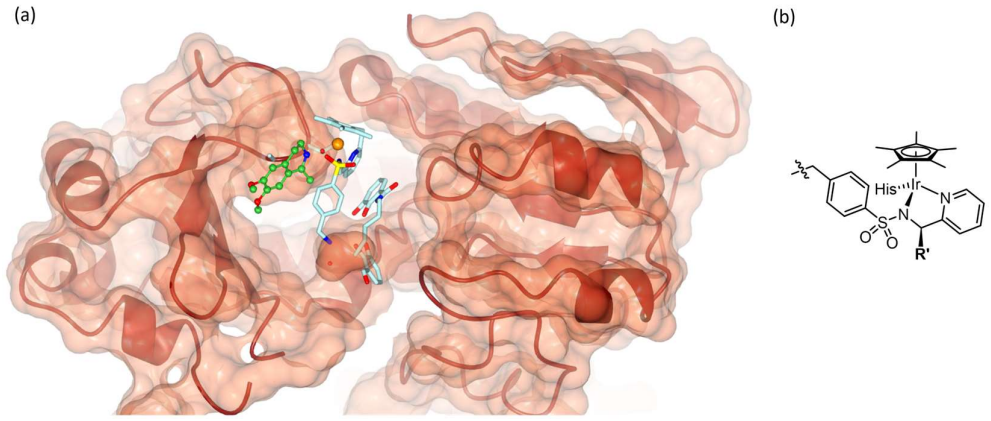


Figure 109 (a) Model of the substrate (green) in the small protein pocket in proximity of the Ir catalyst (orange atom = Ir, blue cylinders = conjugate, protein = red cartoon and surface) and (b) the simplified structure of the proposed conjugate with addition of the substituent R'.

## 5.2.3 Optimisation of the Biological Component of the ArM

Genetic optimisation of the protein scaffold provides the biggest unexplored opportunity for improving the catalytic performance of the PBP ArM. Several reports of genetic optimisation of ArMs have demonstrated enormous improvements in enantioselectivity and also turnover frequency. However, it must be remembered that the process of genetic optimisation can be time-consuming and expensive.

Transfer hydrogenation of imines was selected only as a trial reaction to assess the suitability of the PBP ArM design and develop our understanding of the system; it is a catalytic reaction already accomplished efficiently by organometallic catalysts and natural enzymes alike, with good levels of selectivity. While genetic optimisation of this ArM for the transfer hydrogenation of imines may identify important residues in directing the catalysis, genetic optimisation is often specific to the particular reaction and even the selected substrate. At this time, our understanding of the rational design of proteins for catalysis remains limited and

many genetic optimisation approaches follow a trial-and-error route. As such, genetic optimisation of the PBP ArM for transfer hydrogenation of imines might not necessarily increase our understanding of the ArM system and the time might be more efficiently spent in developing a PBP ArM that can catalyse a more valuable transformation. While genetic optimisation of the PBP ArtIRED would be useful for the sake of a complete story in the development of this ArM, I believe it would be better to attempt this in parallel with the development of a PMP ArM for another catalytic transformation; in this way ArMs for two or more reactions may be optimised for the same amount of work as is necessary to optimise just one. It would also be important to investigate multiple substrates for a selected reaction before conclusions could be made about which mutations led to improved performance. To date, investigations of the periplasmic binding protein ArtIRED have been restricted to only dehydrosalsolidine because of the prohibitive cost of other potential imine substrates.

An alternative approach that follows rational design would be to insert an additional loop into the protein structure to occupy or block the large, unselective pocket for substrate approach. This would hopefully improve the enantioselectivity of the ArM and, by increasing the secondary coordination shell of the Ir complex, provide a stabilising effect. However, it would be extremely complex to determine exactly what sequence should be added.

# Chapter 6 Experimental Methods

## 6.1 General Remarks

### 6.1.1 Materials

Materials were obtained from the following commercial suppliers: Acros, Alfa-Aesar, Fluorochem, Fisher Scientific, Sigma-Aldrich, Tokyo Chemical Industry Ltd. Proteins *Cj*CeuE, Gst and Pth were obtained from Dr. E. V. Blagova.

Analytical thin layer chromatography (TLC) was performed using Merck silica gel 60 F253 aluminium-backed plates using specific solvent systems and visualised under an ultraviolet lamp. Column chromatography was carried out using Fluka Silica, pore size 60 Å, 220-440 mesh, 35-75 μm.

### 6.1.2 Instrumentation

Characterisation data for NMR including $^{1}H$, $^{13}C$, COSY, DEPT135, HMQC and HMBC spectra were recorded on a Jeol ECS 400 and ECX 400 MHz instruments (400 MHz for $^{1}H$ and 101 MHz for $^{13}C$) at ambient temperature, unless otherwise stated. $^{13}C$ spectra are proton decoupled. Variable temperature NMR experiments were carried out by Heather Fish and were measured using a Bruker AV500b instrument (500 MHz for $^{1}H$). $^{1}H$ data are reported as follows: chemical shift (number of protons, multiplicity, coupling constants, *assignment*). 13C data are reported as follows: chemical shift (*assignment*). Chemical shifts are reported in parts per million (ppm), relative to the residual solvent peaks to the nearest 0.01 ppm for $^{1}H$ spectra and 0.1 ppm for $^{13}C$ spectra. Multiplicity is reported as follows: s=singlet, d=doublet, t=triplet, q=quartet, m=multiplet, br=broad. Coupling constants (J) are given in Hz and are quoted to the nearest 0.5 Hz. All NMR spectra were processed MestReNova analysis software.

High-resolution ESI mass spectra were recorded on a Bruker microTOF electrospray mass spectrometer and liquid injection field desorption ionisation (LIFDI) on a Waters GCT Premier TOF mass spectrometer by K. Heaton, R. Cercola and A. Lopez. Melting points were measured using a Stuart Scientific SMP3 melting point apparatus. Infrared spectra were recorded using a Perkin Elmer FT-IR spectrum 2 spectrometer at ambient temperature. Data is reported as peaks of interest. Elemental analysis was measured using an Exeter CE-440 elemental analyser, carried out by G. McAllister and S. Hicks.

Non-chiral analytical HPLC was performed using an Athena C18-WP column (100 Å, 4.6 x 25 mm, CNW). Chiral analytical HPLC was performed with a Lux Cellulose-4 column

(Phenomenex, 250 x 4.6 mm, 5 μM). Measurements were taken using an Agilent 1260 Infinity II Quaternary System equipped with a 1260 Quaternary pump G7111B, 1260 Vialsampler, G7129A, multicolumn thermostat G7116A oven and a 1260 multiwavelength detector G7165A.

## 6.2 Compounds Index

## Chapter 2



## Chapter 3

# Chapter 4

## 6.3 Synthesis of Compounds Related to Chapter 2

## 27. [($\eta^6$-Phenylglycine)$RuCl_2$]$_2$ (dually protected, *N*-acetyl, ethyl ester)

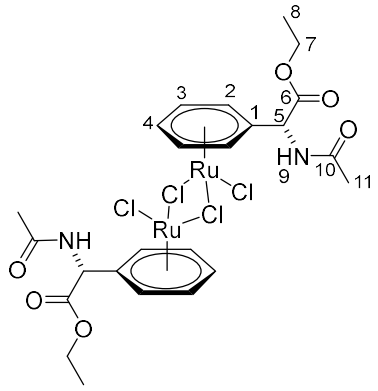


Chemical Formula: $C_{24}H_{30}N_2O_6Cl_4Ru_2$

Molecular Mass: 786.45 g $mol^{-1}$

Complex **27** was prepared by a method modified from the literature[50,142,198].

$RuCl_3 \cdot xH_2O$ (0.1135 g, approx. 0.434 mmol) and **32** (0.3825 g, 1.71 mmol) was placed in a schlenk tube under a nitrogen atmosphere. 4 mL degassed, anhydrous ethanol was then syringed into the tube and the mixture stirred until all solids had dissolved. This solution was then transferred to a microwave vessel and placed inside a CEM Discovery-SP microwave reactor for 20 minutes at 423 K, 150 W, 250 psi. The product formed as an orange precipitate on cooling to room temperature. The reaction mixture was filtered, and the precipitate washed with *n*-pentane. More precipitate was recovered on slow addition of *n*-pentane to the filtrate and separated by filtration.

**Yield:** 0.132 g, 0.17 mmol, 70%

**HRMS (LIFDI):** Calcd. $[M\text{-}Cl]^+$ ($C_{24}H_{30}N_2O_6Cl_3Ru_2$) m/z= 750.92510; Obs. m/z= 750.92827, Mean err 4.2 ppm

**$^1$H NMR:** (400 MHz, $CDCl_3$) δ: 7.93 (2H, d, $J^3$= 5.0 Hz, *H9*), 5.88-5.53 (10H, m, *H2-4*), 5.19 (1H, s, *H5*), 4.30-4.17 (4H, m, *H7*), 1.58 (6H, s, *H11*), 1.31-1.22 (6H, m, *H8*)

**$^{13}$C NMR:** (100 MHz, DMSO-$d_6$) δ: 170.5 (*C6*), 169.1 (*C10*), 97.6, 89.9, 88.2, 88.0, 86.7, 86.3, 86.2 (*C1-4*), 61.9 (*C7*), 54.1 (*C5*), 22.6 (*C11*), 14.4 (*C8*)

# 28. Ruthenium Complex 1

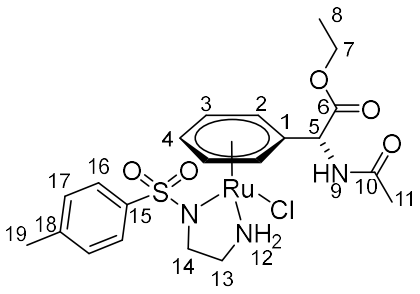

Chemical Formula: $C_{21}H_{28}ClN_3O_5RuS$

Molecular Mass: 571.05 g $mol^{-1}$

Ruthenium Complex 1 was prepared by a method modified from the literature[61].

**27** (0.016 g, 0.020 mmol) and *N*-(2-aminoethyl)-4-methylbenzenesulfonamide (0.017 g, 0.080 mmol) were suspended in dry isopropanol (4 mL). The mixture was stirred at 80 °C for 20 minutes under a nitrogen atmosphere. The mixture was cooled to room temperature then placed on ice to encourage formation of a precipitate. The precipitate was isolated by filtering and washed with a small quantity of ice-cold MeOH followed by *n*-pentane and dried under reduced pressure.

**Yield:** 0.016 g, 0.028 mmol, 72%

**HRMS (ESI):** Calcd. $[M\text{-}Cl]^+$ ($C_{21}H_{28}N_3O_5RuS$) m/z= 536.0788; Obs. m/z= 536.0791, Mean err 0.1 ppm. Calcd. $[M+Na]^+$ ($C_{21}H_{28}ClN_3NaO_5RuS$) m/z= 594.0374; Obs. m/z= 594.0364, Mean err 1.1 ppm

**$^1$H NMR:** (400 MHz, acetone-$d_6$) δ: 8.32 (<1H, d, $J^3$= 6.0 Hz, *H9*), 7.74 (2H, d, $J^3$= 8.0 Hz, *H16*), 7.38 (2H, d, $J^3$= 8.0 Hz, *H17*), 6.70 (<1H, t, $J^3$= 6.0 Hz, *H12*), 6.02 (1H, d, $J^3$= 5.5 Hz, *H2*), 5.89 (1H, t, $J^3$= 5.5 Hz, *H4*), 5.86 (1H, d, $J^3$= 5.5 Hz, *H2*), 5.59 (1H, t, $J^3$= 5.5 Hz, *H3*), 5.48 (1H, t, $J^3$= 5.5 Hz, *H3*), 5.31 (1H, d, $J^3$= 6.0 Hz, *H5*), 4.21-4.10 (2H, m, *H7*), 3.30-3.15 (2H, m, *H14*), 3.06 (2H, q, $J^3$= 6.0 Hz, *H13*), 2.40 (3H, s, *H19*), 1.98 (3H, s, *H11*), 1.19 (3H, t, $J^3$= 7.0 Hz, *H8*)

# 29. Ruthenium Complex 2

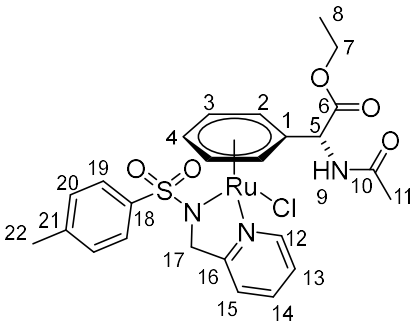


Chemical Formula: $C_{25}H_{28}ClN_3O_5RuS$

Molecular Mass: 619.10 g $mol^{-1}$

Ruthenium Complex 2 was prepared by a method modified from the literature[61].

**27** (0.016 g, 0.02 mmol) and 4-methyl-*N*-(pyridine-2-ylmethyl)benzenesulfonamide (**87**) (0.022 g, 0.08 mmol) were dissolved in dry, degassed ethanol. The solution was heated at 80 °C for 30 minutes in a nitrogen atmosphere. The reaction mixture was filtered through a hot sinter (to remove black precipitate) and the filtrate reduced in volume in vacuo. *n*-Hexane was added as an antisolvent and the solution left at -20 °C to promote formation of precipitate. The precipitate was removed by filtering and washed with more *n*-hexane to leave a pale orange solid.

**Yield:** 0.018 g, 0.03 mmol, 74%

**HRMS (ESI):** Calcd. $[M\text{-}Cl]^+$ ($C_{25}H_{28}N_3O_5RuS$) m/z= 584.0788; Obs. m/z= 584.0772, Mean err 4.6 ppm

**$^1$H NMR:** (400 MHz, acetone-$d_6$) δ: 9.31, 9.26 (1H, d, $J^3$= 5.5 Hz, *H12*), 7.87 (1H, tt, $J^3$= 7.5 Hz, $J^3$= 1.7 Hz, *H14*), 7.81 (2H, dd, $J^3$= 8.0 Hz, $J^3$= 6.0 Hz, *H19*), 7.43-7.36 (2H, m, *H13, H15*), 7.20 (2H, d, $J^3$= 8.0 Hz, *H20*), 6.34-5.76 (5H, m, *H2-4*), 4.19-3.98 (2H, m, *H7*), 2.34 (3H, s, *H22*), 1.18 (3H, t, $J^3$= 7.0 Hz, *H8*). Expect peaks for *H11* and *H17* are hidden by solvent peaks

# 31. Ethyl (2*R*)-2-amino-2-(cyclohexa-1,4-dien-1-yl)acetate

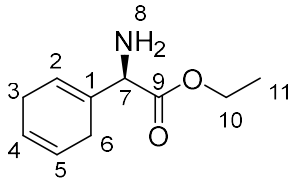


Chemical Formula: $C_{10}H_{15}NO_2$

Molecular Mass: 181.11 g $mol^{-1}$

(*R*)-(-)-2-(2,5-dihydrophenyl)glycine ethyl ester was prepared by a method modified from the literature[199].

Under a nitrogen atmosphere, (*R*)-(-)-2-(2,5-dihydrophenyl)glycine (0.200 g, 1.31 mmol) was suspended in dry ethanol (4 mL) and placed on ice. Addition of thionyl chloride (0.2 mL, 2.74 mmol) drop wise resulted in a pale-yellow solution. The solution was then heated to reflux for 2 hours. The reaction mixture was allowed to cool to room temperature before pouring into 5 mL saturated $NaHCO_3$. The product was extracted with ethyl acetate (3 x 10 mL) before washing with brine (3 x 10 mL). The organic layer was dried over $MgSO_4$ then the solvent removed in vacuo to leave a brown oil.

**Yield:** 0.107 g, 0.59 mmol, 45%

**$R_f$:** 0.36 (2:1 ethyl acetate:hexane)

**HRMS (ESI):** Calcd. $[M+H]^+$ ($C_{10}H_{16}NO_2$) m/z= 182.1176; Meas. m/z= 182.1174, Mean err 0.6 ppm. Calcd. $[M+Na]^+$ ($C_{10}H_{15}NNaO_2$) m/z= 204.0995; Meas. m/z= 204.0994, Mean err 0.6 ppm

**$^1$H NMR:** (400 MHz, $CDCl_3$) δ: 5.73 (1H, br s, H2), 5.71-5.63 (2H, m, $J^3_{H\text{-}H4/5}$= 10.0 Hz, H4-5), 4.25-4.09 (2H, m, H10), 3.96 (1H, s, H7), 2.83-2.48 (4H, m, H3, H6), 1.25 (3H, t, $J^3_{H\text{-}H10}$= 7.0, H11)

**$^1$H NMR:** (400 MHz, DMSO-$d_6$) δ: 5.69-5.57 (3H, m, H2, H4 & H5), 4.10-3.95 (2H, m, H10), 3.78 (1H, s, H7), 2.71-2.37 (4H, m, H3, H6), 1.14 (3H, t, $J^3_{H\text{-}H10}$= 7.0, H11)

**$^{13}$C NMR:** (100 MHz, DMSO-$d_6$) δ: 173.7 (C9), 134.3 (C1), 124.1, 123.7 (C4, C5), 120.7 (C2), 60.3 (C7), 59.9 (C10), 26.2 (C3), 25.3 (C6), 14.1 (C11)

# 32. Ethyl (2*R*)-2-(cyclohexa-1,4-dien-1-yl)-2-acetamidoacetate

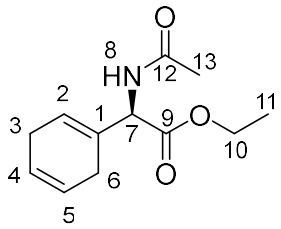


Chemical Formula: $C_{12}H_{17}NO_3$

Molecular Mass: 223.27 g $mol^{-1}$

*N*-acetyl-(*R*)-(-)-2-(2,5-dihydrophenyl)glycine ethyl ester was prepared by a method modified from the literature[77,200].

(*R*)-(-)-2-(2,5-dihydrophenyl)glycine ethyl ester **(31**) was taken up in dry ethanol (20 mL). To this solution were added acetic anhydride (5.105 g, 50 mmol) and triethylamine (2.732 g, 27 mmol) and the reaction mixture refluxed at 80 °C overnight. The reaction mixture was allowed to cool to room temperature before addition of 1 M $NH_4Cl$ solution (20 mL). The product was extracted with ethyl acetate (3 x 20 mL) then washed with brine (2 x 20 mL). The organic layer was dried over $MgSO_4$ followed by removing the solvent in vacuo to leave a thick brown oil which was dried on a high vacuum line. When left for 24 hours at room temperature the oil crystallized.

**Yield:** 1.80 g, 8.06 mmol, 40%

**$R_f$:** 0.61 (1:2 hexane:ethyl acetate)

**HRMS (ESI):** Calcd. $[M+Na]^+$ ($C_{12}H_{17}NNaO_3$) m/z= 246.1101; Obs. m/z= 246.1101, Mean err -0.1 ppm

**$^1$H NMR:** (400 MHz, $CDCl_3$) δ: 6.50 (1H, br, *H8*), 5.73 (1H, s, *H2*), 5.63 (2H, overlapping triplets, *H4-5*), 4.96 (1H, d, $J^3$= 8.0 Hz, *H7*), 4.24-4.04 (2H, m, *H10*), 2.74-2.49 (4H, m, *H3*, *H6*), 2.00 (3H, s, *H13*), 1.24 (3H, t, $J^3$= 7.0 Hz, *H11*)

**$^{13}$C NMR:** (100 MHz, $CDCl_3$) δ: 171.1 (*C12*), 169.6 (*C9*), 130.6 (*C1*), 124.0 (*C2*), 123.8, 123.6 (*C4-5*), 61.8 (*C10*), 56.7 (*C7*), 26.7, 26.4 (*C3, C6*), 23.2 (*C13*), 14.2 (*C11*)

# 34. 2,3-Diacetoxybenzoic acid

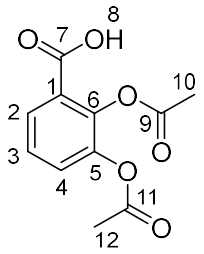


Chemical Formula: $C_{11}H_{10}O_6$

Molecular Mass: 238.20 g $mol^{-1}$

2,3-Diacetoxybenzoic Acid was prepared in accordance with the literature[149].

2,3-Dihydroxybenzoic acid (1.728 g, 11.2 mmol) was suspended in acetic anhydride (4.6 mL, 48.7 mmol) under nitrogen and 1 drop of concentrated sulfuric acid added. The reaction mixture was stirred for 10 minutes before addition of anhydrous diethyl ether (9 mL) before the mixture was left stirring overnight. 20 mL water was added before the product was extracted with dichloromethane (4 x 50 mL). The organic layer was washed with water (2 x 15 mL) and dried over $MgSO_4$ before the solvent removed in vacuo.

**Yield:** 2.494 g, 10.4 mmol, 94%

**HRMS (ESI):** Calcd. $[M+Na]^+$ ($C_{11}H_{10}NaO_6$) m/z= 261.0370; Obs. m/z= 261.0369, Mean err -0.1 ppm

**$^1$H NMR:** (400 MHz, $CDCl_3$) δ: 7.87 (1H, d, $J^3$= 8.0 Hz, *H2*), 7.40 (1H, d, $J^3$= 8.0 Hz, *H4*), 7.33 (1H, t, $J^3$= 8.0 Hz, *H3*), 2.26 (3H, s, *H10*), 2.25 (3H, s, *H12*)

**$^{13}$C NMR:** (100 MHz, $CDCl_3$) δ: 168.8, 168.7 (*C9, C11*), 165.7 (*C7*), 143.7 (*C5*), 142.8 (*C6*), 128.7 (*C2*), 127.6 (*C4*), 125.9 (*C3*), 125.5 (*C1*), 19.3, 19.1 (*C10, C12*)

The characterisation data are consistent with those reported in the literature.

# 37. *tert*-Butyl (2*S*)-2,6-diaminohexanoate

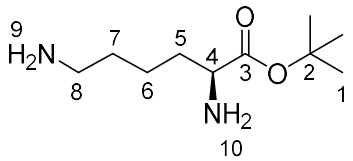


Chemical Formula: $C_{10}H_{22}N_2O_2$

Molecular Mass: 202.30 g $mol^{-1}$

2-Hydroxypropan-2-yl (2S)-2-amino-6-{[(benzyloxy)carbonyl]amino}hexanoate (0.277 g, 0.74 mmol) was added to a solution of *N,N*-diisopropylethylamine (0.2 mL, 1.15 mmol) in anhydrous ethanol (30 mL). 10% Palladium on carbon (0.076 g) was added and the reaction vessel sealed. The vessel was then purged with nitrogen followed by hydrogen at atmospheric pressure and the reaction mixture left stirring overnight at room temperature. The remaining hydrogen was released and the suspension filtered using a Whatman glass microfiber filter GF/F. Volatiles were removed in vacuo to yield the product as a white solid.

**Yield:** 0.146 g, 0.72 mmol, 98%

**HRMS (ESI):** Calcd. $[M+H]^+$ ($C_{10}H_{23}N_2O_2$) m/z= 203.1754; Obs. m/z= 203.1753, Mean err 0.5 ppm

**$^1$H NMR:** (400 MHz, MeOH-$d_4$) δ: 3.33 (1H, dd, $J^3$= 6.0, 7.0 Hz, *H4*), 2.89 (2H, t, $J^3$= 7.5 Hz, *H8*), 1.77-1.53 (4H, m, *H5, H7*), 2.46 (9H, s, *H1*), 1.48-1.37 (2H, m, *H6*)

**$^{13}$C NMR:** (100 MHz, MeOH-$d_4$) δ: 173.9 (*C3*), 81.3 (*C2*), 53.9 (*C4*), 39.2 (*C8*), 33.2 (*C5*), 27.1 (*C7*), 26.9 (*C1*), 22.1 (*C6*)

## 38. *tert*-Butyl (2*S*)-2,6-bis({[2,3-bis(acetyloxy)phenyl]formamido})hexanoatehexanoate

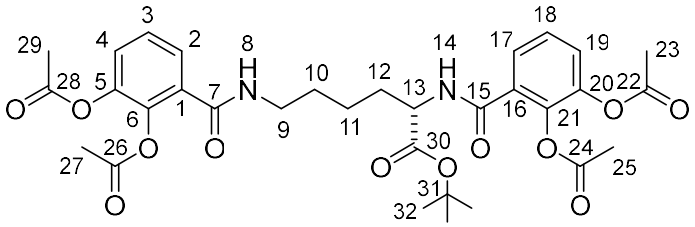

Chemical Formula: $C_{32}H_{38}N_2O_{12}$

Molecular Mass: 642.66 g $mol^{-1}$

2,3-Diacetoxybenzoic acid (**34**) (0.145 g, 0.61 mmol) was dissolved in anhydrous dichloromethane (3.5 mL). Thionyl chloride (0.15 mL, 2.06 mmol) was added drop wise before the solution was brought to reflux for 6 hours. Volatiles were removed in vacuo and the resulting oil resuspended in anhydrous dichloromethane (2 mL). This solution was added drop wise to a solution of tert-Butyl (2S)-2,6-diaminohexanoate (**37**) (0.059 g, 0.29 mmol) in anhydrous dichloromethane(4 mL) and *N,N*-diisopropylethylamine (0.14 mL, 0.57 mmol) over in an ice bath. The solution was stirred for 10 minutes at 0 °C then sonicated at room temperature for a further 20 minutes. The solution was then washed with HCl/$H_20$ at pH 3 until there was no change to the pH of the aqueous layer. The organic layer was dried over $MgSO_4$ and the solvents removed in vacuo to yield a pale yellow oil which produced a foam on drying under vacuum.

**Yield:** 0.106 g, 0.17 mmol, 59%

**HRMS (ESI):** Calcd. $[M+H]^+$ ($C_{32}H_{39}N_2O_{12}$) m/z= 643.2498; Obs. m/z= 643.2488, Mean err -1.6 ppm. Calcd. $[M+Na]^+$ ($C_{32}H_{38}N_2NaO_2$) m/z= 665.2317; Obs. m/z= 665.2314, Mean err 1.1 ppm

**$^1$H NMR:** (400 MHz, DMSO-$d_6$) δ: 8.58 (1H, d, $J^3$= 7.5 Hz, *H14*), 8.33 (1H, t, $J^3$= 5.5 Hz, *H8*), 7.45-7.21 (6H, m, *H2-3, H17-19*), 4.18-4.10 (1H, m, *H13*), 3.18-3.06 (2H, m, *H9*), 2.26-2.17 (12H, 5 x overlapping singlets, *H23,H25, H27, H29*), 1.74-1.59 (2H, m, *H12*), 1.50-1.40 (2H, m, *H10*), 1.37 (9H, s, *H32*), 1.40-1.27 (2H, m, *H11*)

**$^{13}$C NMR:** (100 MHz, DMSO-$d_6$) δ: 171.7 (*C30*), 168.9, 168.9, 168.8, 168.7 (*C22, C24, C26 & C28*), 165.3 & 165.0 (*C7 & C15*), 143.4 & 143.3 (*C5 & C20*), 140.6 & 140.5 (*C6 & C21*), 129.0 & 128.3 (*C2 & C17*), 126.9 & 126.8 (*C4 & C19*), 126.6, 126.3, 126.1, 125.8 (*C1, C3,*

*C16 & C18*), 81.1 (*C31*), 53.7 (*C13*), 39.2 (*C9*), 30.7 (*C12*), 29.0 (*C10*), 28.2 (*C32*), 23.4 (*C11*), 20.9, 20.8, 20.8 & 20.7 (*C23, C25, C27 & C29*),

# 40. (4-Methoxyphenyl)methyl 2,3-bis[(4-methoxyphenyl)methoxy]benzoate

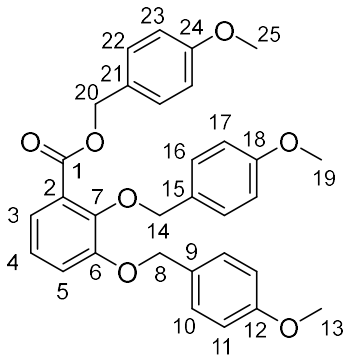


Chemical Formula: $C_{31}H_{30}O_7$

Molecular Mass: 514.57 g $mol^{-1}$

Compound **40** was prepared in accordance with the literature.[201]

2,3-dihydroxybenzoic acid (3.861 g, 25.0 mmol), potassium chloride (13.33 g, 80.0 mmol) and potassium carbonate (24.189 g, 175.0 mmol) were suspended in acetone (200 mL). 4-methyoxybenzylchloride (10.85 mL, 80.0 mmol) was added and the suspension heated to reflux for 3 days. The solvent was removed in vacuo and the resulting solid dissolved in water (150 mL) and the product extracted with DCM (4 x 70 mL). The combine organic layers were dried over $MgSO_4$ and the solvent removed in vacuo. The product was purified by column chromatography (2:3 ethyl acetate: petroleum ether 40-60 °C) to yield a white solid.

**Yield:** 12.193 g, 23.7 mmol, 95%

**$R_f$:** 0.31 (1:4 ethyl acetate: petroleum ether 40-60 °C)

**Melting Point:** 86-88 °C

**HRMS (ESI):** Calcd. $[M+Na]^+$ ($C_{31}H_{30}NaO_7$) m/z= 537.1884; Meas. m/z= 537.1895, Mean err -1.5 ppm. Calcd. $[M+K]^+$ ($C_{31}H_{30}KO_7$) m/z= 553.1623; Meas. m/z= 553.1629, Mean err -1.0 ppm.

**$^1$H NMR:** (400 MHz, $CDCl_3$) δ: 7.37-7.32 (5H, m, *H3, H10 & H16*), 7.18 (2H, d, $J^3_{H\text{-}H23}$= 8.5 Hz, *H22*), 7.11 (1H, dd, $J^3_{H\text{-}H4}$= 8.0 Hz, $J^4_{H\text{-}H3}$= 1.6 Hz, *H5*), 7.04 (1H,apparent t, $J^3_{H\text{-}H3/H5}$= 8.0 Hz, *H4*), 6.90 (2H, d, $J^3_{H\text{-}H10}$= 8.5 Hz, *H11*), 6.87 (2H, d, $J^3_{H\text{-}H16}$= 8.5 Hz, *H17*), 6.76 (2H, d, $J^3_{H\text{-}H22}$= 8.5 Hz, *H23*), 5.25 (2H, s, *H8*), 5.04 (2H, s, *H14*), 4.95 (2H, s, *H20*), 3.81 (3H, s, *H13, H19 or H25*), 3.80 (3H, s, *H13, H19 or H25*), 3.78 (3H, s, *H13, H19 or H25*)

**$^{13}$C NMR:** (100 MHz, $CDCl_3$) δ: 166.5 (*C1*), 159.7 (*C24*), 159.6 (*C12*) & 159.4 (*C18*), 153.0 (*C6*) & 148.4 (C7), 130.4 (C22), 130.3 (C10), 129.7 (C21), 129.5 (*C16*), 128.8 (*C9*), 128.2 (*C15*), 127.1 (*C2*), 123.9 (*C4*), 123.0 (*C3*), 118.2 (*C5*), 114.0 (*C11 & C17*), 113.6 (*C23*), 75.3 (*C20*), 71.2 (*C8*), 66.8 (*C14*), 55.4 (*C25*), 55.4 (*C13*), 55.3 (*C19*)

**IR ATIR ($cm^{-1}$):** 2938 w br (C-H), 1707 s (C=O ester), 1612 m (C-C Ar), 1512 m (C-C Ar)

**Elemental Analysis:** Cald. For [$C_{31}H_{30}O_7$]: %C 72.36, %H 5.88, %N 0.00; Measured for [$C_{31}H_{30}O_7$]: %C 72.53, %H 6.34, %N 0.00

The characterisation data are consistent with those reported in the literature.

# 41. 2,3-Bis[(4-methoxyphenyl)methoxy]benzoic acid

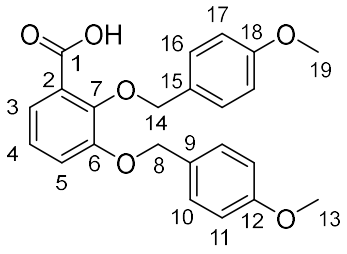


Chemical Formula:$C_{23}H_{22}O_6$

Molecular Mass: 394.42 g $mol^{-1}$

Compound **41** was prepared in accordance with the literature.[201]

Compound **40** (1.162 g, 2.26 mmol) was dissolved in dioxane (11 mL). Sodium hydroxide (2 M aqueous, 6 mL) was added, and the solution stirred at room temperature for 24 hours. The solution was concentrated to remove dioxane. 4 mL water was added, and the solution acidified to pH 2 with 1M HCl. The product formed as a white precipitate on acidification of the aqueous solution and was isolated by filtration and washed with hexane.

**Yield:** 0.822 g, 2.08 mmol, 92%

**$R_f$:** 0.22 (2:3 ethyl acetate: petroleum ether 40-60 °C)

**Melting Point:** 109.8-111.6 °C

**HRMS (ESI):** Calcd. $[M+Na]^+$ ($C_{23}H_{22}NaO_6$) m/z= 417.1309; Meas. m/z= 417.1319, Mean err -2.7 ppm. Calcd. $[M+K]^+$ ($C_{23}H_{22}KO_6$) m/z= 433.1062; Meas. m/z= 433.1062, Mean err -2.1 ppm.

**$^1$H NMR:** (400 MHz, $CDCl_3$) δ: 7.71 (1H, dd, $J^3_{H\text{-}H4}$= 8.0 Hz, $J^4_{H\text{-}H5}$= 1.6 Hz, *H3*), 7.40 (2H, d, $J^3_{H\text{-}H11}$= 8.5 Hz, *H10*), 7.26-7.19 (3H, m, *H5 & H10 or H16*), 7.16 (1H, apparent t, $J^3_{H\text{-}H3/H5}$= 8.0 Hz, *H4*), 6.95 (2H, d, $J^3_{H\text{-}H10}$= 8.5 Hz, *H11*), 6.81 (2H, d, $J^3_{H\text{-}H16}$= 8.5 Hz, *H17*), 5.18 (2H, s, *H8*), 5.10 (2H, s, *H14*), 3.83 (3H, s, *H13*), 3.78 (3H, s, *H19*)

**$^{13}$C NMR:** (100 MHz, $CDCl_3$) δ: 165.3 (*C1*), 160.5 (*C12*), 160.0 (*C18*), 151.4 (*C6*), 147.2 (*C7*), 131.2 (*C10*), 129.7 (*C16*), 128.0 (*C9*), 126.8 (*C15*), 125.0 (*C4*), 124.4 (*C3*), 123.0 (*C2*), 119.1 (*C5*), 114.3 (*C11 & C17*), 76.9 (*C8*), 71.4 (*C14*), 55.5 (*C13*), 55.4 (*C19*)

**IR ATIR ($cm^{-1}$):** 2936 w (C-H), 2696 br (C-H), 1678 m (C=O), 1614 m (C-C Ar), 1515 s (C-C Ar)

**Elemental Analysis:** Cald. For [$C_{23}H_{22}O_6$]: %C 70.04, %H 5.62, %N 0.00; Measured for [$C_{23}H_{22}O_6$]: %C 69.92, %H 5.87, %N 0.00

The characterisation data are consistent with those reported in the literature.

# 42. Methyl (2*S*)-2,6-bis({2,3-bis[(4-methoxyphenyl)methoxy]phenyl}formamido)hexanoate

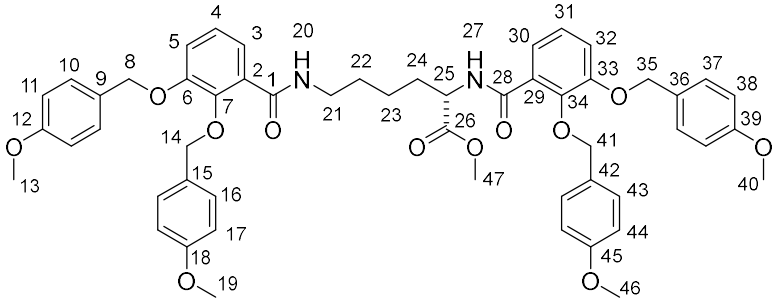

Chemical Formula: $C_{53}H_{56}N_2O_{12}$

Molecular Mass: 913.03 g $mol^{-1}$

Compound **42** was prepared in accordance with the literature.[201]

41 (9.861 g, 25.0 mmol) was dissolved in DMF (200 mL) and placed in an ice bath. *N*,*N*′-Dicyclohexylcarbodiimide (5.236 g, 25.4 mmol) and 1-hydroxybenzotriazole (4.521 g, 25.1 mmol) was added and the reaction mixture stirred at 0 °C for 10 minutes. *N*,*N*-diisopropylethylamine (9 mL, 51.7 mmol) and L-lysine methyl ester dihydrochloride (2.932 g, 12.6 mmol) was added at 0 °C before the reaction mixture was allowed to come to room temperature and was stirred overnight for 22 hours. Ethyl acetate (200 mL) was added, and the reaction mixture stirred on ice for 30 minutes. Byproduct, 1,3-dicyclohexyl urea, was removed by filtration and the organic layer from the filtrate retained and washed with 1 M HCl (2 x 100 mL), saturated aqueous NaHCO3 (2 x 100 mL) and brine (1 x 100 mL). The organic layer was dried over MgSO4 and the solvent removed in vacuo. The remaining solids were taken up in acetonitrile and left stirring on ice for 4 hours before filtering to remove further 1,3-dicyclohexyl urea. The product was purified by column chromatography (3:2 ethyl acetate: petroleum ether 40-60 °C) to yield a colourless oil.

**Yield:** 5.708 g, 6.25 mmol, 50%

**$R_f$:** 0.22 (2:3 ethyl acetate: petroleum ether 40-60 °C)

**HRMS (ESI):** Calcd. $[M+H]^+$ ($C_{53}H_{57}N_2O_{12}$) m/z= 913.3906; Meas. m/z= 913.3936, Mean err -2.3 ppm. Calcd. $[M+Na]^+$ ($C_{53}H_{56}N_2NaO_{12}$) m/z= 935.3725; Meas. m/z= 935.3760, Mean err -3.5 ppm

**$^1$H NMR:** (400 MHz, $CDCl_3$) δ: 8.54 (1H, d, $J^3_{H\text{-}H25}$= 7.5 Hz, *H27*), 7.94 (1H, t, $J^3_{H\text{-}H21}$= 5.5 Hz, *H20*), 7.72-7.66 (2H, m, *H3 & H30*), 7.38 (4H, d, $J^3_{H\text{-}H11/17/38/44}$= 8.5 Hz, *H10, H16, H37*

*or H43*), 7.27 (2H, d, $J^3_{H\text{-}H11/17/38/44}$= 8.5 Hz, *H10, H16, H37 or H43*), 7.18 (2H, d, $J^3_{H\text{-}H11/17/38/44}$= 8.5 Hz, *H10, H16, H37 or H43*), 7.14-7.09 (4H, m, *H4, H5, H31 & H32*), 6.92 (4H, d, $J^3_{H\text{-}H10/16/37/43}$= 8.5 Hz, *H11, H17, H38 or H44*), 6.79 (2H, d, $J^3_{H\text{-}H10/16/37/43}$= 8.5 Hz, *H11, H17, H38 or H44*), 6.76 (2H, d, $J^3_{H\text{-}H10/16/37/43}$= 8.5 Hz, *H11, H17, H38 or H44*), 5.09-4.93 (overlapping singlets, *H8, H14, H35 & H41*, 8H), 4.65-4.57 (m, *H25*, 1H), 3.82 (s, *H13, H19, H40 or H46*, 3H), 3.82 (3H, s, *H13, H19, H40 or H46*), 3.74 (3H, s, *H47*), 3.73 (3H, s, *H13, H19, H40 or H46*), 3.70 (3H, s, *H13, H19, H40 or H46*), 3.22-3.08 (2H, m, *H21*), 1.74-1.61 (2H, m, *H24*), 1.32-1.22 (2H, m, *H22*), 1.22-1.06 (2H, m, *H23*)

**$^{13}$C NMR:** (100 MHz, $CDCl_3$) δ: 172.9 (*C26*), 165.1 (*C1 & C28*), 160.0, 159.9, 159.8 & 159.7 (*C12, C18, C39 & C45*), 151.9 & 151.8 (*C6 & C33*), 147.2 & 146.9 (*C7 & C34*), 130.8, 130.6, 129.8 & 129.6 (*C10, C16, C37 & C43*), 128.6 & 128.5 (*C9, C15, C36 & C42*), 127.4 & 126.6 (*C2 & C29*), 124.3 & 124.3 (*C4 & C31*), 123.3 & 123.3 (*C3 & C30*), 117.3 & 117.0 (*C5 & C32*), 114.1, 114.1 & 113.9 (*C11, C17, C38 & C44*), 76.1, 75.9 & 71.2 (*C8, C14, C35 & C41*), 55.4, 55.3 & 55.3 (*C13, C19, C40 & C46*), 52.7 (*C25*), 52.3 (*C47*), 39.4 (*C21*), 31.8 (*C24*), 29.0 (*C22*), 23.2 (*C23*)

The characterisation data are consistent with those reported in the literature.

# 43. (2*S*)-2,6-Bis({2,3-bis[(4-methoxyphenyl)methoxy]phenyl}formamido)hexanoic acid

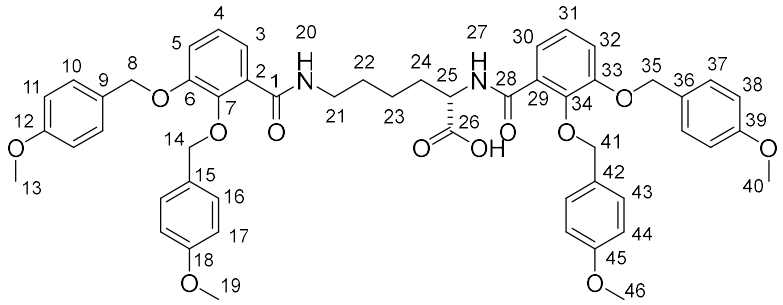

Chemical Formula: $C_{52}H_{54}N_2O_{12}$

Molecular Mass: 899.01 g $mol^{-1}$

Compound **43** was prepared in accordance with the literature.[201]

**42** (7.036 g, 7.71 mmol) was dissolved in 250 mL THF. 1 M LiOH in water (90 mL) was added and the solution was stirred vigorously at room temperature for 6.5 hours. The solution was acidified to pH 2 and the product extracted with ethyl acetate. The combined organic layers were dried over $MgSO_4$ and the solvent removed in vacuo. The product was purified by column chromatography (2% MeOH in chloroform) to yield a white foam solid.

**Yield:** 6.221 g, 6.92 mmol, 90%

**$R_f$:** 0.28 (8% MeOH in DCM)

**Melting Point:** 57-59 °C

**HRMS (ESI):** Calcd. $[M+H]^+$ ($C_{52}H_{55}N_2O_{12}$) m/z= 899.3750; Meas. m/z= 899.3794, Mean err -3.0 ppm. $[M+Na]^+$ ($C_{52}H_{54}N_2NaO_{12}$) m/z= 921.3569; Meas. m/z= 921.3611, Mean err -2.9 ppm

**$^1$H NMR:** (400 MHz, $CDCl_3$) δ: 8.63 (1H, d, $J^3_{H\text{-}H25}$= 7.0 Hz, *H27*), 8.01 (1H, t, $J^3_{H\text{-}H21}$= 5.5 Hz, *H20*), 7.72-7.65 (2H, m, *H3 & H30*), 7.37 (4H, d, $J^3_{H\text{-}H11/17/38/44}$= 8.5 Hz, *H10, H16, H37 or H43*), 7.23 (2H, d, $J^3_{H\text{-}H11/17/38/44}$= 8.5 Hz, *H10, H16, H37 or H43*), 7.18 (2H, d, $J^3_{H\text{-}H11/17/38/44}$= 8.5 Hz, *H10, H16, H37 or H43*), 7.14-7.07 (4H, m, *H4, H5, H31 & H32*), 6.91 (4H, d, $J^3_{H\text{-}H10/16/37/43}$= 8.5 Hz, *H11, H17, H38 or H44*), 6.79 (2H, d, $J^3_{H\text{-}H10/16/37/43}$= 8.5 Hz, *H11, H17, H38 or H44*), 6.74 (2H, d, $J^3_{H\text{-}H10/16/37/43}$= 8.5 Hz, *H11, H17, H38 or H44*), 5.04 (6H, s, *H8, H14, H35 & H41*) 4.95 (2H, s, *H8, H14, H35 & H41*), 4.51 (1H, td, $J^3_{H\text{-}H24}$= 7.5 Hz, $J^3_{H\text{-}H27}$= 5.5 Hz, *H25*), 3.82 (6H, s, *H13, H19, H40 & H46*), 3.72 (3H, s, *H13, H19, H40 & H46*),

3.69 (3H, s, *H13, H19, H40 & H46*), 3.22-3.08 (2H, m, *H21*), 1.81-1.67 (1H, m, *H24*), 1.52-1.40 (1H, m, *H24*), 1.30-1.14 (4H, m, *H22 &H23*)

**$^{13}$C NMR:** (100 MHz, $CDCl_3$) δ: 174.3 (*C26*), 166.1 (*C28*), 165.4 (*C1*), 160.0, 160.0, 159.8 & 159.7 (*C12, C18, C39 & C45*), 151.9 & 151.8 (*C6 & C33*), 147.3 & 147.0 (*C7 & C34*), 130.9, 130.6, 129.7 & 129.6 (*C10, C16, C37 & C43*), 128.6, 128.6, 128.5 & 128.4 (*C9, C15, C36 & C42*), 127.1 & 126.1 (*C2 & C29*), 124.3 (*C4 & C31*), 123.3 &, 123.2 (*C3 & C30*), 117.6 & 117.2 (*C5 &C32*), 114.2, 114.1, 114.1 & 114.0 (*C11, C17, C38 & C44*), 77.4, 76.2, 76.1 & 71.2 (*C8, C14, C35 & C41*), 55.4, 55.4 & 55.3 (*C13, C19, C40 & C46*), 53.0 (*C25*), 39.5 (*C21*), 31.1 (*C24*), 29.0 (*C22*), 23.1 (*C23*)

**IR ATIR ($cm^{-1}$):** 3361 w br (O-H), 2934 w br (C-H), 1734 m (C=O carboxylic acid), 1654 m (C=O amide), 1611 m (N-H), 1513 s (C-C Ar), 1458 m (O-H), 1246 s (C-N)

**Elemental Analysis:** Cald. For [$C_{52}H_{54}N_2O_{12}$]: %C 69.47, %H 6.05, %N 3.12; Measured for [$C_{52}H_{54}N_2O_{12}$]: %C 69.52, %H 6.23, %N 2.81

The characterisation data are consistent with those reported in the literature.

# [(*p*-Cymene)$RuCl_2$]$_2$

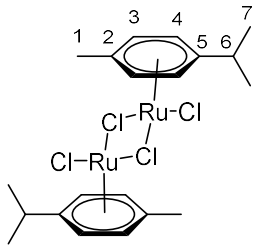


Chemical Formula: $C_{20}H_{28}Cl_4Ru_2$

Molecular Mass: 612.38 g $mol^{-1}$

[(*p*-cymene)$RuCl_2$]$_2$ was prepared in accordance with the literature.[202,203]

$RuCl_3 \cdot xH_2O$ (0.2615 g, 1 mmol) was placed in a Schlenk tube under an atmosphere of nitrogen. A solution of α-phellandrene (1.76 mL) in anhydrous, degassed ethanol (12 mL) was added and the solution heated to reflux for 4 hours. On cooling, the product precipitated as a red-brown solid that was isolated by filtration, washed with ice-cold methanol and dried under vacuum.

**$^1$H NMR:** (400 MHz, $CDCl_3$) δ: 5.46 (4H, d, $J^3_{H\text{-}H3}$ = 6.0 Hz, *H4*), 5.32 (4H, d, $J^3_{H\text{-}H4}$= 6.0 Hz, *H3*), 2.90 (2H, hept, $J^3_{H\text{-}H7}$ = 7.0 Hz, *H6*), 2.14 (6H, s, *H1*), 1.26 (12H, d, $J^3_{H\text{-}H6}$= 7.0 Hz, *H7*)

The characterisation data are consistent with those reported in the literature.

# (*p*-Cymene)Ru(ethylenediamine)Cl

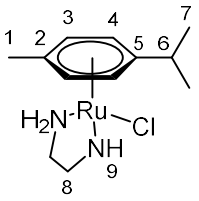


Chemical Formula: $C_{12}H_{21}ClN_2Ru$

Molecular Mass: 329.83 g $mol^{-1}$

(*p*-cymene)Ru(ethylenediamine)Cl was prepared by a method modified from the literature.[61]

[(*p*-cymene)$RuCl_2$]$_2$ (0.057 g, 0.093 mmol) and ethylene diamine (19 μL) were dissolved in dry, degassed ethanol (10 mL) under nitrogen. The reaction mixture was refluxed for 30 minutes. The solution was allowed to cool, concentrated *in vacuo* and the product precipitated from solution by addition of hexane.

**$^1$H NMR:** (400 MHz, MeOH-$d_4$) δ: 5.99 (1H, br, *H9*), 5.59 (2H, d, $J^3_{H\text{-}H3}$ = 6.0 Hz, *H4*), 5.42 (2H, d, $J^3_{H\text{-}H4}$= 6.0 Hz, *H3*), 4.03 (1H, br, *H9*), 2.85 (1H, hept, $J^3_{H\text{-}H7}$ = 7.0 Hz, *H6*), 2.56-2.46 (2H, m, *H8*), 2.44-2.33 (2H, m, *H8*), 2.20 (3H, s, *H1*), 1.26 (6H, d, $J^3_{H\text{-}H6}$= 7.0 Hz, *H7*)

# 44. Ethyl (2*R*)-2-[(2*S*)-2,6-bis({2,3-bis[(4-methoxyphenyl)methoxy]phenyl}formamido)hexanamido]-2-(cyclohexa-1,4-dien-1-yl)acetate

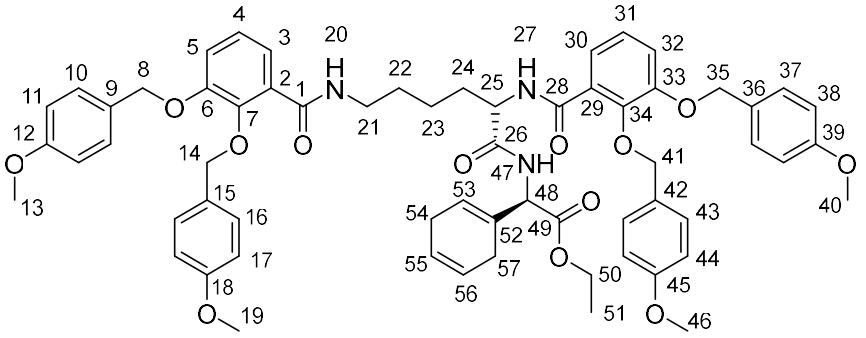

Chemical Formula: $C_{62}H_{67}N_3O_{13}$

Molecular Weight: 1062.23 g $mol^{-1}$

Under a nitrogen atmosphere, **43** (0.359 g, 0.40 mmol) was dissolved in anhydrous DMF (7 mL). HATU (0.137 g, 0.36 mmol) and DIPEA (140 µL, 0.80 mmol) were added and the solution stirred for 20 minutes at room temperature. A solution of **31** (0.220 g, 1.21 mmol) and DIPEA (105 µL, 0.60 mmol) in DMF (2 mL) was prepared and added to the solution of **43**. The reaction mixture was stirred at room temperature for 16 hours. The solvent was removed in vacuo and the resulting slurry taken up in DCM (40 mL) and washed with water (2 x 30 mL) and brine (1 x 30 mL). The organic layer was dried over $MgSO_4$ and volatiles removed in vacuo. The product was purified by column chromatography (7:3 ethyl acetate: petroleum ether 40-60 °C) to yield a white solid.

**Yield:** 0.270 g, 0.25 mmol, 64%

**$R_f$:** 0.31 (7:3 ethyl acetate:hexane)

**Melting Point:** 55-58 °C

**HRMS (ESI):** Calcd. $[M+Na]^+$ ($C_{62}H_{67}N_3NaO_{13}$) m/z= 1084.4566; Meas. m/z= 1084.4552, Mean err -0.7 ppm

**$^1$H NMR:** (400 MHz, $CDCl_3$) δ: 8.46 (1H, t, $J^3_{H\text{-}H21}$ = 8.0 Hz, *H27*), 7.98-7.88 (1H, m, *H20*), 7.77 – 7.59 (2H, m, *H3 & H30*), 7.38 (4H, d, $J^3_{H\text{-}H11/17/38/44}$ = 8.0 Hz, *H10, H16, H37 & H43*), 7.26 – 7.22 (2H, m, *H10, H16, H37 or H43*), 7.21-7.16 (2H, m, *H10, H16, H37 or H43*), 7.14 – 7.08 (4H, m, *H4, H5, H31 & H32*), 6.92 (4H, d, $J^3_{H\text{-}H10/16/37/43}$ = 8.0 Hz, *H11, H17, H38 & H44*), 6.83 – 6.78 (2H, m, *H11, H17, H38 or H44*), 6.78 – 6.74 (2H, m, *H11, H17, H38 or*

*H44*), 5.76 – 5.52 (3H, m, *H53, H55 & H56*), 5.13 – 4.84 (9H, m, *H8, H14, H35, H41 & H48*), 4.54 – 4.41 (1H, m, *H25*), 4.28 – 3.99 (2H, m, *H50*), 3.82 (6H, s, *H13, H19, H40 & H46*), 3.73 (6H, overlapping s, *H13, H19, H40 & H46*), 3.27 – 3.07 (2H, m, *H21*), 2.76 – 2.49 (4H, m, *H54 & H57*), 1.78 – 1.62 (1H, m, *H24*), 1.40 – 1.07 (8H, m, *H22, H23, H24 & H51*).

**$^{13}$C NMR:** (100 MHz, $CDCl_3$) δ: 171.1 (*C49*), 170.5 (*C26*), 165.8 (*C28*), 165.6 (*C52*), 165.1 (*C1*), 160.0, 160.0, 159.8 & 159.7 (*C12, C18, C39 & C45*), 151.9 & 151.8 (*C6 & C33*), 147.1 & 147.0 (*C7 & C34*), 130.9 (C52), 130.9, 130.6, 129.8 & 129.6 (*C10, C16, C37 & C43*), 128.7, 128.7, 128.5 & 128.4 (*C9, C15, C36 & C42*), 127.4 & 126.5 (*C2 & C29*), 124.3 & 124.3 (*C4 & C31*), 124.1, 123.7 & 123.6 (*C53, C55 & C56*), 123.3 (*C3 & C30*), 117.5 & 117.0 (*C5 & C32*), 114.1, 114.1, 114.0 & 114.0 (*C11, C17, C38 & C44*), 76.1, 76.0, 71.2 & 71.2 (*C8, C14, C35 & C41*), 61.7 (*C50*), 57.9 (*C48*), 55.4, 55.4 & 55.3 (*C13, C19, C40 & C46*), 53.5 (*C25*), 39.4 (*C21*), 31.1 or 30.8 (*C24*), 29.1 (*C22*), 26.8 & 26.4 (*C54 & C57*), 23.4 (*C23*), 14.2 (*C51*)

**Elemental Analysis:** Cald. For [$C_{62}H_{67}N_3O_{13}$]: %C 70.11, %H 6.36, %N 3.96; Measured for [$C_{62}H_{67}N_3O_{13}$]: %C 69.62, %H 6.18, %N 3.78

# 46. Ethyl (2R)-2-[(tert-butoxycarbonyl)amino]-2-(cyclohexa-1,4-dien-1-yl)acetate

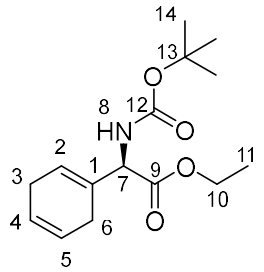


Chemical Formula: $C_{15}H_{23}NO_4$

Molecular Weight: 281.35 g $mol^{-1}$

Under a nitrogen atmosphere, **31** (0.483 g, 2.50 mmol) was dissolved in anhydrous, degassed dichloromethane (10 mL) and placed on ice. Triethylamine (0.835 mL, 6 mmol) was added followed by Boc anhydride (0.704 g, 3.22 mmol) at 0 °C. The solution was stirred at room temperature for 16 hours. The solution was evaporated to dryness then the residues dissolved in ethyl acetate (20 mL). The organic layer was washed with 5% citric acid solution (10 mL) followed by 5% sodium hydrogen carbonate solution (10 mL) then distilled water (10 mL). The organic layer was dried over $MgSO_4$ and the solvent evaporated.

**Yield:** 0.685 g, 2.43 mmol, 97%

**$^1$H NMR:** (400 MHz, $CDCl_3$) δ: 5.74 (1H, s, *H2*), 5.71-5.61 (2H, m, *H4 & H5*), 5.27 (1H, s, *H7*), 4.26-4.12 (2H, m, *H10*), 2.79-2.43 (4H, m, *H3 & H6*), 1.42 (9H, s, *H14*), 1.26 (3H, t, $J^3_{H\text{-}H21}$ = 7.0 Hz, *H11*)

# 47. [($\eta^6$-Phenylglycine)$RuCl_2]_2$ (dually protected, *N*-Boc, ethyl ester)

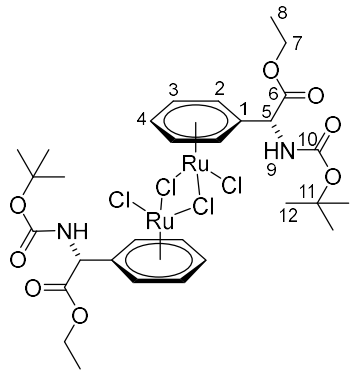


Chemical Formula: $C_{30}H_{42}Cl_4NO_4Ru_2$

Molecular Weight: 902.61 g $mol^{-1}$

**46** (0.5 g, 1.78 mmol) and $RuCl_3 \cdot xH_2O$ (0.080 g, 0.31 mmol) were placed in a Schlenk tube under a nitrogen atmosphere. Degassed anhydrous ethanol (3 mL) was added and the mixture stirred until both additives were completely dissolved. The solution was then transferred to a microwave vessel that had been purged with nitrogen. The solution was irradiated in a CEM Discover microwave reactor for 30 minutes with condition limits of 150 °C, 150 W, 250 psi. After irradiation the product was precipitated from solution by the addition of hexane and isolated by filtration.

# 48. [($\eta^6$-Phenylglycine)$RuCl_2$]$_2$·2HCl (protected, ethyl ester)

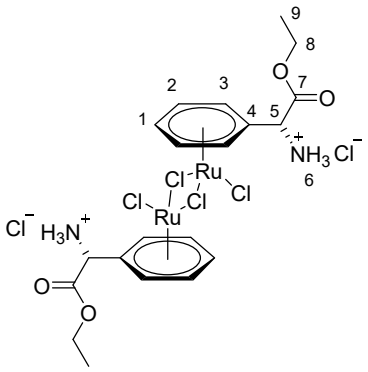


Chemical Formula: $C_{20}H_{28}Cl_6N_2O_4Ru_2$

Molecular Mass: 775.29 g $mol^{-1}$

Complex 48 was prepared in accordance with the literature.[157]

2,5-dihydrophenylglycine (0.539 g, 3.52 mmol) was dissolved in 2M HCl in EtOAc (10 mL) for one hour at room temperature. A solution of ruthenium trichloride hydrate (0.199 g, 0.71 mmol) in ethanol (35 mL) was then added and the solution heated at reflux overnight. The solution was allowed to cool to room temperature, then cooled to 0 °C. A few drops of 6 M HCl was added and the solution stirred for a further 30 minutes at 0 °C to promote the formation of the product as bright orange precipitate. The product was isolated by filtration under vacuum and washed with ice cold ethanol and hexane.

**Yield:** 0.207 g, 0.27 mmol, 75%

**HRMS (ESI):** Calcd. $[M\text{-}2HCl\text{-}Cl]^+$ ($C_{20}H_{26}Cl_3N_2O_4Ru_2$) m/z= 666.9040; Meas. m/z= 666.9063, Mean err -2.0 ppm

**$^1$H NMR:** (400 MHz, DMSO-$d_6$) δ: 8.98 (6H, br, *H6*), 6.36-6.27 (4H, m, *H2*), 6.25-6.19 (2H, m, *H1*), 6.17-6.10 (4H, m, *H3*), 5.15 (2H, s, *H5*), 4.27-4.12 (4H, m, *H8*), 1.18 (6H, t, $J^3_{H\text{-}H8}$= 7.0 Hz, *H9*)

**IR ATIR ($cm^{-1}$):** 3457 w br (N-H), 2982 br (C-H), 1737 s (C=O ester), 1496 s (C-C Ar), 1243 s (C-O ester)

The characterisation data are consistent with those reported in the literature.

# 49. 2,3,4,5,6-Pentafluorophenyl 2,6-bis({2,3-bis[(4-methoxyphenyl)methoxy]phenyl}formamido)hexanoate

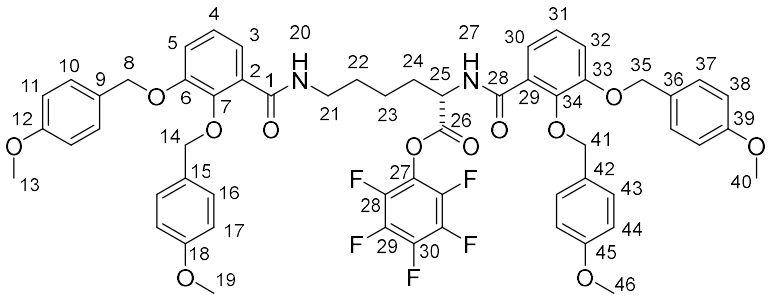

Chemical Formula: $C_{58}H_{53}F_5N_2O_{12}$

Molecular Mass: 1065.06 g $mol^{-1}$

Compound 49 was prepared by the "complex method" in accordance with the literature.[158,159]

Dicyclohexylcarbodiimide (DCC) (0.207 g, 1 mmol) and pentafluorophenol (0.565 g, 3.07 mmol) were dissolved in hexane (4 mL). The solution was refluxed for 70 hours in air with a drying tube attached. The solution was cooled to room temperature the solvent evaporated to dryness. The DCC-PFP complex was then recrystallised from hot hexane to yield 0.294 g of complex as a white solid.

Compound **43** (0.090 g, 0.10 mmol) was dissolved in ethyl acetate (2 mL) and placed on ice. DCC-PFP complex (0.077 g, 0.10 mmol) was added at 0 °C followed by DIPEA (54 µL, 0.3 mmol). The reaction mixture was stirred at room temperature for 16 hours. The solution was then cooled on dry ice for 20 minutes before filtration to remove dicyclohexyl urea (DCU). The filtrate was then evaporated to leave a white powder that was used without any further purification.

**$^1$H NMR:** (400 MHz, $CDCl_3$) δ: 8.63 (1H, d, $J^3_{H\text{-}H25}$= 7.0 Hz, *H27*), 8.01 (1H, t, $J^3_{H\text{-}H21}$= 5.5 Hz, *H20*), 7.72 (1H, dd, , $J^3_{H\text{-}H31}$= 7.5 Hz, $J^4_{H\text{-}H32}$= 2.0 Hz, *H30*), 7.67 (1H, dd, , $J^3_{H\text{-}H4}$= 7.5 Hz, $J^4_{H\text{-}H5}$= 2.0 Hz, *H3*), 7.37 (4H, d, $J^3_{H\text{-}H11/17/38/44}$= 8.5 Hz, *H10, H16, H37 or H43*), 7.22 (2H, d, $J^3_{H\text{-}H11/17/38/44}$= 8.5 Hz, *H10, H16, H37 or H43*), 7.18 (2H, d, $J^3_{H\text{-}H11/17/38/44}$= 8.5 Hz, *H10, H16, H37 or H43*), 7.14-7.07 (4H, m, *H4, H5, H31 & H32*), 6.91 (4H, d, $J^3_{H\text{-}H10/16/37/43}$= 8.5 Hz, *H11, H17, H38 or H44*), 6.79 (2H, d, $J^3_{H\text{-}H10/16/37/43}$= 8.5 Hz, *H11, H17, H38 or H44*), 6.74 (2H, d, $J^3_{H\text{-}H10/16/37/43}$= 8.5 Hz, *H11, H17, H38 or H44*), 5.06 (6H, s, *H8, H14, H35 & H41*) 4.95 (2H, s, *H8, H14, H35 & H41*), 4.85 (1H, td, $J^3_{H\text{-}H24}$= 7.5 Hz, $J^3_{H\text{-}H27}$= 5.5 Hz, *H25*), 3.82 (6H, s, *H13, H19, H40 & H46*), 3.72 (3H, s, *H13, H19, H40 & H46*), 3.69 (3H, s, *H13, H19, H40 &*

*H46*), 3.17 (2H, td, $J^3_{H\text{-}H22}$= 6.5 Hz, $J^3_{H\text{-}H20}$= 6.0 Hz, *H21*), 1.40-1.15 (6H, m, *H22, H23 & H24*)

**$^{19}$F NMR:** ($CDCl_3$) δ: -151.85 (2F, d, $J^3_{F\text{-}F}$= 18.0 Hz, $F_{ortho}$), -157.56 (1F, t, $J^3_{F\text{-}F}$= 22.0 Hz, $F_{para}$), -161.99 (2F, dd, $J^3_{F\text{-}F}$= 22.0 Hz, $J^3_{F\text{-}F}$= 18.0 Hz, $F_{meta}$)

## 6.4 Synthesis of Compounds Related to Chapter 3

## 87. 4-Methyl-*N*-(pyridine-2-ylmethyl)benzenesulfonamide

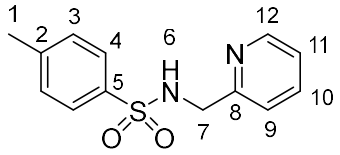


Chemical Formula: $C_{13}H_{14}N_2O_2S$

Molecular Mass: 262.08 g $mol^{-1}$

Compound **87** was prepared by a method modified from the literature.[100]

2-(Aminomethyl)pyridine (0.34 mL, 3.30 mmol) and triethylamine (0.92 mL, 6.60 mmol) were dissolved in dry DCM (60 mL) and placed in an ice bath. In a separate flask, 4-toluenesulfonyl chloride (0.687 g, 3.60 mmol) was dissolved in dry DCM (40 mL) and this solution added dropwise to the 2-(aminomethyl)pyridine solution whilst ensuring the temperature of the reaction remained below 5 °C. Once the addition was complete, the reaction mixture was left stirring in the ice bath for 10 minutes before allowing the mixture to come to room temperature and was left stirring for a further 16 hours. The solution was concentrated to approximately 30 mL on a rotary evaporator and the resulting solution washed with DI water (3 x 15 mL) and brine (1 x 15 mL). The organic layer was dried over $MgSO_4$ and the remaining solvent removed in vacuo. The crude product was purified by column chromatography (1:1 ethyl acetate: petroleum ether 40-60 °C).

**Yield:** 0.430 g, 1.64 mmol, 50%

**$R_f$:** 0.15 (3:2 ethyl acetate:petroleum ether 40-60 °C)

**Melting Point:** 91-94 °C

**HRMS (ESI):** Calcd. $[M+H]^+$ ($C_{13}H_{15}N_2O_2S$) m/z= 263.0849; Meas. m/z= 263.0847, Mean err 0.8 ppm. Calcd. $[M+Na]^+$ ($C_{13}H_{14}N_2NaO_2S$) m/z= 285.0668; Meas. m/z= 285.0665, Mean err 1.8 ppm

**$^1$H NMR:** (400 MHz, DMSO-$d_6$) δ: 8.39 (1H, ddd, $J^3_{H\text{-}H11}$= 5.0 Hz, , $J^4_{H\text{-}H10}$= 2.0 Hz, , $J^5_{H\text{-}H9}$= 1.0 Hz, *H12*), 8.16 (1H, br, *H6*), 7.68 (1H, apparent td, , $J^3_{H\text{-}H9/H11}$= 7.5 Hz, , $J^4_{H\text{-}H12}$= 2.0 Hz, *H10*), 7.66 (2H, d, , $J^3_{H\text{-}H3}$= 8.0 Hz, *H4*), 7.36-7.29 (3H, m, *H3 & H9*), 7.19 (1H, ddd, , $J^3_{H\text{-}H10}$= 7.5 Hz, , $J^3_{H\text{-}H12}$= 5.0 Hz, , $J^4_{H\text{-}H9}$= 1.0 Hz, *H11*), 4.03 (2H, s, *H7*), 2.33 (3H, s, *H1*)

**$^{13}$C NMR:** (100 MHz, DMSO-$d_6$) δ: 157.7 (*C8*), 149.3 (*C12*), 143.2 (*C5*), 138.2 (*C2*), 137.2 (*C10*), 130.1 (*C3*), 127.1 (*C4*), 122.9 (*C11*), 122.1 (*C9*), 48.5 (*C7*), 21.5 (*C1*)

**IR ATIR ($cm^{-1}$):** 3053 w br (C-H Ar), 2880 w br (C-H), 1599 m (C-C Ar), 1328 m (S=O)

**Elemental Analysis:** Cald. For [$C_{13}H_{14}N_2O_2S$]: %C 59.52, %H 5.38, %N 10.68; Measured for [$C_{13}H_{14}N_2O_2S$]: %C 57.65, %H 5.44, %N 10.46

# 88. 4-Methyl-*N*-{[5-(trifluoromethyl)pyridine-2-yl]methyl}benzene-1-sulfonamide

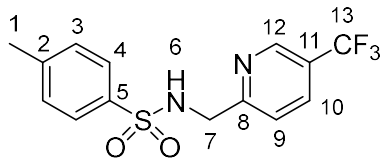


Chemical Formula: $C_{14}H_{13}F_3N_2O_2S$

Molecular Mass: 330.33 g $mol^{-1}$

Compound **88** was prepared by a method modified from the literature.[100]

Tosyl chloride (0.126 g, 0.66 mmol) was suspended in 10 mL DCM. A separate solution of (5-trifluoromethylpyridin-2-yl)methylamine (0.125 g, 0.59 mmol) and *N*,*N*-diisopropylethylamine (0.32 mL, 1.8 mmol) in 15 mL DCM was prepared and placed on ice. The tosyl chloride solution was added dropwise to the solution of (5-trifluoromethylpyridin-2-yl)methylamine at 0°C. Once the addition was complete, the reaction mixture was allowed to come to room temperature and left stirring overnight. The reaction mixture was concentrated to approx. 10 mL then washed with water (3 x 10 mL) and brine (1 x 10 mL). The organic layer was dried over $MgSO_4$ and the solvent removed in vacuo. The resulting solid was column chromatography (2:3 ethyl acetate: petroleum ether 40-60 °C) to yield a white powder.

**Yield:** 0.141 g, 0.43 mmol, 72%

**$R_f$:** 0.33 (2:3 ethyl acetate:petroleum ether 40-60 °C)

**Melting Point:** 130-132 °C

**HRMS (ESI):** Calcd. $[M+H]^+$ ($C_{14}H_{14}F_3N_2O_2S$) m/z= 331.0723; Meas. m/z= 331.0711, Mean err 2.8 ppm. Calcd. $[M+Na]^+$ ($C_{14}H_{13}F_3N_2NaO_2S$) m/z= 353.0542; Meas. m/z= 353.0545, Mean err -1.0 ppm

**$^1$H NMR:** (400 MHz, DMSO-$d_6$) δ: 8.76-8.73 (1H, m, *H12*), 8.34 (1H, t, $J^3_{H\text{-}H7}$= 6.5 Hz, *H6*), 8.08 (1H, dd, $J^3_{H\text{-}H9}$= 8.5 Hz, $J^4_{H\text{-}H12}$= 2.5 Hz, *H10*), 7.59 (2H, d, $J^3_{H\text{-}H3}$= 8.0 Hz, *H4*), 7.52 (1H, d, $J^3_{H\text{-}H10}$= 8.5 Hz, *H9*), 7.28 (2H, d, $J^3_{H\text{-}H4}$= 8.0 Hz, *H3*), 4.15 (2H, d, $J^3_{H\text{-}H6}$= 6.5 Hz, *H7*), 2.31 (3H, s, *H1*)

**$^{13}$C NMR:** (100 MHz, DMSO-$d_6$) δ: 162.5 (*C8*), 146.0 (*C12*), 143.2 (*C5*), 138.1 (*C2*), 134.6 (*C10*), 130.1 (*C3*), 127.1 (*C4*), 124.3 (d, $J^1_{C\text{-}F}$= 272 Hz, *C13*), 124.1 (q, $J^2_{C\text{-}F}$= 32 Hz, *C11*), 122.5 (*C9*), 48.2 (*C7*), 21.4 (*C1*)

**IR ATIR ($cm^{-1}$):** 3160 w br (C-H Ar), 2981 w br (C-H), 1327 m (S=O)

**Elemental Analysis:** Cald. For [$C_{14}H_{13}F_3N_2O_2S$]: %C 50.91, %H 3.97, %N 8.48; Measured for [$C_{14}H_{13}F_3N_2O_2S$]: %C 50.88, %H 4.33, %N 8.40

# 89. *N*-[(5-Chloropyridin-2-yl)methyl]-4-methylbenzene-1-sulfonamide

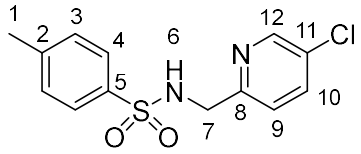


Chemical Formula: $C_{13}H_{13}ClN_2O_2S$

Molecular Mass: 296.77 g $mol^{-1}$

Compound **89** was recovered as a by-product in the synthesis of compound **93**.

**Yield:** 0.063 g, 0.21 mmol, 41%

**$R_f$:** 0.45 (1:1 ethyl acetate:petroleum ether 40-60 °C)

**Melting Point:** 126.9-128.5 °C

**HRMS (ESI):** Calcd. $[M+H]^+$ ($C_{13}H_{14}ClN_2O_2S$) m/z= 297.0459; Meas. m/z= 297.0466, Mean err -1.4 ppm. Calcd. $[M+Na]^+$ ($C_{13}H_{13}ClN_2NaO_2S$) m/z= 319.0278; Meas. m/z= 319.0284, Mean err -2.2 ppm. Calcd. $[M+K]^+$ ($C_{13}H_{13}ClKN_2O_2S$) m/z= 335.0018; Meas. m/z= 335.0013, Mean err -0.4 ppm

**$^1$H NMR:** (400 MHz, DMSO-$d_6$) δ: 8.42 (1H, dd, $J^4_{H\text{-}H10}$= 2.5 Hz, $J^5_{H\text{-}H9}$= 0.5 Hz, *H12*), 8.21 (1H, t, $J^3_{H\text{-}H7}$= 6.0 Hz, *H6*), 7.81 (1H, dd, $J^3_{H\text{-}H9}$= 8.5 Hz, $J^4_{H\text{-}H12}$= 2.5 Hz, *H10*), 7.60 (2H, d, $J^3_{H\text{-}H3}$= 7.5 Hz, *H4*), 7.36-7.28 (3H, m, *H3 & H9 overlap*), 4.02 (2H, d, $J^3_{H\text{-}H6}$= 6.0 Hz, *H7*), 2.33 (3H, s, *H1*)

**$^{13}$C NMR:** (100 MHz, DMSO-$d_6$) δ: 156.5 (*C8*), 147.7 (*C12*), 143.2 (*C5*), 138.2 (*C2*), 137.0 (*C10*), 130.1 (*C11*), 130.1 (*C3*), 127.1 (*C4*), 123.7 (*C9*), 47.8 (*C7*), 21.5 (*C1*)

**IR ATIR ($cm^{-1}$):** 3128 br (C-H), 2877 w (Ar C-H), 1329 m (S=O asymmetric stretch), 1158 m (S=O symmetric stretch)

**Elemental Analysis:** Cald. For [$C_{13}H_{13}ClN_2O_2S$]: %C 52.61, %H 4.42, %N 9.44; Measured for [$C_{13}H_{13}ClN_2O_2S$]: %C 52.76, %H 4.84, %N 9.39

# 90. *N*-[(5-Fluoropyridin-2-yl)methyl]-4-methylbenzene-1-sulfonamide

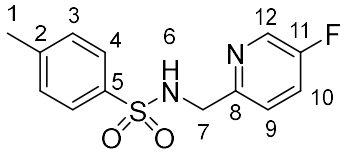


Chemical Formula: $C_{13}H_{13}FN_2O_2S$

Molecular Mass: 280.32 g $mol^{-1}$

Compound **90** was prepared by a method modified from the literature.[100]

Tosyl chloride (0.147 g, 0.77 mmol) was suspended in 10 mL DCM. A separate solution of (5-fluoropyridin-2-yl)methylamine (75 µL, 0.70 mmol) and *N*,*N*-diisopropylethylamine (0.25 mL, 1.4 mmol) in 15 mL DCM was prepared and placed on ice. The tosyl chloride solution was added dropwise to the solution of (5-fluoropyridin-2-yl)methylamine at 0°C. Once the addition was complete, the reaction mixture was allowed to come to room temperature and left stirring overnight. The reaction mixture was concentrated to approx. 10 mL then washed with water (3 x 10 mL) and brine (1 x 10 mL). The organic layer was dried over $MgSO_4$ and the solvent removed in vacuo. The resulting solid was column chromatography (2:3 ethyl acetate: petroleum ether 40-60 °C) to yield a white powder.

**Yield:** 0.131 g, 0.47 mmol, 67%

**$R_f$:** 0.22 (3:7 ethyl acetate:petroleum ether 40-60 °C)

**Melting Point:** 85-88 °C

**HRMS (ESI):** Calcd. $[M+H]^+$ ($C_{13}H_{14}FN_2O_2S$) m/z= 281.0755; Meas. m/z= 281.0759, Mean err -1.4 ppm. Calcd. $[M+Na]^+$ ($C_{13}H_{13}FN_2NaO_2S$) m/z= 303.0574; Meas. m/z= 303.0580, Mean err -0.8 ppm. Calcd. $[M+K]^+$ ($C_{13}H_{13}FKN_2O_2S$) m/z= 319.0313; Meas. m/z= 319.0308, Mean err 0.6 ppm

**$^1$H NMR:** (400 MHz, DMSO-$d_6$) δ: 8.38 (1H, d, $J^3_{H\text{-}F}$= 3.0 Hz, *H12*), 8.20 (1H, t, $J^3_{H\text{-}H7}$= 6.0 Hz, *H6*), 7.66-7.58 (3H, m, *H4 & H10 overlap*), 7.37 (1H, dd, $J^3_{H\text{-}H10}$= 8.5 Hz, $J^4_{H\text{-}F}$= 4.5 Hz, *H9*), 7.32 (2H, d, $J^3_{H\text{-}H4}$= 8.0 Hz, *H3*), 4.02 (2H, d, $J^3_{H\text{-}H6}$= 6.0 Hz, *H7*), 2.33 (3H, s, *H1*)

**$^{13}$C NMR:** (100 MHz, DMSO-$d_6$) δ: 158.8 (d, $J^1_{C\text{-}F}$= 252.0 Hz, *C11*), 154.2 (d, $J^4_{C\text{-}F}$= 3.5 Hz, *C8*), 143.2 (*C5*), 138.2 (*C2*), 137.1 (dd, $J^2_{C\text{-}F}$= 23.5 Hz, 18.0 Hz, *C12*), 130.1 (*C3*), 127.1 (*C4*), 124.1 (dd, $J^2_{C\text{-}F}$= 19.0 Hz, 11.5 Hz, *C10*), 123.7 (d, $J^3_{C\text{-}F}$= 4.0 Hz, *C9*), 47.8 (t, $J^5_{C\text{-}F}$= 9.0 Hz, *C7*), 21.5 (*C1*)

**IR ATIR ($cm^{-1}$):** 3103 w br (C-H Ar), 2931 w br (C-H), 1515 m (C-C Ar), 1324 m (S=O)

**Elemental Analysis:** Cald. For [$C_{13}H_{13}FN_2O_2S$]: %C 55.70, %H 4.67, %N 9.99; Measured for [$C_{13}H_{13}FN_2O_2S$]: %C 55.73, %H 4.96, %N 10.01

# 91. 4-Methyl-*N*-[(4-methylpyridin-2-yl)methyl]benzene-1-sulfonamide

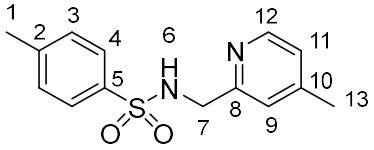


Chemical Formula: $C_{14}H_{16}N_2O_2S$

Molecular Mass: 276.35 g $mol^{-1}$

Compound **91** was prepared by a method modified from the literature.[100]

Tosyl chloride (0.126 g, 0.66 mmol) was suspended in 10 mL DCM. A separate solution of (4-methylpyridin-2-yl)methylamine (0.073 g, 0.59 mmol) and *N*,*N*-diisopropylethylamine (0.2 mL, 1.2 mmol) in 15 mL DCM was prepared and placed on ice. The tosyl chloride solution was added dropwise to the solution of (4-methylpyridin-2-yl)methylamine at 0°C. Once the addition was complete, the reaction mixture was allowed to come to room temperature and left stirring overnight. The reaction mixture was concentrated to approx. 10 mL then washed with water (3 x 10 mL) and brine (1 x 10 mL). The organic layer was dried over $MgSO_4$ and the solvent removed in vacuo. The resulting solid was column chromatography (3:2 ethyl acetate: petroleum ether 40-60 °C) to yield a white powder.

**Yield:** 0.110 g, 0.40 mmol, 68%

**$R_f$:** 0.30 (4:1 ethyl acetate:petroleum ether 40-60 °C)

**Melting Point:** 129-130 °C

**HRMS (ESI):** Calcd. $[M+H]^+$ ($C_{14}H_{17}N_2O_2S$) m/z= 277.1005; Meas. m/z= 277.1007, Mean err -1.3 ppm. Calcd. $[M+Na]^+$ ($C_{14}H_{16}N_2NaO_2S$) m/z= 299.0825; Meas. m/z= 299.0828, Mean err -0.8 ppm. Calcd. $[M+K]^+$ ($C_{14}H_{16}KN_2O_2S$) m/z= 315.0564; Meas. m/z= 315.0565, Mean err -0.8 ppm

**$^1$H NMR:** (400 MHz, DMSO-$d_6$) δ: 8.23 (1H, dd, $J^3_{H\text{-}H11}$= 5.0 Hz, $J^5_{H\text{-}H9}$= 0.5 Hz, *H12*), 8.11 (1H, br, *H6*), 7.62 (2H, d, $J^3_{H\text{-}H3}$= 8.0 Hz, *H4*), 7.32 (2H, d, $J^3_{H\text{-}H4}$= 8.0 Hz, *H3*), 7.05 (1H, s, *H9*), 7.02 (1H, d, $J^3_{H\text{-}H12}$= 5.0 Hz, *H11*), 3.97 (2H, apparent s, *H7*), 2.33 (3H, s, *H1*), 2.20 (3H, s, *H13*)

**$^{13}$C NMR:** (100 MHz, DMSO-$d_6$) δ: 157.4 (*C8*), 149.0 (*C12*), 147.8 (*C10*), 143.2 (*C5*), 138.3 (*C2*), 130.1 (*C3*), 127.1 (*C4*), 123.7 (*C11*), 122.8 (*C9*), 48.4 (*C7*), 21.5 (*C1*), 21.0 (*C13*)

**IR ATIR ($cm^{-1}$):** 3054 br (C-H Ar), 2853 br (C-H), 1610 m (C-C Ar), 1325 s (S=O asymmetric stretch), 1158 (S=O symmetric stretch)

**Elemental Analysis:** Cald. For [$C_{14}H_{16}N_2O_2S$]: %C 60.85, %H 5.84, %N 10.14; Measured for [$C_{14}H_{16}N_2O_2S$]: %C 60.47, %H 5.84, %N 9.94

# 92. 4-Methyl-*N*-[(5-methylpyridin-2-yl)methyl]benzene-1-sulfonamide

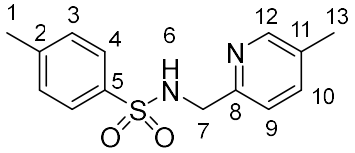


Chemical Formula: $C_{14}H_{16}N_2O_2S$

Molecular Mass: 276.35 g $mol^{-1}$

Compound **92** was prepared by a method modified from the literature.[100]

Tosyl chloride (0.147 g, 0.77 mmol) was suspended in 10 mL DCM. A separate solution of (5-methylpyridin-2-yl)methylamine (84 µL, 0.70 mmol) and triethylamine (0.2 mL, 1.44 mmol) in 15 mL DCM was prepared and placed on ice. The tosyl chloride solution was added dropwise to the (5-methylpyridin-2-yl)methylamine solution at 0°C. Once the addition was complete, the reaction mixture was allowed to come to room temperature and left stirring overnight. The reaction mixture was concentrated to approx. 10 mL then washed with water (3 x 10 mL) and brine (1 x 10 mL). The organic layer was dried over $MgSO_4$ and the solvent removed in vacuo. The resulting solid was column chromatography (3:2 ethyl acetate: petroleum ether 40-60 °C) to yield a white powder.

**Yield:** 0.120 g, 0.43 mmol, 62%

**$R_f$:** 0.23 (1:1 ethyl acetate:petroleum ether 40-60 °C)

**Melting Point:** 124-127 °C

**HRMS (ESI):** Calcd. $[M+H]^+$ ($C_{14}H_{17}N_2O_2S$) m/z= 277.1005; Meas. m/z= 277.1004, Mean err 0.6 ppm. Calcd. $[M+Na]^+$ ($C_{14}H_{16}N_2NaO_2S$) m/z= 299.0825; Meas. m/z= 299.0823, Mean err -1.5 ppm

**$^1$H NMR:** (400 MHz, DMSO-$d_6$) δ: 8.23-8.8.20 (1H, m, *H12*), 8.09 (1H, br, *H6*), 7.63 (2H, d, $J^3_{H\text{-}H3}$= 8.0 Hz, *H4*), 7.49 (1H, dd, $J^3_{H\text{-}H9}$= 8.0 Hz, $J^4_{H\text{-}H12}$= 2.0 Hz, *H10*), 7.32 (2H, d, $J^3_{H\text{-}H4}$= 8.0 Hz, *H3*), 7.19 (1H, d, $J^3_{H\text{-}H10}$= 8.0 Hz, *H9*), 3.95 (2H, br, *H7*), 2.34 (3H, s, *H1*), 2.20 (3H, s, *H13*)

**$^{13}$C NMR:** (100 MHz, DMSO-$d_6$) δ: 154.8 (*C8*), 149.4 (*C12*), 143.1 (*C5*), 138.2 (*C2*), 137.5 (*C10*), 132.0 (*C11*), 130.1 (*C3*), 127.1 (*C4*), 121.7 (*C9*), 48.2 (*C7*), 21.5 (*C1*), 18.1 (*C13*)

**IR ATIR ($cm^{-1}$):** 3043 w br (C-H Ar), 2846 w br (C-H), 1313 m (S=O), 1303 m (S=O)

**Elemental Analysis:** Cald. For [$C_{14}H_{16}N_2O_2S$]: %C 60.85, %H 5.84, %N 10.14; Measured for [$C_{14}H_{16}N_2O_2S$]: %C 60.77, %H 6.08, %N 10.17

# 93. *N*-{[5-(Dimethylamino)pyridin-2-yl]methyl}-4-methylbenzene-1-sulfonamide

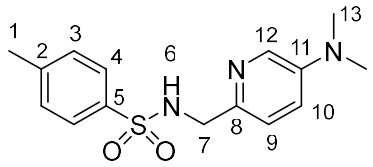


Chemical Formula: $C_{15}H_{19}N_3O_2S$

Molecular Mass: 305.40 g $mol^{-1}$

Compound **93** was prepared by a method modified from the literature.[100]

Tosyl chloride (0.147 g, 0.77 mmol) was suspended in 15 mL DCM. A separate solution of **94** (0.112 g, 0.77 mmol) and *N*,*N*-diisopropylethylamine (0.28 mL, 1.5 mmol) in 15 mL DCM was prepared and placed on ice. The tosyl chloride solution was added dropwise to the solution of **94** at 0°C. Once the addition was complete, the reaction mixture was allowed to come to room temperature and left stirring overnight. The reaction mixture was concentrated to approx. 10 mL then washed with water (3 x 10 mL) and brine (1 x 10 mL). The organic layer was dried over $MgSO_4$ and the solvent removed in vacuo. The resulting solid was column chromatography (1:1 ethyl acetate: petroleum ether 40-60 °C) to yield a white powder.

**Yield:** 0.049 g, 0.16 mmol, 21%

**$R_f$:** 0.23 (4:1 ethyl acetate:petroleum ether 40-60 °C)

**HRMS (ESI):** Calcd. $[M+H]^+$ ($C_{15}H_{20}N_3O_2S$) m/z= 306.1271; Meas. m/z= 306.1274, Mean err -1.3 ppm. Calcd. $[M+Na]^+$ ($C_{15}H_{19}N_3NaO_2S$) m/z= 328.1090; Meas. m/z= 328.1094, Mean err -1.9 ppm

**$^1$H NMR:** (400 MHz, DMSO-$d_6$) δ: 7.94 (1H, t, $J^3_{H\text{-}H7}$= 6.0 Hz, *H6*), 7.88 (1H, d, $J^4_{H\text{-}H10}$= 3.0 Hz, *H12*), 7.61 (2H, d, $J^3_{H\text{-}H3}$= 8.0 Hz, *H4*), 7.31 (2H, d, $J^3_{H\text{-}H4}$= 8.0 Hz, *H3*), 7.06 (1H, d, $J^3_{H\text{-}H10}$= 8.5 Hz, *H9*), 6.98 (1H, dd, $J^3_{H\text{-}H9}$= 8.5 Hz, $J^4_{H\text{-}H12}$= 3.0 Hz, *H10*), 3.87 (2H, d, $J^3_{H\text{-}H6}$= 6.0 Hz, *H7*), 2.84 (6H, s, *H13*), 2.33 (3H, s, *H1*)

**$^{13}$C NMR:** (100 MHz, DMSO-$d_6$) δ: 145.8 (*C8*), 144.5 (*C11*), 142.9 (*C5*), 138.3 (*C2*), 134.1 (*C12*), 130.0 (*C3*), 127.1 (*C4*), 122.3 (*C9*), 119.9 (*C10*), 48.1 (*C7*), 40.3 (*C13*), 21.5 (*C1*)

# 94. 6-(Aminomethyl)-*N*,*N*-dimethylpyridin-3-amine

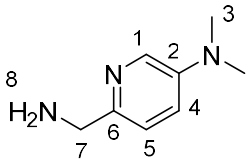


Chemical Formula: $C_8H_{13}N_3$

Molecular Mass: 151.21 g $mol^{-1}$

Compound **94** was prepared by a method modified from the literature.[172]

(5-chloropyridin-2-yl)methylamine (0.255 g, 1.8 mmol) and dimethylamine hydrochloride salt (2.208 g, 27 mmol) was dissolved in water (6 mL) in a microwave vessel. The solution was placed on ice and sodium hydroxide (1.802 g, 45 mmol) was added gradually. The solution was stirred well before being transferred to a CEM Discover microwave reactor and irradiated for 20 minutes intervals with conditions restricted to 190 °C, 250 psi. The reaction was stopped once a brown precipitate started to appear. Water was removed by evaporation under vacuum. The remaining residue was loaded onto a silica plug and eluted with 8% methanol in cholorform. The crude product contained a mixture of (5-chloropyridin-2-yl)methylamine and compound **94**.

**Crude yield:** 0.112 g, 0.74 mmol, 41%

**$R_f$:** 0.21 (8% MeOH in $CHCl_3$)

**HRMS (ESI):** Calcd. $[M+H]^+$ ($C_8H_{14}N_3$) m/z= 152.1182; Meas. m/z= 152.1186, Mean err -2.9 ppm

**$^1$H NMR:** (400 MHz, DMSO-$d_6$) δ: 8.05 (1H, d, $J^4_{H\text{-}H4}$= 3.0 Hz, *H1*), 7.11 (1H, d, $J^3_{H\text{-}H4}$= 8.5 Hz, *H5*), 6.95 (1H, dd, $J^3_{H\text{-}H5}$= 8.5 Hz, $J^4_{H\text{-}H1}$= 3.0 Hz, *H4*), 3.92 (2H, s, *H7*), 2.93 (6H, s, *H3*)

# 95. $[Cp^*IrCl_2]_2$

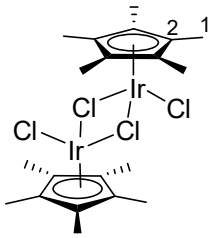


Chemical Formula: $C_{20}H_{30}Cl_4Ir_2$

Molecular Mass: 796.69 g $mol^{-1}$

$[Cp^*IrCl_2]_2$ was prepared based by a method modified from the literature.[173]

Iridium(III) chloride trihydrate (0.846 g, 2.40 mmol) was dissolved in degassed anhydrous methanol (25 mL) under a nitrogen atmosphere. 1,2,3,4,5-Pentamethylcyclopentadiene (0.90 mL, 5.75 mmol) was added, and the reaction mixture heated to reflux for 36 hours. The mixture was cooled to room temperature and the product isolated as a bright red/orange precipitate by filtration. The isolated product was rinsed with ice cold methanol. Further product was recovered by reducing the volume of the filtrate and cooling over ice.

**Yield:** 0.811 g, 1.02 mmol, 85%

**HRMS (LIFDI):** Calcd. $[M\text{-}Cl]^+$ ($C_{10}H_{15}IrCl_2$) m/z= 398.01746; Meas. m/z= 398.01661, Mean err 2.13 ppm

**$^1$H NMR:** (400 MHz, $CDCl_3$) δ: 1.59 (s, *H1*, 15H)

**$^{13}$C NMR:** (100 MHz, $CDCl_3$) δ: 86.3 (*C2*), 9.5 (*C1*)

**IR ATIR ($cm^{-1}$):** 2988 w (C-H), 2967 w (C-H), 2912 w (C-H), 1448 m (C-C Ar)

**Elemental Analysis:** Cald. For $[C_{20}H_{30}Cl_4Ir_2]$: %C 30.15, %H 3.80, %N 0.00; Measured for $[C_{20}H_{30}Cl_4Ir_2]$: %C 29.82, %H 3.88, %N 0.00

# Cp*Ir(87)Cl

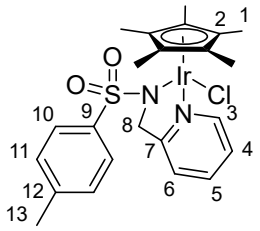


Chemical Formula: $C_{23}H_{28}ClIrN_2O_2S$

Molecular Mass: 624.22 g $mol^{-1}$

Complex Cp*Ir(**87**)Cl was prepared by a method modified from the literature.[100]

$[Cp^*IrCl_2]_2$ (0.050 g, 0.063 mmol) and **87** (0.033 g, 0.126 mmol) were dissolved in dry DCM (2 mL). NaOH (2 M in methanol, 60 µL) was added and the solution was placed in a sonicator for 20 minutes. 2 mL DI water was added, and the mixture stirred vigorously for 30 seconds. The organic layer was removed by syringe and the volume reduced to approximately 1/3$^{rd}$ volume in vacuo. The product was isolated by slow addition of diethyl ether, promoting the formation of the product as orange crystals, which were isolated by filtration.

**Yield:** 0.064 g, 0.10 mmol, 64%

**HRMS (ESI):** Calcd. $[M\text{-}Cl]^+$ ($C_{23}H_{28}IrN_2O_2S$) m/z= 589.1495; Meas. m/z= 589.1495, Mean err -0.1 ppm

**$^1$H NMR:** (400 MHz, $CDCl_3$) δ: 8.52 (1H, dq, $J^3_{H\text{-}H4}$= 5.5 Hz, $J^4_{H\text{-}H5}$= 0.5 Hz, *H3*), 7.87 (2H, d, $J^3_{H\text{-}H11}$= 8.0 Hz, *H10*), 7.65 (1H, td, $J^3_{H\text{-}H4/H6}$= 8.0 Hz, $J^4_{H\text{-}H3}$= 1.5 Hz, *H5*), 7.21 (1H, t, $J^3_{H\text{-}H3/H5}$= 6.5 Hz, *H4*), 7.16 (1H, d, $J^3_{H\text{-}H5}$= 8.0 Hz, *H6*), 7.07 (2H, d, $J^3_{H\text{-}H10}$= 8.0 Hz, *H11*), 4.78 and 4.58 (2H, br, *H8*), 2.27 (3H, s, *H13*), 1.72 (15H, s, *H1*)

**$^{13}$C NMR:** (100 MHz, $CDCl_3$) δ: 164.5 (*C7*), 151.2 (*C3*), 140.6 (*C9*), 139.8 (*C12*), 137.9 (*C5*), 128.9 (*C11*), 128.4 (*C10*), 124.7 (*C6*), 120.5 (*C4*), 86.6 (*C2*), 57.8 (*C8*), 21.5 (*C13*), 9.7 (*C1)*

**Elemental Analysis:** Cald. For $[C_{23}H_{28}ClIrN_2O_2S]$: %C 44.26, %H 4.52, %N 4.49; Measured for $[C_{23}H_{28}ClIrN_2O_2S]$: %C 43.83, %H 4.61, %N 4.99

# Cp*Ir(88)Cl

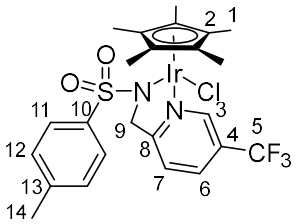


Chemical Formula: $C_{24}H_{27}ClF_3IrN_2O_2S$

Molecular Mass: 692.21 g $mol^{-1}$

Complex Cp*Ir(**88**)Cl was prepared by a method modified from the literature.[100]

$[Cp^*IrCl_2]_2$ (0.048 g, 0.06 mmol) and **88** (0.040 g, 0.12 mmol) were dissolved in dry DCM (2 mL). NaOH (2 M in methanol, 60 μL) was added and the solution was placed in a sonicator for 15 minutes. 2 mL DI water was added, and the mixture stirred vigorously for 30 seconds. The organic layer was removed by syringe and the volume reduced to approximately 1/3rd volume in vacuo. The product was isolated by slow addition of diethyl ether, promoting the formation of the product as yellow-orange crystals, which were isolated by filtration.

**Yield:** 0.047 g, 0.07 mmol, 56%

**HRMS (ESI):** Calcd. $[M\text{-}Cl]^+$ ($C_{24}H_{27}F_3IrN_2O_2S$) m/z= 657.1369; Meas. m/z= 657.1402, Mean err -2.4 ppm

**$^1$H NMR:** (400 MHz, $CDCl_3$) δ: 8.79 (1H, s, *H3*), 7.91 (1H, dd, $J^3_{H\text{-}H7}$= 8.5 Hz, $J^4_{H\text{-}H3}$= 2.0 Hz *H6*), 7.88 (2H, d, $J^3_{H\text{-}H12}$= 8.0 Hz, *H11*), 7.34 (1H, d, $J^3_{H\text{-}H6}$= 8.5 Hz, *H7*), 7.10 (2H, d, $J^3_{H\text{-}H11}$= 8.0 Hz, *H12*), 4.94 and 4.66 (2H, 2 x d, $J^2_{H\text{-}H9}$= 18.0 Hz, *H9*), 2.28 (3H, s, *H14*), 1.72 (15H, s, *H1*)

**$^{13}$C NMR:** (100 MHz, $CDCl_3$) δ: 168.7 (*C8*), 148.2 (*C3*), 141.0 (*C10*), 139.5 (*C13*), 134.7 (*C6*), 129.0 (*C12*), 128.3 (*C11*), 128.0 (*C4*), 122.2 (d, $J^1_{C\text{-}F}$= 272.5 Hz, *C5*), 120.8 (*C7*), 87.1 (*C2*), 57.9 (*C9*), 21.5 (*C14*), 9.6 (*C1*)

**Elemental Analysis:** Cald. For $[C_{24}H_{27}ClF_3IrN_2O_2S]$: %C 41.64, %H 3.93, %N 4.05; Measured for $[C_{24}H_{27}ClF_3IrN_2O_2S]$: %C 41.30, %H 3.94, %N 3.98

# Cp*Ir(89)Cl

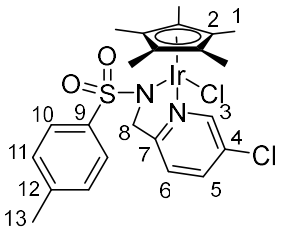


Chemical Formula: $C_{23}H_{27}Cl_2IrN_2O_2S$

Molecular Mass: 658.66 g $mol^{-1}$

Complex Cp*Ir(**89**)Cl was prepared by a method modified from the literature.[100]

$[Cp^*IrCl_2]_2$ (0.046 g, 0.06 mmol) and **89** (0.034 g, 0.12 mmol) were dissolved in dry DCM (2 mL). NaOH (2 M in methanol, 60 μL) was added and the solution was placed in a sonicator for 15 minutes. 2 mL DI water was added, and the mixture stirred vigorously for 30 seconds. The organic layer was removed by syringe and the volume reduced to approximately 1/3$^{rd}$ volume in vacuo. The product was isolated by slow addition of diethyl ether, promoting the formation of the product as yellow-orange crystals, which were isolated by filtration.

**Yield:** 0.041 g, 0.06 mmol, 99%

**HRMS (ESI):** Calcd. $[M\text{-}Cl]^+$ ($C_{23}H_{27}ClIrN_2O_2S$) m/z= 623.1105; Meas. m/z= 623.1107, Mean err -3.4 ppm

**$^1$H NMR:** (400 MHz, $CDCl_3$) δ: 8.48 (1H, dd, $J^4_{H\text{-}H5}$= 2.0 Hz, $J^5_{H\text{-}H6}$= 1.0 Hz *, H3*), 7.87 (2H, d, $J^3_{H\text{-}H11}$= 8.0 Hz, *H10*), 7.64 (1H, dd, $J^3_{H\text{-}H6}$= 8.5 Hz, $J^4_{H\text{-}H3}$= 2.0 Hz, *H5*), 7.14 (1H, dd, $J^3_{H\text{-}H5}$= 8.5 Hz, $J^5_{H\text{-}H3}$= 1.0 Hz, *H6*), 7.09 (2H, d, $J^3_{H\text{-}H10}$= 8.0 Hz, *H11*), 4.83 and 4.54 (2H, 2 x d, $J^2_{H\text{-}H8}$= 17.5 Hz, *H8*), 2.28 (3H, s, *H13*), 1.72 (15H, s, *H1*)

**$^{13}$C NMR:** (100 MHz, $CDCl_3$) δ: 163.1 (*C7*), 149.8 (*C3*), 140.8 (*C9*), 139.7 (*C12*), 137.9 (*C5*), 132.2 (*C4*), 128.9 (*C11*), 128.3 (*C10*), 120.9 (*C6*), 86.9 (*C2*), 57.3 (*C8*), 21.4 (*C13*), 9.6 (*C1*)

**Elemental Analysis:** Cald. For $[C_{23}H_{27}Cl_2IrN_2O_2S]$: %C 41.94, %H 4.13, %N 4.25; Measured for $[C_{23}H_{27}Cl_2IrN_2O_2S]$: %C 41.50, %H 4.28, %N 5.19

# Cp*Ir(90)Cl

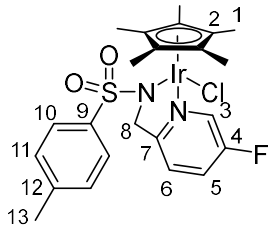


Chemical Formula: $C_{23}H_{27}ClFIrN_2O_2S$

Molecular Mass: 642.21 g $mol^{-1}$

Complex Cp*Ir(**90**)Cl was prepared by a method modified from the literature.[100]

$[Cp^*IrCl_2]_2$ (0.048 g, 0.06 mmol) and **90** (0.034 g, 0.12 mmol) were dissolved in dry DCM (2 mL). NaOH (2 M in methanol, 60 μL) was added and the solution was placed in a sonicator for 15 minutes. 2 mL DI water was added, and the mixture stirred vigorously for 30 seconds. The organic layer was removed by syringe and the volume reduced to approximately 1/3$^{rd}$ volume in vacuo. The product was isolated by slow addition of diethyl ether, promoting the formation of the product as a yellow solid, which were isolated by filtration.

**Yield:** 0.037 g, 0.06 mmol, 48%

**HRMS (ESI):** Calcd. $[M\text{-}Cl]^+$ ($C_{23}H_{27}ClFIrN_2O_2S$) m/z= 607.1401; Meas. m/z= 607.1428, Mean err -1.7 ppm

**$^1$H NMR:** (400 MHz, $CDCl_3$) δ: 8.41 (1H, apparent t, $J^3_{H\text{-}F}$= 2.5 Hz, *H3*), 7.87 (2H, d, $J^3_{H\text{-}H11}$= 8.0 Hz, *H10*), 7.44 (1H, ddd, $J^3_{H\text{-}H6}$= 9.0 Hz, $J^3_{H\text{-}F}$= 6.5 Hz, $J^4_{H\text{-}H3}$= 2.5 Hz, *H5*), 7.18 (1H, dd, $J^3_{H\text{-}H5}$= 9.0 Hz, $J^4_{H\text{-}F}$= 5.0 Hz, *H6*), 7.08 (2H, d, $J^3_{H\text{-}H10}$= 8.0 Hz, *H11*), 4.81 and 4.53 (2H, 2 x br d, $J^2_{H\text{-}H8}$= 16.5 Hz, *H8*), 2.28 (3H, s, *H13*), 1.73 (15H, s, *H1*)

**$^{13}$C NMR:** (100 MHz, $CDCl_3$) δ: 161.0 (d, $J^4_{C\text{-}F}$= 3.5 Hz, *C7*), 160.4 (*C4*), 140.8 (*C9*), 139.8 (*C12*), 139.6 (d, $J^2_{C\text{-}F}$= 23 Hz, *C3*), 128.9 (*C11*), 128.3 (*C10*), 125.5 (d, $J^2_{C\text{-}F}$= 19 Hz, *C5*), 121.0 (d, $J^3_{C\text{-}F}$= 5.5 Hz, *C6*), 86.9 (*C2*), 57.1 (*C8*), 21.4 (*C13*), 9.7 (*C1*)

**Elemental Analysis:** Cald. For $[C_{23}H_{27}ClFIrN_2O_2S]$: %C 43.02, %H 4.24, %N 4.36; Measured for $[C_{23}H_{27}ClFIrN_2O_2S]$: %C 43.07, %H 4.37, %N 4.17

# Cp*Ir(91)Cl

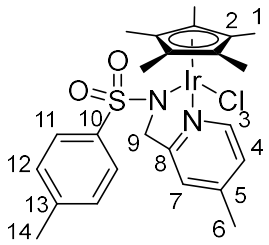


Chemical Formula: $C_{24}H_{30}ClIrN_2O_2S$

Molecular Mass: 638.24 g $mol^{-1}$

Complex Cp*Ir(**91**)Cl was prepared by a method modified from the literature.[100]

$[Cp^*IrCl_2]_2$ (0.048 g, 0.06 mmol) and **91** (0.033 g, 0.12 mmol) were dissolved in dry DCM (2 mL). NaOH (2 M in methanol, 60 μL) was added and the solution was placed in a sonicator for 15 minutes. 2 mL DI water was added, and the mixture stirred vigorously for 30 seconds. The organic layer was removed by syringe and the volume reduced to approximately 1/3$^{rd}$ volume in vacuo. The product was isolated by slow addition of diethyl ether, promoting the formation of the product as orange crystals, which were isolated by filtration.

**Yield:** 0.056 g, 0.09 mmol, 74%

**HRMS (ESI):** Calcd. $[M\text{-}Cl]^+$ ($C_{24}H_{30}IrN_2O_2S$) m/z= 603.1652; Meas. m/z= 603.1659, Mean err -2.7 ppm

**$^1$H NMR:** (400 MHz, $CDCl_3$) δ: 8.34 (1H, d, $J^3_{H\text{-}H4}$= 6.0 Hz, *H3*), 7.89 (2H, d, $J^3_{H\text{-}H12}$= 8.0 Hz, *H11*), 7.08 (2H, d, $J^3_{H\text{-}H11}$= 8.0 Hz, *H12*), 7.01 (1H, d, $J^3_{H\text{-}H3}$= 6.0 Hz, *H4*), 6.98 (1H, s, *H7*), 4.70 and 4.48 (2H, br, *H9*), 2.32 (3H, s, *H6*), 2.28 (3H, s, *H14*), 1.72 (15H, s, *H1*)

**$^{13}$C NMR:** (100 MHz, $CDCl_3$) δ: 163.9 (*C8*), 150.4 (*C3*), 150.1 (*C5*), 140.5 (*C10*), 139.9 (*C13*), 128.9 (*C12*), 128.4 (*C11*), 125.9 (*C4*), 121.1 (*C7*), 86.4 (*C2*), 57.6 (*C9*), 21.4 (*C14*), 21.1 (*C6*), 9.7 (*C1*)

**Elemental Analysis:** Cald. For $[C_{24}H_{30}ClIrN_2O_2S]$: %C 45.17, %H 4.74, %N 4.39; Measured for $[C_{24}H_{30}ClIrN_2O_2S]$: %C 44.95, %H 4.89, %N 4.36

# Cp*Ir(92)Cl

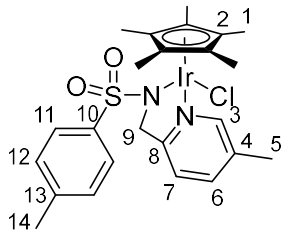


Chemical Formula: $C_{24}H_{30}ClIrN_2O_2S$

Molecular Mass: 638.24 g $mol^{-1}$

Complex Cp*Ir(**92**)Cl was prepared by a method modified from the literature.[100]

$[Cp^*IrCl_2]_2$ (0.048 g, 0.06 mmol) and **92** (0.034 g, 0.12 mmol) were dissolved in dry DCM (2 mL). NaOH (2 M in methanol, 60 μL) was added and the solution was placed in a sonicator for 15 minutes. 2 mL DI water was added, and the mixture stirred vigorously for 30 seconds. The organic layer was removed by syringe and the volume reduced to approximately 1/3$^{rd}$ volume in vacuo. The product was isolated by slow addition of diethyl ether, promoting the formation of the product as orange crystals, which were isolated by filtration.

**Yield:** 0.049 g, 0.08 mmol, 64%

**HRMS (ESI):** Calcd. $[M\text{-}Cl]^+$ ($C_{24}H_{30}IrN_2O_2S$) m/z= 603.1652; Meas. m/z= 603.1670, Mean err -1.4 ppm

**$^1$H NMR:** (400 MHz, $CDCl_3$) δ: 8.32 (1H, s, *H3*), 7.87 (2H, d, $J^3_{H\text{-}H12}$= 8.0 Hz, *H11*), 7.45 (1H, d, $J^3_{H\text{-}H7}$= 8.0 Hz, *H6*), 7.16-7.03 (3H, m, *H7 & H12*), 4.76 and 4.50 (2H, br, *H9*), 2.32 (3H, s, *H5*), 2.27 (3H, s, *H14*), 1.72 (15H, s, *H1*)

**$^{13}$C NMR:** (100 MHz, $CDCl_3$) δ: 161.7 (*C8*), 151.0 (*C3*), 138.8 (*C10*), 134.6 (*C13*), 129.8 (*C6*), 128.9 (*C12*), 128.4 (*C11*), 126.6 (*C4*), 119.8 (*C7*), 86.5 (*C2*), 57.4 (*C9*), 21.4 (*C14*), 18.1 (*C5*), 9.7 (*C1*)

**Elemental Analysis:** Cald. For $[C_{24}H_{30}ClIrN_2O_2S]$: %C 45.17, %H 4.74, %N 4.39; Measured for $[C_{24}H_{30}ClIrN_2O_2S]$: %C 44.07, %H 4.49, %N 4.14

# Cp*Ir(93)Cl

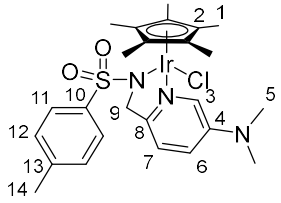

Chemical Formula: $C_{25}H_{33}ClIrN_3O_2S$

Molecular Mass: 667.29 g $mol^{-1}$

Complex Cp*Ir(**93**)Cl was prepared by a method modified from the literature.[100]

**Yield:** Quantitative

**HRMS (ESI):** Calcd. $[M\text{-}Cl]^+$ ($C_{25}H_{33}IrN_3O_2S$) m/z= 632.1917; Meas. m/z= 632.1919, Mean err -0.8 ppm

**$^1$H NMR:** (400 MHz, $CDCl_3$) δ: 7.92 (1H, m, *H3*), 7.88 (2H, d, $J^3_{H\text{-}H12}$= 7.0 Hz, *H11*), 7.07 (2H, d, $J^3_{H\text{-}H11}$= 7.0 Hz, *H12*), 6.93 (2H, m, *H6 & H7*), 4.67 and 4.41 (2H, 2 x br, *H9*), 2.96 (6H, s, *H5*), 2.27 (3H, s, *H14*), 1.73 (15H, s, *H1*)

**$^{13}$C NMR:** (100 MHz, $CDCl_3$) δ: 151.3 (*C8*), 146.7 (*C4*), 140.4 (*C10*), 140.1 (*C13*), 135.2 (*C3*), 128.8 (*C12*), 128.4 (*C11*), 121.2 (*C6*), 119.8 (*C7*), 86.3 (*C2*), 56.8 (*C9*), 40.1 (*C5*), 21.4 (*C14*), 9.7 (*C1*)

**Elemental Analysis:** Cald. For $[C_{25}H_{33}ClIrN_3O_2S]$: %C 45.00, %H 4.98, %N 6.30; Measured for $[C_{25}H_{33}ClIrN_3O_2S]$: %C 44.57, %H 4.79, %N 6.15

## 6.5 Synthesis of Compounds Related to Chapter 4

## 4-Cyano-*N*-[(pyrimidin-2-yl)methyl]benzene-1-sulfonamide

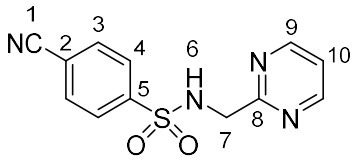


Chemical Formula: $C_{12}H_{10}N_4O_2S$

Molecular Mass: 274.30 g $mol^{-1}$

4-Cyano-*N*-[(pyrimidin-2-yl)methyl]benzene-1-sulfonamide was prepared by a method modified from the literature.[100]

2-(Aminomethyl)pyrimidine hydrochloride (0.582 g, 4.0 mmol) and triethylamine (1.73 mL, 12.40 mmol) were dissolved in anhydrous dichloromethane (60 mL) and placed in an ice bath. A solution of 4-cyanobenzenesulfonyl chloride (0.886 g, 4.40 mmol) in dichloromethane (50 mL) was prepared and added dropwise to the 2-(aminomethyl)pyrimidine solution whilst ensuring the temperature did not rise above 5 °C. Once the addition was complete, the reaction mixture was allowed to come to room temperature and left stirring overnight. The reaction mixture was concentrated to approx. 40 mL and washed with water (30 mL). The combine mixture was filtered to isolate the product as a white solid.

**Yield:** 0.727 g, 2.65 mmol, 66%

**$R_f$:** 0.41 (3:2 ethyl acetate:petroleum ether 40-60 °C)

**HRMS (ESI):** Calcd. $[M+H]^+$ ($C_{12}H_{11}N_4O_2S$) m/z= 275.0597; Obs. m/z= 275.0600, Mean err -0.1 ppm. Calcd. $[M+Na]^+$ ($C_{12}H_{10}N_4NaO_2S$) m/z= 297.0417; Obs. m/z= 297.0418, Mean err -1.5 ppm

**$^1$H NMR:** (400 MHz, DMSO-$d_6$) δ: 8.65 (t, $J^3$= 6.0 Hz, *H6*, 1H), 8.59 (d, $J^3$= 5.0 Hz, *H9*, 2H), 7.94 (d, $J^3$= 8.0 Hz, *H4*, 2H), 7.83 (d, $J^3$= 8.0 Hz, *H3*, 2H), 7.28 (t, $J^3$= 5.0 Hz, *H10*, 1H), 4.27 (d, $J^3$= 6.0 Hz, *H7*, 2H)

**$^{13}$C NMR:** (100 MHz, DMSO-$d_6$) δ: 165.7 (*C8*), 157.8 (*C9*), 145.7 (*C5*), 133.6 (*C3*), 127.8 (*C4*), 120.5 (*C10*), 118.3 (*C2*), 115.1 (*C1*), 49.1 (*C7*)

# 102. General Method

Compound **102a**-**102c** were prepared by a method modified from the literature.[100]

4-(Bromomethyl)benzenesulfonyl chloride (1 eq.) was dissolved in DCM in a round-bottom flask with a dropping funnel attached and placed in an ice bath. A separate solution of the necessary 2-(aminomethyl)pyridine compound (1.3 eq.) and DIPEA (2 eq.) in DCM was added to the dropping funnel and added to the 4-(bromomethyl)benzenesulfonyl chloride solution dropwise at 0 °C. The solution was stirred at 0 °C for 30 minutes then allowed to come to room temperature overnight. The solution was reduced ½ volume then washed with water and brine. The organic layer was dried over $MgSO_4$ and the solvent removed in vacuo. The product was purified by column chromatography (1:1 ethyl acetate: petroleum ether 40-60 °C).

# 102a. 4-(Bromomethyl)-*N*-[(pyridin-2-yl)methyl]benzene-1-sulfonamide

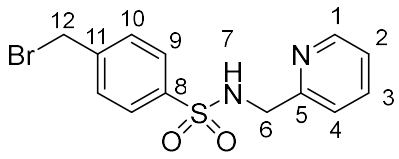


Chemical Formula: $C_{13}H_{13}BrN_2O_2S$

Molecular Mass: 341.22 g $mol^{-1}$

**Yield:** 1.533 g, 4.49 mmol, 90%

**$R_f$:** 0.30 (1:1 ethyl acetate: petroleum ether 40-60 °C)

**Melting Point:** decomposes 118 °C

**HRMS (ESI):** Calcd. $[M+H]^+$ ($C_{13}H_{14}BrN_2O_2S$) m/z= 340.9954; Meas. m/z= 340.9957, Mean err -0.8 ppm. Calcd. $[M+Na]^+$ ($C_{13}H_{13}BrN_2NaO_2S$) m/z= 362.9773; Meas. m/z= 362.9776, Mean err -0.6 ppm

**$^1$H NMR:** (400 MHz, DMSO-$d_6$) δ: 8.38 (1H, dq, $J^3_{H\text{-}H2}$= 5.0 Hz, $J^4_{H\text{-}H3}$= 1.0 Hz, *H1*), 8.31 (1H, t, $J^3_{H\text{-}H6}$= 6.5 Hz, *H7*), 7.73 (2H, d, $J^3_{H\text{-}H10}$= 8.0 Hz, *H9*), 7.67 (1H, apparent td, $J^3_{H\text{-}H2}$= 7.5 Hz, $J^3_{H\text{-}H4}$= 7.5 Hz, $J^4_{H\text{-}H1}$= 2.0 Hz, *H3*), 7.57 (2H, d, $J^3_{H\text{-}H9}$= 8.0 Hz, *H10*), 7.29 (1H, d, $J^3_{H\text{-}H3}$= 8.0 Hz, *H4*), 7.18 (1H, dd, $J^3_{H\text{-}H3}$= 7.5 Hz, $J^3_{H\text{-}H1}$= 5.0 Hz, *H2*), 4.71 (2H, s, *H12*), 4.07 (2H, d, $J^3_{H\text{-}H7}$= 6.5 Hz, *H6*)

**$^{13}$C NMR:** (100 MHz, DMSO-$d_6$) δ: 157.5 (*C5*), 149.3 (*C1*), 143.0 (*C11*), 140.8 (*C8*), 137.3 (*C3*), 130.5 (*C10*), 127.5 (*C9*), 123.0 (*C2*), 122.2 (*C4*), 48.5 (*C6*), 33.3 (*C12*)

**IR ATIR ($cm^{-1}$):** 3295 m (N-H), 3024 w br (C-H), 1325 m (S=O asymmetric stretch), 1161 m (S=O symmetric stretch)

**Elemental Analysis:** Cald. For [$C_{13}H_{13}BrN_2O_2S$]: %C 45.76, %H 3.84, %N 8.21; Measured for [$C_{13}H_{13}BrN_2O_2S$]: %C 46.41, %H 4.17, %N 8.19

# 102b. 4-(Bromomethyl)-*N*-[(4-methylpyridin-2-yl)methyl]benzene-1-sulfonamide

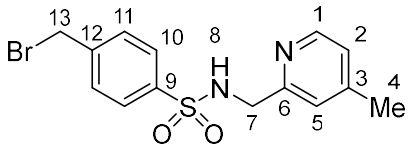


Chemical Formula: $C_{14}H_{15}BrN_2O_2S$

Molecular Mass: 355.25 g $mol^{-1}$

**Yield:** 0.981 g, 2.76 mmol, 69%

**$R_f$:** 0.18 (3:2 ethyl acetate: petroleum ether 40-60 °C)

**Melting Point:** decomposes on heating

**HRMS (ESI):** Calcd. $[M+H]^+$ ($C_{14}H_{16}BrN_2O_2S$) m/z= 355.0110; Meas. m/z= 355.0112, Mean err -1.5 ppm. Calcd. $[M+Na]^+$ ($C_{14}H_{15}BrN_2NaO_2S$) m/z= 376.9930; Meas. m/z= 376.9932, Mean err -0.9 ppm. Calcd. $[M+K]^+$ ($C_{14}H_{15}BrKN_2O_2S$) m/z= 392.9669; Meas. m/z= 392.9671, Mean err -1.9 ppm

**$^1$H NMR:** (400 MHz, DMSO-$d_6$) δ: 8.26 (1H, t, $J^3_{H\text{-}H7}$= 6.5, *H8*), 8.22 (1H, d, $J^3_{H\text{-}H2}$= 5.0 Hz, *H1*), 7.72 (2H, d, $J^3_{H\text{-}H11}$= 8.5 Hz, *H10*), 7.56 (2H, d, $J^3_{H\text{-}H10}$= 8.5 Hz, *H11*), 7.06 (1H, s, *H5*), 6.99 (1H, d, $J^3_{H\text{-}H1}$= 5.0 Hz, *H2*), 4.71 (2H, s, *H13*), 4.04 (2H, d, $J^3_{H\text{-}H8}$= 6.5 Hz, *H7*), 2.19 (3H, s, *H4*)

**$^{13}$C NMR:** (100 MHz, DMSO-$d_6$) δ: 157.1 (*C6*), 149.0 (*C1*), 147.9 (*C3*), 142.9 (*C12*), 140.9 (*C9*), 130.4 (*C11*), 127.5 (*C10*), 123.8 (*C2*), 122.9 (*C5*), 48.4 (*C7*), 33.3 (*C13*), 21.1 (*C4*)

**IR ATIR ($cm^{-1}$):** 3023 br (C-H), 2827 br (Ar C-H), 2687 br (Ar C-H), 1323 m (S=O asymmetric stretch), 1154 s (S=O symmetric stretch), 664 s (C-Br)

**Elemental Analysis:** Cald. For [$C_{14}H_{15}BrN_2O_2S$]: %C 47.33, %H 4.26, %N 7.89; Measured for [$C_{14}H_{15}BrN_2O_2S$]: %C 48.43, %H 4.65, %N 8.82

# 102c. 4-(Bromomethyl)-*N*-[(5-methylpyridin-2-yl)methyl]benzene-1-sulfonamide

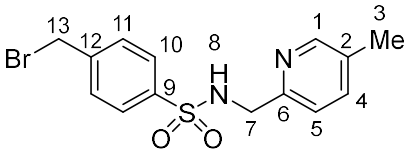


Chemical Formula: $C_{14}H_{15}BrN_2O_2S$

Molecular Mass: 355.25 g $mol^{-1}$

**Yield:** 1.8794 g, 5.51 mmol, 67%

**$R_f$:** 0.23 (3:2 ethyl acetate: petroleum ether 40-60 °C)

**Melting Point:** decomposes at 105-107 °C

**HRMS (ESI):** Calcd. $[M+H]^+$ ($C_{14}H_{16}BrN_2O_2S$) m/z= 355.0110; Meas. m/z= 355.0107, Mean err 0.6 ppm. Calcd. $[M+Na]^+$ ($C_{14}H_{15}BrN_2NaO_2S$) m/z= 376.9930; Meas. m/z= 376.9924, Mean err 1.1 ppm. Calcd. $[M+K]^+$ ($C_{14}H_{15}BrKN_2O_2S$) m/z= 392.9669; Meas. m/z= 392.9664, Mean err 0.5 ppm

**$^1$H NMR:** (400 MHz, DMSO-$d_6$) δ: 8.25 (1H, t, $J^3_{H\text{-}H7}$= 6.5, *H8*), 8.20 (1H, dt, $J^4_{H\text{-}H4}$= 2.5 Hz, $J^5_{H\text{-}H5}$= 1.0 Hz, *H1*), 7.71 (2H, d, $J^3_{H\text{-}H11}$= 8.5 Hz, *H10*), 7.55 (2H, d, $J^3_{H\text{-}H10}$= 8.5 Hz, *H11*), 7.45 (1H, dd, $J^3_{H\text{-}H5}$= 8.0 Hz, $J^4_{H\text{-}H1}$= 2.5 Hz, *H4*), 7.16 (1H, dd, $J^3_{H\text{-}H4}$= 8.0 Hz, $J^5_{H\text{-}H1}$= 1.0 Hz, *H5*), 4.71 (2H, s, *H13*), 4.03 (2H, d, $J^3_{H\text{-}H8}$= 6.5 Hz, *H7*), 2.91 (3H, s, *H3*)

**$^{13}$C NMR:** (100 MHz, DMSO-$d_6$) δ: 154.5 (*C6*), 149.4 (*C1*), 142.9 (*C12*), 140.9 (*C9*), 137.5 (*C4*), 132.0 (*C2*), 130.4 (*C11*), 127.6 (*C10*), 121.7 (*C5*), 48.2 (*C7*), 33.2 (*C13*), 18.1 (*C3*)

**IR ATIR ($cm^{-1}$):** 3047 br (C-H), 2858 br (Ar C-H), 1329 m (S=O asymmetric stretch), 1157 s (S=O symmetric stretch), 665 s (C-Br)

**Elemental Analysis:** Cald. For [$C_{14}H_{15}BrN_2O_2S$]: %C 47.33, %H 4.26, %N 7.89; Measured for [$C_{14}H_{15}BrN_2O_2S$]: %C 47.57, %H 4.30, %N 7.92

# 103. General Method

Compound **103a**-**103c** were prepared by a method modified from the literature.[204]

**102** (1 eq.) and potassium phthalimide salt (1.6 eq.) were dissolved in dry, degassed DMF in a round-bottomed flask fitted with a reflux condenser. The reaction mixture was heated to 100 °C under nitrogen overnight. The solution was concentrated under reduced pressure before water was added. The product was extracted with DCM and the combine organic layers washed brine, dried over $MgSO_4$, and the solvent removed in vacuo. The crude product was purified by column chromatography (30:19:1 ethyl acetate: petroleum ether 40-60 °C: methanol) to yield an off-white solid.

# 103a. 4-[(1,3-Dioxo-2,3-dihydro-1H-isoindol-2-yl)methyl]-*N*-[(pyridin-2-yl)methyl]benzene-1-sulfonamide

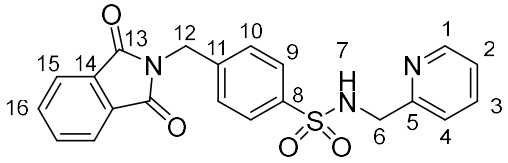


Chemical Formula: $C_{21}H_{17}N_3O_4S$

Molecular Mass: 407.44 g $mol^{-1}$

**Yield:** 1.107 g, 2.72 mmol, 65%

**$R_f$:** 0.14 (3:2 ethyl acetate: petroleum ether 40-60 °C)

**Melting Point:** 175.7-177.2 °C

**HRMS (ESI):** Calcd. $[M+H]^+$ ($C_{21}H_{18}N_3O_4S$) m/z= 408.1013; Meas. m/z= 408.1014, Mean err 1.1 ppm. Calcd. $[M+Na]^+$ ($C_{21}H_{17}N_3NaO_4S$) m/z= 430.0832; Meas. m/z= 430.0830, Mean err -0.3 ppm

**$^1$H NMR:** (400 MHz, DMSO-$d_6$) δ: 8.33 (1H, dq, $J^3_{H\text{-}H2}$= 5.0 Hz, $J^4_{H\text{-}H3}$= 1.0 Hz, *H1*), 8.24 (1H, t, $J^3_{H\text{-}H6}$= 6.0 Hz, *H7*), 7.92-7.81 (4H, m, *H15 & H16*), 7.69 (2H, d, $J^3_{H\text{-}H10}$= 8.0 Hz, *H9*), 7.61 (1H, apparent td, $J^3_{H\text{-}H2}$= 7.5 Hz, $J^3_{H\text{-}H4}$= 7.5 Hz, $J^4_{H\text{-}H1}$= 2.0 Hz, *H3*), 7.44 (2H, d, $J^3_{H\text{-}H9}$= 8.0 Hz, *H10*), 7.25 (1H, d, $J^3_{H\text{-}H3}$= 8.0 Hz, *H4*), 7.10 (1H, dd, $J^3_{H\text{-}H3}$= 7.5 Hz, $J^3_{H\text{-}H1}$= 5.0 Hz, *H2*), 4.80 (2H, s, *H12*), 4.02 (2H, d, $J^3_{H\text{-}H7}$= 5.0 Hz, *H6*)

**$^{13}$C NMR:** (100 MHz, DMSO-$d_6$) δ: 168.2 (*C13*), 157.6 (*C5*), 149.2 (*C1*), 141.7 (*C11*), 140.2 (*C8*), 137.1 (*C3*), 135.2 (*C16*), 132.1 (*C14*), 128.5 (*C10*), 127.4 (*C9*), 123.9 (*C15*), 122.8 (*C2*), 122.1 (*C4*), 48.5 (*C6*), 41.0 (*C12*)

**IR ATIR ($cm^{-1}$):** 3255 w (N-H sulfonamide), 1700 s (C=O amide), 1321 s (S=O asymmetric stretch), 1154 s (S=O symmetric stretch)

**Elemental Analysis:** Cald. For [$C_{21}H_{17}N_3O_4S$]: %C 61.91, %H 4.21, %N 10.31; Measured for [$C_{21}H_{17}N_3O_4S$]: %C 61.19, %H 4.82, %N 10.39

# 103b. 4-[(1,3-Dioxo-2,3-dihydro-1H-isoindol-2-yl)methyl]-*N*-[(4-methylpyridin-2-yl)methyl]benzene-1-sulfonamide

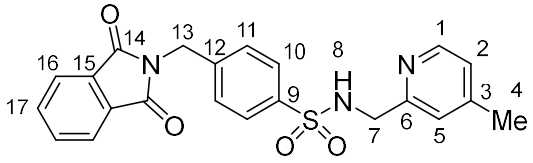


Chemical Formula: $C_{22}H_{19}N_3O_4S$

Molecular Mass: 421.47 g $mol^{-1}$

**Yield:** 0.584 g, 1.39 mmol, 57%

**$R_f$:** 0.16 (3:2 ethyl acetate: petroleum ether 40-60 °C with 2% EtOH)

**Melting Point:** 121.9-125.3 °C

**HRMS (ESI):** Calcd. $[M+H]^+$ ($C_{22}H_{20}N_3O_4S$) m/z= 422.1169; Meas. m/z= 422.1175, Mean err -2.1 ppm. Calcd. $[M+Na]^+$ ($C_{22}H_{19}N_3NaO_4S$) m/z= 444.0988; Meas. m/z= 444.0990, Mean err -1.0 ppm. Calcd. $[M+K]^+$ ($C_{22}H_{19}KN_3O_4S$) m/z= 460.0728; Meas. m/z= 460.0727, Mean err -3.1 ppm

**$^1$H NMR:** (400 MHz, DMSO-$d_6$) δ: 8.24-8.13 (2H, m, *H1 & H8*), 7.91-7.80 (4H, m, *H16 & H17*), 7.68 (2H, d, $J^3_{H\text{-}H11}$= 8.5 Hz, *H10*), 7.43 (2H, d, $J^3_{H\text{-}H10}$= 8.5 Hz, *H11*), 7.01 (1H, s, *H5*), 6.91 (1H, dd, $J^3_{H\text{-}H1}$= 5.0 Hz, $J^4_{H\text{-}H5}$= 1.0 Hz, *H2*), 4.80 (2H, s, *H13*), 3.99 (2H, d, $J^3_{H\text{-}H8}$= 6.5 Hz, *H7*), 2.14 (3H, s, *H4*)

**$^{13}$C NMR:** (100 MHz, DMSO-$d_6$) δ: 168.2 (*C14*), 157.2 (*C6*), 149.0 (*C1*), 147.7 (*C3*), 141.2 (*C12*), 140.3 (*C9*), 135.2 (*C17*), 132.1 (*C15*), 128.4 (*C11*), 127.4 (*C10*), 123.9 (*C16*), 123.6 (*C2*), 122.8 (*C5*), 48.4 (*C7*), 41.0 (*C13*), 20.9 (*C4*)

**IR ATIR ($cm^{-1}$):** 3259 br (N-H), 2962 m (C-H), 1710 s (C=O), 1330 m (S=O asymmetric stretch), 1156 m (S=O symmetric stretch)

**Elemental Analysis:** Cald. For [$C_{22}H_{19}N_3O_4S$]: %C 62.7, %H 4.54, %N 9.97; Measured for [$C_{22}H_{19}N_3O_4S$]: %C 57.45, %H 5.11, %N 7.85

# 103c. 4-[(1,3-Dioxo-2,3-dihydro-1H-isoindol-2-yl)methyl]-*N*-[(5-methylpyridin-2-yl)methyl]benzene-1-sulfonamide

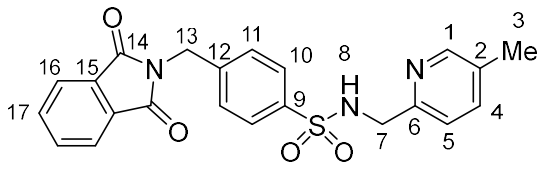


Chemical Formula: $C_{22}H_{19}N_3O_4S$

Molecular Mass: 421.47 g $mol^{-1}$

**Yield:** 0.900 g, 2.13 mmol, 46%

**$R_f$:** 0.24 (3:2 ethyl acetate: petroleum ether 40-60 °C with 6% EtOH)

**Melting Point:** 140.8-144.5 °C

**HRMS (ESI):** Calcd. $[M+H]^+$ ($C_{22}H_{20}N_3O_4S$) m/z= 422.1169; Meas. m/z= 422.1175, Mean err -1.6 ppm. Calcd. $[M+Na]^+$ ($C_{22}H_{19}N_3NaO_4S$) m/z= 444.0988; Meas. m/z= 444.0993, Mean err -2.0 ppm. Calcd. $[M+K]^+$ ($C_{22}H_{19}KN_3O_4S$) m/z= 460.0728; Meas. m/z= 460.0734, Mean err -1.5 ppm

**$^1$H NMR:** (400 MHz, DMSO-$d_6$) δ: 8.21-8.15 (2H, m, *H1 & H18*), 7.90-7.80 (4H, m, *H16 & H17*), 7.68 (2H, d, $J^3_{H\text{-}H11}$= 8.0 Hz, *H10*), 7.46-7.39 (3H, m, *H11 & H4*), 7.12 (1H, d, $J^3_{H\text{-}H4}$= 8.0 Hz, *H5*), 4.81 (2H, s, *H13*), 3.98 (2H, s, *H7*), 2.16 (3H, s, *H3*)

**$^{13}$C NMR:** (100 MHz, DMSO-$d_6$) δ: 168.2 (*C14*), 154.6 (*C6*), 149.4 (*C1*), 141.6 (*C12*), 140.3 (*C9*), 137.4 (*C4*), 135.2 (*C17*), 132.1 (*C15*), 132.0 (*C2*), 128.4 (*C11*), 127.4 (*C10*), 123.9 (*C16*), 121.7 (*C5*), 48.2 (*C7*), 41.0 (*C13*), 18.0 (*C3*)

**IR ATIR ($cm^{-1}$):** 3283 m (N-H), 1710 s (C=O), 1329 m (S=O asymmetric stretch), 1163 m (S=O symmetric stretch)

**Elemental Analysis:** Cald. For [$C_{22}H_{19}N_3O_4S$]: %C 62.70, %H 4.54, %N 9.97; Measured for [$C_{22}H_{19}N_3O_4S$]: %C 62.36, %H 4.44, %N 10.00

# 104. General Method

Compound **104a**-**104c** were prepared by a method modified from the literature.[205]

Under nitrogen, **103** (1 eq.) was dissolved in THF:ethanol. Hydrazine hydrate (10 eq.) was then added, and the reaction mixture stirred at room temperature for 5 minutes. The reaction mixture was then heated to reflux for 3 hours. The formation of a white precipitate (phthalhydrazide) indicates the progress of the reaction. The mixture was allowed to room to room temperature and the white precipitate was removed by filtration. The filtrate was concentrated in vacuo to leave a yellow oil which was redissolved and coevaporated with ethanol multiple times to give an off-white solid.

# 104a. 4-(Aminomethyl)-*N*-[(pyridin-2-yl)methyl]benzene-1-sulfonamide

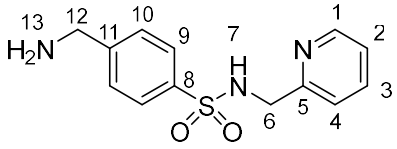


Chemical Formula: $C_{13}H_{15}N_3O_2S$

Molecular Mass: 277.34 g $mol^{-1}$

**Yield:** 0.253 g, 1.11 mmol, 94%

**$R_f$:** 0 (5% MeOH in $CDCl_3$)

**Melting Point:** 103-107 °C

**HRMS (ESI):** Calcd. $[M+H]^+$ ($C_{13}H_{16}N_3O_2S$) m/z= 278.0958; Meas. m/z= 278.0959, Mean err -0.7 ppm. Calcd. $[M+Na]^+$ ($C_{13}H_{15}N_3NaO_2S$) m/z= 300.0777; Meas. m/z= 300.0779, Mean err 0.6 ppm. Calcd. $[M+K]^+$ ($C_{13}H_{15}KN_3O_2S$) m/z= 316.0517; Meas. m/z= 316.0522, Mean err -1.3 ppm

**$^1$H NMR:** (400 MHz, DMSO-$d_6$) δ: 8.39 (1H, dq, $J^3_{H\text{-}H2}$= 5.0 Hz, $J^4_{H\text{-}H3}$= 1.0 Hz, *H1*), 7.73-7.65 (3H, m, *H3 & H9*), 7.48 (2H, d, $J^3_{H\text{-}H9}$= 8.0 Hz, *H10*), 7.32 (1H, d, $J^3_{H\text{-}H3}$= 8.0 Hz, *H4*), 7.20 (1H, dd, $J^3_{H\text{-}H3}$= 7.5 Hz, $J^3_{H\text{-}H1}$= 5.0 Hz, *H2*), 4.01 (2H, s, *H6*), 3.75 (2H, s, *H12*)

**$^{13}$C NMR:** (100 MHz, DMSO-$d_6$) δ: 157.7 (*C5*), 149.5 (*C11*), 149.3 (*C1*), 138.8 (*C8*), 137.3 (*C3*), 128.1 (*C10*), 127.0 (*C9*), 122.9 (*C2*), 122.1 (*C4*), 48.5 (*C6*), 45.6 (*C12*)

**IR ATIR ($cm^{-1}$):** 3342 m (N-H), 2853 w br (C-H), 1315 s (S=O asymmetric stretch), 1148 m (S=O symmetric stretch)

**Elemental Analysis:** Cald. For [$C_{13}H_{15}N_3O_2S$]: %C 56.30, %H 5.45, %N 15.15; Measured for [$C_{13}H_{15}N_3O_2S$]: %C 55.47, %H 6.01, %N 15.30

# 104b. 4-(Aminomethyl)-*N*-[(4-methylpyridin-2-yl)methyl]benzene-1-sulfonamide

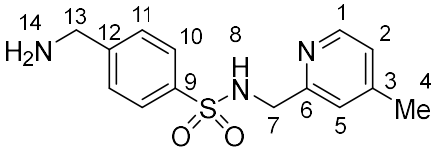


Chemical Formula: $C_{14}H_{17}N_3O_2S$

Molecular Mass: 291.37 g $mol^{-1}$

**Yield:** 0.129 g, 0.44 mmol, 41%

**$R_f$:** 0.0 (1:2 ethyl acetate: petroleum ether 40-60 °C)

**Melting Point:** 139.5-140.8 °C

**HRMS (ESI):** Calcd. $[M+H]^+$ ($C_{14}H_{18}N_3O_2S$) m/z= 292.1114; Meas. m/z= 292.1116, Mean err 0.2 ppm. Calcd. $[M+Na]^+$ ($C_{14}H_{17}N_3NaO_2S$) m/z= 314.0934; Meas. m/z= 314.0937, Mean err 0.4 ppm. Calcd. $[M+K]^+$ ($C_{14}H_{17}KN_3O_2S$) m/z= 330.0673; Meas. m/z= 330.0674, Mean err -0.6 ppm

**$^1$H NMR:** (400 MHz, DMSO-$d_6$) δ: 8.23 (1H, d, $J^3_{H\text{-}H2}$= 5.0 Hz, *H1*), 7.67 (2H, d, $J^3_{H\text{-}H11}$= 8.0 Hz, *H10*), 7.47 (2H, d, $J^3_{H\text{-}H10}$= 8.0 Hz, *H11*), 7.08 (1H, s, *H5*), 7.02 (1H, d, $J^3_{H\text{-}H1}$= 5.0 Hz, *H2*), 3.96 (2H, s, *H7*), 3.74 (2H, s, *H13*), 2.21 (3H, s, *H4*)

**$^{13}$C NMR:** (100 MHz, DMSO-$d_6$) δ: 157.4 (*C6*), 149.7 (*C12*), 149.0 (*C1*), 147.8 (*C3*), 138.8 (*C9*), 128.0 (*C11*), 127.0 (*C10*), 123.7 (*C2*), 122.8 (*C5*), 48.4 (*C7*), 45.7 (*C13*), 21.0 (*C4*)

**IR ATIR ($cm^{-1}$):** 3340 m (1° amine N-H), 3258 w (C-H), 3167 w (C-H), 2662 br (Ar C-H), 1309 m (S=O asymmetric stretch), 1149 s (S=O symmetric stretch)

**Elemental Analysis:** Cald. For [$C_{14}H_{17}N_3O_2S$]: %C 57.71, %H 5.88, %N 14.42; Measured for [$C_{14}H_{17}N_3O_2S$]: %C 57.45, %H 6.28, %N 14.68

# 104c. 4-(Aminomethyl)-*N*-[(5-methylpyridin-2-yl)methyl]benzene-1-sulfonamide

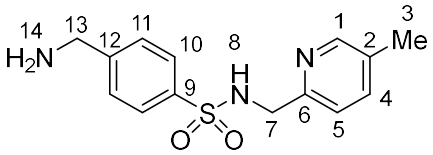


Chemical Formula: $C_{14}H_{17}N_3O_2S$

Molecular Mass: 291.37 g $mol^{-1}$

**Yield:** 0.214 g, 0.73 mmol, 81%

**$R_f$:** 0.0 (1:2 ethyl acetate: petroleum ether 40-60 °C)

**Melting Point:** 117-119 °C

**HRMS (ESI):** Calcd. $[M+H]^+$ ($C_{14}H_{18}N_3O_2S$) m/z= 292.1114; Meas. m/z= 292.1113, Mean err 0.1 ppm. Calcd. $[M+Na]^+$ ($C_{14}H_{17}N_3NaO_2S$) m/z= 314.0934; Meas. m/z= 314.0935, Mean err -1.3 ppm. Calcd. $[M+K]^+$ ($C_{14}H_{17}KN_3O_2S$) m/z= 330.0673; Meas. m/z= 330.0672, Mean err -3.1 ppm

**$^1$H NMR:** (400 MHz, DMSO-$d_6$) δ: 8.23-8.20 (1H, m, *H1*), 7.68 (2H, d, $J^3_{H\text{-}H11}$= 8.5 Hz, *H10*), 7.53-7.45 (3H, m, *H11 & H4*), 7.20 (1H, dd, $J^3_{H\text{-}H4}$= 8.0 Hz, $J^5_{H\text{-}H1}$= 1.0 Hz, *H5*), 3.96 (2H, s, *H7*), 3.74 (2H, s, *H13*), 2.21 (3H, s, *H3*)

**$^{13}$C NMR:** (100 MHz, DMSO-$d_6$) δ: 154.8 (*C6*), 149.7 (*C12*), 149.4 (*C1*), 138.8 (*C9*), 137.5 (*C4*), 132.0 (*C2*), 128.0 (*C11*), 127.0 (*C10*), 121.7 (*C5*), 48.2 (*C7*), 45.7 (*C13*), 18.1 (*C3*)

**IR ATIR ($cm^{-1}$):** 3332 m (1° amine N-H), 3169 w (C-H), 2660 br (Ar C-H), 1308 m (S=O asymmetric stretch), 1149 s (S=O symmetric stretch)

**Elemental Analysis:** Cald. For [$C_{14}H_{17}N_3O_2S$]: %C 57.71, %H 5.88, %N 14.42; Measured for [$C_{14}H_{17}N_3O_2S$]: %C 57.36, %H 5.61, %N 14.34

# 2,3-Bis(benzyloxy)benzaldehyde

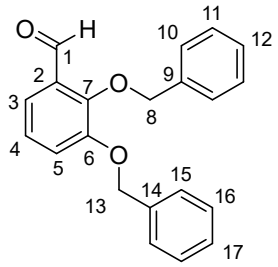


Chemical Formula: $C_{21}H_{18}O_3$

Molecular Mass: 318.37 g $mol^{-1}$

2,3-Bis(benzyloxy)benzaldehyde was prepared based on a preparation from the literature[177,206].

2,3-Dihydroxybenzaldehyde (4.073 g, 29.49 mmol) and benzyl chloride (8 mL, 69.50 mmol) were dissolved in dry ethanol (90 mL). To this solution was added anhydrous $K_2CO_3$ (5.217 g, 37.75 mmol). The solution was refluxed at 82 °C for 20 hours then left to cool. The resulting brown precipitate was dissolved in ethyl acetate (150 mL) and this solution washed with water (2 x 50 mL), brine (1 x 50 mL) and brine:water (1:1) (1 x 50 mL). The solvent was removed in vacuo to yield a beige solid. The crude product was purified by flash column chromatography (5:1 petroleum ether 40-60 °C: ethyl acetate).

**Yield:** 6.620 g, 20.8 mmol, 71%

**$R_f$:** 0.31 (1:5 ethyl acetate: petroleum ether 40-60 °C)

**Melting Point:** 94-96 °C

**HRMS (ESI):** Calcd. $[M+Na]^+$ ($C_{21}H_{18}NaO_3$) m/z= 341.1148; Meas. m/z= 341.1150, Mean err -0.7 ppm. Calcd. $[M+K]^+$ ($C_{21}H_{18}KO_3$) m/z= 357.0888; Meas. m/z= 357.0888, Mean err -1.6 ppm

**$^1$H NMR:** (400 MHz, $CDCl_3$) δ: 10.29 (1H, s, *H1*), 7.49 (2H, d, $J^3_{H\text{-}H11}$= 8.0 Hz, *H10*), 7.46-7.30 (9H, m, *H3, H11-12 & H15-17*), 7.25 (1H, dd, $J^3_{H\text{-}H4}$= 8.0 Hz, $J^4_{H\text{-}H3}$= 1.5 Hz, *H5*), 7.12 (1H, apparent t, $J^3_{H\text{-}H3/5}$= 8.0 Hz, *H4*), 5.22 (2H, s, *H8*), 5.19 (2H, s, *H13*)

**$^{13}$C NMR:** (100 MHz, $CDCl_3$) δ: 190.3 (*C1*), 152.3 (*C6*), 151.7 (*C7*), 136.5 & 136.4 (*C9 & C14*), 130.6 (*C2*), 128.9 & 128.9 (*C11 & C16*), 128.7 & 128.7 &128.4 (*C12, C15 & C17*), 127.7 (*C10*), 124.4 (*C4*), 120.0 (*C5*), 119.7 (*C3*), 76.6 (*C8*), 71.4 (*C13*)

**IR ATIR ($cm^{-1}$):** 3029 w (C-H Ar), 2878 w br (C-H), 1691 s (C=O), 1582 s (C-C Ar)

**Elemental Analysis:** Cald. For [$C_{21}H_{18}O_3$]: %C 79.23, %H 5.70, %N 0.00; Measured for [$C_{21}H_{18}O_3$]: %C 78.95, %H 6.08, %N 0.00

# 2,3-Bis(benzyloxy)benzoic acid

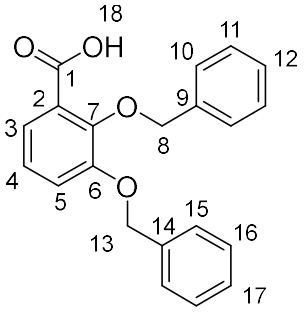


Chemical Formula: $C_{21}H_{18}O_4$

Molecular Mass: 334.37 g $mol^{-1}$

2,3-Bis(benzyloxy)benzoic acid was prepared based on a preparation from the literature[177,206].

2,3-Bis(benzyloxy)benzaldehyde (6.620 g, 20.8 mmol) was ground to a fine powder and suspended in 40 mL acetone and 40 mL water. Solutions of sodium chlorite (3.213 g, 35.53 mmol) in DI water (30 mL) and a second solution of sulfamic acid (4.300 g, 44.29 mmol) in DI water (40 mL) were prepared and these were added dropwise and alternately to the aldehyde suspension over 30 minutes. The reaction mixture was stirred in air for 3.5 hours. Acetone was removed in vacuo and the suspension cooled before the solid was filtered under vacuum. The collected solid was recrystallised from hot ethanol and stored in a dessicator.

**Yield:** 6.301 g, 18.8 mmol, 91%

**$R_f$:** 0.43 (20:1 chloroform:methanol)

**Melting Point:** 124-125 °C

**HRMS (ESI):** Calcd. $[M+Na]^+$ ($C_{21}H_{18}NaO_4$) m/z= 357.1097; Meas. m/z= 357.1096, Mean err 0.4 ppm

**$^1$H NMR:** (400 MHz, $CDCl_3$) δ: 11.39 (1H, br, *H18*), 7.71 (1H, dd, $J^3_{H\text{-}H4}$= 8.0 Hz, $J^4_{H\text{-}H5}$= 1.5 Hz, *H3*), 7.50-7.22 (11H, m, *H5, H10-12*, *H15-17*), 7.19 (1H, apparent t, $J^3_{H\text{-}H3/H5}$= 8.0 Hz, *H4*), 5.24 (s, *H8*, 2H), 5.18 (s, *H13*, 2H)

**$^{13}$C NMR:** (100 MHz, $CDCl_3$) δ: 165.3 (*C1*), 151.4 (*C6*), 147.2 (*C7*), 135.9 (*C14*), 134.7 (*C9*), 129.4, 129.0, 128.9, 128.7 & 127.9 (*C10-12 & C15-17*), 125.2 (*C4*), 124.6 (*C3*), 123.1 (*C2*), 119.1 (*C5*), 77.2 (*C8*), 71.6 (*C13*)

**IR ATIR ($cm^{-1}$):** 3062 w (C-H), 3031 w (C-H), 2872 w br (O-H), 1684 s (C=O), 1257 s (C-O)

**Elemental Analysis:** Cald. For [$C_{21}H_{18}O_4$]: %C 75.43, %H 5.43, %N 0.00; Measured for [$C_{21}H_{18}O_4$]: %C 75.05, %H 5.60, %N 0.00

# 2,3-Bis(benzyloxy)benzoic acid-*N*-hydroxysuccinimide ester

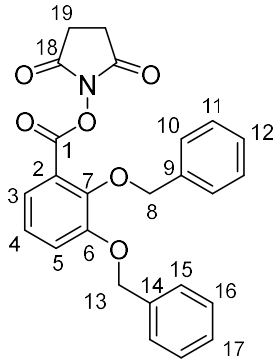


Chemical Formula: $C_{25}H_{21}NO_6$

Molecular Mass: 431.44 g $mol^{-1}$

2,3-Bis(benzyloxy)benzoic acid-*N*-hydroxysuccinimide ester was prepared based on a preparation from the literature[177].

2,3-Bis(benzyloxy)benzoic acid (4.502 g, 13.5 mmol) and *N*-hydroxysuccinimide (1.561 g, 13.6 mmol) were dissolved in dioxane (30 mL) and placed on ice. To this solution was added *N*,*N*'-dicyclohexylcarbodiimide (2.788 g, 13.5 mmol) and reaction mixture was stirred for 10 minutes on ice. The flask was then removed from the ice bath and the reaction mixture left to stir overnight at room temperature. The reaction mixture was then filtered under gravity to remove urea then the volatiles removed in vacuo to leave an orange oil. Isopropanol was added drop wise to the vigorously stirring oil to promote formation of a solid. The resulting solid was filtered and washed with isopropanol/ethanol (1:1). The product was then left in a desiccator overnight before being recrystallized with hot ethyl acetate to yield off-white crystals.

**Yield:** 3.465 g, 8.0 mmol, 59%

**$R_f$**: 0.87 (10:1 acetone:methanol)

**Melting Point:**115-117 °C

**HRMS (ESI):** Calcd. $[M+Na]^+$ ($C_{25}H_{21}NNaO_6$) m/z= 454.1261; Meas. m/z= 454.1259, Mean err 0.8 ppm

**$^1$H NMR:** (400 MHz, $CDCl_3$) δ: 7.59 (1H, dq, $J^3_{H\text{-}H4}$= 8.0 Hz, $J^4_{H\text{-}H5}$= 0.6 Hz, *H3*), 7.45-7.21 (11H, m, *H5, H10-12, H15-17*), 7.13 (1H, apparent td, $J^3_{H\text{-}H3/H5}$= 8.0 Hz, $J^{Ar}$= 0.6 Hz, *H4*), 5.14 (4H, s, *H8, H13*), 2.87 (4H, br, *H19*)

**$^{13}$C NMR:** (100 MHz, $CDCl_3$) δ: 169.4 (*C18*), 160.8 (*C1*), 153.1 (*C7*), 149.9 (*C6*), 137.1 (*C9*), 136.3 (*C14*), 128.8, 128.7, 128.4, 128.3, 128.1 & 127.7 (*C10-12 & C15-17*), 124.4 (*C4*), 123.8 (*C3*), 121.1 (*C2*), 120.2 (*C5*), 76.0 (*C8*), 71.5 (*C13*), 25.8 (*C19*)

**IR ATIR ($cm^{-1}$):** 1764 m (C=O ester), 1733 s (C=O amide), 1206 s (C-O ester), 1010 s (C-N amide)

**Elemental Analysis:** Cald. For [$C_{25}H_{21}NO_6$]: %C 69.60, %H 4.91, %N 3.25; Measured for [$C_{25}H_{21}NO_6$]: %C 69.45, %H 4.72, %N 3.26

# (2*S*)-2,6-Bis({[2,3-bis(benzyloxy)phenyl]formamido})hexanoic acid = ($Bn_4$-azotochelin)

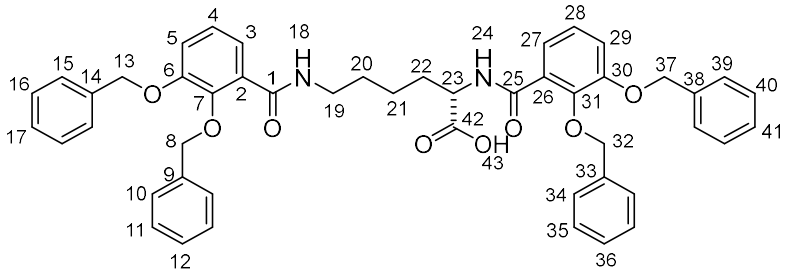

Chemical Formula: $C_{48}H_{46}N_2O_8$

Molecular Mass: 778.90 g $mol^{-1}$

Benzyl-protected Azotochelin was prepared based on a preparation from the literature[177].

2,3-Bis(benzyloxy)benzoic acid-NHE (3.465 g, 8.03 mmol) was dissolved in acetone (29 mL). A solution of *L*-lysine (0.741 g, 4.06 mmol) and triethylamine (3.2 mL, 22.96 mmol) in water (11 mL) was prepared separately then added to the solution of NHE and the reaction mixture left stirring overnight at room temperature. Acetone was removed in vacuo to give an orange oil below a layer of water. The oil was taken up in ethyl acetate (50 mL) and washed with 0.1 M HCl (3 x 30 mL) to remove excess triethylamine. The organic layer was dried over $MgSO_4$ and the solvent removed in vacuo. The resulting yellow oil was dried to a white foam on the vacuum line. The crude product was purified by flash column chromatography (chloroform:methanol 9:1).

**Yield:** 2.69 g, 3.45 mmol, 43%

**$R_f$:** 0.24 (10:1 chloroform:methanol)

**Melting Point:** 60-64 °C

**HRMS (ESI):** Calcd. $[M+H]^+$ ($C_{48}H_{47}N_2O_8$) m/z= 779.3327; Meas. m/z= 779.3346, Mean err -2.3 ppm. Calcd. $[M+Na]^+$ ($C_{48}H_{46}N_2NaO_8$) m/z= 801.3146; Meas. m/z= 801.3162, Mean err -1.8 ppm

**$^1$H NMR:** (400 MHz, $CDCl_3$) δ: 8.54 (1H, d, $J^3_{H\text{-}H23}$= 7.0 Hz, *H24*), 7.92 (1H, t, $J^3_{H\text{-}H19}$= 5.5 Hz, *H18*), 7.76-7.67 (2H, m, *H3 & H27*), 7.49-7.18 (20 H, m, *H10-12, H15-17, H34-36 & H39-41*), 7.16-7.07 (4H, m, *H4-5 & H28-29*) 5.12 (4H, s, *H8 & H32*), 5.11 (2H, s, *H37*), 5.03 (2H, s, *H13*), 4.53 (1H, td, $J^3_{H\text{-}H22}$= 7.5 Hz, $J^3_{H\text{-}H24}$= 5.5 Hz, *H23*), 3.19-3.03 (2H, m, *H19*), 1.76-1.62 & 1.45-1.31 (2H, 2 x m, *H22*), 1.22-1.05 (4H, m, *H20-21*)

**$^{13}$C NMR:** (100 MHz, $CDCl_3$) δ: 174.4 (*C42*), 166.0 (*C25*), 165.3 (*C1*), 151.8 & 151.8 (*C7 & C31*), 147.2 & 146.9 (*C6 & C30*), 136.5, 136.4, 136.4 & 136.2 (*C9, C14, C33 & C38*), 129.0, 128.9, 128.8, 128.8, 128.8, 128.7, 128.4, 128.4, 127.9, 127.8 (*C10-12, C15-17, C34-36 & C39-41*), 127.2 & 126.3 (*C2 & C26*), 124.5 & 124.5 (*C4 & C28*), 123.5 & 123.4 (*C3 & C27*), 117.6 & 117.1 (*C5 & C29*), 76.5 & 76.4 (*C13 & C37*), 71.4 & 71.4 (*C8 & C32*), 53.0 (*C23*), 39.5 (*C19*), 31.0 (*C22*), 28.8 & 23.0 (*C20-21*)

**IR ATIR ($cm^{-1}$):** 3363 br (O-H carboxylic acid), 2932 br (C-H), 1734 m (C=O carboxylic acid), 1653 m (C=O amide), 1626 m (C=O amide), 1524 m (N-H), 1453 s (C-H)

**Elemental Analysis:** Cald. For [$C_{48}H_{46}N_2O_8$]: %C 74.02, %H 5.95, %N 3.06; Measured for [$C_{48}H_{46}N_2O_8$]: %C 73.74, %H 6.09, %N 3.65

# 105. General Method

$Bn_4$-azotochelin (1 eq.) was dissolved in anhydrous DMF. HATU (0.9 eq.) and DIPEA (2 eq.) were added and the solution stirred for 30 minutes at room temperature. A second solution of **104** (3 eq.) and DIPEA (2 eq.) in DMF was prepared and added to the $Bn_4$-azotochelin mixture. The solution was then stirred overnight at room temperature before the volatiles were removed in vacuo. The residue was taken up in DCM and washed with water and brine. The organic phase was dried over $MgSO_4$ and the solvent removed under reduced pressure. The product was purified by column chromatography (loaded in 100% EtOAc before being eluted with a MeOH/EtOAc mixture run on a gradient of 3% MeOH to 10% MeOH).

# 105a. (2*S*)-2,6-Bis({[2,3-bis(benzyloxy)phenyl]formamido})-*N*-[(4-{[(pyridin-2-yl)methyl]sulfamoyl}phenyl)methyl]hexanamide

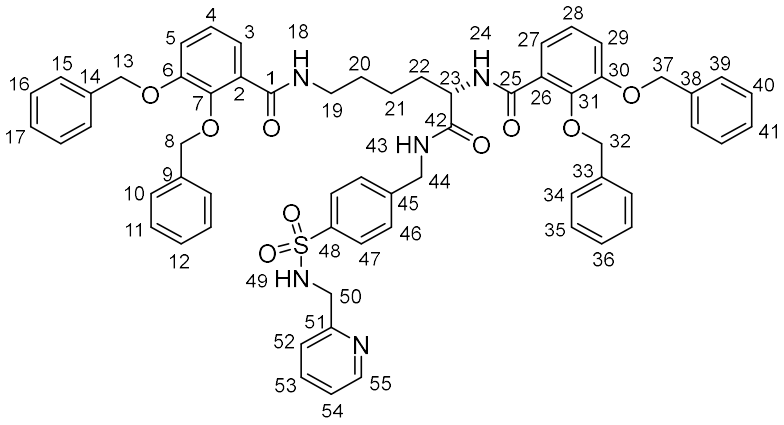

Chemical Formula: $C_{61}H_{59}N_5O_9S$

Molecular Mass: 1038.23 g $mol^{-1}$

**Yield:** 0.205 g, 0.20 mmol, 60%

**$R_f$:** 0.25 (3% MeOH in EtOAc)

**Melting Point:** 59.3-63.2 °C

**HRMS (ESI):** Calcd. $[M+H]^+$ ($C_{61}H_{60}N_3O_9S$) m/z= 1038.4106; Meas. m/z= 1038.4157, Mean err -3.6 ppm. Calcd. $[M+Na]^+$ ($C_{61}H_{59}N_3NaO_9S$) m/z= 1060.3926; Meas. m/z= 1060.3981, Mean err -3.7 ppm. Calcd. $[M+K]^+$ ($C_{61}H_{59}KN_3O_9S$) m/z= 1076.3665; Meas. m/z= 1076.3710, Mean err -4.1 ppm

**$^{1}$H NMR:** (400 MHz, $CDCl_3$) δ: 8.41-8.35 (1H, m, *H24 & H55*), 7.91 (1H, t, $J^{3}_{H\text{-}H19}$= 5.5 Hz, *H18*), 7.71 (2H, d, $J^{3}_{H\text{-}H46}$= 8.5 Hz, *H47*), 7.66-7.59 (2H, m, *H3 & H27*), 7.53 (1H, apparent td, $J^{3}_{H\text{-}H52/54}$= 7.5 Hz, $J^{4}_{H\text{-}H55}$= 2.0 Hz, *H53*), 7.47-7.21 (22H, m, *H10-12, H15-17, H34-36, H39-41 & H46*), 7.16-7.06 (7H, m, *H4-5, H28-29, H49, H52 & H54*), 6.06 (1H, t, $J^{3}_{H\text{-}H44}$= 5.5 Hz, *H43*), 5.13 (2H, s, *H8 or H32*), 5.13 (2H, s, *H8 or H32*), 5.08 (2H, s, *H37*), 5.03 (2H, s, *H13*), 4.46-4.34 (3H, m, *H23 & H44*), 4.17 (2H, d, $J^{3}_{H\text{-}H43}$= 5.5 Hz, *H50*), 3.13 (2H, apparent q, $J^{3}_{H\text{-}H18/20}$= 6.5 Hz, *H19*), 1.72-1.62 (1H, m, *H22*), 1.38-1.26 (1H, m, *H22*), 1.26-1.17 (2H, m, *H20*), 1.17-1.06 (2H, m, *H21*)

**$^{13}$C NMR:** (100 MHz, $CDCl_3$) δ: 171.8 (*C42*), 165.9 (*C25*), 165.2 (*C1*), 154.8 (*C51*), 151.8 & 151.8 (*C7 & C31*), 149.0 (*C55*), 147.0 & 146.8 (*C6 & C30*), 143.7 (*C45*), 138.4 (*C48*), 136.8 (*C53*), 136.5, 136.4, 136.3 & 136.2 (*C9, C14, C33 & C38*), 129.0, 128.9, 128.8, 128.8, 128.8, 128.5, 128.4, 127.9, 127.8 (*C10-12, C15-17, C34-36, C39-41 & C46*), 127.5 (*C47*), 127.3 & 126.5 (*C2 & C26*), 124.6 & 124.5 (*C4 & C28*), 123.3 & 123.1 (*C3 & C27*), 122.7 (*C54*), 122.0 (*C52*), 117.5 & 117.0 (*C5 & C29*), 76.5 (*C13*), 76.3 (*C37*), 71.4 & 71.4 (*C8 & C32*), 53.8 (*C23*), 47.4 (*C44*), 42.8 (*C50*), 39.1 (*C19*), 30.5 (*C22*), 28.9 (*C20*), 23.2 (*C21*)

**IR ATIR ($cm^{-1}$):** 2934 w (N-H), 1637 s (C=O), 1312 s (S=O asymmetric stretch), 1208 s (C-O alkyl aryl ether), 1156 s (S=O symmetric stretch)

**Elemental Analysis:** Cald. For [$C_{61}H_{59}N_5O_9S$]: %C 70.57, %H 5.73, %N 6.75; Measured for [$C_{61}H_{59}N_5O_9S$]: %C 69.31, %H 5.84, %N 6.63

# 105b. (2*S*)-2,6-Bis({[2,3-bis(benzyloxy)phenyl]formamido})-*N*-[(4-{[(4-methylpyridin-2-yl)methyl]sulfamoyl}phenyl)methyl]hexanamide

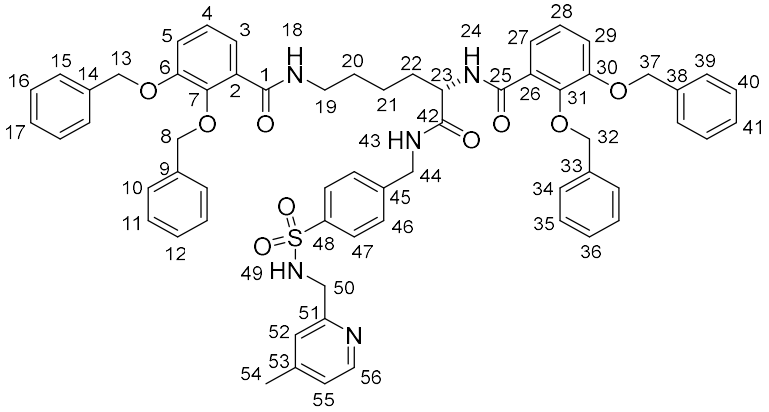

Chemical Formula: $C_{62}H_{61}N_5O_9S$

Molecular Mass: 1052.26 g $mol^{-1}$

**Yield:** 0.091 g, 0.09 mmol, 53%

**$R_f$:** 0.26 (6% MeOH in EtOAc)

**Melting Point:** 70-76 °C

**HRMS (ESI):** Calcd. $[M+H]^+$ ($C_{62}H_{62}N_5O_9S$) m/z= 1052.4263; Meas. m/z= 1052.4296, Mean err -3.7 ppm. Calcd. $[M+Na]^+$ ($C_{62}H_{61}N_5NaO_9S$) m/z= 1074.4082; Meas. m/z= 1074.4139, Mean err -3.8 ppm. Calcd. $[M+K]^+$ ($C_{62}H_{61}KN_5O_9S$) m/z= 1090.3822; Meas. m/z= 1090.3871, Mean err -4.2 ppm

**$^1$H NMR:** (400 MHz, $CDCl_3$) δ: 8.38 (1H, d, $J^3_{H\text{-}H23}$= 7.0 Hz, *H24*), 8.23 (1H, dd, $J^3_{H\text{-}H55}$= 5.0 Hz, $J^5_{H\text{-}H52}$= 1.0 Hz, *H56*), 7.91 (1H, t, $J^3_{H\text{-}H19}$= 6.0 Hz, *H18*), 7.71 (2H, d, $J^3_{H\text{-}H46}$= 8.5 Hz, *H47*), 7.65-7.58 (2H, m, *H3 & H27*), 7.47-7.20 (22H, m, *H10-12, H15-17, H34-36, H39-41 & H46*), 7.17-7.06 (5H, m, *H4-5, H28-29, H49*), 6.94-6.89 (2H, m, *H52 & H55*), 6.10 (1H, t, $J^3_{H\text{-}H44}$= 5.5 Hz, *H43*), 5.13 (2H, s, *H8 or H32*), 5.13 (2H, s, *H8 or H32*), 5.07 (2H, s, *H37*), 5.03 (2H, s, *H13*), 4.45-4.34 (3H, m, *H23 & H44*), 4.11 (2H, d, $J^3_{H\text{-}H43}$= 5.5 Hz, *H50*), 3.12 (2H, apparent q, $J^3_{H\text{-}H18/20}$= 6.5 Hz, *H19*), 2.23 (3H, m, *H54*), 1.75-1.61 (1H, m, *H22*), 1.38-1.26 (1H, m, *H22*), 1.26-1.16 (2H, m, *H20*), 1.16-1.06 (2H, m, *H21*)

**$^{13}$C NMR:** (100 MHz, $CDCl_3$) δ: 171.9 (*C42*), 165.9 (*C25*), 165.2 (*C1*), 154.7 (*C51*), 151.8 & 151.8 (*C7 & C31*), 148.7 (*C56*), 148.2 (*C53*), 147.0 & 146.8 (*C6 & C30*), 143.7 (*C45*), 138.5

(*C48*), 136.5, 136.4, 136.3 & 136.2 (*C9, C14, C33 & C38*), 129.0, 128.9, 128.8, 128.8, 128.8, 128.4, 128.4, 127.9, 127.9, 127.8 (*C10-12, C15-17, C34-36, C39-41 & C46*), 127.5 (*C47*), 127.3 & 126.5 (*C2 & C26*), 124.6 & 124.5 (*C4 & C28*), 123.7 (*C55*), 123.3 & 123.1 (*C3 & C27*), 122.8 (*C52*), 117.6 & 117.0 (*C5 & C29*), 76.5 (*C13*), 76.3 (*C37*), 71.5 & 71.4 (*C8 & C32*), 53.8 (*C23*), 47.4 (*C44*), 42.7 (*C50*), 39.1 (*C19*), 30.5 (*C22*), 28.9 (*C20*), 23.2 (*C21*), 21.0 (*C54*)

**IR ATIR ($cm^{-1}$):** 3212 br (C-H), 2930 w (Ar C-H), 2862 w (Ar C-H), 1640 m (C=O amide), 1574 m (N-H), 1312 m (S=O asymmetric stretch), 1155 m (S=O symmetric stretch)

**Elemental Analysis:** Cald. For [$C_{62}H_{61}N_5O_9S$]: %C 70.77, %H 5.84, %N 6.66; Measured for [$C_{62}H_{61}N_5O_9S$]: %C 69.56, %H 5.85, %N 6.62

# 105c. (2*S*)-2,6-Bis({[2,3-bis(benzyloxy)phenyl]formamido})-*N*-[(4-{[(5-methylpyridin-2-yl)methyl]sulfamoyl}phenyl)methyl]hexanamide

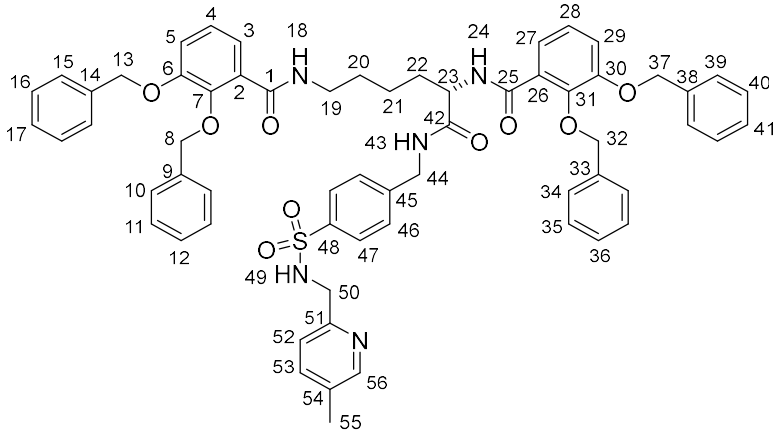

Chemical Formula: $C_{62}H_{61}N_5O_9S$

Molecular Mass: 1052.26 g $mol^{-1}$

**Yield:** 0.545 g, 0.52 mmol, 69%

**$R_f$:** 0.32 (6% MeOH in EtOAc)

**Melting Point:** 64-66 °C

**HRMS (ESI):** Calcd. $[M+H]^+$ ($C_{62}H_{62}N_5O_9S$) m/z= 1052.4263; Meas. m/z= 1052.4302, Mean err -3.6 ppm. Calcd. $[M+Na]^+$ ($C_{62}H_{61}N_5NaO_9S$) m/z= 1074.4082; Meas. m/z= 1074.4115, Mean err -3.4 ppm. Calcd. $[M+K]^+$ ($C_{62}H_{61}KN_5O_9S$) m/z= 1090.3822; Meas. m/z= 1090.3856, Mean err -2.1 ppm

**$^1$H NMR:** (400 MHz, $CDCl_3$) δ: 8.36 (1H, d, $J^3_{H\text{-}H23}$= 7.0 Hz, *H24*), 8.24-8.20 (1H, m, *H56*), 7.91 (1H, t, $J^3_{H\text{-}H19}$= 5.5 Hz, *H18*), 7.72 (2H, d, $J^3_{H\text{-}H46}$= 8.5 Hz, *H47*), 7.67-7.60 (2H, m, *H3 & H27*), 7.48-7.19 (23H, m, *H10-12, H15-17, H34-36, H39-41, H46 & H53*), 7.18-7.06 (4H, m, *H4-5, H28-29*), 7.03 (1H, t, $J^3_{H\text{-}H50}$= 6.0 Hz, *H49*), 6.99 (1H, d, $J^3_{H\text{-}H53}$= 8.0 Hz, *H52*), 5.92 (1H, t, $J^3_{H\text{-}H44}$= 5.5 Hz, *H43*), 5.14 & 5.13 (4H, 2 overlapping s, *H8 & H32*), 5.07 (2H, s, *H37*), 5.03 (2H, s, *H13*), 4.44-4.33 (3H, m, *H23 & H44*), 4.12 (2H, d, $J^3_{H\text{-}H43}$= 5.5 Hz, *H50*), 3.13 (2H, apparent q, $J^3_{H\text{-}H18/20}$= 6.5 Hz, *H19*), 2.25 (3H, m, *H55*), 1.75-1.65 (1H, m, *H22*), 1.37-1.27 (1H, m, *H22*), 1.27-1.16 (2H, m, *H20*), 1.16-1.06 (2H, m, *H21*)

**$^{13}$C NMR:** (100 MHz, $CDCl_3$) δ: 171.8 (*C42*), 165.9 (*C25*), 165.2 (*C1*), 151.8 (*C51*), 151.8 & 151.8 (*C7 & C31*), 149.3 (*C56*), 147.0 & 146.8 (*C6 & C30*), 143.7 (*C45*), 138.4 (*C48*), 137.4

(*C53*), 136.5, 136.5, 136.3 & 136.2 (*C9, C14, C33 & C38*), 132.2 (*C54*), 129.0, 128.9, 128.8, 128.8, 128.8, 128.4, 128.4, 127.9, 127.8 (*C10-12, C15-17, C34-36, C39-41 & C46*), 127.6 (*C47*), 127.3 & 126.4 (*C2 & C26*), 124.6 & 124.5 (*C4 & C28*), 123.3 & 123.1 (*C3 & C27*), 121.5 (*C52*), 117.6 & 117.0 (*C5 & C29*), 76.5 (*C13*), 76.3 (*C37*), 71.5 & 71.4 (*C8 & C32*), 53.8 (*C23*), 47.2 (*C44*), 42.8 (*C50*), 39.1 (*C19*), 30.5 (*C22*), 28.9 (*C20*), 23.2 (*C21*), 18.2 (*C55*)

**IR ATIR ($cm^{-1}$):** 3047 br (C-H), 2932 w (Ar C-H), 2864 w (Ar C-H), 1640 m (C=O amide), 1574 m (N-H), 1311 m (S=O asymmetric stretch), 1156 m (S=O symmetric stretch)

**Elemental Analysis:** Cald. For [$C_{62}H_{61}N_5O_9S$]: %C 70.77, %H 5.84, %N 6.66; Measured for [$C_{62}H_{61}N_5O_9S$]: %C 69.56, %H 5.85, %N 6.79

## 106. General Method

Glassware for this reaction was pre-soaked in 6 M HCL for several hours. The glassware was rinsed with generous amounts of DI water, 2 M NaOH, DI water and anhydrous ethanol. **105** and palladium hydroxide on carbon (20%) was suspended in anhydrous ethanol/ammonia (in methanol, 7 M) (5:1 v/v). The vessel was sealed and flushed with nitrogen, then hydrogen. The reaction was stirred vigorously at room temperature for 4 hours. Palladium on carbon was removed by filtration using Whatmann glass GF/F filter paper. The filtrate was evaporated to leave the product as a white foam.

## 106a. (2*S*)-2,6-Bis[(2,3-dihydroxyphenyl)formamido]-*N*-[(4-{[(pyridin-2-yl)methyl]sulfamoyl}phenyl)methyl]hexanamide

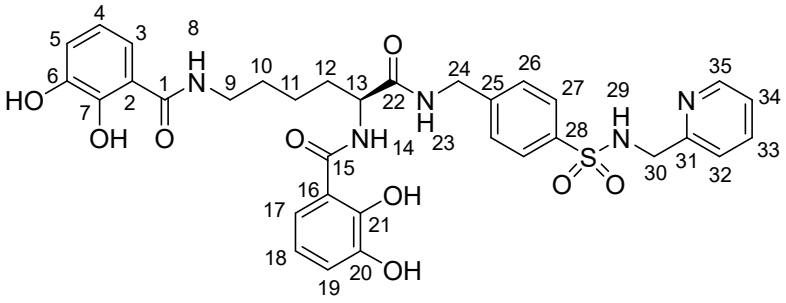

Chemical Formula: $C_{33}H_{35}N_5O_9S$

Molecular Mass: 677.73 g $mol^{-1}$

**Yield:** 0.205 g, 0.20 mmol, 60%

**$R_f$:** 0 (5% MeOH in $CDCl_3$)

**Melting Point:** 107.6-108.9 °C

**HRMS (ESI):** Calcd. $[M+H]^+$ ($C_{33}H_{36}N_5O_9S$) m/z= 678.2228; Meas. m/z= 678.2233, Mean err 0.2 ppm. Calcd. $[M+Na]^+$ ($C_{33}H_{35}N_5NaO_9S$) m/z= 700.2048; Meas. m/z= 700.2064, Mean err -2.2 ppm. Calcd. $[M+K]^+$ ($C_{33}H_{35}KN_5O_9S$) m/z= 716.1787; Meas. m/z= 716.1768, Mean err 0.7 ppm

**$^1$H NMR:** (400 MHz, methanol-d4) δ: 8.32 (1H, ddd, $J^3_{H\text{-}H34}$= 5.0 Hz, $J^4_{H\text{-}H33}$= 2.0 Hz, $J^5_{H\text{-}H32}$= 1.0 Hz, *H35*), 7.73 (2H, d, $J^3_{H\text{-}H26}$= 8.5 Hz, *H27*), 7.67 (1H, td, $J^3_{H\text{-}H32/34}$= 7.5 Hz, $J^4_{H\text{-}H35}$= 2.0 Hz, *H33*), 7.41 (2H, d, $J^3_{H\text{-}H27}$= 8.5 Hz, *H26*), 7.34 (1H, dt, $J^3_{H\text{-}H33}$= 7.5 Hz, $J^4_{H\text{-}H34}$= 1.0 Hz, $J^5_{H\text{-}H35}$= 1.0 Hz, *H32*), 7.31 (1H, dd, $J^3_{H\text{-}H18}$= 8.0 Hz, $J^4_{H\text{-}H19}$= 1.5 Hz, *H17*), 7.20 (1H, ddd, $J^3_{H\text{-}}$

$_{H33}$= 7.5 Hz, $J^{3}_{H\text{-}H35}$= 5.0 Hz, $J^{4}_{H\text{-}H32}$= 1.0 Hz, *H34*), 7.16 (1H, dd, $J^{3}_{H\text{-}H4}$= 8.0 Hz, $J^{4}_{H\text{-}H5}$= 1.5 Hz, *H3*), 6.90 (1H, dd, $J^{3}_{H\text{-}H18}$= 8.0 Hz, $J^{4}_{H\text{-}H17}$= 1.5 Hz, *H19*), 6.88 (1H, dd, $J^{3}_{H\text{-}H4}$= 8.0 Hz, $J^{4}_{H\text{-}H3}$= 1.5 Hz, *H5*), 6.69 (1H, t, $J^{3}_{H\text{-}H17/19}$= 8.0 Hz, *H18*), 6.66 (1H, t, $J^{3}_{H\text{-}H3/5}$= 8.0 Hz, *H4*), 4.56 (1H, dd - diastereotopic *H12*, $J^{3}_{H\text{-}H12\alpha}$= 8.5 Hz, $J^{4}_{H\text{-}H12\beta}$= 6.0 Hz, *H13*), 4.48-4.36 (2H, m, *H24*), 4.13 (2H, s, *H30*), 3.37 (2H, t, $J^{3}_{H\text{-}H10}$= 7.0 Hz, *H9*), 2.02-1.80 (2H, m, *H12*), 1.73-1.60 (2H, m, *H10*), 1.58-1.40 (2H, m, *H11*)

**$^{13}$C NMR:** (100 MHz, methanol-d4) δ: 173.4 (*C22*), 170.2 (*C15*), 169.8 (*C1*), 156.9 (*C31*), 148.2 (*C35*), 146.1 (*C7 & C21*), 146.0 (*C6 & C20*), 143.9 (*C25*), 139.2 (*C28*), 137.4 (*C33*), 127.6 (*C26*), 126.9 (*C27*), 122.6 (*C34*), 122.2 (*C32*), 118.3, 118.3 & 118.2 (*C4-5 & C17-19*), 117.3 (*C3*), 115.8 & 115.5 (*C2 & C16*), 53.9 (*C13*), 47.5 (*C24*), 42.2 (*C30*), 38.8 (*C9*), 31.3 (*C12*), 28.7 (*C10*), 23.1 (*C11*)

**IR ATIR (cm$^{-1}$):** 3266 br (O-H), 2933 m (N-H), 1637 s (C=O), 1325 m (S=O asymmetric stretch), 1154 s (S=O symmetric stretch)

**Elemental Analysis:** Cald. For [$C_{33}H_{35}N_5O_9S$]: %C 58.48, %H 5.21, %N 10.33; Measured for [$C_{33}H_{35}N_5O_9S$]: %C 55.79, %H 4.87, %N 9.86

# 106b. (2*S*)-2,6-Bis[(2,3-dihydroxyphenyl)formamido]-*N*-[(4-{[(4-methylpyridin-2-yl)methyl]sulfamoyl}phenyl)methyl]hexanamide

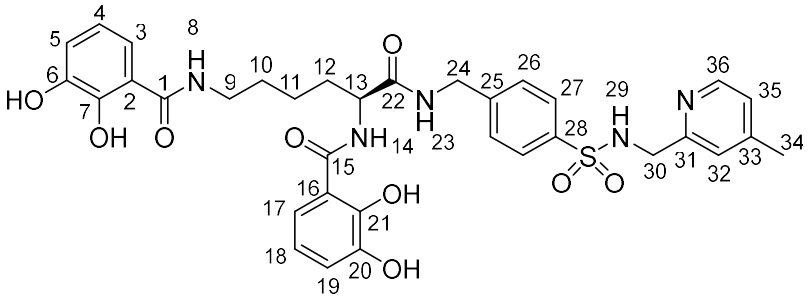

Chemical Formula: $C_{34}H_{37}N_5O_9S$

Molecular Mass: 691.76 g $mol^{-1}$

**Yield:** 0.109 g, 0.16 mmol, 88%

**$R_f$:** 0 (5% MeOH in $CDCl_3$)

**Melting Point:** 110.1-113.5 °C

**HRMS (ESI):** Calcd. $[M+H]^+$ ($C_{34}H_{38}N_5O_9S$) m/z= 692.2385; Meas. m/z= 692.2377, Mean err -0.5 ppm. Calcd. $[M+Na]^+$ ($C_{34}H_{37}N_5NaO_9S$) m/z= 714.2204; Meas. m/z= 714.2217, Mean err -4.1 ppm

**$^1$H NMR:** (400 MHz, methanol-d4) δ: 8.15 (1H, d, $J^3_{H\text{-}H35}$= 5.0 Hz, *H36*), 7.71 (2H, d, $J^3_{H\text{-}H26}$= 8.5 Hz, *H27*), 7.40 (2H, d, $J^3_{H\text{-}H27}$= 8.5 Hz, *H26*), 7.31 (1H, dd, $J^3_{H\text{-}H18}$= 8.0 Hz, $J^4_{H\text{-}H19}$= 1.5 Hz, *H17*), 7.17 (1H, dd, $J^3_{H\text{-}H4}$= 8.0 Hz, $J^4_{H\text{-}H5}$= 1.5 Hz, *H3*), 7.13 (1H, s, *H32*), 7.02 (1H, d, $J^3_{H\text{-}H36}$= 5.0 Hz, *H35*), 6.88 (1H, dd, $J^3_{H\text{-}H18}$= 8.0 Hz, $J^4_{H\text{-}H17}$= 1.5 Hz, *H19*), 6.87 (1H, dd, $J^3_{H\text{-}H4}$= 8.0 Hz, $J^4_{H\text{-}H3}$= 1.5 Hz, *H5*), 6.64 (1H, t, $J^3_{H\text{-}H17/19}$= 8.0 Hz, *H18*), 6.63 (1H, t, $J^3_{H\text{-}H3/5}$= 8.0 Hz, *H4*), 4.56 (1H, dd - diastereotopic *H12*, $J^3_{H\text{-}H12\alpha}$= 8.5 Hz, $J^4_{H\text{-}H12\beta}$= 5.5 Hz, *H13*), 4.42 (2H, s, *H24*), 4.10 (2H, s, *H30*), 3.37 (2H, t, $J^3_{H\text{-}H10}$= 7.0 Hz, *H9*), 2.24 (3H, s, *H34*), 2.01-1.81 (2H, m, *H12*), 1.73-1.60 (2H, m, *H10*), 1.59-1.43 (2H, m, *H11*)

**$^{13}$C NMR:** (100 MHz, methanol-d4) δ: 173.6 (*C22*), 170.2 (*C15*), 169.9 (*C1*), 156.5 (*C31*), 149.3 (*C33*), 147.9 (*C36*), 146.5 (*C7 & C21*), 146.2 (*C6 & C20*), 143.9 (*C25*), 139.3 (*C28*), 127.6 (*C26*), 126.9 (*C27*), 123.5 (*C35*), 123.0 (*C32*), 118.5 (*C17*), 117.9 & 117.9 (*C5 & C19*), 117.7 (*C4 & C18*), 117.5 (*C3*), 116.0 & 115.7 (*C2 & C16*), 54.0 (*C13*), 47.4 (*C24*), 42.1 (*C30*), 38.8 (*C9*), 31.4 (*C12*), 28.7 (*C10*), 23.1 (*C11*), 19.7 (*C34*)

**IR ATIR ($cm^{-1}$):** 3230 br (O-H), 2930 w (N-H), 1635 s (C=O), 1323 m (S=O asymmetric stretch), 1154 m (S=O symmetric stretch)

**Elemental Analysis:** Cald. For [$C_{34}H_{37}N_5O_9S$]: %C 59.03, %H 5.39, %N 10.12; Measured for [$C_{34}H_{37}N_5O_9S$]: %C 55.45, %H 4.94, %N 9.52

# 106c. (2*S*)-2,6-Bis[(2,3-dihydroxyphenyl)formamido]-*N*-[(4-{[(5-methylpyridin-2-yl)methyl]sulfamoyl}phenyl)methyl]hexanamide

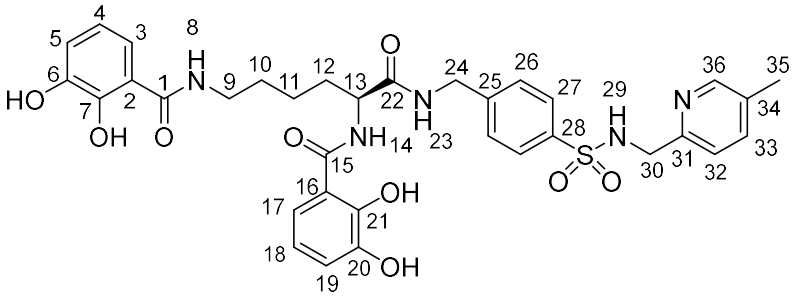

Chemical Formula: $C_{34}H_{37}N_5O_9S$

Molecular Mass: 691.76 g $mol^{-1}$

**Yield:** 0.117 g, 0.17 mmol, 96%

**$R_f$:** 0 (5% MeOH in $CDCl_3$)

**Melting Point:** 106.4-109.2 °C

**HRMS (ESI):** Calcd. $[M+H]^+$ ($C_{34}H_{38}N_5O_9S$) m/z= 692.2385; Meas. m/z= 692.2406, Mean err -2.5 ppm. Calcd. $[M+Na]^+$ ($C_{34}H_{37}N_5NaO_9S$) m/z= 714.2204; Meas. m/z= 714.2234, Mean err -0.9 ppm

**$^1$H NMR:** (400 MHz, methanol-d4) δ: 8.16 (1H, d, $J^4_{H\text{-}H33}$= 2.0 Hz, *H36*), 7.73 (2H, d, $J^3_{H\text{-}H26}$= 8.5 Hz, *H27*), 7.50 (1H, dd, $J^3_{H\text{-}H32}$= 7.5 Hz, $J^4_{H\text{-}H36}$= 2.0 Hz, *H33*), 7.42 (2H, d, $J^3_{H\text{-}H27}$= 8.5 Hz, *H26*), 7.31 (1H, dd, $J^3_{H\text{-}H18}$= 8.0 Hz, $J^4_{H\text{-}H19}$= 1.5 Hz, *H17*), 7.23 (1H, d, $J^3_{H\text{-}H33}$= 8.0 Hz, *H32*), 7.16 (1H, dd, $J^3_{H\text{-}H4}$= 8.0 Hz, $J^4_{H\text{-}H5}$= 1.5 Hz, *H3*), 6.90 (1H, dd, $J^3_{H\text{-}H18}$= 8.0 Hz, $J^4_{H\text{-}H17}$= 1.5 Hz, *H19*), 6.88 (1H, dd, $J^3_{H\text{-}H4}$= 8.0 Hz, $J^4_{H\text{-}H3}$= 1.5 Hz, *H5*), 6.69 (1H, t, $J^3_{H\text{-}H17/19}$= 8.0 Hz, *H18*), 6.66 (1H, t, $J^3_{H\text{-}H3/5}$= 8.0 Hz, *H4*), 4.56 (1H, dd - diastereotopic H12, $J^3_{H\text{-}H12\alpha}$= 8.5 Hz, $J^4_{H\text{-}H12\beta}$= 6.0 Hz, *H13*), 4.48-4.37 (2H, m, *H24*), 4.08 (2H, s, *H30*), 3.36 (2H, t, $J^3_{H\text{-}H10}$= 7.0 Hz, *H9*), 2.25 (3H, s, *H35*), 2.00-1.81 (2H, m, *H12*), 1.72-1.60 (2H, m, *H10*), 1.57-1.41 (2H, m, *H11*)

**$^{13}$C NMR:** (100 MHz, methanol-d4) δ: 173.4 (*C22*), 170.2 (*C15*), 169.8 (*C1*), 153.9 (*C31*), 148.4 (*C36*), 146.0 (*C7 & C21*), 146.0 (*C6 & C20*), 143.9 (*C25*), 139.2 (*C28*), 137.9 (*C33*), 132.7 (*C34*), 127.6 (*C26*), 126.9 (*C27*), 121.8 (*C32*), 118.4, 118.3, 118.3 & 118.2 (*C4-5 &*

*C17-19*), 117.3 (*C3*), 115.8 & 115.5 (*C2 & C16*), 54.0 (*C13*), 47.3 (*C24*), 42.2 (*C30*), 38.8 (*C9*), 31.3 (*C12*), 28.7 (*C10*), 23.1 (*C11*), 16.7 (*C35*)

**IR ATIR ($cm^{-1}$):** 3250 br (O-H), 2930 w (N-H), 1635 m (C=O), 1323 m (S=O asymmetric stretch), 1154 m (S=O symmetric stretch)

**Elemental Analysis:** Cald. For [$C_{34}H_{37}N_5O_9S$]: %C 59.03, %H 5.39, %N 10.12; Measured for [$C_{34}H_{37}N_5O_9S$]: %C 54.95, %H 4.65, %N 9.12

## 107a-c. Siderophore-catalyst conjugates

The following stock solutions were prepared:

- 10 mM Fe-NTA (as previously described[181])
- 5 mM $[Cp^*IrCl_2]_2$ (**95**) in DMF
- 10 mM **106** in DMF

To 120 µL MOPS buffer (0.2 MOPS, 0.15 M NaCl at pH 7.0) 75 µL of 10 mM Fe-NTA solution was added and the solution sonicated for 1 minute. 75 µL 10 mM **106** solution was then added and the solution sonicated for a further 1 minute. Finally, 75 µL of 5 mM $[Cp^*IrCl_2]_2$ solution was added and the solution sonicated again for 1 minute.

## 6.6 Other Methods

## Preparation of proteins *Cj*CeuE, Pth and Gst

Proteins were prepared by Dr. E. Blagova.

Following previous investigations of *Cj*CeuE, it had been identified that crystallisation only succeeded when the first 23 residues, proposed to link the protein to the membrane anchor in the native protein, was removed.[207] Likewise, constructs for Gst and Pth were designed where like-sections were removed (*Cj*CeuE = residues 24-310, Pth = residues 16-297 and Gst = residues 19-300).

Synthetic DNA genes for Gst and Pth were purchased from ThermoFisher Scientific (UK) and the DNA amplified so the constructs begin at residue 37 for Pth and 39 for Gst. These strands were then cloned into the Lic-adapted pET 28a vector (YSBLic3C). This vector provides an N-terminal hexa-histidine tag linked to our protein of interest *via* a Human Rhinovirus 3C protease cleavage site that allows removal of the tag. After cleavage of this tag, three residues remain attached at the N-terminal, which are glycine, proline and alanine. Preparation of a plasmid encoding for *Cj*CeuE with an N-terminal hexa-histidine tag has previously been described.[105]

All three proteins were expressed in *E. coli.* BL21 (DE3) cells. Cell cultures were grown in Luria-Bertani broth with 30 μg/ml kanamycin with shaking as 37 °C. Once an $OD_{600}$ of 0.6-0.8 was achieved, the cultures were induced with 1 mM isopropyl β-d-thiogalactopyranoside (IPTG) for 3.5-4 hours.

The cells were harvested by centrifugation and the cell pellets resuspended in TRIS buffer (50 mM TRIS, 500 mM NaCl, pH 7.5) with complete EDTA-free Protease Inhibitor Cocktail (Roche Diagnostics). Cells were lysed by sonication and the soluble crude extract isolated following centrifugation at 19,900 rpm to remove insoluble material in the pellet. The supernatant solution was then loaded onto a 5 mL HisTrap Ni-chelating column (Amersham Pharmacia) and eluted using a gradient of imidazole. The N-terminal His-tag was cleaved by addition of 3C protease (1:100 ratio protease:protein). The solution was then dialysed in a second TRIS buffer (20 mM TRIS, 150 mM NaCl, pH 7.5) overnight. Remaining His-tagged protein and protease were removed by passing through a HisTrap Ni-chelating column. The proteins were concentrated to approximately 100-150 mg/mL and stored at -80 °C until use.

## Preparation of Artificial Metalloenzymes

All proteins were received as concentrated stock samples from Dr. E. Blagova. These concentrated samples were diluted to approximately 30-40 μM in MOPS buffer (0.2 M MOPS, 0.15 M NaCl at pH 7.4) and the concentration measured using the absorbance at 280 nm in UV-vis spectroscopy. The concentration was calculated using the Beer-Lambert law using the following extinction coefficients measured by Dr. A. Miller[182]:

- *Cj*CeuE = 18585 $dm^3$ $mol^{-1}$ $cm^{-1}$
- Pth = 29196 $dm^3$ $mol^{-1}$ $cm^{-1}$
- Gst = 34239 $dm^3$ $mol^{-1}$ $cm^{-1}$

A volume of **107** stock solution was added such that a 1:1 ratio of protein:conjugate was achieved. The solutions were left for 3 hours at 4 °C to ensure equilibrium binding was reached. The ArM solution was then concentrated using spin concentrators with a 10 kDa cut-off. Sample were concentrated to approximately 1-2 mM and stored at 4 °C overnight before use.

## Testing Catalytic Activity

Stock solutions were prepared:

- MES buffer: 0.6 M MES, 3M sodium formate adjusted to achieve pH 5.8 at reaction temperature
- Substrate stock: 6,7-dimethoxy-1-methyl-3,4-dihydroisoquinoline in MES buffer. Concentration depended on the stock concentration of ArM/complex being added so that the correct final concentrations were reached
- ArM or catalyst stock. ArM stock volume is measured following concentration of the samples and the concentration then calculated. Catalyst stocks were prepared at 3.125 mM catalyst in DMF
- 250 mM L-glutathione in DI water
- Quenching solutions: 625 µL methanol, 300 µL water, 50 µL 250 mM L-glutathione stock, per sample
- Concentrated caffeine stock (internal standard)

The appropriate volume of substrate stock was measured into a vial with a stirrer bar and incubated at the reaction temperature for 15 minutes. The reaction was initiated by the appropriate volume of ArM/catalyst stock solution (final concentrations: 50 mM substrate, 0.125 mM catalyst). 25 µL aliquots were taken at selected time intervals and quenched by addition to quenching solutions.

## Non-Chiral HPLC Method

Samples were filtered through 0.22 µm nylon membranes. The samples were analysed by HPLC (Agilent 1260) using Athena C18-WP column (100 Å, 4.6 x 25 mm, CNW); solvent A: $H_20$ + 0.1% TFA, solvent B: MeOH + 0.1% TFA. 10% B ramping to 50% B at 20 min, 90% B 20.5-24 min, 10% B 24.5-35 min; flow rate 1 mL $min^{-1}$, 35 °C. Retention times: product = 11.4 min, substrate = 12.9 min, caffeine = 15.2 min

Conversion of substrate to product was calculated from the peak areas using multiplication factors from calibration curves of the absorbance of the two components to adjust for the differences in the absorption coefficient of the substrate and the product.

## Chiral HPLC Method

Samples were filtered through 0.22 µm nylon membranes. The samples were analysed by HPLC (Agilent 1260) using a Lux Cellulose-4 column (Phenomenex, 250 mm x 4.6 mm, 5µm); solvent A: $H_20$ + 20 mM $(NH_4)HCO_3$ adjusted to pH 8.75 using DEA, solvent B: MeCN. 10% B ramping to 13% B at 12 mins, ramping to 40% B at 12-25 mins, ramping back to 10% B 20-25 mins and maintaining 10% B 25-30 mins; flow rate 1.5 mL $min^{-1}$, 35 °C. Retention times (*S*)-product = 9.6 min, (*R*)-product = 10.6 min, substrate = 13.0 mins, caffeine =

Conversion of substrate to product was calculated from the peak areas using multiplication factors from calibration curves of the absorbance of the two components relative to the peak area of the internal standard, caffeine, to adjust for the differences in the absorption coefficient of the substrate and the product.

# Appendix 1: Control Reactions and HPLC calibrations for Catalysis Experiments

## a) Substrate under reaction conditions in the absence of catalyst/ArM

To test that imine **1a** does not convert to **1b** under the standard reaction conditions, a control experiment was carried out where the reaction conditions were repeated, but with an absence of any catalyst/ArM present. Conditions: 50 mM imine **1a**, 3 M sodium formate, pH 5.8 (0.6 M MES), 40 °C, stirring. 72 hours. Conversion was measured using the non-chiral HPLC method.

No **1b** observed after 72 hours.

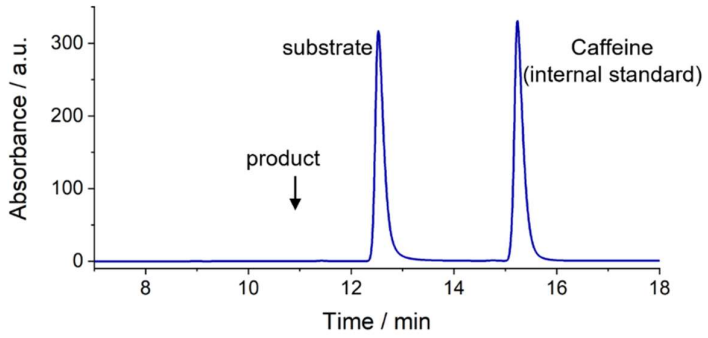


## b) Substrate in absence of catalyst/ArM at 60 °C (variable temperature experiments)

For the variable temperature experiments with the 5-Me-pyr_azoto_Gst and 5-Me-pyr_azoto_Pth ArMs at variable temperatures, it was necessary to repeat the substrate control experiment at 60 °C. Since there is no conversion of **1a** to **1b** at 40 °C it was not necessary to carry out controls at 20 °C and 5 °C but at 60 °C any background reaction would be accelerated. Conditions: 50 mM imine **1a**, 3 M sodium formate, pH 5.8 (0.6 M MES), 60 °C, stirring. 2 hours was sufficient for this measurement since both ArMs catalyse the reaction to competition well within this time. Conversion was measured using the non-chiral HPLC method.

There was 1.9% conversion to **1b** after 2 hours, however, as this is very low and much slower than the ArM catalysed reactions, the background reaction can be ignored.

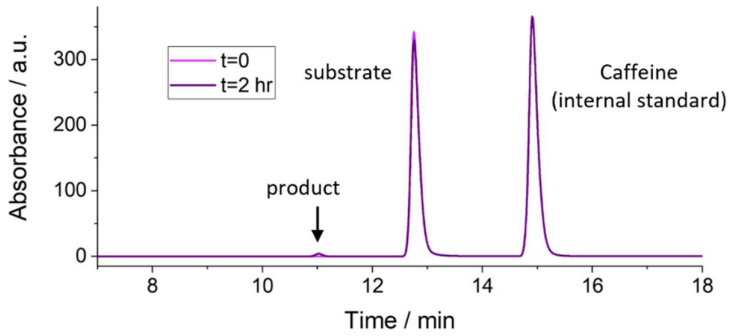


## c) Siderophore-catalyst conjugate without Cp*Ir

To test that there is no background reaction from the conjugate in the absence of the Cp*Ir unit, the conjugate was prepared with only Fe coordinated as catalysis measured under the standard reaction conditions. Conditions: 50 mM imine **1a**, 0.125 mM conjugate, 3 M sodium formate, pH 5.8 (0.6 M MES), 40 °C, stirring. 24 hours. Conversion was measured using the non-chiral HPLC method.

There was 3.2% conversion to **1b** after 24 hours, which could perhaps be attributed to trace amounts of Pd leached during the hydrogenation step to remove the Bn-protecting groups. Since, under the same conditions, the catalytic conjugate with Cp*Ir reached completion within 30 minutes, such a low conversion in 24 hours can be treated as being negligible.

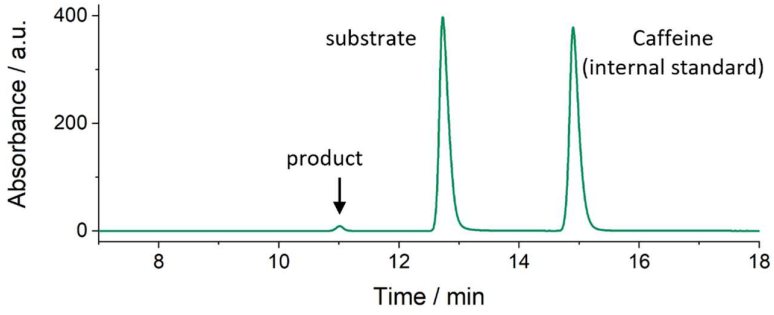

## d) Substrate and product peak area calibration plots

Calibration plots for the peak area of the substrate/product at a range of concentrations was used in calculating the conversion at each time point. Calibration samples were prepared with each experiment individually but an example of the plots is given here. In the case of ArM experiments, the peak areas of the substrate/product were calculated relative to the peak area of the internal standard (caffeine).

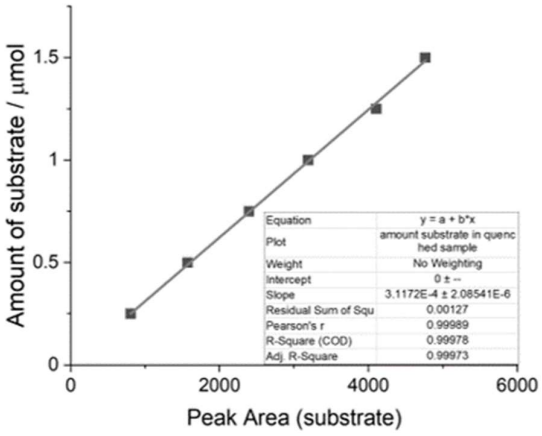


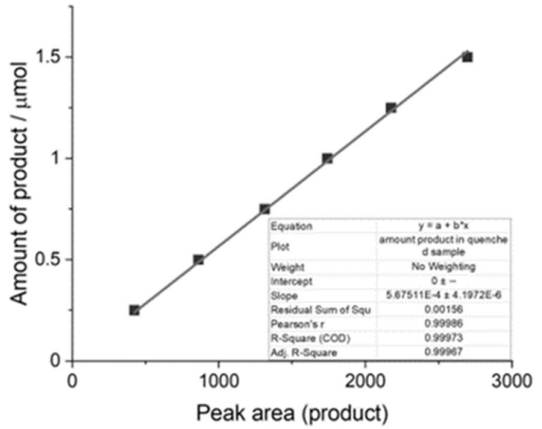

# Appendix 2: Crystal Structures of Compounds 87-92

## 87:4-Methyl-*N*-(pyridine-2-ylmethyl)benzenesulfonamide

Data collected, solved and refined by Adrian C Whitwood

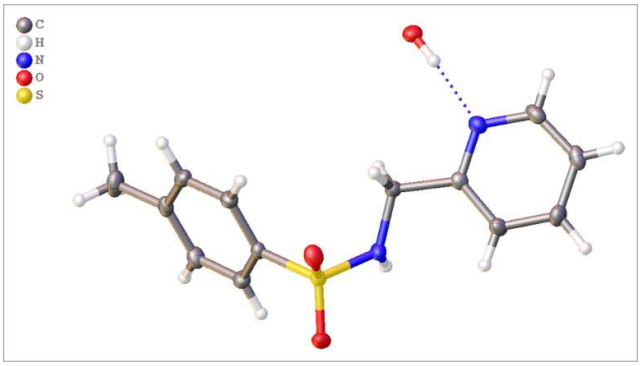


**Table 1 Crystal data and structure refinement for akdk21001.**

| | |
|---|---|
| Identification code | akdk21001 |
| Empirical formula | $C_{26}H_{30}N_4O_5S_2$ |
| Formula weight | 542.66 |
| Temperature/K | 110.00(10) |
| Crystal system | monoclinic |
| Space group | C2/c |
| a/Å | 26.8204(7) |
| b/Å | 5.95132(14) |
| c/Å | 16.5535(4) |
| α/° | 90 |
| β/° | 99.998(3) |
| γ/° | 90 |
| Volume/Å$^3$ | 2602.09(12) |
| Z | 4 |
| $\rho_{calc}$g/cm$^3$ | 1.385 |
| μ/mm$^{-1}$ | 2.230 |
| F(000) | 1144.0 |
| Crystal size/mm$^3$ | 0.23 × 0.191 × 0.082 |
| Radiation | Cu Kα (λ = 1.54184) |
| 2Θ range for data collection/° | 10.854 to 134.13 |
| Index ranges | -32 ≤ h ≤ 30, -7 ≤ k ≤ 6, -19 ≤ l ≤ 16 |
| Reflections collected | 4255 |
| Independent reflections | 2318 [$R_{int}$ = 0.0126, $R_{sigma}$ = 0.0186] |
| Data/restraints/parameters | 2318/0/229 |
| Goodness-of-fit on F$^2$ | 1.063 |
| Final R indexes [I>=2σ (I)] | $R_1$ = 0.0282, $wR_2$ = 0.0717 |
| Final R indexes [all data] | $R_1$ = 0.0315, $wR_2$ = 0.0742 |
| Largest diff. peak/hole / e Å$^{-3}$ | 0.31/-0.35 |

**Table 2 Fractional Atomic Coordinates ($x10^4$) and Equivalent Isotropic Displacement Parameters ($Å^2x10^3$) for akdk21001. $U_{eq}$ is defined as 1/3 of the trace of the orthogonalised $U_{IJ}$ tensor**

| Atom | *x* | *y* | *z* | U(eq) |
|---|---|---|---|---|
| C1 | 5528.9(5) | 6381(3) | 3529.4(9) | 17.3(3) |
| C2 | 5024.6(5) | 6170(2) | 3822.2(8) | 15.9(3) |
| C3 | 4817.4(6) | 7883(3) | 4219.8(9) | 21.0(3) |
| C4 | 4366.8(6) | 7512(3) | 4503.4(10) | 23.7(3) |
| C5 | 4134.9(6) | 5439(3) | 4377.2(9) | 22.5(3) |
| C6 | 4360.3(6) | 3847(3) | 3959.2(10) | 23.1(3) |
| C7 | 6591.0(5) | 8523(2) | 2983.0(9) | 16.0(3) |
| C8 | 6579.6(6) | 10072(3) | 2351.7(10) | 20.0(3) |
| C9 | 6783.7(6) | 9496(3) | 1664.8(10) | 22.4(3) |
| C10 | 7002.1(5) | 7392(3) | 1603.4(9) | 20.4(3) |
| C11 | 7009.4(6) | 5874(3) | 2242.1(10) | 21.1(3) |
| C12 | 6803.8(5) | 6408(3) | 2932.5(9) | 19.0(3) |
| C13 | 7231.0(7) | 6802(4) | 861.6(11) | 30.3(4) |
| N1 | 5712.8(5) | 8695(2) | 3609.4(8) | 18.1(3) |
| N2 | 4795.7(5) | 4176(2) | 3677.4(8) | 20.4(3) |
| O1 | 6523.7(4) | 7838.5(19) | 4509.9(6) | 23.4(3) |
| O2 | 6342.4(4) | 11654.0(19) | 3923.0(7) | 24.6(3) |
| S1 | 6311.6(2) | 9252.1(6) | 3837.4(2) | 16.95(13) |
| O3 | 5000 | 11177(3) | 2500 | 21.2(3) |

**Table 3 Anisotropic Displacement Parameters ($Å^2x10^3$) for akdk21001. The Anisotropic displacement factor exponent takes the form: $-2\pi^2[h^2a^{*2}U_{11}+2hka^*b^*U_{12}+\ldots]$.**

| Atom | $U_{11}$ | $U_{22}$ | $U_{33}$ | $U_{23}$ | $U_{13}$ | $U_{12}$ |
|---|---|---|---|---|---|---|
| C1 | 18.5(7) | 15.8(7) | 18.4(7) | -1.6(6) | 5.7(6) | -0.7(6) |
| C2 | 16.6(7) | 18.6(7) | 12.2(7) | 1.3(6) | 1.4(5) | -0.5(6) |
| C3 | 22.6(8) | 20.8(8) | 21.0(8) | -3.5(6) | 7.9(6) | -4.4(6) |
| C4 | 22.6(8) | 28.1(9) | 22.9(8) | -2.6(7) | 10.4(6) | 1.5(7) |
| C5 | 15.4(7) | 31.7(9) | 20.4(8) | 9.0(7) | 3.5(6) | -0.5(6) |
| C6 | 18.6(7) | 21.1(8) | 28.2(8) | 4.4(7) | 0.6(6) | -5.2(6) |
| C7 | 12.9(6) | 18.6(7) | 16.9(7) | -1.5(6) | 4.0(5) | -1.8(6) |
| C8 | 19.0(7) | 17.0(8) | 25.0(8) | 1.6(6) | 6.1(6) | 1.1(6) |
| C9 | 20.5(8) | 26.7(9) | 20.9(8) | 4.9(7) | 5.9(6) | -1.4(6) |
| C10 | 12.9(7) | 28.9(8) | 19.7(7) | -4.4(6) | 3.4(5) | -3.4(6) |
| C11 | 17.2(7) | 19.2(8) | 27.2(8) | -4.8(6) | 4.8(6) | 1.4(6) |
| C12 | 18.3(7) | 16.4(7) | 22.6(8) | 1.9(6) | 4.4(6) | -0.4(6) |
| C13 | 23.3(9) | 45.6(12) | 24.0(9) | -6.1(8) | 9.6(7) | 0.1(8) |
| N1 | 16.0(6) | 16.1(7) | 23.2(7) | 3.0(5) | 6.5(5) | 1.0(5) |
| N2 | 18.8(6) | 18.2(7) | 23.8(7) | -0.1(5) | 2.6(5) | -2.2(5) |

| | | | | | | |
|---|---|---|---|---|---|---|
| O1 | 22.7(5) | 29.6(6) | 18.4(5) | 2.3(5) | 4.5(4) | -2.2(5) |
| O2 | 27.5(6) | 17.8(6) | 31.4(6) | -7.3(5) | 13.8(5) | -5.7(4) |
| S1 | 17.2(2) | 16.8(2) | 18.3(2) | -1.78(14) | 7.00(13) | -2.33(13) |
| O3 | 24.7(8) | 15.7(8) | 24.2(8) | 0 | 6.8(6) | 0 |

**Table 4 Bond Lengths for akdk21001.**

| Atom | Atom | Length/Å | Atom | Atom | Length/Å |
|---|---|---|---|---|---|
| C1 | C2 | 1.5192(19) | C7 | S1 | 1.7657(14) |
| C1 | N1 | 1.4610(19) | C8 | C9 | 1.388(2) |
| C2 | C3 | 1.381(2) | C9 | C10 | 1.393(2) |
| C2 | N2 | 1.3386(19) | C10 | C11 | 1.388(2) |
| C3 | C4 | 1.388(2) | C10 | C13 | 1.507(2) |
| C4 | C5 | 1.381(2) | C11 | C12 | 1.389(2) |
| C5 | C6 | 1.374(2) | N1 | S1 | 1.6192(13) |
| C6 | N2 | 1.345(2) | O1 | S1 | 1.4320(11) |
| C7 | C8 | 1.390(2) | O2 | S1 | 1.4374(12) |
| C7 | C12 | 1.390(2) | | | |

**Table 5 Bond Angles for akdk21001.**

| Atom | Atom | Atom | Angle/° | Atom | Atom | Atom | Angle/° |
|---|---|---|---|---|---|---|---|
| N1 | C1 | C2 | 110.73(12) | C9 | C10 | C13 | 120.34(15) |
| C3 | C2 | C1 | 123.04(13) | C11 | C10 | C9 | 118.67(14) |
| N2 | C2 | C1 | 114.96(13) | C11 | C10 | C13 | 120.99(15) |
| N2 | C2 | C3 | 121.98(13) | C10 | C11 | C12 | 121.48(15) |
| C2 | C3 | C4 | 119.31(15) | C11 | C12 | C7 | 118.85(14) |
| C5 | C4 | C3 | 119.13(15) | C1 | N1 | S1 | 121.31(10) |
| C6 | C5 | C4 | 117.80(14) | C2 | N2 | C6 | 117.77(13) |
| N2 | C6 | C5 | 123.96(15) | N1 | S1 | C7 | 107.74(7) |
| C8 | C7 | C12 | 120.71(13) | O1 | S1 | C7 | 108.17(7) |
| C8 | C7 | S1 | 118.84(11) | O1 | S1 | N1 | 107.75(7) |
| C12 | C7 | S1 | 120.42(11) | O1 | S1 | O2 | 119.96(7) |
| C9 | C8 | C7 | 119.47(15) | O2 | S1 | C7 | 107.36(7) |
| C8 | C9 | C10 | 120.82(15) | O2 | S1 | N1 | 105.32(7) |

**Table 6 Hydrogen Bonds for akdk21001**

| D | H | A | d(D-H)/Å | d(H-A)/Å | d(D-A)/Å | D-H-A/° |
|---|---|---|---|---|---|---|
| N1 | H1 | O3 | 0.82(2) | 2.04(2) | 2.8267(16) | 161.6(18) |
| O3 | H3A | N2[1] | 0.86(2) | 1.90(2) | 2.7669(16) | 176(2) |

**Table 7 Torsion Angles for akdk21001**

| A | B | C | D | Angle/° | A | B | C | D | Angle/° |
|---|---|---|---|---|---|---|---|---|---|
| C1 | C2 | C3 | C4 | -176.81(14) | C8 | C7 | S1 | O2 | -28.35(13) |
| C1 | C2 | N2 | C6 | 176.71(13) | C8 | C9 | C10 | C11 | 0.4(2) |
| C1 | N1 | S1 | C7 | 69.94(13) | C8 | C9 | C10 | C13 | -178.88(15) |
| C1 | N1 | S1 | O1 | -46.56(13) | C9 | C10 | C11 | C12 | 0.2(2) |
| C1 | N1 | S1 | O2 | -175.71(11) | C10 | C11 | C12 | C7 | -0.6(2) |
| C2 | C1 | N1 | S1 | 145.78(11) | C12 | C7 | C8 | C9 | -0.1(2) |
| C2 | C3 | C4 | C5 | -0.3(2) | C12 | C7 | S1 | N1 | -93.30(13) |
| C3 | C2 | N2 | C6 | -2.4(2) | C12 | C7 | S1 | O1 | 22.92(13) |
| C3 | C4 | C5 | C6 | -1.2(2) | C12 | C7 | S1 | O2 | 153.70(12) |
| C4 | C5 | C6 | N2 | 1.0(2) | C13 | C10 | C11 | C12 | 179.38(14) |
| C5 | C6 | N2 | C2 | 0.7(2) | N1 | C1 | C2 | C3 | -8.9(2) |
| C7 | C8 | C9 | C10 | -0.4(2) | N1 | C1 | C2 | N2 | 172.02(12) |
| C8 | C7 | C12 | C11 | 0.6(2) | N2 | C2 | C3 | C4 | 2.2(2) |
| C8 | C7 | S1 | N1 | 84.64(13) | S1 | C7 | C8 | C9 | -178.01(12) |
| C8 | C7 | S1 | O1 | -159.14(11) | S1 | C7 | C12 | C11 | 178.47(11) |

**Table 8 Hydrogen Atom Coordinates (Åx10$^4$) and Isotropic Displacement Parameters (Å$^2$x10$^3$) for akdk21001**

| Atom | *x* | *y* | *z* | U(eq) |
|---|---|---|---|---|
| H1A | 5775(7) | 5390(30) | 3860(11) | 22(4) |
| H1B | 5491(7) | 5880(30) | 2948(11) | 24(5) |
| H3 | 4980(7) | 9240(30) | 4305(11) | 22(4) |
| H4 | 4224(7) | 8720(30) | 4794(12) | 33(5) |
| H5 | 3829(7) | 5110(30) | 4581(11) | 28(5) |
| H6 | 4205(7) | 2430(30) | 3858(11) | 26(5) |
| H8 | 6439(6) | 11470(30) | 2388(10) | 20(4) |
| H9 | 6777(7) | 10560(30) | 1235(12) | 31(5) |
| H11 | 7160(7) | 4420(30) | 2193(12) | 29(5) |
| H12 | 6815(7) | 5400(30) | 3373(12) | 27(5) |
| H13A | 7573(10) | 7210(40) | 935(14) | 54(7) |
| H13B | 7050(10) | 7390(50) | 385(17) | 67(8) |
| H13C | 7231(10) | 5170(50) | 773(16) | 66(8) |
| H1 | 5564(7) | 9570(30) | 3266(12) | 24(5) |
| H3A | 5068(8) | 12050(40) | 2117(13) | 43(6) |

# 88: 4-Methyl-*N*-{[5-(trifluoromethyl)pyridine-2-yl]methyl}benzene-1-sulfonamide

Data collected, solved and refined by Adrian C Whitwood

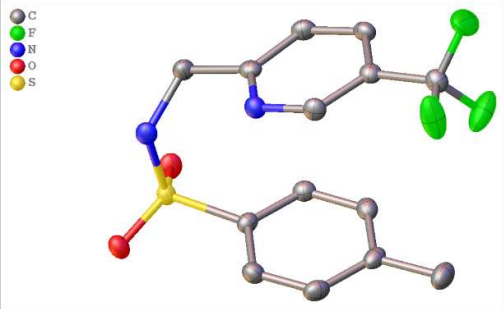


**Table 1 Crystal data and structure refinement for akdk21008.**

| | |
|---|---|
| Identification code | akdk21008 |
| Empirical formula | $C_{14}H_{13}F_3N_2O_2S$ |
| Formula weight | 330.32 |
| Temperature/K | 110.00(10) |
| Crystal system | triclinic |
| Space group | P-1 |
| a/Å | 9.2225(8) |
| b/Å | 9.5210(9) |
| c/Å | 9.9139(8) |
| α/° | 77.525(8) |
| β/° | 64.985(8) |
| γ/° | 62.690(10) |
| Volume/Å$^3$ | 700.67(13) |
| Z | 2 |
| $\rho_{calc}$g/cm$^3$ | 1.566 |
| μ/mm$^{-1}$ | 2.479 |
| F(000) | 340.0 |
| Crystal size/mm$^3$ | 0.209 × 0.159 × 0.061 |
| Radiation | Cu Kα (λ = 1.54184) |
| 2Θ range for data collection/° | 9.848 to 134.096 |
| Index ranges | -11 ≤ h ≤ 10, -11 ≤ k ≤ 10, -10 ≤ l ≤ 11 |
| Reflections collected | 4370 |
| Independent reflections | 2495 [$R_{int}$ = 0.0297, $R_{sigma}$ = 0.0440] |
| Data/restraints/parameters | 2495/0/251 |
| Goodness-of-fit on F$^2$ | 1.046 |
| Final R indexes [I>=2σ (I)] | $R_1$ = 0.0412, $wR_2$ = 0.1058 |
| Final R indexes [all data] | $R_1$ = 0.0513, $wR_2$ = 0.1154 |
| Largest diff. peak/hole / e Å$^{-3}$ | 0.57/-0.43 |

**Table 2 Fractional Atomic Coordinates (x$10^4$) and Equivalent Isotropic Displacement Parameters (Å$^2$x$10^3$) for akdk21008. $U_{eq}$ is defined as 1/3 of the trace of the orthogonalised $U_{IJ}$ tensor**

| Atom | *x* | *y* | *z* | U(eq) |
|---|---|---|---|---|
| C1 | 7300(3) | 5242(3) | 8610(2) | 17.4(5) |
| C2 | 6259(3) | 5258(3) | 7915(3) | 21.4(5) |
| C3 | 4729(3) | 6578(3) | 8002(3) | 24.3(5) |
| C4 | 4214(3) | 7910(3) | 8754(3) | 22.3(5) |
| C5 | 5264(3) | 7848(3) | 9467(3) | 21.7(5) |
| C6 | 6794(3) | 6530(3) | 9410(2) | 19.8(5) |
| C7 | 2577(4) | 9361(3) | 8805(3) | 30.2(6) |
| C8 | 11226(3) | 5364(3) | 6877(3) | 20.6(5) |
| C9 | 9935(3) | 7004(3) | 6629(2) | 17.8(5) |
| C10 | 9636(3) | 8298(3) | 7312(3) | 21.5(5) |
| C11 | 8425(3) | 9777(3) | 7097(3) | 20.0(5) |
| C12 | 7531(3) | 9908(3) | 6209(2) | 18.8(5) |
| C13 | 7942(3) | 8572(3) | 5539(2) | 19.9(5) |
| C14 | 6108(3) | 11451(3) | 6041(3) | 21.5(5) |
| F1 | 6605(2) | 12638.0(18) | 5625(2) | 47.9(5) |
| F2 | 5491(3) | 11431.2(19) | 5053(2) | 48.7(5) |
| F3 | 4716(2) | 11901(2) | 7306.1(18) | 45.9(5) |
| N1 | 10797(3) | 4071(2) | 6855(2) | 18.6(4) |
| N2 | 9130(3) | 7143(2) | 5725(2) | 18.9(4) |
| O1 | 9322(2) | 2300.2(18) | 7941.6(18) | 22.2(4) |
| O2 | 9830(2) | 3532.7(19) | 9571.8(17) | 22.7(4) |
| S1 | 9364.5(7) | 3641.0(6) | 8330.5(6) | 16.90(18) |

**Table 3 Anisotropic Displacement Parameters (Å$^2$x$10^3$) for akdk21008. The Anisotropic displacement factor exponent takes the form: - $2\pi^2$[$h^2a^{*2}U_{11}$+2hka*b*$U_{12}$+…].**

| Atom | $U_{11}$ | $U_{22}$ | $U_{33}$ | $U_{23}$ | $U_{13}$ | $U_{12}$ |
|---|---|---|---|---|---|---|
| C1 | 15.7(11) | 18.8(11) | 16.5(10) | 1.9(8) | -6.8(9) | -6.4(9) |
| C2 | 23.8(13) | 20.0(12) | 23.8(12) | -0.4(9) | -10.5(10) | -10.4(10) |
| C3 | 20.9(13) | 28.7(13) | 27.6(13) | 3.9(10) | -13.1(11) | -12.2(11) |
| C4 | 16.1(12) | 21.5(12) | 23.9(12) | 4.8(9) | -5.7(10) | -7.3(10) |
| C5 | 22.2(13) | 19.5(12) | 19.6(11) | -1.2(9) | -3.4(10) | -9.3(10) |
| C6 | 20.5(12) | 22.7(12) | 18.0(11) | 0.5(9) | -7.9(9) | -10.4(10) |
| C7 | 20.4(14) | 25.4(14) | 34.6(15) | 3.0(12) | -8.7(12) | -4.5(11) |

| | | | | | | |
|---|---|---|---|---|---|---|
| C8 | 18.8(12) | 20.6(12) | 25.1(12) | -1.4(9) | -11.0(10) | -7.4(10) |
| C9 | 18.0(12) | 21.5(12) | 15.2(10) | 1.0(8) | -4.4(9) | -11.4(10) |
| C10 | 21.9(13) | 27.3(13) | 20.8(11) | -0.2(10) | -10.6(10) | -12.5(11) |
| C11 | 21.7(12) | 22.2(12) | 19.6(11) | -3.9(9) | -6.4(9) | -11.7(10) |
| C12 | 20.3(12) | 20.2(12) | 16.6(10) | 1.4(9) | -6.3(9) | -10.4(10) |
| C13 | 22.7(12) | 23.3(12) | 17.6(11) | -1.9(9) | -11.0(10) | -9.1(10) |
| C14 | 25.9(13) | 21.3(12) | 19.4(11) | -0.9(9) | -10.3(10) | -9.6(11) |
| F1 | 37.1(10) | 20.8(8) | 83.6(14) | 10.1(8) | -23.9(10) | -13.9(8) |
| F2 | 66.6(13) | 28.6(9) | 58.4(11) | -9.6(8) | -51.1(10) | 3.1(8) |
| F3 | 26.5(9) | 48.2(11) | 30.2(8) | 1.0(7) | -4.0(7) | 3.7(8) |
| N1 | 21.2(11) | 21.3(10) | 16.8(10) | -2.6(8) | -10.6(8) | -7.5(8) |
| N2 | 22.1(11) | 19.4(10) | 17.3(9) | -1.2(7) | -9.2(8) | -8.3(9) |
| O1 | 26.2(9) | 16.0(8) | 27.5(9) | -0.4(6) | -14.8(7) | -7.1(7) |
| O2 | 24.4(9) | 23.7(9) | 22.1(8) | -0.1(7) | -15.9(7) | -5.3(7) |
| S1 | 18.4(3) | 15.4(3) | 17.9(3) | -0.1(2) | -10.0(2) | -5.1(2) |

**Table 4 Bond Lengths for akdk21008.**

| Atom | Atom | Length/Å | Atom | Atom | Length/Å |
|---|---|---|---|---|---|
| C1 | C2 | 1.392(3) | C10 | C11 | 1.379(3) |
| C1 | C6 | 1.391(3) | C11 | C12 | 1.394(3) |
| C1 | S1 | 1.760(2) | C12 | C13 | 1.383(3) |
| C2 | C3 | 1.376(4) | C12 | C14 | 1.489(3) |
| C3 | C4 | 1.396(4) | C13 | N2 | 1.334(3) |
| C4 | C5 | 1.396(4) | C14 | F1 | 1.331(3) |
| C4 | C7 | 1.497(3) | C14 | F2 | 1.332(3) |
| C5 | C6 | 1.381(3) | C14 | F3 | 1.330(3) |
| C8 | C9 | 1.514(3) | N1 | S1 | 1.630(2) |
| C8 | N1 | 1.463(3) | O1 | S1 | 1.4319(17) |
| C9 | C10 | 1.394(3) | O2 | S1 | 1.4358(16) |
| C9 | N2 | 1.339(3) | | | |

**Table 5 Bond Angles for akdk21008.**

| Atom | Atom | Atom | Angle/° | Atom | Atom | Atom | Angle/° |
|---|---|---|---|---|---|---|---|
| C2 | C1 | S1 | 119.12(18) | C13 | C12 | C11 | 118.9(2) |
| C6 | C1 | C2 | 120.8(2) | C13 | C12 | C14 | 120.9(2) |
| C6 | C1 | S1 | 119.88(18) | N2 | C13 | C12 | 123.3(2) |
| C3 | C2 | C1 | 119.4(2) | F1 | C14 | C12 | 113.2(2) |
| C2 | C3 | C4 | 121.3(2) | F1 | C14 | F2 | 106.5(2) |
| C3 | C4 | C7 | 121.0(2) | F2 | C14 | C12 | 113.2(2) |
| C5 | C4 | C3 | 118.1(2) | F3 | C14 | C12 | 112.55(19) |
| C5 | C4 | C7 | 120.9(2) | F3 | C14 | F1 | 105.1(2) |
| C6 | C5 | C4 | 121.7(2) | F3 | C14 | F2 | 105.5(2) |
| C5 | C6 | C1 | 118.8(2) | C8 | N1 | S1 | 120.12(17) |
| N1 | C8 | C9 | 115.3(2) | C13 | N2 | C9 | 117.8(2) |
| C10 | C9 | C8 | 120.3(2) | N1 | S1 | C1 | 107.32(10) |
| N2 | C9 | C8 | 117.2(2) | O1 | S1 | C1 | 108.20(11) |
| N2 | C9 | C10 | 122.5(2) | O1 | S1 | N1 | 105.23(10) |
| C11 | C10 | C9 | 119.4(2) | O1 | S1 | O2 | 120.08(10) |
| C10 | C11 | C12 | 118.0(2) | O2 | S1 | C1 | 108.12(10) |
| C11 | C12 | C14 | 120.2(2) | O2 | S1 | N1 | 107.24(11) |

**Table 6 Torsion Angles for akdk21008**

| A | B | C | D | Angle/° | A | B | C | D | Angle/° |
|---|---|---|---|---|---|---|---|---|---|
| C1 | C2 | C3 | C4 | 1.0(4) | C9 | C8 | N1 | S1 | -81.2(2) |
| C2 | C1 | C6 | C5 | -1.9(3) | C9 | C10 | C11 | C12 | 0.7(3) |
| C2 | C1 | S1 | N1 | 88.6(2) | C10 | C9 | N2 | C13 | -3.1(3) |
| C2 | C1 | S1 | O1 | -24.5(2) | C10 | C11 | C12 | C13 | -2.5(3) |
| C2 | C1 | S1 | O2 | -156.04(18) | C10 | C11 | C12 | C14 | 175.0(2) |
| C2 | C3 | C4 | C5 | -2.3(4) | C11 | C12 | C13 | N2 | 1.7(3) |
| C2 | C3 | C4 | C7 | 178.1(2) | C11 | C12 | C14 | F1 | 52.6(3) |
| C3 | C4 | C5 | C6 | 1.6(3) | C11 | C12 | C14 | F2 | 174.0(2) |
| C4 | C5 | C6 | C1 | 0.5(3) | C11 | C12 | C14 | F3 | -66.4(3) |
| C6 | C1 | C2 | C3 | 1.2(3) | C12 | C13 | N2 | C9 | 1.2(3) |
| C6 | C1 | S1 | N1 | -86.0(2) | C13 | C12 | C14 | F1 | -129.9(2) |
| C6 | C1 | S1 | O1 | 160.95(17) | C13 | C12 | C14 | F2 | -8.5(3) |
| C6 | C1 | S1 | O2 | 29.4(2) | C13 | C12 | C14 | F3 | 111.0(3) |
| C7 | C4 | C5 | C6 | -178.9(2) | C14 | C12 | C13 | N2 | -175.9(2) |
| C8 | C9 | C10 | C11 | -178.6(2) | N1 | C8 | C9 | C10 | 147.9(2) |
| C8 | C9 | N2 | C13 | 177.7(2) | N1 | C8 | C9 | N2 | -32.9(3) |
| C8 | N1 | S1 | C1 | 67.2(2) | N2 | C9 | C10 | C11 | 2.2(3) |
| C8 | N1 | S1 | O1 | -177.69(17) | S1 | C1 | C2 | C3 | -173.33(18) |
| C8 | N1 | S1 | O2 | -48.8(2) | S1 | C1 | C6 | C5 | 172.54(17) |

**Table 7 Hydrogen Atom Coordinates (Åx10$^4$) and Isotropic Displacement Parameters (Å$^2$x10$^3$) for akdk21008**

| Atom | *x* | *y* | *z* | U(eq) |
|---|---|---|---|---|
| H2 | 6570(40) | 4400(30) | 7430(30) | 23(7) |
| H3 | 4050(40) | 6580(40) | 7540(30) | 37(8) |
| H5 | 4880(40) | 8780(30) | 10010(30) | 27(7) |
| H6 | 7470(40) | 6550(30) | 9880(30) | 21(7) |
| H7A | 2540(50) | 10240(50) | 9070(40) | 62(12) |
| H7B | 1540(50) | 9240(40) | 9520(40) | 58(11) |
| H7C | 2520(50) | 9640(50) | 7900(50) | 74(13) |
| H8A | 12340(40) | 5220(30) | 6080(30) | 26(7) |
| H8B | 11350(40) | 5290(30) | 7810(30) | 29(7) |
| H10 | 10170(40) | 8180(30) | 7930(30) | 27(7) |
| H11 | 8180(40) | 10670(30) | 7560(30) | 32(8) |
| H13 | 7420(30) | 8600(30) | 4950(30) | 16(6) |
| H1 | 10710(40) | 4010(30) | 6200(30) | 17(8) |

# 89: *N*-[(5-Chloropyridin-2-yl)methyl]-4-methylbenzene-1-sulfonamide

Data collected, solved and refined by Adrian C Whitwood

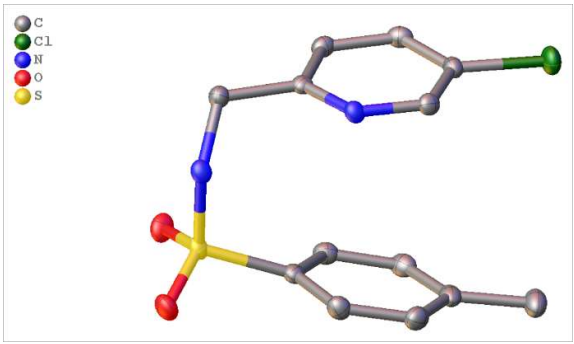


**Table 1 Crystal data and structure refinement for akdk22006.**

| | |
|---|---|
| Identification code | akdk22006 |
| Empirical formula | $C_{13}H_{13}N_2O_2SCl$ |
| Formula weight | 296.76 |
| Temperature/K | 109.90(14) |
| Crystal system | triclinic |
| Space group | P-1 |
| a/Å | 7.5078(6) |
| b/Å | 9.1089(5) |
| c/Å | 10.0161(7) |
| α/° | 77.771(6) |
| β/° | 82.101(6) |
| γ/° | 81.171(6) |
| Volume/Å$^3$ | 657.59(8) |
| Z | 2 |
| $\rho_{calc}$g/cm$^3$ | 1.499 |
| μ/mm$^{-1}$ | 4.058 |
| F(000) | 308.0 |
| Crystal size/mm$^3$ | 0.141 × 0.107 × 0.096 |
| Radiation | Cu Kα (λ = 1.54184) |
| 2Θ range for data collection/° | 9.088 to 134.144 |
| Index ranges | $-8 \leq h \leq 8$, $-10 \leq k \leq 7$, $-11 \leq l \leq 11$ |
| Reflections collected | 3934 |
| Independent reflections | 2325 [$R_{int}$ = 0.0150, $R_{sigma}$ = 0.0232] |
| Data/restraints/parameters | 2325/0/178 |
| Goodness-of-fit on F$^2$ | 1.063 |
| Final R indexes [I>=2σ (I)] | $R_1$ = 0.0269, $wR_2$ = 0.0658 |
| Final R indexes [all data] | $R_1$ = 0.0315, $wR_2$ = 0.0682 |
| Largest diff. peak/hole / e Å$^{-3}$ | 0.36/-0.40 |

**Table 2 Fractional Atomic Coordinates (x$10^4$) and Equivalent Isotropic Displacement Parameters (Å$^2$x$10^3$) for akdk22006. $U_{eq}$ is defined as 1/3 of the trace of the orthogonalised $U_{IJ}$ tensor**

| Atom | *x* | *y* | *z* | U(eq) |
|---|---|---|---|---|
| C1 | 1987(2) | 6933.7(19) | 9938.9(18) | 16.6(4) |
| C2 | 3446(2) | 7930.0(19) | 9314.2(16) | 13.7(3) |
| C3 | 3017(2) | 9467.6(19) | 8812.4(17) | 16.3(4) |
| C4 | 4382(2) | 10347.5(19) | 8237.4(17) | 17.3(4) |
| C5 | 6141(2) | 9623.9(19) | 8170.9(17) | 15.7(3) |
| C6 | 6489(2) | 8086.5(19) | 8699.2(17) | 16.1(4) |
| C7 | 3831(2) | 5851.6(19) | 6923.4(17) | 15.2(3) |
| C8 | 5499(2) | 4940(2) | 6942.2(18) | 18.9(4) |
| C9 | 7015(2) | 5507(2) | 6187.9(19) | 21.1(4) |
| C10 | 6894(2) | 6976(2) | 5399.9(18) | 20.1(4) |
| C11 | 5196(2) | 7829(2) | 5352.4(18) | 20.3(4) |
| C12 | 3667(2) | 7288(2) | 6114.3(17) | 18.2(4) |
| C13 | 8560(3) | 7625(2) | 4642.4(19) | 26.8(4) |
| Cl1 | 7949.9(6) | 10624.2(5) | 7422.9(4) | 22.26(13) |
| N1 | 2273.1(19) | 5434.7(16) | 9584.7(15) | 15.1(3) |
| N2 | 5167.4(18) | 7251.1(15) | 9279.4(14) | 14.8(3) |
| O1 | 385.6(16) | 6223.7(14) | 7666.4(13) | 21.2(3) |
| O2 | 2048.2(17) | 3621.4(14) | 8157.9(13) | 22.5(3) |
| S1 | 1973.1(5) | 5225.9(5) | 8070.3(4) | 15.20(12) |

**Table 3 Anisotropic Displacement Parameters (Å$^2$x$10^3$) for akdk22006. The Anisotropic displacement factor exponent takes the form: - $2\pi^2[h^2a^{*2}U_{11}+2hka^*b^*U_{12}+\ldots]$.**

| Atom | $U_{11}$ | $U_{22}$ | $U_{33}$ | $U_{23}$ | $U_{13}$ | $U_{12}$ |
|---|---|---|---|---|---|---|
| C1 | 14.6(8) | 17.4(9) | 18.0(9) | -4.3(7) | -0.7(7) | -2.6(7) |
| C2 | 14.0(8) | 16.4(8) | 11.9(8) | -4.5(6) | -3.3(6) | -1.8(6) |
| C3 | 14.1(8) | 18.2(9) | 16.1(8) | -4.5(7) | -2.9(7) | 1.9(7) |
| C4 | 22.5(9) | 13.3(8) | 15.5(8) | -2.1(6) | -4.2(7) | 0.2(7) |
| C5 | 16.9(9) | 17.2(9) | 14.1(8) | -3.0(7) | -1.4(6) | -5.8(7) |
| C6 | 12.6(8) | 18.7(9) | 17.7(8) | -4.8(7) | -4.0(7) | -0.5(7) |
| C7 | 14.7(8) | 17.7(8) | 15.0(8) | -5.5(7) | -3.3(6) | -2.5(7) |
| C8 | 18.1(9) | 15.5(9) | 23.4(9) | -4.1(7) | -4.0(7) | -0.9(7) |
| C9 | 16.1(9) | 24.4(10) | 23.8(9) | -8.8(7) | -1.9(7) | -0.3(7) |
| C10 | 21.9(9) | 26.3(10) | 15.1(9) | -7.5(7) | -0.4(7) | -9.1(7) |
| C11 | 27.8(10) | 18.8(9) | 14.6(9) | -1.6(7) | -1.9(7) | -6.0(7) |
| C12 | 19.7(9) | 18.0(9) | 17.2(9) | -4.2(7) | -4.9(7) | 0.2(7) |
| C13 | 25.0(10) | 36.9(11) | 20.9(10) | -6.7(8) | 1.7(8) | -13.8(8) |

| | | | | | | |
|---|---|---|---|---|---|---|
| Cl1 | 20.3(2) | 20.6(2) | 25.3(2) | −0.71(17) | 1.02(17) | −9.27(17) |
| N1 | 13.2(7) | 14.4(7) | 17.3(7) | -0.4(6) | -4.8(6) | -1.1(6) |
| N2 | 13.0(7) | 14.4(7) | 17.4(7) | -2.6(6) | -4.3(6) | -1.3(5) |
| O1 | 12.5(6) | 28.6(7) | 21.7(6) | -2.2(5) | -5.7(5) | -0.2(5) |
| O2 | 21.6(7) | 17.7(7) | 30.1(7) | -5.8(5) | -2.2(5) | -7.3(5) |
| S1 | 11.7(2) | 15.9(2) | 18.7(2) | −2.74(16) | −3.83(15) | −2.94(15) |

**Table 4 Bond Lengths for akdk22006.**

| Atom | Atom | Length/Å | Atom | Atom | Length/Å |
|---|---|---|---|---|---|
| C1 | C2 | 1.514(2) | C7 | C12 | 1.383(2) |
| C1 | N1 | 1.460(2) | C7 | S1 | 1.7653(17) |
| C2 | C3 | 1.388(2) | C8 | C9 | 1.383(3) |
| C2 | N2 | 1.343(2) | C9 | C10 | 1.398(3) |
| C3 | C4 | 1.385(2) | C10 | C11 | 1.389(3) |
| C4 | C5 | 1.382(2) | C10 | C13 | 1.505(2) |
| C5 | C6 | 1.386(2) | C11 | C12 | 1.385(3) |
| C5 | Cl1 | 1.7457(17) | N1 | S1 | 1.6177(15) |
| C6 | N2 | 1.337(2) | O1 | S1 | 1.4333(12) |
| C7 | C8 | 1.392(2) | O2 | S1 | 1.4383(13) |

**Table 5 Bond Angles for akdk22006.**

| Atom | Atom | Atom | Angle/° | Atom | Atom | Atom | Angle/° |
|---|---|---|---|---|---|---|---|
| N1 | C1 | C2 | 115.18(14) | C8 | C9 | C10 | 121.00(16) |
| C3 | C2 | C1 | 121.34(15) | C9 | C10 | C13 | 121.03(17) |
| N2 | C2 | C1 | 116.62(14) | C11 | C10 | C9 | 118.15(16) |
| N2 | C2 | C3 | 122.03(15) | C11 | C10 | C13 | 120.82(17) |
| C4 | C3 | C2 | 119.99(15) | C12 | C11 | C10 | 121.62(17) |
| C5 | C4 | C3 | 117.28(16) | C7 | C12 | C11 | 119.12(16) |
| C4 | C5 | C6 | 120.17(16) | C1 | N1 | S1 | 120.81(12) |
| C4 | C5 | Cl1 | 120.75(13) | C6 | N2 | C2 | 118.29(14) |
| C6 | C5 | Cl1 | 119.09(13) | N1 | S1 | C7 | 107.68(8) |
| N2 | C6 | C5 | 122.20(15) | O1 | S1 | C7 | 107.21(8) |
| C8 | C7 | S1 | 119.05(13) | O1 | S1 | N1 | 107.52(8) |
| C12 | C7 | C8 | 120.63(16) | O1 | S1 | O2 | 120.01(8) |
| C12 | C7 | S1 | 120.03(13) | O2 | S1 | C7 | 108.10(8) |
| C9 | C8 | C7 | 119.37(16) | O2 | S1 | N1 | 105.78(8) |

**Table 6 Hydrogen Bonds for akdk22006**

| D | H | A | d(D-H)/Å | d(H-A)/Å | d(D-A)/Å | D-H-A/° |
|---|---|---|---|---|---|---|
| N1 | H1 | N2[1] | 0.83(2) | 2.19(2) | 2.992(2) | 162(2) |

**Table 7 Torsion Angles for akdk22006**

| A | B | C | D | Angle/° | A | B | C | D | Angle/° |
|---|---|---|---|---|---|---|---|---|---|
| C1 | C2 | C3 | C4 | −179.53(15) | C8 | C7 | S1 | O2 | -38.95(16) |
| C1 | C2 | N2 | C6 | 178.10(14) | C8 | C9 | C10 | C11 | -2.5(3) |
| C1 | N1 | S1 | C7 | 74.66(14) | C8 | C9 | C10 | C13 | 176.53(16) |
| C1 | N1 | S1 | O1 | -40.57(14) | C9 | C10 | C11 | C12 | 3.3(3) |
| C1 | N1 | S1 | O2 | −169.93(12) | C10 | C11 | C12 | C7 | -1.2(3) |
| C2 | C1 | N1 | S1 | -74.00(17) | C12 | C7 | C8 | C9 | 2.8(3) |
| C2 | C3 | C4 | C5 | 1.1(2) | C12 | C7 | S1 | N1 | -99.02(15) |
| C3 | C2 | N2 | C6 | -2.3(2) | C12 | C7 | S1 | O1 | 16.42(16) |
| C3 | C4 | C5 | C6 | -1.7(2) | C12 | C7 | S1 | O2 | 147.13(14) |
| C3 | C4 | C5 | Cl1 | 178.27(13) | C13 | C10 | C11 | C12 | −175.67(16) |
| C4 | C5 | C6 | N2 | 0.3(3) | Cl1 | C5 | C6 | N2 | −179.66(13) |
| C5 | C6 | N2 | C2 | 1.7(2) | N1 | C1 | C2 | C3 | 140.05(16) |
| C7 | C8 | C9 | C10 | -0.5(3) | N1 | C1 | C2 | N2 | -40.3(2) |
| C8 | C7 | C12 | C11 | -2.0(3) | N2 | C2 | C3 | C4 | 0.8(2) |
| C8 | C7 | S1 | N1 | 74.91(15) | S1 | C7 | C8 | C9 | −171.11(13) |
| C8 | C7 | S1 | O1 | −169.65(13) | S1 | C7 | C12 | C11 | 171.88(13) |

**Table 8 Hydrogen Atom Coordinates (Åx10$^4$) and Isotropic Displacement Parameters (Å$^2$x10$^3$) for akdk22006**

| Atom | *x* | *y* | *z* | U(eq) |
|---|---|---|---|---|
| H1A | 1894.66 | 6807.16 | 10951.39 | 20 |
| H1B | 811.51 | 7463.08 | 9642.29 | 20 |
| H3 | 1787.16 | 9916.71 | 8863.13 | 20 |
| H4 | 4120.33 | 11405.18 | 7902.55 | 21 |
| H6 | 7707.85 | 7610.45 | 8647.18 | 19 |
| H8 | 5593.94 | 3937.8 | 7468.05 | 23 |
| H9 | 8156.42 | 4890.03 | 6205.4 | 25 |
| H11 | 5081.03 | 8808.5 | 4783.11 | 24 |
| H12 | 2519.63 | 7895.76 | 6081.83 | 22 |
| H13A | 8836.53 | 7312.66 | 3750.71 | 40 |
| H13B | 9586.87 | 7252.29 | 5184.15 | 40 |
| H13C | 8341.65 | 8733.06 | 4499.31 | 40 |
| H1 | 3140(30) | 4840(20) | 9890(20) | 22(5) |

# 90: *N*-[(5-Fluoropyridin-2-yl)methyl]-4-methylbenzene-1-sulfonamide

Data collected, solved and refined by Adrian C Whitwood

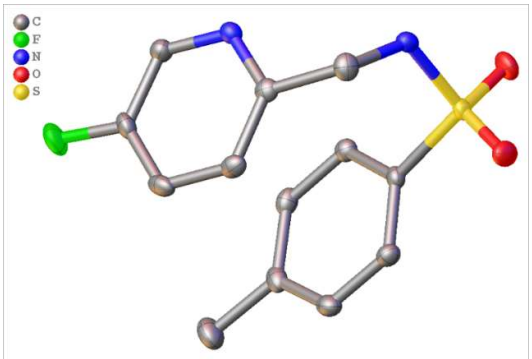


**Table 1 Crystal data and structure refinement for akdk21012.**

| | |
|---|---|
| Identification code | akdk21012 |
| Empirical formula | $C_{13}H_{13}FN_2O_2S$ |
| Formula weight | 280.31 |
| Temperature/K | 109.9(2) |
| Crystal system | monoclinic |
| Space group | $P2_1/n$ |
| a/Å | 6.78284(16) |
| b/Å | 13.0054(3) |
| c/Å | 14.5983(3) |
| α/° | 90 |
| β/° | 98.976(2) |
| γ/° | 90 |
| Volume/Å$^3$ | 1272.00(5) |
| Z | 4 |
| $\rho_{calc}$g/cm$^3$ | 1.464 |
| μ/mm$^{-1}$ | 2.390 |
| F(000) | 584.0 |
| Crystal size/mm$^3$ | 0.308 × 0.264 × 0.079 |
| Radiation | Cu Kα (λ = 1.54184) |
| 2Θ range for data collection/° | 9.158 to 134.12 |
| Index ranges | $-6 \le h \le 8$, $-15 \le k \le 9$, $-17 \le l \le 17$ |
| Reflections collected | 4401 |
| Independent reflections | 2267 [$R_{int}$ = 0.0182, $R_{sigma}$ = 0.0252] |
| Data/restraints/parameters | 2267/0/177 |
| Goodness-of-fit on F$^2$ | 1.040 |
| Final R indexes [I>=2σ (I)] | $R_1$ = 0.0316, $wR_2$ = 0.0807 |
| Final R indexes [all data] | $R_1$ = 0.0354, $wR_2$ = 0.0837 |
| Largest diff. peak/hole / e Å$^{-3}$ | 0.26/-0.40 |

**Table 2 Fractional Atomic Coordinates (x$10^4$) and Equivalent Isotropic Displacement Parameters (Å$^2$x$10^3$) for akdk21012. $U_{eq}$ is defined as 1/3 of the trace of the orthogonalised $U_{IJ}$ tensor**

| Atom | *x* | *y* | *z* | U(eq) |
|---|---|---|---|---|
| C1 | 5765(2) | 3181.9(13) | 640.3(12) | 19.5(4) |
| C2 | 6128(2) | 3886.6(12) | 1474.5(11) | 15.8(3) |
| C3 | 6331(2) | 3515.7(13) | 2377.8(12) | 17.9(3) |
| C4 | 6602(2) | 4195.8(14) | 3117.6(11) | 19.9(4) |
| C5 | 6681(2) | 5220.9(13) | 2903.1(11) | 18.4(3) |
| C6 | 6482(2) | 5554.0(13) | 1995.6(11) | 17.0(3) |
| C7 | 1518(2) | 3297.4(12) | 1352.9(11) | 14.3(3) |
| C8 | 1700(2) | 2567.0(13) | 2056.4(12) | 16.7(3) |
| C9 | 1727(2) | 2882.3(13) | 2965.3(12) | 19.1(4) |
| C10 | 1574(2) | 3917.7(14) | 3184.3(11) | 18.6(4) |
| C11 | 1330(2) | 4634.2(13) | 2460.9(12) | 17.8(3) |
| C12 | 1304(2) | 4335.0(13) | 1546.6(11) | 15.6(3) |
| C13 | 1688(3) | 4250.9(16) | 4177.9(12) | 29.1(4) |
| F1 | 6978.2(17) | 5934.2(8) | 3587.9(7) | 29.3(3) |
| N1 | 3897(2) | 3404.4(11) | 15.5(9) | 16.5(3) |
| N2 | 6204.6(19) | 4895.9(10) | 1286.1(9) | 15.6(3) |
| O1 | 1997.9(19) | 1824.3(9) | 231.9(8) | 23.6(3) |
| O2 | 284.2(18) | 3397.0(10) | -439.4(8) | 24.2(3) |
| S1 | 1806.1(6) | 2922.4(3) | 220.6(3) | 15.62(13) |

**Table 3 Anisotropic Displacement Parameters (Å$^2$x$10^3$) for akdk21012. The Anisotropic displacement factor exponent takes the form: - $2\pi^2[h^2a^{*2}U_{11}+2hka^*b^*U_{12}+\ldots]$.**

| Atom | $U_{11}$ | $U_{22}$ | $U_{33}$ | $U_{23}$ | $U_{13}$ | $U_{12}$ |
|---|---|---|---|---|---|---|
| C1 | 17.9(8) | 19.0(8) | 21.5(9) | -2.5(7) | 2.7(7) | 3.1(7) |
| C2 | 10.9(8) | 18.0(8) | 18.4(8) | 1.1(7) | 1.5(6) | 1.5(6) |
| C3 | 13.5(8) | 17.8(8) | 21.4(8) | 6.6(7) | -0.7(6) | 0.8(6) |
| C4 | 14.2(8) | 30.6(10) | 14.1(8) | 7.3(7) | -0.4(6) | -0.4(7) |
| C5 | 16.8(8) | 24.6(9) | 12.7(8) | -3.7(7) | -1.3(6) | -0.9(7) |
| C6 | 17.6(8) | 16.2(8) | 16.6(8) | 1.2(6) | 0.7(6) | -1.0(6) |
| C7 | 12.5(7) | 16.9(8) | 12.9(7) | -1.8(6) | 0.4(6) | -1.6(6) |
| C8 | 16.8(8) | 14.5(8) | 18.7(8) | 2.0(6) | 2.5(6) | -0.8(6) |
| C9 | 17.4(8) | 23.2(9) | 16.5(8) | 3.8(7) | 2.6(6) | -2.2(7) |
| C10 | 12.2(8) | 27.3(9) | 16.4(8) | -4.3(7) | 2.6(6) | -3.2(7) |
| C11 | 14.3(8) | 16.5(8) | 22.6(9) | -4.6(7) | 3.2(6) | -0.5(6) |
| C12 | 12.5(8) | 17.0(8) | 17.0(8) | 1.6(6) | 0.7(6) | 0.1(6) |
| C13 | 28.7(10) | 40.1(11) | 18.7(9) | -7.3(8) | 4.0(8) | -4.1(8) |
| F1 | 39.8(6) | 31.3(6) | 15.1(5) | -7.6(4) | -1.4(4) | -2.2(5) |
| N1 | 21.5(8) | 15.2(7) | 12.7(7) | 1.0(6) | 2.4(5) | -1.7(6) |

| | | | | | | |
|---|---|---|---|---|---|---|
| N2 | 15.3(7) | 17.6(7) | 13.5(6) | 1.0(5) | 1.0(5) | 0.2(5) |
| O1 | 36.7(7) | 16.0(6) | 18.8(6) | -5.1(5) | 7.0(5) | -5.6(5) |
| O2 | 23.0(7) | 31.7(7) | 15.1(6) | 1.4(5) | -5.5(5) | -2.4(5) |
| S1 | 20.0(2) | 15.0(2) | 11.1(2) | −1.80(14) | 0.26(15) | −3.10(15) |

**Table 4 Bond Lengths for akdk21012.**

| Atom | Atom | Length/Å | Atom | Atom | Length/Å |
|---|---|---|---|---|---|
| C1 | C2 | 1.513(2) | C7 | C12 | 1.391(2) |
| C1 | N1 | 1.470(2) | C7 | S1 | 1.7631(16) |
| C2 | C3 | 1.391(2) | C8 | C9 | 1.386(2) |
| C2 | N2 | 1.344(2) | C9 | C10 | 1.392(2) |
| C3 | C4 | 1.386(2) | C10 | C11 | 1.399(2) |
| C4 | C5 | 1.372(2) | C10 | C13 | 1.504(2) |
| C5 | C6 | 1.380(2) | C11 | C12 | 1.388(2) |
| C5 | F1 | 1.3556(19) | N1 | S1 | 1.6209(14) |
| C6 | N2 | 1.334(2) | O1 | S1 | 1.4338(13) |
| C7 | C8 | 1.390(2) | O2 | S1 | 1.4370(12) |

**Table 5 Bond Angles for akdk21012.**

| Atom | Atom | Atom | Angle/° | Atom | Atom | Atom | Angle/° |
|---|---|---|---|---|---|---|---|
| N1 | C1 | C2 | 113.35(13) | C8 | C9 | C10 | 121.05(16) |
| C3 | C2 | C1 | 122.18(15) | C9 | C10 | C11 | 118.39(15) |
| N2 | C2 | C1 | 115.69(14) | C9 | C10 | C13 | 120.39(16) |
| N2 | C2 | C3 | 122.12(15) | C11 | C10 | C13 | 121.23(16) |
| C4 | C3 | C2 | 119.93(16) | C12 | C11 | C10 | 121.45(16) |
| C5 | C4 | C3 | 116.58(15) | C11 | C12 | C7 | 118.78(15) |
| C4 | C5 | C6 | 121.49(15) | C1 | N1 | S1 | 120.24(11) |
| F1 | C5 | C4 | 120.20(15) | C6 | N2 | C2 | 118.23(14) |
| F1 | C5 | C6 | 118.30(15) | N1 | S1 | C7 | 107.11(7) |
| N2 | C6 | C5 | 121.65(15) | O1 | S1 | C7 | 106.73(7) |
| C8 | C7 | C12 | 120.85(15) | O1 | S1 | N1 | 107.87(8) |
| C8 | C7 | S1 | 119.57(13) | O1 | S1 | O2 | 119.34(7) |
| C12 | C7 | S1 | 119.30(12) | O2 | S1 | C7 | 109.68(8) |
| C9 | C8 | C7 | 119.43(15) | O2 | S1 | N1 | 105.53(8) |

**Table 6 Torsion Angles for akdk21012**

| A | B | C | D | Angle/° | A | B | C | D | Angle/° |
|---|---|---|---|---|---|---|---|---|---|
| C1 | C2 | C3 | C4 | −178.06(15) | C8 | C7 | S1 | O2 | 136.53(13) |
| C1 | C2 | N2 | C6 | 178.71(14) | C8 | C9 | C10 | C11 | 1.9(2) |

| | | | | | | | | |
|---|---|---|---|---|---|---|---|---|
| C1 | N1 | S1 | C7 | 55.74(14) | C8 | C9 | C10 | C13 | −177.55(16) |
| C1 | N1 | S1 | O1 | -58.83(13) | C9 | C10 | C11 | C12 | -2.1(2) |
| C1 | N1 | S1 | O2 | 172.57(12) | C10 | C11 | C12 | C7 | 0.3(2) |
| C2 | C1 | N1 | S1 | -84.44(16) | C12 | C7 | C8 | C9 | -1.9(2) |
| C2 | C3 | C4 | C5 | -0.9(2) | C12 | C7 | S1 | N1 | 64.46(14) |
| C3 | C2 | N2 | C6 | -0.1(2) | C12 | C7 | S1 | O1 | 179.79(12) |
| C3 | C4 | C5 | C6 | 0.6(2) | C12 | C7 | S1 | O2 | -49.60(15) |
| C3 | C4 | C5 | F1 | −178.82(14) | C13 | C10 | C11 | C12 | 177.39(15) |
| C4 | C5 | C6 | N2 | 0.0(3) | F1 | C5 | C6 | N2 | 179.38(14) |
| C5 | C6 | N2 | C2 | -0.2(2) | N1 | C1 | C2 | C3 | 120.48(17) |
| C7 | C8 | C9 | C10 | 0.0(2) | N1 | C1 | C2 | N2 | -58.36(19) |
| C8 | C7 | C12 | C11 | 1.8(2) | N2 | C2 | C3 | C4 | 0.7(2) |
| C8 | C7 | S1 | N1 | −109.41(14) | S1 | C7 | C8 | C9 | 171.84(12) |
| C8 | C7 | S1 | O1 | 5.92(15) | S1 | C7 | C12 | C11 | −172.01(12) |

**Table 7 Hydrogen Atom Coordinates (Åx10$^4$) and Isotropic Displacement Parameters (Å$^2$x10$^3$) for akdk21012**

| Atom | *x* | *y* | *z* | U(eq) |
|---|---|---|---|---|
| H1A | 6895.06 | 3246.04 | 289.02 | 23 |
| H1B | 5730.62 | 2461.98 | 857.63 | 23 |
| H3 | 6284.74 | 2796.76 | 2487.71 | 21 |
| H4 | 6726.25 | 3964.35 | 3741.16 | 24 |
| H6 | 6543.92 | 6269.68 | 1873.11 | 20 |
| H8 | 1804.95 | 1857.9 | 1915.44 | 20 |
| H9 | 1852.02 | 2383.59 | 3446.41 | 23 |
| H11 | 1179.48 | 5341.12 | 2598.48 | 21 |
| H12 | 1142.63 | 4829.75 | 1061.85 | 19 |
| H13A | 598.57 | 3931.97 | 4445.06 | 44 |
| H13B | 1569.5 | 5000.83 | 4204.91 | 44 |
| H13C | 2971.12 | 4036.84 | 4531.03 | 44 |
| H1 | 3750(30) | 3991(17) | -204(15) | 27(6) |

# 91: 4-Methyl-*N*-[(4-methylpyridin-2-yl)methyl]benzene-1-sulfonamide

Data collected, solved and refined by Adrian C Whitwood

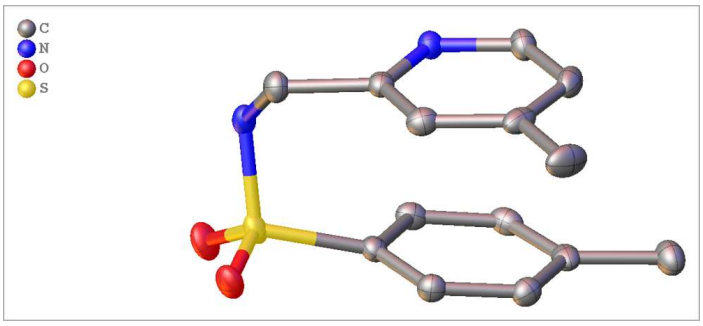


**Table 1 Crystal data and structure refinement for akdk22005.**

| | |
|---|---|
| Identification code | akdk22005 |
| Empirical formula | $C_{14}H_{16}N_2O_2S$ |
| Formula weight | 276.35 |
| Temperature/K | 110.00(10) |
| Crystal system | triclinic |
| Space group | P-1 |
| a/Å | 7.3158(3) |
| b/Å | 9.1955(5) |
| c/Å | 10.4433(6) |
| α/° | 90.509(5) |
| β/° | 100.314(4) |
| γ/° | 106.325(4) |
| Volume/Å$^3$ | 662.02(6) |
| Z | 2 |
| $\rho_{calc}$g/cm$^3$ | 1.386 |
| μ/mm$^{-1}$ | 2.173 |
| F(000) | 292.0 |
| Crystal size/mm$^3$ | 0.17 × 0.14 × 0.08 |
| Radiation | Cu Kα (λ = 1.54184) |
| 2Θ range for data collection/° | 8.624 to 134.002 |
| Index ranges | $-7 \leq h \leq 8$, $-10 \leq k \leq 10$, $-11 \leq l \leq 12$ |
| Reflections collected | 3914 |
| Independent reflections | 2356 [$R_{int}$ = 0.0149, $R_{sigma}$ = 0.0240] |
| Data/restraints/parameters | 2356/0/179 |
| Goodness-of-fit on F$^2$ | 1.068 |
| Final R indexes [I>=2σ (I)] | $R_1$ = 0.0307, $wR_2$ = 0.0772 |
| Final R indexes [all data] | $R_1$ = 0.0349, $wR_2$ = 0.0803 |
| Largest diff. peak/hole / e Å$^{-3}$ | 0.35/-0.32 |

**Table 2 Fractional Atomic Coordinates (x10$^4$) and Equivalent Isotropic Displacement Parameters (Å$^2$x10$^3$) for akdk22005. $U_{eq}$ is defined as 1/3 of the trace of the orthogonalised $U_{IJ}$ tensor**

| Atom | *x* | *y* | *z* | U(eq) |
|---|---|---|---|---|
| C1 | 7425(2) | 5997.4(18) | 2164.6(16) | 18.7(3) |
| C2 | 6916(2) | 4288.6(18) | 2248.7(15) | 15.9(3) |
| C3 | 7523(2) | 3656.7(19) | 3388.0(16) | 19.4(3) |
| C4 | 7003(2) | 2084.0(19) | 3460.4(16) | 21.2(4) |
| C5 | 5867(2) | 1217.6(19) | 2356.5(17) | 21.8(4) |
| C6 | 5351(2) | 1938.0(18) | 1248.4(16) | 20.1(4) |
| C7 | 7626(3) | 1359(2) | 4683.8(18) | 31.3(4) |
| C8 | 2669(2) | 4658.4(18) | 2383.7(15) | 16.1(3) |
| C9 | 2947(2) | 3768.5(18) | 3426.0(15) | 17.4(3) |
| C10 | 1976(2) | 2232.8(18) | 3297.6(15) | 18.8(3) |
| C11 | 717(2) | 1565.2(18) | 2143.4(16) | 18.7(3) |
| C12 | 409(2) | 2492.4(19) | 1127.2(15) | 19.7(3) |
| C13 | 1390(2) | 4023.4(18) | 1234.1(15) | 17.9(3) |
| C14 | -235(2) | -121.9(19) | 2007.4(18) | 25.9(4) |
| N1 | 5800(2) | 6580.4(15) | 1604.2(13) | 17.5(3) |
| N2 | 5854.9(18) | 3445.1(14) | 1172.6(12) | 16.4(3) |
| O1 | 5053.3(17) | 7028.9(13) | 3752.1(11) | 22.9(3) |
| O2 | 2930.7(18) | 7405.0(13) | 1718.6(11) | 25.4(3) |
| S1 | 4111.4(6) | 6554.2(4) | 2424.0(4) | 17.39(13) |

**Table 3 Anisotropic Displacement Parameters (Å$^2$x10$^3$) for akdk22005. The Anisotropic displacement factor exponent takes the form: - $2\pi^2[h^2a^{*2}U_{11}+2hka^*b^*U_{12}+\ldots]$.**

| Atom | $U_{11}$ | $U_{22}$ | $U_{33}$ | $U_{23}$ | $U_{13}$ | $U_{12}$ |
|---|---|---|---|---|---|---|
| C1 | 18.2(8) | 15.7(8) | 20.3(8) | 0.3(6) | 1.1(6) | 3.2(6) |
| C2 | 13.8(7) | 16.1(8) | 19.1(8) | 1.4(6) | 4.3(6) | 5.3(6) |
| C3 | 16.2(8) | 23.8(9) | 18.7(8) | 2.3(6) | 2.7(6) | 6.7(7) |
| C4 | 20.4(8) | 25.1(9) | 25.1(9) | 11.2(7) | 10.7(7) | 13.7(7) |
| C5 | 20.5(8) | 15.2(8) | 33.4(9) | 6.9(7) | 10.2(7) | 8.1(7) |
| C6 | 18.6(8) | 15.9(8) | 25.3(9) | -0.5(6) | 3.2(6) | 4.8(6) |
| C7 | 37.7(11) | 38.7(11) | 28.0(10) | 18.2(8) | 13.5(8) | 23.0(9) |
| C8 | 16.5(7) | 15.1(8) | 18.0(8) | 0.3(6) | 4.1(6) | 6.2(6) |
| C9 | 17.1(8) | 19.5(8) | 15.2(8) | 0.7(6) | 1.5(6) | 5.6(6) |
| C10 | 17.9(8) | 20.1(8) | 19.6(8) | 4.7(6) | 3.7(6) | 7.4(7) |
| C11 | 13.3(7) | 18.7(8) | 24.9(8) | -1.2(6) | 5.7(6) | 4.8(6) |
| C12 | 14.8(7) | 25.2(9) | 18.3(8) | -4.9(6) | -0.1(6) | 6.5(7) |
| C13 | 17.5(8) | 22.4(8) | 15.5(8) | 1.8(6) | 1.3(6) | 9.5(7) |

| | | | | | | |
|---|---|---|---|---|---|---|
| C14 | 22.4(9) | 20.2(9) | 33.5(10) | -3.7(7) | 4.6(7) | 4.0(7) |
| N1 | 23.5(7) | 12.9(7) | 15.0(7) | 2.2(5) | 2.0(6) | 4.3(5) |
| N2 | 17.2(7) | 14.3(7) | 18.2(7) | 1.5(5) | 3.0(5) | 5.5(5) |
| O1 | 32.9(7) | 17.0(6) | 17.3(6) | -3.1(4) | 2.0(5) | 6.3(5) |
| O2 | 35.1(7) | 17.7(6) | 26.7(6) | 3.3(5) | 2.0(5) | 15.1(5) |
| S1 | 24.7(2) | 12.4(2) | 15.8(2) | 0.27(14) | 1.75(15) | 7.81(15) |

**Table 4 Bond Lengths for akdk22005.**

| Atom | Atom | Length/Å | Atom | Atom | Length/Å |
|---|---|---|---|---|---|
| C1 | C2 | 1.517(2) | C8 | C13 | 1.391(2) |
| C1 | N1 | 1.469(2) | C8 | S1 | 1.7615(16) |
| C2 | C3 | 1.385(2) | C9 | C10 | 1.384(2) |
| C2 | N2 | 1.342(2) | C10 | C11 | 1.396(2) |
| C3 | C4 | 1.395(2) | C11 | C12 | 1.394(2) |
| C4 | C5 | 1.387(2) | C11 | C14 | 1.505(2) |
| C4 | C7 | 1.504(2) | C12 | C13 | 1.382(2) |
| C5 | C6 | 1.385(2) | N1 | S1 | 1.6192(14) |
| C6 | N2 | 1.337(2) | O1 | S1 | 1.4377(12) |
| C8 | C9 | 1.388(2) | O2 | S1 | 1.4363(12) |

**Table 5 Bond Angles for akdk22005.**

| Atom | Atom | Atom | Angle/° | Atom | Atom | Atom | Angle/° |
|---|---|---|---|---|---|---|---|
| N1 | C1 | C2 | 115.20(13) | C9 | C10 | C11 | 121.27(15) |
| C3 | C2 | C1 | 120.84(14) | C10 | C11 | C14 | 120.05(15) |
| N2 | C2 | C1 | 116.46(13) | C12 | C11 | C10 | 118.38(15) |
| N2 | C2 | C3 | 122.70(15) | C12 | C11 | C14 | 121.56(15) |
| C2 | C3 | C4 | 120.16(15) | C13 | C12 | C11 | 120.94(15) |
| C3 | C4 | C7 | 121.59(16) | C12 | C13 | C8 | 119.64(15) |
| C5 | C4 | C3 | 116.96(15) | C1 | N1 | S1 | 119.79(11) |
| C5 | C4 | C7 | 121.45(16) | C6 | N2 | C2 | 116.93(13) |
| C6 | C5 | C4 | 119.26(15) | N1 | S1 | C8 | 107.61(7) |
| N2 | C6 | C5 | 123.96(15) | O1 | S1 | C8 | 108.19(7) |
| C9 | C8 | C13 | 120.43(15) | O1 | S1 | N1 | 106.98(7) |
| C9 | C8 | S1 | 120.66(12) | O2 | S1 | C8 | 107.70(7) |
| C13 | C8 | S1 | 118.55(12) | O2 | S1 | N1 | 106.15(7) |
| C10 | C9 | C8 | 119.26(14) | O2 | S1 | O1 | 119.67(7) |

**Table 6 Hydrogen Bonds for akdk22005**

| D | H | A | d(D-H)/Å | d(H-A)/Å | d(D-A)/Å | D-H-A/° |
|---|---|---|---|---|---|---|
| N1 | H1 | N2[1] | 0.85(2) | 2.11(2) | 2.9328(19) | 160.8(19) |

**Table 7 Torsion Angles for akdk22005**

| A | B | C | D | Angle/° | A | B | C | D | Angle/° |
|---|---|---|---|---|---|---|---|---|---|
| C1 | C2 | C3 | C4 | 178.41(14) | C9 | C8 | S1 | O1 | -16.31(15) |
| C1 | C2 | N2 | C6 | -178.13(13) | C9 | C8 | S1 | O2 | -146.99(13) |
| C1 | N1 | S1 | C8 | -73.84(13) | C9 | C10 | C11 | C12 | -1.9(2) |
| C1 | N1 | S1 | O1 | 42.22(13) | C9 | C10 | C11 | C14 | 176.73(15) |
| C1 | N1 | S1 | O2 | 171.07(11) | C10 | C11 | C12 | C13 | 2.9(2) |
| C2 | C1 | N1 | S1 | 70.84(16) | C11 | C12 | C13 | C8 | -1.6(2) |
| C2 | C3 | C4 | C5 | -0.3(2) | C13 | C8 | C9 | C10 | 1.7(2) |
| C2 | C3 | C4 | C7 | -179.63(15) | C13 | C8 | S1 | N1 | -74.28(13) |
| C3 | C2 | N2 | C6 | 1.6(2) | C13 | C8 | S1 | O1 | 170.45(12) |
| C3 | C4 | C5 | C6 | 1.4(2) | C13 | C8 | S1 | O2 | 39.77(14) |
| C4 | C5 | C6 | N2 | -1.2(2) | C14 | C11 | C12 | C13 | -175.72(15) |
| C5 | C6 | N2 | C2 | -0.3(2) | N1 | C1 | C2 | C3 | -132.17(15) |
| C7 | C4 | C5 | C6 | -179.21(15) | N1 | C1 | C2 | N2 | 47.55(19) |
| C8 | C9 | C10 | C11 | -0.4(2) | N2 | C2 | C3 | C4 | -1.3(2) |
| C9 | C8 | C13 | C12 | -0.7(2) | S1 | C8 | C9 | C10 | -171.42(12) |
| C9 | C8 | S1 | N1 | 98.96(13) | S1 | C8 | C13 | C12 | 172.53(12) |

**Table 8 Hydrogen Atom Coordinates (Åx10$^4$) and Isotropic Displacement Parameters (Å$^2$x10$^3$) for akdk22005**

| Atom | *x* | *y* | *z* | U(eq) |
|---|---|---|---|---|
| H1A | 7980.07 | 6481.99 | 3052.92 | 22 |
| H1B | 8446.17 | 6310.25 | 1632.31 | 22 |
| H3 | 8295.55 | 4296.1 | 4121.8 | 23 |
| H5 | 5447.41 | 141.9 | 2360.15 | 26 |
| H6 | 4593.26 | 1324.27 | 496.69 | 24 |
| H7A | 9044.81 | 1625.46 | 4889.76 | 47 |
| H7B | 7087.98 | 253.67 | 4552.29 | 47 |
| H7C | 7149.85 | 1726.15 | 5406.62 | 47 |
| H9 | 3793.65 | 4208.57 | 4218.74 | 21 |
| H10 | 2170.74 | 1620.92 | 4008.45 | 23 |
| H12 | -488.55 | 2065.9 | 349.9 | 24 |
| H13 | 1192.6 | 4638.79 | 526.38 | 22 |
| H14A | 756.77 | -653.81 | 2028.11 | 39 |
| H14B | -1156.55 | -386.95 | 1176.95 | 39 |
| H14C | -925.74 | -423.48 | 2728.43 | 39 |

| | | | | |
|---|---|---|---|---|
| H1 | 5330(30) | 6350(20) | 790(20) | 31(6) |

# 92: 4-Methyl-*N*-[(5-methylpyridin-2-yl)methyl]benzene-1-sulfonamide

Data collected, solved and refined by Adrian C Whitwood

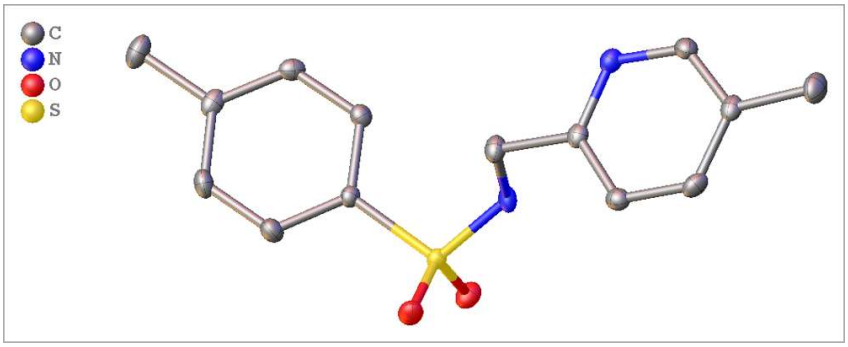


**Table 1 Crystal data and structure refinement for akdk21006.**

| | |
|---|---|
| Identification code | akdk21006 |
| Empirical formula | $C_{14}H_{16}N_2O_2S$ |
| Formula weight | 276.35 |
| Temperature/K | 110.00(10) |
| Crystal system | monoclinic |
| Space group | $P2_1/c$ |
| a/Å | 15.5913(2) |
| b/Å | 12.0597(2) |
| c/Å | 7.12032(12) |
| α/° | 90 |
| β/° | 99.8509(16) |
| γ/° | 90 |
| Volume/Å$^3$ | 1319.06(4) |
| Z | 4 |
| $\rho_{calc}$g/cm$^3$ | 1.392 |
| μ/mm$^{-1}$ | 2.181 |
| F(000) | 584.0 |
| Crystal size/mm$^3$ | 0.237 × 0.168 × 0.11 |
| Radiation | Cu Kα (λ = 1.54184) |
| 2Θ range for data collection/° | 9.324 to 134.124 |
| Index ranges | $-17 \leq h \leq 18$, $-14 \leq k \leq 11$, $-8 \leq l \leq 6$ |
| Reflections collected | 4586 |
| Independent reflections | 2355 [$R_{int}$ = 0.0164, $R_{sigma}$ = 0.0240] |
| Data/restraints/parameters | 2355/0/179 |
| Goodness-of-fit on F$^2$ | 1.053 |
| Final R indexes [I>=2σ (I)] | $R_1$ = 0.0334, $wR_2$ = 0.0839 |
| Final R indexes [all data] | $R_1$ = 0.0375, $wR_2$ = 0.0867 |
| Largest diff. peak/hole / e Å$^{-3}$ | 0.37/-0.36 |

**Table 2 Fractional Atomic Coordinates (x$10^4$) and Equivalent Isotropic Displacement Parameters (Å$^2$x$10^3$) for akdk21006. $U_{eq}$ is defined as 1/3 of the trace of the orthogonalised $U_{IJ}$ tensor**

| Atom | *x* | *y* | *z* | U(eq) |
|---|---|---|---|---|
| C1 | 1238.3(10) | 5944.0(14) | 2969(2) | 12.1(4) |
| C2 | 1090.1(11) | 6972.6(15) | 3732(2) | 14.3(4) |
| C3 | 249.9(11) | 7253.0(15) | 3947(2) | 15.6(4) |
| C4 | -446.4(11) | 6535.6(16) | 3386(2) | 16.2(4) |
| C5 | -279.5(11) | 5506.5(15) | 2630(3) | 18.2(4) |
| C6 | 557.0(11) | 5202.1(15) | 2432(3) | 16.9(4) |
| C7 | -1357.9(11) | 6850.1(17) | 3624(3) | 23.8(4) |
| C8 | 2986.5(11) | 5927.1(16) | 6254(2) | 17.2(4) |
| C9 | 3900.1(11) | 6084.0(14) | 7329(2) | 13.8(4) |
| C10 | 4558.1(11) | 5330.3(15) | 7159(2) | 16.2(4) |
| C11 | 5396.9(11) | 5533.9(15) | 8101(2) | 16.9(4) |
| C12 | 5568.5(11) | 6493.2(15) | 9178(2) | 15.7(4) |
| C13 | 4867.4(11) | 7187.9(15) | 9272(2) | 15.9(4) |
| C14 | 6463.0(11) | 6771.6(18) | 10244(3) | 23.6(4) |
| N1 | 2975.9(9) | 6159.4(13) | 4228(2) | 14.4(3) |
| N2 | 4048.4(9) | 7002.0(12) | 8380(2) | 15.2(3) |
| O1 | 2445.7(8) | 6012.5(11) | 816.2(17) | 18.8(3) |
| O2 | 2355.2(8) | 4381.9(10) | 2877.1(18) | 19.2(3) |
| S1 | 2294.5(2) | 5563.0(3) | 2604.8(6) | 12.57(15) |

**Table 3 Anisotropic Displacement Parameters (Å$^2$x$10^3$) for akdk21006. The Anisotropic displacement factor exponent takes the form: - $2\pi^2[h^2a^{*2}U_{11}+2hka^*b^*U_{12}+\ldots]$.**

| Atom | $U_{11}$ | $U_{22}$ | $U_{33}$ | $U_{23}$ | $U_{13}$ | $U_{12}$ |
|---|---|---|---|---|---|---|
| C1 | 10.4(8) | 14.4(8) | 11.0(8) | 1.2(6) | 0.6(6) | 0.5(7) |
| C2 | 13.7(8) | 14.9(9) | 13.5(8) | 0.5(7) | -0.1(6) | -0.6(7) |
| C3 | 18.0(8) | 15.2(9) | 13.0(8) | 0.4(7) | 1.1(7) | 3.8(7) |
| C4 | 13.7(8) | 22.4(9) | 12.5(8) | 6.1(7) | 2.2(6) | 3.5(7) |
| C5 | 13.4(8) | 19.8(9) | 20.5(9) | 1.7(7) | 0.0(7) | -4.7(7) |
| C6 | 16.2(9) | 15.5(9) | 18.0(9) | -2.1(7) | 0.3(7) | -1.3(7) |
| C7 | 14.7(9) | 30.2(11) | 27.7(10) | 7.5(9) | 6.7(7) | 3.5(8) |
| C8 | 13.4(8) | 23.7(10) | 14.5(8) | 2.7(7) | 2.0(7) | -2.2(7) |
| C9 | 13.3(8) | 16.9(9) | 11.6(8) | 3.5(7) | 3.0(6) | -0.6(7) |
| C10 | 18.3(9) | 15.7(8) | 14.9(8) | -0.7(7) | 4.0(7) | -0.6(7) |
| C11 | 15.2(9) | 19.3(9) | 17.0(9) | 2.8(7) | 4.9(7) | 5.7(7) |
| C12 | 13.3(8) | 22.9(9) | 11.0(8) | 2.9(7) | 2.3(7) | -0.5(7) |
| C13 | 16.6(8) | 16.9(9) | 14.5(8) | -2.7(7) | 3.3(7) | -1.8(7) |
| C14 | 14.3(9) | 34.4(11) | 20.8(9) | -0.9(8) | -0.3(7) | -0.4(8) |
| N1 | 11.4(7) | 15.9(8) | 15.2(7) | 3.3(6) | 0.3(6) | -3.6(6) |

| | | | | | | |
|---|---|---|---|---|---|---|
| N2 | 13.7(7) | 17.3(8) | 14.7(7) | 2.0(6) | 2.9(6) | 1.4(6) |
| O1 | 16.9(6) | 25.1(7) | 15.0(6) | 2.1(5) | 4.1(5) | 2.0(5) |
| O2 | 17.5(6) | 13.3(7) | 27.5(7) | -1.4(5) | 5.8(5) | 1.8(5) |
| S1 | 10.6(2) | 13.1(2) | 14.0(2) | -0.35(15) | 2.08(15) | 0.62(15) |

**Table 4 Bond Lengths for akdk21006.**

| Atom | Atom | Length/Å | Atom | Atom | Length/Å |
|---|---|---|---|---|---|
| C1 | C2 | 1.389(2) | C9 | C10 | 1.391(2) |
| C1 | C6 | 1.392(2) | C9 | N2 | 1.334(2) |
| C1 | S1 | 1.7709(16) | C10 | C11 | 1.386(2) |
| C2 | C3 | 1.387(2) | C11 | C12 | 1.389(3) |
| C3 | C4 | 1.392(3) | C12 | C13 | 1.388(2) |
| C4 | C5 | 1.395(3) | C12 | C14 | 1.507(2) |
| C4 | C7 | 1.508(2) | C13 | N2 | 1.344(2) |
| C5 | C6 | 1.385(2) | N1 | S1 | 1.6003(15) |
| C8 | C9 | 1.509(2) | O1 | S1 | 1.4402(12) |
| C8 | N1 | 1.467(2) | O2 | S1 | 1.4384(13) |

**Table 5 Bond Angles for akdk21006.**

| Atom | Atom | Atom | Angle/° | Atom | Atom | Atom | Angle/° |
|---|---|---|---|---|---|---|---|
| C2 | C1 | C6 | 120.75(16) | C11 | C10 | C9 | 119.40(16) |
| C2 | C1 | S1 | 120.66(13) | C10 | C11 | C12 | 119.45(16) |
| C6 | C1 | S1 | 118.57(13) | C11 | C12 | C14 | 122.55(16) |
| C3 | C2 | C1 | 118.98(16) | C13 | C12 | C11 | 116.78(16) |
| C2 | C3 | C4 | 121.45(16) | C13 | C12 | C14 | 120.65(17) |
| C3 | C4 | C5 | 118.42(16) | N2 | C13 | C12 | 124.67(16) |
| C3 | C4 | C7 | 121.00(17) | C8 | N1 | S1 | 121.24(12) |
| C5 | C4 | C7 | 120.57(17) | C9 | N2 | C13 | 117.58(15) |
| C6 | C5 | C4 | 121.07(16) | N1 | S1 | C1 | 107.26(8) |
| C5 | C6 | C1 | 119.31(17) | O1 | S1 | C1 | 109.19(7) |
| N1 | C8 | C9 | 109.00(13) | O1 | S1 | N1 | 106.29(8) |
| C10 | C9 | C8 | 121.33(16) | O2 | S1 | C1 | 106.18(8) |
| N2 | C9 | C8 | 116.52(15) | O2 | S1 | N1 | 109.12(8) |
| N2 | C9 | C10 | 122.10(16) | O2 | S1 | O1 | 118.36(8) |

**Table 6 Hydrogen Bonds for akdk21006**

| D | H | A | d(D-H)/Å | d(H-A)/Å | d(D-A)/Å | D-H-A/° |
|---|---|---|---|---|---|---|
| N1 | H1 | N2[1] | 0.84(2) | 2.09(2) | 2.902(2) | 162(2) |

**Table 7 Torsion Angles for akdk21006**

| A | B | C | D | Angle/° | A | B | C | D | Angle/° |
|---|---|---|---|---|---|---|---|---|---|
| C1 | C2 | C3 | C4 | -1.1(3) | C8 | N1 | S1 | C1 | 61.14(15) |
| C2 | C1 | C6 | C5 | 1.3(3) | C8 | N1 | S1 | O1 | 177.85(13) |
| C2 | C1 | S1 | N1 | 31.47(16) | C8 | N1 | S1 | O2 | -53.47(15) |
| C2 | C1 | S1 | O1 | -83.32(15) | C9 | C8 | N1 | S1 | 150.85(13) |
| C2 | C1 | S1 | O2 | 148.03(14) | C9 | C10 | C11 | C12 | -0.8(2) |
| C2 | C3 | C4 | C5 | 1.3(3) | C10 | C9 | N2 | C13 | 0.6(2) |
| C2 | C3 | C4 | C7 | −179.89(16) | C10 | C11 | C12 | C13 | 1.3(2) |
| C3 | C4 | C5 | C6 | -0.2(3) | C10 | C11 | C12 | C14 | 179.93(16) |
| C4 | C5 | C6 | C1 | -1.1(3) | C11 | C12 | C13 | N2 | -0.9(3) |
| C6 | C1 | C2 | C3 | -0.2(2) | C12 | C13 | N2 | C9 | 0.0(3) |
| C6 | C1 | S1 | N1 | −150.06(14) | C14 | C12 | C13 | N2 | −179.57(16) |
| C6 | C1 | S1 | O1 | 95.16(15) | N1 | C8 | C9 | C10 | -72.3(2) |
| C6 | C1 | S1 | O2 | -33.49(16) | N1 | C8 | C9 | N2 | 105.03(17) |
| C7 | C4 | C5 | C6 | −179.00(16) | N2 | C9 | C10 | C11 | -0.2(3) |
| C8 | C9 | C10 | C11 | 176.97(15) | S1 | C1 | C2 | C3 | 178.25(13) |
| C8 | C9 | N2 | C13 | −176.68(15) | S1 | C1 | C6 | C5 | −177.20(13) |

**Table 8 Hydrogen Atom Coordinates (Åx10$^4$) and Isotropic Displacement Parameters (Å$^2$x10$^3$) for akdk21006**

| Atom | *x* | *y* | *z* | U(eq) |
|---|---|---|---|---|
| H2 | 1557.19 | 7476.08 | 4100.61 | 17 |
| H3 | 147.17 | 7950.02 | 4489.71 | 19 |
| H5 | -747.26 | 5006.45 | 2243.59 | 22 |
| H6 | 664.45 | 4494.14 | 1934.88 | 20 |
| H7A | -1493.06 | 6510.92 | 4789.68 | 36 |
| H7B | -1772.36 | 6585.12 | 2523.42 | 36 |
| H7C | -1400.74 | 7658.47 | 3713.3 | 36 |
| H8A | 2792.33 | 5156.43 | 6414.06 | 21 |
| H8B | 2583.38 | 6435.76 | 6762.39 | 21 |
| H10 | 4433.38 | 4681.93 | 6403.62 | 19 |
| H11 | 5850.77 | 5021.41 | 8009.83 | 20 |
| H13 | 4973.98 | 7841.55 | 10019.84 | 19 |
| H14A | 6502.24 | 7571.12 | 10490.35 | 35 |
| H14B | 6901.2 | 6555.43 | 9477.33 | 35 |
| H14C | 6567.24 | 6369.41 | 11457.73 | 35 |
| H1 | 3180(14) | 6760(20) | 3920(30) | 24(6) |

# Appendix 3: Crystal Structures of Complexes Cp*Ir(87)Cl and Cp*Ir(88)Cl

## Cp*Ir(87)Cl

Data collected, solved and refined by Adrian C Whitwood

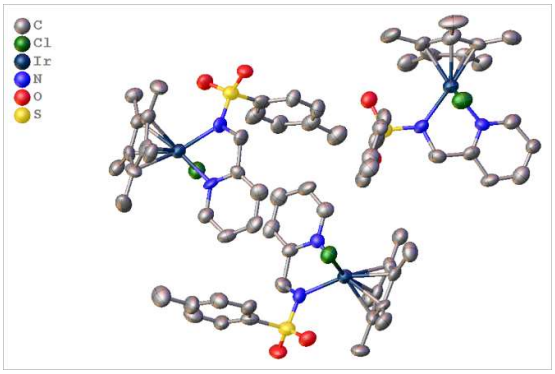


**Table 1 Crystal data and structure refinement for akdk21004.**

| | |
|---|---|
| Identification code | akdk21004 |
| Empirical formula | $C_{23}H_{28}N_2O_2SClIr$ |
| Formula weight | 624.18 |
| Temperature/K | 110.00(10) |
| Crystal system | monoclinic |
| Space group | $P2_1/c$ |
| a/Å | 11.1726(2) |
| b/Å | 40.4331(8) |
| c/Å | 15.2296(3) |
| α/° | 90 |
| β/° | 92.1501(17) |
| γ/° | 90 |
| Volume/Å$^3$ | 6875.0(2) |
| Z | 12 |
| $\rho_{calc}$g/cm$^3$ | 1.809 |
| μ/mm$^{-1}$ | 13.379 |
| F(000) | 3672.0 |
| Crystal size/mm$^3$ | 0.18 × 0.12 × 0.09 |
| Radiation | Cu Kα (λ = 1.54184) |
| 2Θ range for data collection/° | 7.27 to 134.154 |
| Index ranges | -13 ≤ h ≤ 13, -31 ≤ k ≤ 48, -18 ≤ l ≤ 18 |
| Reflections collected | 28419 |
| Independent reflections | 12275 [$R_{int}$ = 0.0624, $R_{sigma}$ = 0.0818] |
| Data/restraints/parameters | 12275/6/829 |
| Goodness-of-fit on F$^2$ | 1.072 |
| Final R indexes [I>=2σ (I)] | $R_1$ = 0.0862, $wR_2$ = 0.2114 |
| Final R indexes [all data] | $R_1$ = 0.1224, $wR_2$ = 0.2428 |
| Largest diff. peak/hole / e Å$^{-3}$ | 5.16/-2.44 |

**Table 2 Fractional Atomic Coordinates (x10$^4$) and Equivalent Isotropic Displacement Parameters (Å$^2$x10$^3$) for akdk21004. $U_{eq}$ is defined as 1/3 of the trace of the orthogonalised $U_{IJ}$ tensor**

| Atom | *x* | *y* | *z* | U(eq) |
|---|---|---|---|---|
| C1 | 8165(13) | 5765(3) | 2646(10) | 46(4) |
| C2 | 8544(16) | 5494(4) | 3206(9) | 58(5) |
| C3 | 9448(15) | 5315(4) | 2744(11) | 56(4) |
| C4 | 9627(14) | 5491(4) | 1950(11) | 57(4) |
| C5 | 8843(13) | 5765(3) | 1881(11) | 48(4) |
| C6 | 7304(15) | 6022(4) | 2960(12) | 66(5) |
| C7 | 8128(16) | 5407(5) | 4103(11) | 72(5) |
| C8 | 10222(15) | 5043(4) | 3097(14) | 75(6) |
| C9 | 10589(14) | 5403(5) | 1301(14) | 88(7) |
| C10 | 8848(15) | 6017(4) | 1152(11) | 64(5) |
| C11 | 5673(14) | 4868(3) | 1692(11) | 54(4) |
| C12 | 5309(13) | 5197(4) | 1315(9) | 47(4) |
| C13 | 4187(13) | 5230(4) | 904(10) | 50(4) |
| C14 | 3934(16) | 5536(4) | 552(11) | 59(4) |
| C15 | 4694(13) | 5795(4) | 626(10) | 52(4) |
| C16 | 5771(14) | 5731(4) | 1066(11) | 60(4) |
| C17 | 7361(15) | 4277(4) | 2052(10) | 57(4) |
| C18 | 8386(16) | 4307(4) | 1526(12) | 63(5) |
| C19 | 8552(13) | 4073(3) | 876(10) | 49(4) |
| C20 | 7770(15) | 3820(4) | 718(11) | 57(4) |
| C21 | 6764(15) | 3784(4) | 1226(11) | 55(4) |
| C22 | 6564(13) | 4018(3) | 1889(10) | 48(4) |
| C23 | 7916(16) | 3585(4) | -36(12) | 65(5) |
| Cl1 | 8034(4) | 5060.9(11) | 507(3) | 61.7(10) |
| Ir1 | 7818.3(5) | 5318.7(2) | 1938.0(4) | 43.2(2) |
| N1 | 6725(11) | 4915(3) | 2278(8) | 48(3) |
| N2 | 6080(10) | 5443(3) | 1406(8) | 41(3) |
| O1 | 8099(10) | 4640(3) | 3372(7) | 56(3) |
| O2 | 5977(9) | 4470(2) | 3264(7) | 55(3) |
| S1 | 7030(4) | 4588.1(9) | 2833(3) | 50.5(9) |
| C24 | 2045(13) | 4149(3) | 2557(10) | 43(3) |
| C25 | 2203(13) | 3979(3) | 1723(9) | 43(3) |
| C26 | 1341(12) | 3713(3) | 1638(10) | 44(3) |
| C27 | 621(14) | 3731(4) | 2368(11) | 54(4) |
| C28 | 1024(14) | 3994(3) | 2953(10) | 49(4) |
| C29 | 2667(15) | 4448(4) | 2882(12) | 61(4) |
| C30 | 3127(15) | 4080(4) | 1088(11) | 63(5) |
| C31 | 1256(14) | 3483(4) | 885(10) | 59(4) |
| C32 | -477(13) | 3520(4) | 2559(11) | 57(4) |
| C33 | 418(14) | 4104(4) | 3788(11) | 59(4) |

| | | | | |
|---|---|---|---|---|
| C34 | 2261(15) | 3287(4) | 4536(10) | 55(4) |
| C35 | 3341(12) | 3510(4) | 4644(9) | 43(3) |
| C36 | 4018(14) | 3539(4) | 5409(10) | 52(4) |
| C37 | 4989(16) | 3749(4) | 5471(11) | 56(4) |
| C38 | 5207(13) | 3939(4) | 4742(12) | 56(4) |
| C39 | 4532(13) | 3902(4) | 3980(10) | 50(4) |
| C40 | 2342(13) | 2559(4) | 3658(11) | 48(4) |
| C41 | 3201(14) | 2440(4) | 3073(11) | 54(4) |
| C42 | 3928(15) | 2166(4) | 3323(12) | 59(4) |
| C43 | 3782(17) | 2026(4) | 4166(15) | 69(5) |
| C44 | 2982(15) | 2152(4) | 4722(13) | 63(5) |
| C45 | 2242(14) | 2410(4) | 4494(12) | 58(4) |
| C46 | 4606(17) | 1742(4) | 4389(14) | 81(6) |
| Cl2 | 4064(3) | 3347.9(9) | 2140(2) | 53.9(9) |
| Ir2 | 2437.9(6) | 3636.9(2) | 2813.9(4) | 42.8(2) |
| N3 | 2175(10) | 3216(3) | 3583(8) | 46(3) |
| N4 | 3579(11) | 3697(3) | 3941(8) | 42(3) |
| O3 | 1233(10) | 2879(2) | 2384(7) | 57(3) |
| O4 | 360(9) | 2847(3) | 3878(9) | 66(3) |
| S2 | 1400(3) | 2893.9(9) | 3336(3) | 52.5(9) |
| C47 | 8248(14) | 2660(3) | 7805(10) | 49(4) |
| C48 | 8063(13) | 2468(3) | 7036(11) | 49(4) |
| C49 | 9023(12) | 2553(3) | 6504(10) | 47(4) |
| C50 | 9806(14) | 2789(4) | 6933(10) | 48(4) |
| C51 | 9278(14) | 2866(4) | 7775(10) | 49(4) |
| C52 | 7444(14) | 2653(4) | 8588(11) | 58(4) |
| C53 | 7146(18) | 2205(4) | 6896(12) | 70(6) |
| C54 | 9295(16) | 2385(4) | 5640(11) | 60(4) |
| C55 | 10913(13) | 2935(4) | 6599(12) | 58(4) |
| C56 | 9826(14) | 3075(4) | 8504(11) | 55(4) |
| C57 | 8305(14) | 3389(4) | 5074(9) | 50(4) |
| C58 | 7193(13) | 3196(3) | 4914(9) | 39(3) |
| C59 | 6510(15) | 3204(4) | 4150(11) | 54(4) |
| C60 | 5486(14) | 3017(4) | 4039(12) | 55(4) |
| C61 | 5184(13) | 2816(4) | 4739(10) | 52(4) |
| C62 | 5875(13) | 2816(4) | 5497(10) | 50(4) |
| C63 | 8314(15) | 4058(4) | 6317(10) | 52(4) |
| C64 | 7497(16) | 4104(5) | 6982(12) | 69(5) |
| C65 | 6658(16) | 4353(4) | 6945(9) | 57(4) |
| C66 | 6536(15) | 4565(4) | 6231(12) | 59(4) |
| C67 | 7370(16) | 4524(4) | 5559(11) | 60(4) |
| C68 | 8250(14) | 4280(3) | 5616(9) | 47(4) |
| C69 | 5551(16) | 4816(4) | 6141(13) | 75(5) |
| Cl3 | 6454(3) | 3309.0(9) | 7363(3) | 54.4(9) |
| Ir3 | 8026.4(6) | 2992.0(2) | 6712.9(4) | 42.7(2) |

| | | | | |
|---|---|---|---|---|
| N5 | 8566(11) | 3411(3) | 6033(7) | 45(3) |
| N6 | 6904(9) | 2999(3) | 5574(8) | 40(3) |
| O5 | 9627(10) | 3676(2) | 7276(7) | 58(3) |
| O6 | 10215(8) | 3817(2) | 5746(7) | 49(2) |
| S3 | 9288(3) | 3727.2(9) | 6364(2) | 47.6(9) |

**Table 3 Anisotropic Displacement Parameters ($Å^2x10^3$) for akdk21004. The Anisotropic displacement factor exponent takes the form: $-2\pi^2[h^2a^{*2}U_{11}+2hka^*b^*U_{12}+\ldots]$.**

| Atom | $U_{11}$ | $U_{22}$ | $U_{33}$ | $U_{23}$ | $U_{13}$ | $U_{12}$ |
|---|---|---|---|---|---|---|
| C1 | 45(8) | 47(7) | 46(8) | -26(7) | 10(7) | -6(7) |
| C2 | 68(11) | 80(11) | 27(7) | -20(8) | 2(7) | -42(9) |
| C3 | 53(10) | 58(9) | 55(10) | -2(8) | -24(8) | -6(8) |
| C4 | 43(9) | 67(10) | 61(11) | -15(8) | -4(8) | 10(8) |
| C5 | 37(8) | 38(7) | 67(10) | -8(7) | -1(7) | -9(7) |
| C6 | 57(11) | 70(10) | 71(12) | -24(9) | -13(9) | 10(9) |
| C7 | 67(12) | 102(13) | 46(10) | -8(10) | -7(9) | -8(11) |
| C8 | 47(10) | 65(10) | 111(17) | -13(11) | -29(11) | 4(9) |
| C9 | 31(8) | 132(17) | 102(16) | -56(14) | 18(9) | -12(10) |
| C10 | 57(10) | 76(11) | 58(11) | 1(9) | 4(8) | -24(9) |
| C11 | 44(9) | 50(8) | 69(11) | -5(8) | 1(8) | -9(7) |
| C12 | 42(8) | 61(9) | 37(8) | -7(7) | -7(6) | -5(8) |
| C13 | 30(7) | 59(9) | 60(10) | -10(8) | -4(7) | -1(7) |
| C14 | 57(10) | 68(10) | 52(10) | -8(8) | -1(8) | 15(9) |
| C15 | 42(8) | 60(9) | 52(9) | 12(8) | -5(7) | -4(8) |
| C16 | 43(9) | 80(11) | 56(10) | 11(9) | -1(8) | -6(9) |
| C17 | 60(10) | 78(11) | 31(8) | 5(8) | -1(7) | 10(9) |
| C18 | 56(10) | 53(9) | 81(13) | 16(9) | 2(9) | 13(9) |
| C19 | 42(8) | 51(8) | 53(9) | 0(7) | 5(7) | 7(7) |
| C20 | 51(9) | 70(10) | 52(10) | -2(8) | 13(8) | 11(9) |
| C21 | 51(9) | 45(8) | 67(11) | 1(8) | -4(8) | 8(8) |
| C22 | 38(8) | 52(8) | 51(9) | -2(7) | -19(7) | 0(7) |
| C23 | 54(10) | 79(11) | 63(11) | -9(9) | 5(9) | 14(9) |
| Cl1 | 55(2) | 82(3) | 49(2) | -16(2) | 7.1(18) | -1(2) |
| Ir1 | 37.1(3) | 50.5(4) | 41.8(4) | -3.4(3) | -0.1(3) | -3.1(3) |
| N1 | 39(7) | 44(6) | 59(8) | -1(6) | -17(6) | 0(6) |
| N2 | 33(6) | 44(6) | 45(7) | 4(5) | 2(5) | -8(5) |
| O1 | 53(7) | 69(6) | 46(6) | 8(5) | -1(5) | -2(6) |
| O2 | 51(6) | 57(6) | 60(7) | 2(5) | 23(5) | -6(5) |
| S1 | 44(2) | 56(2) | 52(2) | -3.1(18) | 6.3(17) | -1.7(18) |
| C24 | 39(8) | 42(7) | 50(9) | 11(6) | 16(7) | 10(7) |
| C25 | 38(7) | 58(8) | 31(7) | 7(6) | -9(6) | 5(7) |
| C26 | 23(6) | 53(8) | 54(9) | 3(7) | -12(6) | 2(6) |
| C27 | 37(8) | 58(9) | 67(11) | 27(8) | -1(8) | 2(8) |
| C28 | 56(10) | 46(7) | 45(9) | 1(7) | -14(7) | 18(7) |
| C29 | 50(10) | 61(9) | 72(12) | 10(8) | -6(9) | 6(8) |

| | | | | | | |
|---|---|---|---|---|---|---|
| C30 | 64(11) | 67(10) | 58(11) | 17(8) | 17(9) | 13(9) |
| C31 | 50(9) | 80(11) | 45(9) | -1(8) | -10(7) | 13(9) |
| C32 | 34(8) | 70(10) | 68(11) | 4(9) | 2(7) | -17(8) |
| C33 | 48(9) | 64(9) | 65(11) | 9(8) | 3(8) | 16(8) |
| C34 | 55(10) | 57(9) | 53(10) | 8(7) | 7(8) | -11(8) |
| C35 | 33(7) | 57(8) | 39(8) | -4(7) | 2(6) | 0(7) |
| C36 | 52(9) | 72(10) | 34(8) | -5(7) | 6(7) | 19(9) |
| C37 | 64(11) | 52(8) | 51(10) | -13(8) | -1(8) | 12(8) |
| C38 | 34(8) | 53(8) | 80(12) | -11(8) | -14(8) | 6(7) |
| C39 | 43(8) | 59(9) | 47(9) | -6(7) | 8(7) | 1(8) |
| C40 | 33(7) | 60(9) | 52(9) | -9(7) | 3(7) | -12(7) |
| C41 | 47(9) | 55(9) | 58(10) | 0(8) | -17(8) | 0(8) |
| C42 | 46(9) | 52(8) | 80(13) | -2(9) | 13(9) | 1(8) |
| C43 | 53(11) | 55(9) | 99(16) | 16(9) | -3(11) | 11(8) |
| C44 | 48(10) | 67(10) | 75(12) | 1(9) | 20(9) | -10(9) |
| C45 | 35(8) | 59(9) | 81(13) | 16(9) | -3(8) | -1(8) |
| C46 | 66(12) | 72(11) | 106(17) | 10(11) | 20(12) | 19(10) |
| Cl2 | 51(2) | 64(2) | 46(2) | 1.4(17) | 5.6(17) | 8.2(19) |
| Ir2 | 36.9(3) | 48.3(4) | 43.2(4) | 2.0(3) | 0.2(3) | -0.2(3) |
| N3 | 40(7) | 58(7) | 41(7) | 15(6) | 1(5) | 3(6) |
| N4 | 38(6) | 43(6) | 45(7) | 1(5) | 4(5) | 0(5) |
| O3 | 50(6) | 61(6) | 61(7) | -4(5) | -10(5) | -2(5) |
| O4 | 31(5) | 68(7) | 99(10) | 19(7) | 3(6) | -5(5) |
| S2 | 37.7(19) | 53(2) | 66(3) | 0.6(19) | -0.9(18) | -3.8(18) |
| C47 | 56(9) | 40(7) | 50(9) | 17(7) | -8(7) | -4(7) |
| C48 | 32(7) | 46(7) | 72(11) | 6(7) | 18(7) | -4(7) |
| C49 | 31(7) | 52(8) | 58(9) | 9(7) | 2(7) | 24(7) |
| C50 | 51(9) | 53(8) | 41(8) | -1(7) | -9(7) | 2(8) |
| C51 | 40(8) | 67(9) | 41(8) | 9(7) | -1(7) | -1(8) |
| C52 | 45(9) | 69(10) | 58(10) | 10(8) | -8(8) | 5(8) |
| C53 | 97(15) | 50(9) | 62(11) | 4(8) | -26(11) | -21(10) |
| C54 | 68(11) | 57(9) | 52(10) | -1(8) | -17(9) | 17(9) |
| C55 | 38(8) | 64(9) | 73(12) | 7(8) | 14(8) | -7(8) |
| C56 | 47(9) | 66(9) | 53(10) | -4(8) | -5(8) | -4(8) |
| C57 | 55(9) | 62(9) | 31(7) | 7(7) | -7(7) | -2(8) |
| C58 | 44(8) | 35(6) | 39(8) | -5(6) | 3(6) | -5(6) |
| C59 | 62(11) | 53(8) | 49(9) | -14(7) | 2(8) | 0(8) |
| C60 | 46(9) | 56(9) | 62(11) | -6(8) | -7(8) | 19(8) |
| C61 | 35(8) | 68(10) | 53(9) | -14(8) | -3(7) | -2(8) |
| C62 | 41(8) | 59(9) | 48(9) | 3(7) | 0(7) | 4(8) |
| C63 | 55(9) | 63(9) | 38(8) | -6(7) | -13(7) | -19(8) |
| C64 | 64(12) | 89(13) | 53(11) | -15(10) | -16(9) | 9(10) |
| C65 | 69(11) | 77(10) | 25(7) | -5(7) | -4(7) | 0(9) |
| C66 | 50(10) | 60(9) | 65(11) | -18(8) | -8(8) | 8(8) |
| C67 | 69(12) | 61(9) | 48(10) | 9(8) | -6(8) | 8(9) |
| C68 | 51(9) | 56(8) | 35(8) | -1(7) | -1(7) | 11(8) |
| C69 | 68(12) | 81(12) | 75(13) | -13(10) | -9(10) | 15(10) |
| Cl3 | 50(2) | 62(2) | 51(2) | 1.8(17) | 7.5(17) | 6.2(18) |
| Ir3 | 39.5(4) | 48.1(4) | 40.2(4) | 1.9(3) | -2.2(3) | 0.2(3) |

| | | | | | |
|---|---|---|---|---|---|
| N5 | 50(7) | 60(7) | 24(6) | 9(5) | -4(5) | -4(6) |
| N6 | 19(5) | 54(6) | 46(6) | 1(5) | -8(4) | 3(5) |
| O5 | 66(7) | 61(6) | 47(6) | 4(5) | -15(5) | -14(6) |
| O6 | 35(5) | 58(6) | 53(6) | 6(5) | 3(5) | -8(5) |
| S3 | 44(2) | 53.9(19) | 45(2) | 2.3(16) | 1.0(16) | -7.4(17) |

**Table 4 Bond Lengths for akdk21004.**

| Atom | Atom | Length/Å | Atom | Atom | Length/Å |
|---|---|---|---|---|---|
| C1 | C2 | 1.44(2) | C36 | C37 | 1.38(2) |
| C1 | C5 | 1.41(2) | C37 | C38 | 1.38(2) |
| C1 | C6 | 1.51(2) | C38 | C39 | 1.37(2) |
| C1 | Ir1 | 2.131(12) | C39 | N4 | 1.351(18) |
| C2 | C3 | 1.45(2) | C40 | C41 | 1.42(2) |
| C2 | C7 | 1.50(2) | C40 | C45 | 1.42(2) |
| C2 | Ir1 | 2.184(13) | C40 | S2 | 1.773(16) |
| C3 | C4 | 1.42(2) | C41 | C42 | 1.42(2) |
| C3 | C8 | 1.49(2) | C42 | C43 | 1.42(3) |
| C3 | Ir1 | 2.157(15) | C43 | C44 | 1.35(3) |
| C4 | C5 | 1.41(2) | C43 | C46 | 1.50(2) |
| C4 | C9 | 1.53(2) | C44 | C45 | 1.37(2) |
| C4 | Ir1 | 2.137(17) | Cl2 | Ir2 | 2.421(4) |
| C5 | C10 | 1.51(2) | Ir2 | N3 | 2.092(11) |
| C5 | Ir1 | 2.139(13) | Ir2 | N4 | 2.114(12) |
| C11 | C12 | 1.50(2) | N3 | S2 | 1.601(12) |
| C11 | N1 | 1.461(17) | O3 | S2 | 1.456(11) |
| C12 | C13 | 1.386(18) | O4 | S2 | 1.463(12) |
| C12 | N2 | 1.318(17) | C47 | C48 | 1.41(2) |
| C13 | C14 | 1.37(2) | C47 | C51 | 1.42(2) |
| C14 | C15 | 1.35(2) | C47 | C52 | 1.52(2) |
| C15 | C16 | 1.38(2) | C47 | Ir3 | 2.143(13) |
| C16 | N2 | 1.316(18) | C48 | C49 | 1.41(2) |
| C17 | C18 | 1.43(2) | C48 | C53 | 1.49(2) |
| C17 | C22 | 1.39(2) | C48 | Ir3 | 2.175(14) |
| C17 | S1 | 1.778(17) | C49 | C50 | 1.44(2) |
| C18 | C19 | 1.39(2) | C49 | C54 | 1.52(2) |
| C19 | C20 | 1.36(2) | C49 | Ir3 | 2.124(13) |
| C20 | C21 | 1.40(2) | C50 | C51 | 1.46(2) |
| C20 | C23 | 1.51(2) | C50 | C55 | 1.48(2) |
| C21 | C22 | 1.41(2) | C50 | Ir3 | 2.165(15) |
| Cl1 | Ir1 | 2.436(4) | C51 | C56 | 1.51(2) |
| Ir1 | N1 | 2.116(12) | C51 | Ir3 | 2.159(14) |
| Ir1 | N2 | 2.136(11) | C57 | C58 | 1.479(19) |

| | | | | | |
|---|---|---|---|---|---|
| N1 | S1 | 1.597(12) | C57 | N5 | 1.482(16) |
| O1 | S1 | 1.439(10) | C58 | C59 | 1.368(19) |
| O2 | S1 | 1.450(10) | C58 | N6 | 1.329(17) |
| C24 | C25 | 1.46(2) | C59 | C60 | 1.38(2) |
| C24 | C28 | 1.45(2) | C60 | C61 | 1.39(2) |
| C24 | C29 | 1.47(2) | C61 | C62 | 1.37(2) |
| C24 | Ir2 | 2.150(13) | C62 | N6 | 1.369(18) |
| C25 | C26 | 1.448(19) | C63 | C64 | 1.40(2) |
| C25 | C30 | 1.50(2) | C63 | C68 | 1.39(2) |
| C25 | Ir2 | 2.170(13) | C63 | S3 | 1.724(17) |
| C26 | C27 | 1.40(2) | C64 | C65 | 1.38(2) |
| C26 | C31 | 1.48(2) | C65 | C66 | 1.39(2) |
| C26 | Ir2 | 2.153(14) | C66 | C67 | 1.42(2) |
| C27 | C28 | 1.45(2) | C66 | C69 | 1.50(2) |
| C27 | C32 | 1.53(2) | C67 | C68 | 1.39(2) |
| C27 | Ir2 | 2.150(15) | Cl3 | Ir3 | 2.417(4) |
| C28 | C33 | 1.53(2) | Ir3 | N5 | 2.087(11) |
| C28 | Ir2 | 2.157(14) | Ir3 | N6 | 2.103(11) |
| C34 | C35 | 1.510(19) | N5 | S3 | 1.583(12) |
| C34 | N3 | 1.479(19) | O5 | S3 | 1.441(11) |
| C35 | C36 | 1.370(19) | O6 | S3 | 1.471(10) |
| C35 | N4 | 1.344(18) | | | |

**Table 5 Bond Angles for akdk21004.**

| Atom | Atom | Atom | Angle/° | Atom | Atom | Atom | Angle/° |
|---|---|---|---|---|---|---|---|
| C2 | C1 | C6 | 121.0(15) | C44 | C43 | C42 | 121.1(16) |
| C2 | C1 | Ir1 | 72.5(7) | C44 | C43 | C46 | 124.1(19) |
| C5 | C1 | C2 | 109.4(13) | C43 | C44 | C45 | 122.4(18) |
| C5 | C1 | C6 | 129.0(15) | C44 | C45 | C40 | 119.0(17) |
| C5 | C1 | Ir1 | 71.0(7) | C24 | Ir2 | C25 | 39.5(5) |
| C6 | C1 | Ir1 | 129.7(11) | C24 | Ir2 | C26 | 66.8(6) |
| C1 | C2 | C3 | 106.7(13) | C24 | Ir2 | C28 | 39.4(5) |
| C1 | C2 | C7 | 128.4(16) | C24 | Ir2 | Cl2 | 122.6(4) |
| C1 | C2 | Ir1 | 68.5(8) | C25 | Ir2 | Cl2 | 93.1(4) |
| C3 | C2 | C7 | 124.8(17) | C26 | Ir2 | C25 | 39.1(5) |
| C3 | C2 | Ir1 | 69.6(8) | C26 | Ir2 | C28 | 65.8(5) |
| C7 | C2 | Ir1 | 127.6(11) | C26 | Ir2 | Cl2 | 97.4(4) |
| C2 | C3 | C8 | 127.0(17) | C27 | Ir2 | C24 | 65.7(6) |
| C2 | C3 | Ir1 | 71.5(9) | C27 | Ir2 | C25 | 63.9(5) |
| C4 | C3 | C2 | 106.6(14) | C27 | Ir2 | C26 | 37.9(6) |
| C4 | C3 | C8 | 125.4(17) | C27 | Ir2 | C28 | 39.4(6) |
| C4 | C3 | Ir1 | 69.9(9) | C27 | Ir2 | Cl2 | 131.8(5) |
| C8 | C3 | Ir1 | 132.5(11) | C28 | Ir2 | C25 | 65.2(6) |

| | | | | | | | |
|---|---|---|---|---|---|---|---|
| C3 | C4 | C9 | 123.9(16) | C28 | Ir2 | Cl2 | 158.3(4) |
| C3 | C4 | Ir1 | 71.4(10) | N3 | Ir2 | C24 | 148.6(5) |
| C5 | C4 | C3 | 110.4(15) | N3 | Ir2 | C25 | 158.6(5) |
| C5 | C4 | C9 | 125.7(17) | N3 | Ir2 | C26 | 119.6(5) |
| C5 | C4 | Ir1 | 70.8(9) | N3 | Ir2 | C27 | 99.8(5) |
| C9 | C4 | Ir1 | 127.3(11) | N3 | Ir2 | C28 | 111.8(5) |
| C1 | C5 | C10 | 128.5(14) | N3 | Ir2 | Cl2 | 88.2(3) |
| C1 | C5 | Ir1 | 70.4(8) | N3 | Ir2 | N4 | 74.4(4) |
| C4 | C5 | C1 | 106.8(14) | N4 | Ir2 | C24 | 98.7(5) |
| C4 | C5 | C10 | 124.4(16) | N4 | Ir2 | C25 | 126.9(5) |
| C4 | C5 | Ir1 | 70.6(9) | N4 | Ir2 | C26 | 165.1(5) |
| C10 | C5 | Ir1 | 128.2(11) | N4 | Ir2 | C27 | 140.4(6) |
| N1 | C11 | C12 | 108.6(11) | N4 | Ir2 | C28 | 105.4(5) |
| C13 | C12 | C11 | 119.0(13) | N4 | Ir2 | Cl2 | 87.7(3) |
| N2 | C12 | C11 | 117.5(13) | C34 | N3 | Ir2 | 112.7(9) |
| N2 | C12 | C13 | 123.5(14) | C34 | N3 | S2 | 113.7(9) |
| C14 | C13 | C12 | 115.5(15) | S2 | N3 | Ir2 | 128.0(7) |
| C15 | C14 | C13 | 123.2(16) | C35 | N4 | C39 | 119.4(13) |
| C14 | C15 | C16 | 115.3(15) | C35 | N4 | Ir2 | 116.8(9) |
| N2 | C16 | C15 | 124.7(16) | C39 | N4 | Ir2 | 123.8(10) |
| C18 | C17 | S1 | 120.5(14) | N3 | S2 | C40 | 104.3(7) |
| C22 | C17 | C18 | 119.0(16) | O3 | S2 | C40 | 107.2(7) |
| C22 | C17 | S1 | 120.3(13) | O3 | S2 | N3 | 108.4(6) |
| C19 | C18 | C17 | 118.3(16) | O3 | S2 | O4 | 118.8(7) |
| C20 | C19 | C18 | 122.5(16) | O4 | S2 | C40 | 102.7(7) |
| C19 | C20 | C21 | 120.5(15) | O4 | S2 | N3 | 114.0(7) |
| C19 | C20 | C23 | 121.6(15) | C48 | C47 | C51 | 112.9(14) |
| C21 | C20 | C23 | 117.9(15) | C48 | C47 | C52 | 124.5(14) |
| C20 | C21 | C22 | 118.6(15) | C48 | C47 | Ir3 | 72.1(9) |
| C17 | C22 | C21 | 121.1(16) | C51 | C47 | C52 | 122.7(14) |
| C1 | Ir1 | C2 | 39.0(6) | C51 | C47 | Ir3 | 71.3(8) |
| C1 | Ir1 | C3 | 65.4(6) | C52 | C47 | Ir3 | 124.5(11) |
| C1 | Ir1 | C4 | 64.2(6) | C47 | C48 | C53 | 126.2(15) |
| C1 | Ir1 | C5 | 38.7(6) | C47 | C48 | Ir3 | 69.7(8) |
| C1 | Ir1 | Cl1 | 142.5(4) | C49 | C48 | C47 | 104.5(13) |
| C1 | Ir1 | N2 | 98.0(5) | C49 | C48 | C53 | 128.8(16) |
| C2 | Ir1 | Cl1 | 152.1(5) | C49 | C48 | Ir3 | 68.9(8) |
| C3 | Ir1 | C2 | 38.9(6) | C53 | C48 | Ir3 | 131.2(12) |
| C3 | Ir1 | Cl1 | 113.4(5) | C48 | C49 | C50 | 111.3(14) |
| C4 | Ir1 | C2 | 64.3(6) | C48 | C49 | C54 | 124.6(15) |
| C4 | Ir1 | C3 | 38.7(6) | C48 | C49 | Ir3 | 72.8(8) |
| C4 | Ir1 | C5 | 38.6(6) | C50 | C49 | C54 | 123.5(14) |
| C4 | Ir1 | Cl1 | 91.2(5) | C50 | C49 | Ir3 | 72.0(8) |
| C5 | Ir1 | C2 | 65.2(6) | C54 | C49 | Ir3 | 128.7(10) |
| C5 | Ir1 | C3 | 65.6(6) | C49 | C50 | C51 | 106.3(14) |

| | | | | | | | |
|---|---|---|---|---|---|---|---|
| C5 | Ir1 | Cl1 | 104.7(5) | C49 | C50 | C55 | 127.7(15) |
| N1 | Ir1 | C1 | 128.8(5) | C49 | C50 | Ir3 | 68.9(8) |
| N1 | Ir1 | C2 | 103.5(5) | C51 | C50 | C55 | 126.0(14) |
| N1 | Ir1 | C3 | 109.8(5) | C51 | C50 | Ir3 | 70.0(9) |
| N1 | Ir1 | C4 | 143.5(5) | C55 | C50 | Ir3 | 124.8(11) |
| N1 | Ir1 | C5 | 167.3(6) | C47 | C51 | C50 | 104.9(14) |
| N1 | Ir1 | Cl1 | 88.0(4) | C47 | C51 | C56 | 127.7(15) |
| N1 | Ir1 | N2 | 75.5(4) | C47 | C51 | Ir3 | 70.1(8) |
| N2 | Ir1 | C2 | 124.1(6) | C50 | C51 | C56 | 126.7(14) |
| N2 | Ir1 | C3 | 162.4(5) | C50 | C51 | Ir3 | 70.4(8) |
| N2 | Ir1 | C4 | 140.6(5) | C56 | C51 | Ir3 | 130.9(11) |
| N2 | Ir1 | C5 | 105.5(5) | C58 | C57 | N5 | 109.1(12) |
| N2 | Ir1 | Cl1 | 83.1(3) | C59 | C58 | C57 | 124.3(13) |
| C11 | N1 | Ir1 | 114.1(9) | N6 | C58 | C57 | 114.7(12) |
| C11 | N1 | S1 | 111.6(9) | N6 | C58 | C59 | 121.0(13) |
| S1 | N1 | Ir1 | 130.8(7) | C58 | C59 | C60 | 121.6(16) |
| C12 | N2 | Ir1 | 116.4(9) | C59 | C60 | C61 | 116.9(15) |
| C16 | N2 | C12 | 117.7(13) | C62 | C61 | C60 | 120.2(15) |
| C16 | N2 | Ir1 | 125.3(10) | C61 | C62 | N6 | 121.2(15) |
| N1 | S1 | C17 | 106.0(7) | C64 | C63 | S3 | 120.0(13) |
| O1 | S1 | C17 | 107.2(7) | C68 | C63 | C64 | 116.8(16) |
| O1 | S1 | N1 | 109.7(6) | C68 | C63 | S3 | 123.1(13) |
| O1 | S1 | O2 | 117.3(7) | C65 | C64 | C63 | 121.9(18) |
| O2 | S1 | C17 | 105.2(7) | C64 | C65 | C66 | 122.1(17) |
| O2 | S1 | N1 | 110.5(7) | C65 | C66 | C67 | 116.6(15) |
| C25 | C24 | C29 | 127.5(13) | C65 | C66 | C69 | 122.7(17) |
| C25 | C24 | Ir2 | 71.0(7) | C67 | C66 | C69 | 120.7(17) |
| C28 | C24 | C25 | 106.3(13) | C68 | C67 | C66 | 121.1(15) |
| C28 | C24 | C29 | 125.6(14) | C67 | C68 | C63 | 121.4(15) |
| C28 | C24 | Ir2 | 70.6(7) | C47 | Ir3 | C48 | 38.2(6) |
| C29 | C24 | Ir2 | 129.7(11) | C47 | Ir3 | C50 | 64.2(6) |
| C24 | C25 | C30 | 122.8(13) | C47 | Ir3 | C51 | 38.6(6) |
| C24 | C25 | Ir2 | 69.5(7) | C47 | Ir3 | Cl3 | 94.5(5) |
| C26 | C25 | C24 | 109.1(13) | C48 | Ir3 | Cl3 | 115.6(4) |
| C26 | C25 | C30 | 128.2(14) | C49 | Ir3 | C47 | 63.1(6) |
| C26 | C25 | Ir2 | 69.8(8) | C49 | Ir3 | C48 | 38.3(5) |
| C30 | C25 | Ir2 | 127.0(10) | C49 | Ir3 | C50 | 39.1(5) |
| C25 | C26 | C31 | 124.1(14) | C49 | Ir3 | C51 | 65.6(6) |
| C25 | C26 | Ir2 | 71.0(7) | C49 | Ir3 | Cl3 | 153.8(4) |
| C27 | C26 | C25 | 106.9(13) | C50 | Ir3 | C48 | 65.6(5) |
| C27 | C26 | C31 | 129.0(14) | C50 | Ir3 | Cl3 | 144.6(4) |
| C27 | C26 | Ir2 | 70.9(9) | C51 | Ir3 | C48 | 66.1(6) |
| C31 | C26 | Ir2 | 125.1(10) | C51 | Ir3 | C50 | 39.6(6) |
| C26 | C27 | C28 | 110.6(14) | C51 | Ir3 | Cl3 | 106.2(4) |
| C26 | C27 | C32 | 127.6(15) | N5 | Ir3 | C47 | 150.0(5) |

| | | | | | | | |
|---|---|---|---|---|---|---|---|
| C26 | C27 | Ir2 | 71.2(8) | N5 | Ir3 | C48 | 154.2(5) |
| C28 | C27 | C32 | 121.7(16) | N5 | Ir3 | C49 | 116.2(5) |
| C28 | C27 | Ir2 | 70.6(8) | N5 | Ir3 | C50 | 95.9(5) |
| C32 | C27 | Ir2 | 126.6(10) | N5 | Ir3 | C51 | 111.8(5) |
| C24 | C28 | C33 | 126.9(13) | N5 | Ir3 | Cl3 | 90.0(3) |
| C24 | C28 | Ir2 | 70.0(8) | N5 | Ir3 | N6 | 75.7(4) |
| C27 | C28 | C24 | 107.0(14) | N6 | Ir3 | C47 | 134.2(5) |
| C27 | C28 | C33 | 126.0(15) | N6 | Ir3 | C48 | 101.9(5) |
| C27 | C28 | Ir2 | 70.1(8) | N6 | Ir3 | C49 | 100.8(5) |
| C33 | C28 | Ir2 | 128.7(10) | N6 | Ir3 | C50 | 130.5(5) |
| N3 | C34 | C35 | 104.1(12) | N6 | Ir3 | C51 | 166.2(5) |
| C36 | C35 | C34 | 123.8(14) | N6 | Ir3 | Cl3 | 84.8(3) |
| N4 | C35 | C34 | 115.5(13) | C57 | N5 | Ir3 | 112.9(9) |
| N4 | C35 | C36 | 120.7(14) | C57 | N5 | S3 | 116.3(9) |
| C35 | C36 | C37 | 121.2(15) | S3 | N5 | Ir3 | 130.6(6) |
| C38 | C37 | C36 | 116.9(15) | C58 | N6 | C62 | 119.1(12) |
| C39 | C38 | C37 | 120.9(15) | C58 | N6 | Ir3 | 118.5(9) |
| N4 | C39 | C38 | 120.8(15) | C62 | N6 | Ir3 | 122.4(10) |
| C41 | C40 | S2 | 119.5(12) | N5 | S3 | C63 | 107.4(7) |
| C45 | C40 | C41 | 120.0(15) | O5 | S3 | C63 | 107.1(7) |
| C45 | C40 | S2 | 120.5(12) | O5 | S3 | N5 | 107.7(6) |
| C40 | C41 | C42 | 119.4(16) | O5 | S3 | O6 | 119.1(7) |
| C43 | C42 | C41 | 118.0(16) | O6 | S3 | C63 | 103.9(7) |
| C42 | C43 | C46 | 114.7(18) | O6 | S3 | N5 | 111.0(6) |

**Table 6 Torsion Angles for akdk21004**

| A | B | C | D | Angle/° | A | B | C | D | Angle/° |
|---|---|---|---|---|---|---|---|---|---|
| C1 | C2 | C3 | C4 | 2.8(16) | C36 | C35 | N4 | C39 | 3(2) |
| C1 | C2 | C3 | C8 | 171.5(14) | C36 | C35 | N4 | Ir2 | −178.4(11) |
| C1 | C2 | C3 | Ir1 | -58.7(10) | C36 | C37 | C38 | C39 | -4(2) |
| C2 | C1 | C5 | C4 | 1.1(16) | C37 | C38 | C39 | N4 | 5(2) |
| C2 | C1 | C5 | C10 | −173.6(14) | C38 | C39 | N4 | C35 | -4(2) |
| C2 | C1 | C5 | Ir1 | 62.7(10) | C38 | C39 | N4 | Ir2 | 177.4(11) |
| C2 | C3 | C4 | C5 | -2.2(18) | C40 | C41 | C42 | C43 | -2(2) |
| C2 | C3 | C4 | C9 | 174.5(15) | C41 | C40 | C45 | C44 | 0(2) |
| C2 | C3 | C4 | Ir1 | -62.5(10) | C41 | C40 | S2 | N3 | -85.2(13) |
| C3 | C4 | C5 | C1 | 0.7(18) | C41 | C40 | S2 | O3 | 29.7(13) |
| C3 | C4 | C5 | C10 | 175.7(14) | C41 | C40 | S2 | O4 | 155.6(12) |
| C3 | C4 | C5 | Ir1 | -60.7(12) | C41 | C42 | C43 | C44 | -1(3) |
| C5 | C1 | C2 | C3 | -2.4(16) | C41 | C42 | C43 | C46 | −178.5(15) |
| C5 | C1 | C2 | C7 | 176.5(14) | C42 | C43 | C44 | C45 | 3(3) |

| | | | | | | | | | | | |
|---|---|---|---|---|---|---|---|---|---|---|---|
| C5 | C1 | C2 | Ir1 | -61.8(10) | | C43 | C44 | C45 | C40 | -2(3) | |
| C6 | C1 | C2 | C3 | 174.4(13) | | C45 | C40 | C41 | C42 | 2(2) | |
| C6 | C1 | C2 | C7 | 5(2) | | C45 | C40 | S2 | N3 | 94.9(13) | |
| C6 | C1 | C2 | Ir1 | 126.3(14) | | C45 | C40 | S2 | O3 | 150.3(12) | |
| C6 | C1 | C5 | C4 | 172.2(15) | | C45 | C40 | S2 | O4 | -24.3(14) | |
| C6 | C1 | C5 | C10 | -3(3) | | C46 | C43 | C44 | C45 | 179.6(17) | |
| C6 | C1 | C5 | Ir1 | 126.2(16) | | Ir2 | C24 | C25 | C26 | 58.8(9) | |
| C7 | C2 | C3 | C4 | 176.3(14) | | Ir2 | C24 | C25 | C30 | 121.6(13) | |
| C7 | C2 | C3 | C8 | -8(2) | | Ir2 | C24 | C28 | C27 | -60.6(10) | |
| C7 | C2 | C3 | Ir1 | 122.3(15) | | Ir2 | C24 | C28 | C33 | 124.0(14) | |
| C8 | C3 | C4 | C5 | 171.1(14) | | Ir2 | C25 | C26 | C27 | 62.2(10) | |
| C8 | C3 | C4 | C9 | 6(3) | | Ir2 | C25 | C26 | C31 | 120.1(13) | |
| C8 | C3 | C4 | Ir1 | 128.5(15) | | Ir2 | C26 | C27 | C28 | 59.8(10) | |
| C9 | C4 | C5 | C1 | 175.9(15) | | Ir2 | C26 | C27 | C32 | 122.2(15) | |
| C9 | C4 | C5 | C10 | -1(3) | | Ir2 | C27 | C28 | C24 | 60.6(10) | |
| C9 | C4 | C5 | Ir1 | 122.7(16) | | Ir2 | C27 | C28 | C33 | 123.9(14) | |
| C11 | C12 | C13 | C14 | 178.0(15) | | Ir2 | N3 | S2 | C40 | 134.0(9) | |
| C11 | C12 | N2 | C16 | 179.1(14) | | Ir2 | N3 | S2 | O3 | 20.0(11) | |
| C11 | C12 | N2 | Ir1 | 7.4(18) | | Ir2 | N3 | S2 | O4 | -114.8(9) | |
| C11 | N1 | S1 | C17 | 62.1(13) | | N3 | C34 | C35 | C36 | 154.7(14) | |
| C11 | N1 | S1 | O1 | 177.6(11) | | N3 | C34 | C35 | N4 | 28.4(17) | |
| C11 | N1 | S1 | O2 | -51.5(13) | | N4 | C35 | C36 | C37 | -3(2) | |
| C12 | C11 | N1 | Ir1 | -28.7(16) | | S2 | C40 | C41 | C42 | 178.1(12) | |
| C12 | C11 | N1 | S1 | 170.0(11) | | S2 | C40 | C45 | C44 | 180.0(12) | |
| C12 | C13 | C14 | C15 | -3(2) | | C47 | C48 | C49 | C50 | 1.0(16) | |
| C13 | C12 | N2 | C16 | -2(2) | | C47 | C48 | C49 | C54 | 173.4(13) | |
| C13 | C12 | N2 | Ir1 | 173.6(12) | | C47 | C48 | C49 | Ir3 | -61.0(10) | |
| C13 | C14 | C15 | C16 | 2(3) | | C48 | C47 | C51 | C50 | -2.0(17) | |
| C14 | C15 | C16 | N2 | 0(3) | | C48 | C47 | C51 | C56 | 172.8(15) | |
| C15 | C16 | N2 | C12 | 1(3) | | C48 | C47 | C51 | Ir3 | 60.3(11) | |
| C15 | C16 | N2 | Ir1 | 171.4(13) | | C48 | C49 | C50 | C51 | -2.2(17) | |
| C17 | C18 | C19 | C20 | 1(2) | | C48 | C49 | C50 | C55 | 179.1(15) | |
| C18 | C17 | C22 | C21 | 1(2) | | C48 | C49 | C50 | Ir3 | -62.5(10) | |
| C18 | C17 | S1 | N1 | 65.3(15) | | C49 | C50 | C51 | C47 | 2.4(16) | |
| C18 | C17 | S1 | O1 | -51.9(15) | | C49 | C50 | C51 | C56 | 173.4(14) | |

| | | | | | | | | | |
|---|---|---|---|---|---|---|---|---|---|
| C18 | C17 | S1 | O2 | −177.6(13) | C49 | C50 | C51 | Ir3 | -59.6(10) |
| C18 | C19 | C20 | C21 | -1(3) | C51 | C47 | C48 | C49 | 0.7(17) |
| C18 | C19 | C20 | C23 | 175.1(15) | C51 | C47 | C48 | C53 | 173.4(15) |
| C19 | C20 | C21 | C22 | 1(2) | C51 | C47 | C48 | Ir3 | -59.9(11) |
| C20 | C21 | C22 | C17 | -1(2) | C52 | C47 | C48 | C49 | −179.4(13) |
| C22 | C17 | C18 | C19 | -1(2) | C52 | C47 | C48 | C53 | -7(2) |
| C22 | C17 | S1 | N1 | −108.8(13) | C52 | C47 | C48 | Ir3 | 120.1(14) |
| C22 | C17 | S1 | O1 | 134.0(12) | C52 | C47 | C51 | C50 | 178.1(13) |
| C22 | C17 | S1 | O2 | 8.4(14) | C52 | C47 | C51 | C56 | 7(2) |
| C23 | C20 | C21 | C22 | −175.1(14) | C52 | C47 | C51 | Ir3 | −119.6(14) |
| Ir1 | C1 | C2 | C3 | 59.3(10) | C53 | C48 | C49 | C50 | −171.4(15) |
| Ir1 | C1 | C2 | C7 | −121.7(16) | C53 | C48 | C49 | C54 | 1(3) |
| Ir1 | C1 | C5 | C4 | -61.6(10) | C53 | C48 | C49 | Ir3 | 126.5(17) |
| Ir1 | C1 | C5 | C10 | 123.7(15) | C54 | C49 | C50 | C51 | −174.7(13) |
| Ir1 | C2 | C3 | C4 | 61.4(10) | C54 | C49 | C50 | C55 | 7(2) |
| Ir1 | C2 | C3 | C8 | −129.9(16) | C54 | C49 | C50 | Ir3 | 125.0(14) |
| Ir1 | C3 | C4 | C5 | 60.4(11) | C55 | C50 | C51 | C47 | −178.8(14) |
| Ir1 | C3 | C4 | C9 | −123.0(16) | C55 | C50 | C51 | C56 | -8(3) |
| Ir1 | C4 | C5 | C1 | 61.4(10) | C55 | C50 | C51 | Ir3 | 119.1(16) |
| Ir1 | C4 | C5 | C10 | −123.6(15) | C57 | C58 | C59 | C60 | 179.6(14) |
| Ir1 | N1 | S1 | C17 | -95.2(11) | C57 | C58 | N6 | C62 | 178.6(13) |
| Ir1 | N1 | S1 | O1 | 20.3(12) | C57 | C58 | N6 | Ir3 | 0.1(16) |
| Ir1 | N1 | S1 | O2 | 151.3(9) | C57 | N5 | S3 | C63 | 74.6(12) |
| N1 | C11 | C12 | C13 | −165.3(14) | C57 | N5 | S3 | O5 | −170.3(11) |
| N1 | C11 | C12 | N2 | 14(2) | C57 | N5 | S3 | O6 | -38.3(12) |
| N2 | C12 | C13 | C14 | 3(2) | C58 | C57 | N5 | Ir3 | 32.9(14) |
| S1 | C17 | C18 | C19 | −174.7(11) | C58 | C57 | N5 | S3 | −152.0(10) |
| S1 | C17 | C22 | C21 | 175.0(11) | C58 | C59 | C60 | C61 | 0(2) |
| C24 | C25 | C26 | C27 | 3.7(15) | C59 | C58 | N6 | C62 | -3(2) |
| C24 | C25 | C26 | C31 | −178.7(13) | C59 | C58 | N6 | Ir3 | 178.5(10) |
| C24 | C25 | C26 | Ir2 | -58.6(9) | C59 | C60 | C61 | C62 | 1(2) |
| C25 | C24 | C28 | C27 | 1.8(15) | C60 | C61 | C62 | N6 | -3(2) |
| C25 | C24 | C28 | C33 | −173.6(13) | C61 | C62 | N6 | C58 | 4(2) |
| C25 | C24 | C28 | Ir2 | 62.4(9) | C61 | C62 | N6 | Ir3 | −177.7(11) |

| | | | | | | | | | |
|---|---|---|---|---|---|---|---|---|---|
| C25 | C26 | C27 | C28 | -2.5(16) | C63 | C64 | C65 | C66 | 3(3) |
| C25 | C26 | C27 | C32 | 175.5(14) | C64 | C63 | C68 | C67 | -3(2) |
| C25 | C26 | C27 | Ir2 | -62.3(9) | C64 | C63 | S3 | N5 | 79.5(13) |
| C26 | C27 | C28 | C24 | 0.5(16) | C64 | C63 | S3 | O5 | -35.9(14) |
| C26 | C27 | C28 | C33 | 175.9(13) | C64 | C63 | S3 | O6 | −162.8(12) |
| C26 | C27 | C28 | Ir2 | -60.1(11) | C64 | C65 | C66 | C67 | -4(2) |
| C28 | C24 | C25 | C26 | -3.4(15) | C64 | C65 | C66 | C69 | 174.0(16) |
| C28 | C24 | C25 | C30 | 176.3(13) | C65 | C66 | C67 | C68 | 1(2) |
| C28 | C24 | C25 | Ir2 | -62.1(9) | C66 | C67 | C68 | C63 | 3(2) |
| C29 | C24 | C25 | C26 | −175.2(13) | C68 | C63 | C64 | C65 | 1(2) |
| C29 | C24 | C25 | C30 | 4(2) | C68 | C63 | S3 | N5 | -97.3(13) |
| C29 | C24 | C25 | Ir2 | 126.0(15) | C68 | C63 | S3 | O5 | 147.3(12) |
| C29 | C24 | C28 | C27 | 173.8(13) | C68 | C63 | S3 | O6 | 20.4(14) |
| C29 | C24 | C28 | C33 | -2(2) | C69 | C66 | C67 | C68 | −176.7(15) |
| C29 | C24 | C28 | Ir2 | −125.5(15) | Ir3 | C47 | C48 | C49 | 60.5(10) |
| C30 | C25 | C26 | C27 | −176.0(14) | Ir3 | C47 | C48 | C53 | −126.8(16) |
| C30 | C25 | C26 | C31 | 2(2) | Ir3 | C47 | C51 | C50 | -62.3(10) |
| C30 | C25 | C26 | Ir2 | 121.8(15) | Ir3 | C47 | C51 | C56 | 126.9(16) |
| C31 | C26 | C27 | C28 | 180.0(13) | Ir3 | C48 | C49 | C50 | 62.0(10) |
| C31 | C26 | C27 | C32 | -2(3) | Ir3 | C48 | C49 | C54 | −125.6(14) |
| C31 | C26 | C27 | Ir2 | 120.2(15) | Ir3 | C49 | C50 | C51 | 60.3(10) |
| C32 | C27 | C28 | C24 | −177.7(13) | Ir3 | C49 | C50 | C55 | −118.4(16) |
| C32 | C27 | C28 | C33 | -2(2) | Ir3 | C50 | C51 | C47 | 62.1(10) |
| C32 | C27 | C28 | Ir2 | 121.7(14) | Ir3 | C50 | C51 | C56 | −127.0(16) |
| C34 | C35 | C36 | C37 | −179.3(14) | Ir3 | N5 | S3 | C63 | −111.2(10) |
| C34 | C35 | N4 | C39 | −179.8(13) | Ir3 | N5 | S3 | O5 | 3.8(12) |
| C34 | C35 | N4 | Ir2 | -1.4(16) | Ir3 | N5 | S3 | O6 | 135.9(8) |
| C34 | N3 | S2 | C40 | -74.4(12) | N5 | C57 | C58 | C59 | 160.5(13) |
| C34 | N3 | S2 | O3 | 171.6(10) | N5 | C57 | C58 | N6 | -21.2(17) |
| C34 | N3 | S2 | O4 | 36.8(13) | N6 | C58 | C59 | C60 | 1(2) |
| C35 | C34 | N3 | Ir2 | -43.6(14) | S3 | C63 | C64 | C65 | −176.2(13) |
| C35 | C34 | N3 | S2 | 160.3(10) | S3 | C63 | C68 | C67 | 173.4(12) |
| C35 | C36 | C37 | C38 | 3(2) | | | | | |

**Table 7 Hydrogen Atom Coordinates (Åx10$^4$) and Isotropic Displacement Parameters (Å$^2$x10$^3$) for akdk21004**

| Atom | *x* | *y* | *z* | U(eq) |
|---|---|---|---|---|
| H6A | 7005.23 | 6154.64 | 2458.51 | 100 |
| H6B | 7717.19 | 6167 | 3389.53 | 100 |
| H6C | 6630.75 | 5913.17 | 3234.24 | 100 |
| H7A | 7351.33 | 5511.89 | 4194.41 | 107 |
| H7B | 8714.3 | 5485.79 | 4549.79 | 107 |
| H7C | 8045.52 | 5166.41 | 4150.83 | 107 |
| H8A | 9978.39 | 4984.3 | 3688.91 | 113 |
| H8B | 11059.18 | 5115.06 | 3122.08 | 113 |
| H8C | 10136.06 | 4849.1 | 2712.44 | 113 |
| H9A | 10944.68 | 5188.95 | 1460.05 | 132 |
| H9B | 11213.33 | 5573.76 | 1320.32 | 132 |
| H9C | 10226.79 | 5390.85 | 705.53 | 132 |
| H10A | 8728.79 | 5905.95 | 584.1 | 96 |
| H10B | 9618.73 | 6133.55 | 1168.43 | 96 |
| H10C | 8200.67 | 6177.11 | 1229.91 | 96 |
| H11A | 5008.09 | 4772.67 | 2021.48 | 65 |
| H11B | 5863.3 | 4713.25 | 1212.41 | 65 |
| H13 | 3629.95 | 5052.52 | 868.25 | 60 |
| H14 | 3189.78 | 5566.64 | 240.69 | 71 |
| H15 | 4500.57 | 6007.42 | 392.33 | 62 |
| H16 | 6329.63 | 5907.31 | 1128.1 | 72 |
| H18 | 8941.05 | 4483.16 | 1618.29 | 76 |
| H19 | 9237.15 | 4090.1 | 528.54 | 59 |
| H21 | 6225.45 | 3604.63 | 1125.41 | 65 |
| H22 | 5873.7 | 3997.99 | 2231.54 | 57 |
| H23A | 7716.47 | 3698.52 | -590.87 | 98 |
| H23B | 7378.87 | 3395.43 | 28.67 | 98 |
| H23C | 8746.6 | 3507.25 | -37.14 | 98 |
| H29A | 3480.74 | 4452.16 | 2664.28 | 92 |
| H29B | 2704.54 | 4445.91 | 3526.17 | 92 |
| H29C | 2229.1 | 4644.35 | 2673.36 | 92 |
| H30A | 3165.52 | 3914.87 | 619.76 | 94 |
| H30B | 3910.55 | 4096.88 | 1396.83 | 94 |
| H30C | 2910.36 | 4295.47 | 832.13 | 94 |
| H31A | 2050.98 | 3453.64 | 645.79 | 88 |
| H31B | 708.67 | 3574.92 | 429.51 | 88 |
| H31C | 951.8 | 3269.19 | 1079.32 | 88 |
| H32A | -484.67 | 3471.62 | 3188.95 | 86 |
| H32B | -442.54 | 3312.2 | 2228.8 | 86 |
| H32C | -1205.78 | 3640.89 | 2379.95 | 86 |
| H33A | 1022.03 | 4192.18 | 4208.65 | 88 |
| H33B | 18.01 | 3914.09 | 4049.32 | 88 |
| H33C | -174.78 | 4275.85 | 3641.8 | 88 |
| H34A | 2376.64 | 3080.75 | 4878.98 | 66 |

| | | | | |
|---|---|---|---|---|
| H34B | 1529.42 | 3399.86 | 4729 | 66 |
| H36 | 3814.86 | 3411.02 | 5905.73 | 63 |
| H37 | 5483.55 | 3762.87 | 5990.47 | 67 |
| H38 | 5835.19 | 4097.83 | 4769.93 | 67 |
| H39 | 4735.77 | 4023.21 | 3471.9 | 59 |
| H41 | 3288.58 | 2543.84 | 2518.97 | 65 |
| H42 | 4494.95 | 2078.02 | 2935.9 | 71 |
| H44 | 2933.14 | 2058.55 | 5291.13 | 75 |
| H45 | 1668.58 | 2487.69 | 4890.47 | 70 |
| H46A | 5187.58 | 1810.14 | 4851.7 | 121 |
| H46B | 5029.98 | 1677.07 | 3864.49 | 121 |
| H46C | 4136.94 | 1554.91 | 4595.16 | 121 |
| H52A | 7472.84 | 2868 | 8884.71 | 87 |
| H52B | 7721.26 | 2480.3 | 8999.18 | 87 |
| H52C | 6618.68 | 2605.49 | 8385.4 | 87 |
| H53A | 6862.52 | 2204.74 | 6279.1 | 106 |
| H53B | 6471.01 | 2246.41 | 7273.09 | 106 |
| H53C | 7501.5 | 1989.09 | 7043.01 | 106 |
| H54A | 8605.65 | 2251.68 | 5440.8 | 90 |
| H54B | 9998.73 | 2242.63 | 5725.44 | 90 |
| H54C | 9456.84 | 2553.76 | 5196.65 | 90 |
| H55A | 10819.74 | 2965.91 | 5961.35 | 87 |
| H55B | 11588.66 | 2786.61 | 6730.74 | 87 |
| H55C | 11063.28 | 3149.56 | 6881.61 | 87 |
| H56A | 10559.16 | 3179.08 | 8303.25 | 83 |
| H56B | 10020.52 | 2934.63 | 9014.44 | 83 |
| H56C | 9256.19 | 3246.15 | 8667.48 | 83 |
| H57A | 8206.09 | 3613.35 | 4822.41 | 59 |
| H57B | 8979.11 | 3279.47 | 4785.47 | 59 |
| H59 | 6747.84 | 3343.32 | 3684.61 | 65 |
| H60 | 5009.53 | 3023.94 | 3509.77 | 66 |
| H61 | 4493.85 | 2679.2 | 4688.72 | 63 |
| H62 | 5638.06 | 2686.18 | 5980.48 | 59 |
| H64 | 7522.42 | 3958.67 | 7472.96 | 83 |
| H65 | 6145.59 | 4380.87 | 7423.69 | 68 |
| H67 | 7328.03 | 4666.2 | 5061.03 | 72 |
| H68 | 8817.32 | 4264.54 | 5169.04 | 57 |
| H69A | 4843.66 | 4715.08 | 5851.94 | 112 |
| H69B | 5819.17 | 5003.07 | 5788.37 | 112 |
| H69C | 5346.49 | 4895.49 | 6725.38 | 112 |

# Cp*Ir(88)Cl

Data collected, solved and refined by Adrian C Whitwood

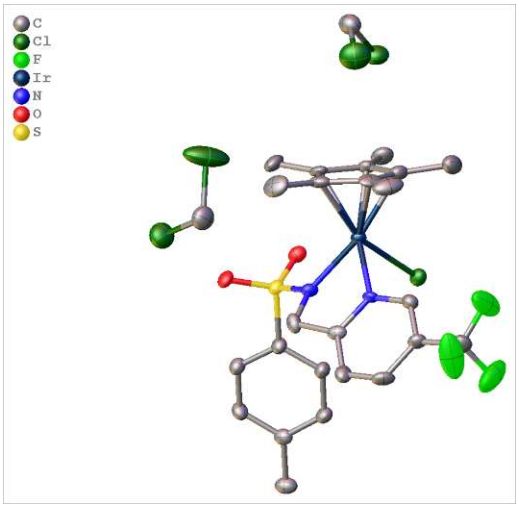


**Table 1 Crystal data and structure refinement for akdk21007.**

| | |
|---|---|
| Identification code | akdk21007 |
| Empirical formula | $C_{26}H_{31}Cl_5F_3IrN_2O_2S$ |
| Formula weight | 862.04 |
| Temperature/K | 110.00(14) |
| Crystal system | monoclinic |
| Space group | $P2_1/c$ |
| a/Å | 8.4043(3) |
| b/Å | 14.5366(6) |
| c/Å | 25.6967(8) |
| α/° | 90 |
| β/° | 94.965(3) |
| γ/° | 90 |
| Volume/Å$^3$ | 3127.59(18) |
| Z | 4 |
| $\rho_{calc}$g/cm$^3$ | 1.831 |
| μ/mm$^{-1}$ | 13.221 |
| F(000) | 1688.0 |
| Crystal size/mm$^3$ | 0.178 × 0.121 × 0.017 |
| Radiation | Cu Kα (λ = 1.54184) |
| 2Θ range for data collection/° | 6.992 to 134.138 |
| Index ranges | $-10 \le h \le 5$, $-17 \le k \le 16$, $-30 \le l \le 29$ |
| Reflections collected | 11554 |
| Independent reflections | 5559 [$R_{int}$ = 0.0381, $R_{sigma}$ = 0.0500] |
| Data/restraints/parameters | 5559/0/367 |
| Goodness-of-fit on F$^2$ | 1.075 |
| Final R indexes [I>=2σ (I)] | $R_1$ = 0.0481, $wR_2$ = 0.1095 |
| Final R indexes [all data] | $R_1$ = 0.0570, $wR_2$ = 0.1144 |
| Largest diff. peak/hole / e Å$^{-3}$ | 1.49/-1.87 |

**Table 2 Fractional Atomic Coordinates (x$10^4$) and Equivalent Isotropic Displacement Parameters (Å$^2$x$10^3$) for akdk21007. $U_{eq}$ is defined as 1/3 of the trace of the orthogonalised $U_{IJ}$ tensor**

| Atom | *x* | *y* | *z* | U(eq) |
|---|---|---|---|---|
| C1 | 1214(9) | 4918(6) | 3574(3) | 21.9(17) |
| C2 | 1541(9) | 4622(6) | 4090(3) | 23.9(17) |
| C3 | 292(9) | 4427(6) | 4386(3) | 24.8(18) |
| C4 | -1295(9) | 4501(6) | 4176(3) | 23.0(17) |
| C5 | -1580(9) | 4800(6) | 3660(3) | 25.4(18) |
| C6 | -342(9) | 5011(6) | 3362(3) | 24.1(18) |
| C7 | -2657(10) | 4295(6) | 4502(3) | 29.7(19) |
| C8 | 2126(10) | 3816(6) | 2590(3) | 24.1(18) |
| C9 | 1143(9) | 3629(5) | 2086(3) | 21.2(16) |
| C10 | 207(9) | 2847(6) | 1989(3) | 28.2(19) |
| C11 | -607(10) | 2726(6) | 1508(3) | 29.1(19) |
| C12 | -501(9) | 3412(6) | 1132(3) | 24.2(18) |
| C13 | 399(9) | 4184(6) | 1251(3) | 23.0(17) |
| C14 | -1349(11) | 3314(6) | 599(4) | 35(2) |
| C15 | 5012(10) | 5298(6) | 1735(3) | 28.3(19) |
| C16 | 4015(10) | 5496(7) | 1253(3) | 31(2) |
| C17 | 3284(10) | 6367(6) | 1321(3) | 28.9(19) |
| C18 | 3875(9) | 6733(6) | 1826(3) | 23.4(17) |
| C19 | 4962(9) | 6086(6) | 2072(3) | 23.2(17) |
| C20 | 6106(11) | 4472(7) | 1829(4) | 44(3) |
| C21 | 3801(12) | 4905(8) | 781(4) | 48(3) |
| C22 | 2263(12) | 6891(8) | 912(4) | 44(3) |
| C23 | 3444(11) | 7651(6) | 2041(4) | 36(2) |
| C24 | 5964(10) | 6206(7) | 2573(3) | 36(2) |
| Cl1 | -5(2) | 6159.3(13) | 1988.8(7) | 23.8(4) |
| F1 | -939(9) | 3937(5) | 264(2) | 72(2) |
| F2 | -1133(11) | 2520(5) | 394(3) | 89(3) |
| F3 | -2919(8) | 3412(7) | 605(3) | 86(3) |
| Ir1 | 2586.3(4) | 5467.2(2) | 1918.9(2) | 17.47(11) |
| N1 | 2308(7) | 4811(5) | 2629(2) | 19.8(14) |
| N2 | 1225(7) | 4290(4) | 1715(2) | 17.6(13) |
| O1 | 4224(6) | 4741(4) | 3453(2) | 23.5(12) |
| O2 | 2897(6) | 6186(4) | 3170(2) | 23.2(12) |
| S1 | 2827(2) | 5201.3(13) | 3198.8(7) | 19.0(4) |
| C26 | 5498(13) | 6624(8) | 4142(4) | 46(3) |
| Cl4 | 6906(5) | 7273(3) | 3862.1(15) | 95.8(14) |
| Cl5 | 5721(3) | 6703(2) | 4825.6(10) | 53.1(7) |
| C25 | 8145(11) | 7067(7) | 827(4) | 39(2) |
| Cl2 | 7644(4) | 6027(2) | 511.6(13) | 63.2(8) |
| Cl3 | 6519(3) | 7577.6(18) | 1098.8(10) | 44.3(6) |

**Table 3 Anisotropic Displacement Parameters ($Å^2x10^3$) for akdk21007. The Anisotropic displacement factor exponent takes the form: $-2\pi^2[h^2a^{*2}U_{11}+2hka^*b^*U_{12}+\ldots]$.**

| Atom | $U_{11}$ | $U_{22}$ | $U_{33}$ | $U_{23}$ | $U_{13}$ | $U_{12}$ |
|---|---|---|---|---|---|---|
| C1 | 18(4) | 25(5) | 23(4) | 1(3) | 3(3) | 4(3) |
| C2 | 19(4) | 28(5) | 24(4) | -1(3) | 1(3) | 2(3) |
| C3 | 27(4) | 28(5) | 20(4) | 4(3) | 6(3) | 5(4) |
| C4 | 24(4) | 17(4) | 29(4) | -2(3) | 8(3) | 2(3) |
| C5 | 18(4) | 30(5) | 28(4) | 3(4) | 3(3) | 0(3) |
| C6 | 19(4) | 28(5) | 25(4) | 2(3) | 0(3) | 0(3) |
| C7 | 31(4) | 23(5) | 37(5) | -3(4) | 13(4) | -1(4) |
| C8 | 28(4) | 24(5) | 21(4) | 2(3) | 3(3) | 10(4) |
| C9 | 21(4) | 15(4) | 29(4) | -5(3) | 10(3) | 0(3) |
| C10 | 25(4) | 39(6) | 21(4) | 6(4) | 5(3) | 1(4) |
| C11 | 30(5) | 23(5) | 35(5) | -7(4) | 10(4) | -13(4) |
| C12 | 23(4) | 18(4) | 32(4) | -2(3) | 2(3) | -6(3) |
| C13 | 24(4) | 20(4) | 26(4) | 4(3) | 5(3) | -1(3) |
| C14 | 39(5) | 23(5) | 42(5) | 0(4) | 0(4) | -9(4) |
| C15 | 24(4) | 21(5) | 42(5) | 1(4) | 15(4) | -7(3) |
| C16 | 30(4) | 42(6) | 22(4) | -1(4) | 17(3) | -12(4) |
| C17 | 24(4) | 32(5) | 30(4) | 3(4) | 1(3) | -10(4) |
| C18 | 22(4) | 18(4) | 31(4) | 3(3) | 3(3) | -7(3) |
| C19 | 16(4) | 19(4) | 36(5) | 4(3) | 6(3) | -6(3) |
| C20 | 27(5) | 37(6) | 71(7) | -4(5) | 17(5) | 11(4) |
| C21 | 43(6) | 62(8) | 42(6) | -17(5) | 22(5) | -21(5) |
| C22 | 40(5) | 54(7) | 36(5) | 14(5) | -6(4) | -15(5) |
| C23 | 32(5) | 23(5) | 52(6) | -3(4) | 1(4) | -9(4) |
| C24 | 18(4) | 53(7) | 36(5) | 5(4) | -1(4) | -9(4) |
| Cl1 | 21.8(9) | 19.1(10) | 30.5(10) | -1.4(8) | 1.7(7) | 3.0(7) |
| F1 | 105(6) | 71(5) | 35(3) | 10(3) | -22(3) | -46(4) |
| F2 | 155(8) | 38(4) | 65(5) | -30(3) | -50(5) | 27(5) |
| F3 | 40(4) | 156(9) | 58(4) | -8(5) | -14(3) | -10(4) |
| Ir1 | 16.97(17) | 14.96(18) | 20.77(17) | -0.04(13) | 3.29(12) | -2.08(13) |
| N1 | 20(3) | 18(4) | 21(3) | -2(3) | 3(3) | -6(3) |
| N2 | 18(3) | 11(3) | 25(3) | 3(3) | 4(3) | -3(2) |
| O1 | 14(3) | 29(3) | 27(3) | 0(2) | 2(2) | 4(2) |
| O2 | 20(3) | 21(3) | 28(3) | -6(2) | 4(2) | 1(2) |
| S1 | 14.9(8) | 20.1(10) | 22.2(9) | -2.7(7) | 2.4(7) | 0.7(7) |
| C26 | 47(6) | 50(7) | 39(5) | -4(5) | -6(5) | -6(5) |
| Cl4 | 135(3) | 85(3) | 76(2) | -18(2) | 56(2) | -63(3) |
| Cl5 | 56.6(16) | 63.6(19) | 39.1(13) | -1.0(12) | 4.5(11) | -1.6(14) |

| | | | | | | |
|---|---|---|---|---|---|---|
| C25 | 37(5) | 34(6) | 47(6) | 5(5) | 8(4) | 1(4) |
| Cl2 | 71.0(19) | 49.6(18) | 70.2(19) | -16.3(15) | 13.3(15) | -6.9(15) |
| Cl3 | 39.4(13) | 46.2(15) | 49.2(14) | 1.6(11) | 15.4(10) | -4.4(11) |

**Table 4 Bond Lengths for akdk21007.**

| Atom | Atom | Length/Å | Atom | Atom | Length/Å |
|---|---|---|---|---|---|
| C1 | C2 | 1.399(11) | C15 | Ir1 | 2.146(8) |
| C1 | C6 | 1.379(11) | C16 | C17 | 1.424(13) |
| C1 | S1 | 1.778(8) | C16 | C21 | 1.484(13) |
| C2 | C3 | 1.380(11) | C16 | Ir1 | 2.174(7) |
| C3 | C4 | 1.399(11) | C17 | C18 | 1.448(11) |
| C4 | C5 | 1.396(11) | C17 | C22 | 1.506(12) |
| C4 | C7 | 1.507(11) | C17 | Ir1 | 2.138(8) |
| C5 | C6 | 1.378(11) | C18 | C19 | 1.421(11) |
| C8 | C9 | 1.500(11) | C18 | C23 | 1.502(12) |
| C8 | N1 | 1.456(11) | C18 | Ir1 | 2.159(8) |
| C9 | C10 | 1.393(12) | C19 | C24 | 1.487(11) |
| C9 | N2 | 1.358(10) | C19 | Ir1 | 2.194(7) |
| C10 | C11 | 1.372(12) | Cl1 | Ir1 | 2.4196(18) |
| C11 | C12 | 1.396(12) | Ir1 | N1 | 2.091(6) |
| C12 | C13 | 1.373(11) | Ir1 | N2 | 2.100(6) |
| C12 | C14 | 1.495(12) | N1 | S1 | 1.595(6) |
| C13 | N2 | 1.336(10) | O1 | S1 | 1.456(5) |
| C14 | F1 | 1.316(11) | O2 | S1 | 1.435(6) |
| C14 | F2 | 1.288(11) | C26 | Cl4 | 1.719(11) |
| C14 | F3 | 1.329(11) | C26 | Cl5 | 1.755(10) |
| C15 | C16 | 1.464(12) | C25 | Cl2 | 1.748(10) |
| C15 | C19 | 1.437(12) | C25 | Cl3 | 1.753(10) |
| C15 | C20 | 1.518(12) | | | |

**Table 5 Bond Angles for akdk21007.**

| Atom | Atom | Atom | Angle/° | Atom | Atom | Atom | Angle/° |
|---|---|---|---|---|---|---|---|
| C2 | C1 | S1 | 119.2(6) | C23 | C18 | Ir1 | 125.2(6) |
| C6 | C1 | C2 | 120.4(7) | C15 | C19 | C24 | 124.8(8) |
| C6 | C1 | S1 | 120.3(6) | C15 | C19 | Ir1 | 68.9(4) |
| C3 | C2 | C1 | 119.4(7) | C18 | C19 | C15 | 108.2(7) |
| C2 | C3 | C4 | 121.1(7) | C18 | C19 | C24 | 127.0(8) |
| C3 | C4 | C7 | 120.9(7) | C18 | C19 | Ir1 | 69.6(4) |
| C5 | C4 | C3 | 118.1(7) | C24 | C19 | Ir1 | 129.9(6) |
| C5 | C4 | C7 | 121.0(7) | C15 | Ir1 | C16 | 39.6(3) |

| | | | | | | | |
|---|---|---|---|---|---|---|---|
| C6 | C5 | C4 | 121.4(7) | C15 | Ir1 | C18 | 65.0(3) |
| C5 | C6 | C1 | 119.6(8) | C15 | Ir1 | C19 | 38.7(3) |
| N1 | C8 | C9 | 106.7(6) | C15 | Ir1 | Cl1 | 160.4(2) |
| C10 | C9 | C8 | 124.2(7) | C16 | Ir1 | C19 | 65.0(3) |
| N2 | C9 | C8 | 114.8(7) | C16 | Ir1 | Cl1 | 127.8(3) |
| N2 | C9 | C10 | 120.9(7) | C17 | Ir1 | C15 | 65.6(3) |
| C11 | C10 | C9 | 119.7(8) | C17 | Ir1 | C16 | 38.6(4) |
| C10 | C11 | C12 | 118.3(8) | C17 | Ir1 | C18 | 39.4(3) |
| C11 | C12 | C14 | 120.7(7) | C17 | Ir1 | C19 | 64.9(3) |
| C13 | C12 | C11 | 119.8(8) | C17 | Ir1 | Cl1 | 95.9(2) |
| C13 | C12 | C14 | 119.4(8) | C18 | Ir1 | C16 | 65.1(3) |
| N2 | C13 | C12 | 121.8(7) | C18 | Ir1 | C19 | 38.1(3) |
| F1 | C14 | C12 | 113.8(7) | C18 | Ir1 | Cl1 | 96.7(2) |
| F1 | C14 | F3 | 104.4(9) | C19 | Ir1 | Cl1 | 128.9(2) |
| F2 | C14 | C12 | 112.8(8) | N1 | Ir1 | C15 | 108.7(3) |
| F2 | C14 | F1 | 107.1(9) | N1 | Ir1 | C16 | 143.8(3) |
| F2 | C14 | F3 | 106.0(9) | N1 | Ir1 | C17 | 164.8(3) |
| F3 | C14 | C12 | 112.0(8) | N1 | Ir1 | C18 | 125.5(3) |
| C16 | C15 | C20 | 125.8(8) | N1 | Ir1 | C19 | 101.5(3) |
| C16 | C15 | Ir1 | 71.2(4) | N1 | Ir1 | Cl1 | 87.44(18) |
| C19 | C15 | C16 | 107.9(8) | N1 | Ir1 | N2 | 75.3(2) |
| C19 | C15 | C20 | 125.7(8) | N2 | Ir1 | C15 | 111.1(3) |
| C19 | C15 | Ir1 | 72.4(4) | N2 | Ir1 | C16 | 98.4(3) |
| C20 | C15 | Ir1 | 129.0(6) | N2 | Ir1 | C17 | 119.8(3) |
| C15 | C16 | C21 | 126.7(9) | N2 | Ir1 | C18 | 159.2(3) |
| C15 | C16 | Ir1 | 69.2(4) | N2 | Ir1 | C19 | 147.8(3) |
| C17 | C16 | C15 | 107.0(7) | N2 | Ir1 | Cl1 | 83.27(17) |
| C17 | C16 | C21 | 126.3(9) | C8 | N1 | Ir1 | 114.3(5) |
| C17 | C16 | Ir1 | 69.3(5) | C8 | N1 | S1 | 115.9(5) |
| C21 | C16 | Ir1 | 126.5(6) | S1 | N1 | Ir1 | 126.6(4) |
| C16 | C17 | C18 | 108.6(8) | C9 | N2 | Ir1 | 117.4(5) |
| C16 | C17 | C22 | 126.1(8) | C13 | N2 | C9 | 119.4(7) |
| C16 | C17 | Ir1 | 72.1(5) | C13 | N2 | Ir1 | 123.1(5) |
| C18 | C17 | C22 | 124.7(9) | N1 | S1 | C1 | 104.7(4) |
| C18 | C17 | Ir1 | 71.1(5) | O1 | S1 | C1 | 105.8(3) |
| C22 | C17 | Ir1 | 129.5(6) | O1 | S1 | N1 | 113.2(3) |
| C17 | C18 | C23 | 125.6(8) | O2 | S1 | C1 | 107.2(4) |
| C17 | C18 | Ir1 | 69.5(5) | O2 | S1 | N1 | 108.5(3) |
| C19 | C18 | C17 | 108.2(8) | O2 | S1 | O1 | 116.5(3) |
| C19 | C18 | C23 | 126.2(8) | Cl4 | C26 | Cl5 | 111.4(6) |
| C19 | C18 | Ir1 | 72.3(5) | Cl2 | C25 | Cl3 | 112.7(5) |

**Table 6 Torsion Angles for akdk21007**

| A | B | C | D | Angle/° | A | B | C | D | Angle/° |
|---|---|---|---|---|---|---|---|---|---|
| C1 | C2 | C3 | C4 | 1.3(13) | C16 | C17 | C18 | C19 | -0.5(9) |
| C2 | C1 | C6 | C5 | -0.7(13) | C16 | C17 | C18 | C23 | 177.9(7) |
| C2 | C1 | S1 | N1 | 140.6(7) | C16 | C17 | C18 | Ir1 | -62.8(6) |
| C2 | C1 | S1 | O1 | 20.8(8) | C17 | C18 | C19 | C15 | -2.3(9) |
| C2 | C1 | S1 | O2 | -104.3(7) | C17 | C18 | C19 | C24 | 174.2(8) |
| C2 | C3 | C4 | C5 | -1.5(13) | C17 | C18 | C19 | Ir1 | -60.5(5) |
| C2 | C3 | C4 | C7 | -179.5(8) | C19 | C15 | C16 | C17 | -4.3(9) |
| C3 | C4 | C5 | C6 | 0.5(13) | C19 | C15 | C16 | C21 | 175.7(8) |
| C4 | C5 | C6 | C1 | 0.6(13) | C19 | C15 | C16 | Ir1 | -63.6(5) |
| C6 | C1 | C2 | C3 | -0.2(13) | C20 | C15 | C16 | C17 | −175.7(8) |
| C6 | C1 | S1 | N1 | -41.0(8) | C20 | C15 | C16 | C21 | 4.3(13) |
| C6 | C1 | S1 | O1 | -160.9(7) | C20 | C15 | C16 | Ir1 | 125.0(8) |
| C6 | C1 | S1 | O2 | 74.1(8) | C20 | C15 | C19 | C18 | 175.4(8) |
| C7 | C4 | C5 | C6 | 178.5(8) | C20 | C15 | C19 | C24 | -1.1(13) |
| C8 | C9 | C10 | C11 | -177.8(8) | C20 | C15 | C19 | Ir1 | −125.8(8) |
| C8 | C9 | N2 | C13 | 179.6(7) | C21 | C16 | C17 | C18 | −177.1(8) |
| C8 | C9 | N2 | Ir1 | -3.1(8) | C21 | C16 | C17 | C22 | -5.5(14) |
| C8 | N1 | S1 | C1 | -63.9(6) | C21 | C16 | C17 | Ir1 | 120.8(8) |
| C8 | N1 | S1 | O1 | 50.9(6) | C22 | C17 | C18 | C19 | −172.2(8) |
| C8 | N1 | S1 | O2 | -178.1(5) | C22 | C17 | C18 | C23 | 6.2(13) |
| C9 | C8 | N1 | Ir1 | -37.4(7) | C22 | C17 | C18 | Ir1 | 125.5(8) |
| C9 | C8 | N1 | S1 | 161.7(5) | C23 | C18 | C19 | C15 | 179.4(8) |
| C9 | C10 | C11 | C12 | -1.7(12) | C23 | C18 | C19 | C24 | -4.2(13) |
| C10 | C9 | N2 | C13 | -0.2(11) | C23 | C18 | C19 | Ir1 | 121.1(8) |
| C10 | C9 | N2 | Ir1 | 177.1(6) | Ir1 | C15 | C16 | C17 | 59.3(5) |
| C10 | C11 | C12 | C13 | -0.2(12) | Ir1 | C15 | C16 | C21 | −120.7(8) |
| C10 | C11 | C12 | C14 | 179.4(8) | Ir1 | C15 | C19 | C18 | -58.7(5) |
| C11 | C12 | C13 | N2 | 2.0(12) | Ir1 | C15 | C19 | C24 | 124.7(8) |
| C11 | C12 | C14 | F1 | -169.8(9) | Ir1 | C16 | C17 | C18 | 62.1(6) |
| C11 | C12 | C14 | F2 | -47.4(12) | Ir1 | C16 | C17 | C22 | −126.3(9) |
| C11 | C12 | C14 | F3 | 72.1(11) | Ir1 | C17 | C18 | C19 | 62.3(5) |
| C12 | C13 | N2 | C9 | -1.7(11) | Ir1 | C17 | C18 | C23 | −119.3(8) |
| C12 | C13 | N2 | Ir1 | -178.9(6) | Ir1 | C18 | C19 | C15 | 58.3(5) |
| C13 | C12 | C14 | F1 | 9.8(13) | Ir1 | C18 | C19 | C24 | −125.3(8) |
| C13 | C12 | C14 | F2 | 132.1(9) | Ir1 | N1 | S1 | C1 | 137.9(4) |
| C13 | C12 | C14 | F3 | −108.4(10) | Ir1 | N1 | S1 | O1 | −107.3(5) |
| C14 | C12 | C13 | N2 | -177.6(8) | Ir1 | N1 | S1 | O2 | 23.6(5) |
| C15 | C16 | C17 | C18 | 3.0(9) | N1 | C8 | C9 | C10 | −154.7(7) |

| | | | | | | | | | |
|---|---|---|---|---|---|---|---|---|---|
| C15 | C16 | C17 | C22 | 174.6(8) | N1 | C8 | C9 | N2 | 25.6(9) |
| C15 | C16 | C17 | Ir1 | -59.2(5) | N2 | C9 | C10 | C11 | 1.9(12) |
| C16 | C15 | C19 | C18 | 4.1(9) | S1 | C1 | C2 | C3 | 178.2(7) |
| C16 | C15 | C19 | C24 | -172.5(7) | S1 | C1 | C6 | C5 | -179.1(7) |
| C16 | C15 | C19 | Ir1 | 62.8(5) | | | | | |

**Table 7 Hydrogen Atom Coordinates (Åx10$^4$) and Isotropic Displacement Parameters (Å$^2$x10$^3$) for akdk21007**

| Atom | *x* | *y* | *z* | U(eq) |
|---|---|---|---|---|
| H2 | 2614.08 | 4556.14 | 4234.76 | 29 |
| H3 | 511.64 | 4238.4 | 4739.25 | 30 |
| H5 | -2649.15 | 4860.19 | 3511.04 | 31 |
| H6 | -559.84 | 5218.74 | 3012.5 | 29 |
| H7A | -2361.69 | 3783.76 | 4739.61 | 45 |
| H7B | -3605.98 | 4126.68 | 4273.28 | 45 |
| H7C | -2890.65 | 4841.15 | 4706.05 | 45 |
| H8A | 1582.61 | 3576.08 | 2888.36 | 29 |
| H8B | 3184.14 | 3516.53 | 2589.97 | 29 |
| H10 | 133.73 | 2398.69 | 2254.92 | 34 |
| H11 | -1228.04 | 2188.45 | 1431.83 | 35 |
| H13 | 436.15 | 4655.6 | 996.37 | 28 |
| H20A | 6191.62 | 4313.7 | 2201.46 | 66 |
| H20B | 7167.05 | 4621.46 | 1722.59 | 66 |
| H20C | 5664.46 | 3948.1 | 1624.78 | 66 |
| H21A | 3789.1 | 4257.05 | 887.32 | 72 |
| H21B | 4683.64 | 5008.67 | 563.2 | 72 |
| H21C | 2787.31 | 5057.15 | 582.48 | 72 |
| H22A | 1551.24 | 6462.97 | 709.96 | 66 |
| H22B | 2948.2 | 7203.56 | 677.72 | 66 |
| H22C | 1623.38 | 7348.04 | 1081.62 | 66 |
| H23A | 2337.09 | 7801.56 | 1919.32 | 54 |
| H23B | 4158.2 | 8124.12 | 1921.2 | 54 |
| H23C | 3554.1 | 7626.93 | 2423.71 | 54 |
| H24A | 5544.15 | 6716.32 | 2769.34 | 54 |
| H24B | 7065.71 | 6342.73 | 2500.32 | 54 |
| H24C | 5944.03 | 5639.79 | 2778.65 | 54 |
| H26A | 5601.11 | 5972.37 | 4036.97 | 55 |
| H26B | 4417.18 | 6837.71 | 4012.24 | 55 |
| H25A | 8560.62 | 7497.67 | 572.55 | 47 |
| H25B | 9007.64 | 6954.54 | 1106.8 | 47 |

# Abbreviations

| | |
|---|---|
| Ac | Acetyl (protecting group) |
| ArM | Artificial metalloenzyme |
| Bipy | bipyridine |
| Boc | *tert*-Butyloxycarbonyl |
| *Cj*CeuE | Periplasmic binding protein from *Campylobacter jejuni* |
| Cp*Ir | Pentamethylcyclopentadienyl iridium |
| Cym | Cymene ($\eta^6$-arene ligand) |
| DCM | Dichloromethane |
| DMF | Dimethylformamide |
| e.e. | Enatiomeric excess |
| EtOAc | Ethyl acetate |
| EtOH | Ethanol |
| Gst | Periplasmic binding protein from *Geobacillus stearothermophilus* |
| HATU | 1-[Bis(dimethylamino)methylene]-1*H*-1,2,3-triazolo[4,5-*b*]pyridinium 3-oxid hexafluorophosphate |
| His | Histidine |
| HMB | Hexamethylbenzene ($\eta^6$-arene ligand) |
| HPLC | High-performance liquid chromatography |
| HRMS | High-resolution mass spectrometry |
| HRMS-ESI | High-resolution mass spectrometry – electrospray ionisation |
| $K_d$ | Dissociation constant |
| Me | Methyl (protecting group) |
| MeOH | Methanol |
| NaOH | Sodium hydroxide |
| PBP | Periplasmic binding protein |
| PG | Protecting group |
| PMB | *para*-Methyloxybenzyl (protecting group) |
| Pth | Periplasmic binding protein from *Parageobacillus thermoglucosidasius* |
| $^t$Bu | *tert*-Butyl (protecting group) |
| TLC | Thin layer chromatography |
| TMU | Tetramethylurea |
| TOF | Turnover frequency |
| TON | Turnover number |
| Trp | Tryptophan |
| Tyr | Tyrosine |

# References


1 J. Choi, S. Han and H. Kim, *Biotechnol. Adv.*, 2015, **33**, 1443–1454.

2 R. A. Sheldon and D. Brady, *Chem. Commun.*, 2018, **54**, 6088–6104.

3 J. M. Woodley, *Trends Biotechnol.*, 2008, **26**, 321–327.

4 U. T. Bornscheuer, G. W. Huisman, R. J. Kazlauskas, S. Lutz, J. C. Moore and K. Robins, *Nature*, 2012, **485**, 185–194.

5 E. Vazquez-Figueroa, V. Yeh, J. M. Broering, J. F. Chaparro-Riggers and A. S. Bommarius, *Protein Eng. Des. Sel.*, 2008, **21**, 673–680.

6 J. M. Woodley, *Appl. Microbiol. Biotechnol.*, 2019, **103**, 4733–4739.

7 E. L. Bell, W. Finnigan, S. P. France, A. P. Green, M. A. Hayes, L. J. Hepworth, S. L. Lovelock, H. Niikura, S. Osuna, E. Romero, K. S. Ryan, N. J. Turner and S. L. Flitsch, *Nat Rev Methods Prim.*, 2021, **1**, 1–21.

8 N. Ran, L. Zhao, Z. Chen and J. Tao, *Green Chem.*, 2008, **10**, 361–372.

9 R. Wohlgemuth, *Curr. Opin. Biotechnol.*, 2010, **21**, 713–724.

10 I. S. Young and P. S. Baran, *Nat. Chem.*, 2009, **1**, 193–205.

11 M. D. Truppo, *ACS Med. Chem. Lett.*, 2017, **8**, 476–480.

12 R. N. Patel, *Bioorg. Med. Chem.*, 2018, **26**, 1252–1274.

13 D. J. Pollard and J. M. Woodley, *Trends Biotechnol.*, 2007, **25**, 66–73.

14 M. Breuer, K. Ditrich, T. Habicher, B. Hauer, M. Keßeler, R. Stürmer and T. Zelinski, *Angew. Chem. Int. Ed.*, 2004, **43**, 788–824.

15 R. A. Sheldon, *Green Chem.*, 2007, **9**, 1273–1283.

16 S. Wu, R. Snajdrova, J. C. Moore, K. Baldenius and U. T. Bornscheuer, *Angew. Chem. Int. Ed.*, 2021, **60**, 88–119.

17 C. A. Denard, H. Ren and H. Zhao, *Curr. Opin. Chem. Biol.*, 2015, **25**, 55–64.

18 E. T. Farinas, T. Bulter and F. H. Arnold, *Curr. Opin. Biotchnol.*, 2001, **12**, 545–551.

19 B. Hauer, *ACS Catal.*, 2020, **10**, 8418–8427.

20 J. P. Adams, M. J. B. Brown, A. Diaz-Rodriguez, R. C. Lloyd and G.-D. Roiban, *Adv. Synth. Catal.*, 2019, **361**, 2421–2432.

21 S. M. A. De Wildeman, T. Sonke, H. E. Schoemaker and O. May, *Acc. Chem. Res.*, 2007, **40**, 1260–1266.

22 B. Jandeleit, D. J. Schaefer, T. S. Powers, H. W. Turner and W. H. Weinberg, *Angew. Chem. Int. Ed.*, 1999, **38**, 2494–2532.

23 F. Schwizer, Y. Okamoto, T. Heinisch, Y. Gu, M. M. Pellizzoni, V. Lebrun, R. Reuter, V. Köhler, J. C. Lewis and T. R. Ward, *Chem. Rev.*, 2018, **118**, 142–231.

24 T. Kokubo, S. Sassa and E. T. Kaiser, *J. Am. Chem. Soc.*, 1987, **109**, 606–607.

25 B. Imperiali and R. S. Roy, *J. Am. Chem. Soc.*, 1994, **116**, 12083–12084.

26 C. J. Suckling and L.-M. Zhu, *Bioorg. Med. Chem. Lett.*, 1993, **3**, 531–534.

27 C. Letondor, A. Pordea, N. Humbert, A. Ivanova, S. Mazurek, M. Novic and T. R. Ward, *J. Am. Chem. Soc.*, 2006, **128**, 8320–8328.

28 T. K. Hyster, L. Knörr, T. R. Ward and T. Rovis, *Science*, 2012, **338**, 500–505.

29 T. Heinisch and T. R. Ward, *Acc. Chem. Res.*, 2016, **49**, 1711–1721.

30 Z. Liu, V. Lebrun, T. Kitanosono, H. Mallin, V. Köhler, D. Häussinger, D. Hilvert, S. Kobayashi and T. R. Ward, *Angew. Chem. Int. Ed.*, 2016, **55**, 11587–11590.

31 C.-C. Lin, C.-W. Lin and A. S. C. Chan, *Asymmetry*, 1999, **10**, 1887–1893.

32 J. G. Rebelein, Y. Cotelle, B. Garabedian and T. R. Ward, *ACS Catal.*, 2019, **9**, 4173–4178.

33 R. R. Davies and M. D. Distefano, *J. Am. Chem. Soc.*, 1997, **119**, 11643–11652.

34 A. D. Liang, J. Serrano-Plana, R. L. Peterson and T. R. Ward, *Acc. Chem. Res.*, 2019, **52**, 585–595.

35 J. Collot, J. Gradinaru, N. Humbert, M. Skander, A. Zocchi and T. R. Ward, *J. Am. Chem. Soc.*, 2003, **125**, 9030–9031.

36 M. E. Wilson and G. M. Whitesides, *J. Am. Chem. Soc.*, 1978, **100**, 306–307.

37 I. Drienovská, A. Rioz-Martínez, A. Draksharapu and G. Roelfes, *Chem. Sci.*, 2015, **6**, 770–776.

38 J. Bos, W. R. Browne, A. J. M. Driessen and G. Roelfes, *J. Am. Chem. Soc.*, 2015, **137**, 9796–9799.

39 J. Bos, F. Fusetti, A. J. M. Driessen and G. Roelfes, *Angew. Chem. Int. Ed.*, 2012, **51**,

7472–7475.

40 F. W. Monnard, E. S. Nogueira, T. Heinisch, T. Schirmer and T. R. Ward, *Chem. Sci.*, 2013, **4**, 3269–3274.

41 P. Dydio, H. M. Key, A. Nazarenko, J. Y.-E. Rha, V. Seyedkazemi, D. S. Clark and H. J. F, *Science*, 2016, **354**, 102–106.

42 Y. Gu, S. N. Natoli, Z. Liu, D. S. Clark and J. F. Hartwig, *Angew. Chem. Int. Ed.*, 2019, **58**, 13954–13960.

43 F. Richter, A. Leaver-Fay, S. D. Khare, S. Bjelic and D. Baker, *PLoS One*, 2011, **6**, e19230.

44 S. Basler, S. Studer, Y. Zou, T. Mori, Y. Ota, A. Camus, H. A. Bunzel, R. C. Helgeson, K. N. Houk, G. Jiménez-Osés and D. Hilvert, *Nat. Chem.*, 2021, **13**, 231–235.

45 M. Jeschek, R. Reuter, T. Heinisch, C. Trindler, J. Klehr, S. Panke and T. R. Ward, *Nature*, 2016, **537**, 661–665.

46 C. Gutiérrez de Souza, M. Bersellini and G. Roelfes, *ChemCatChem*, 2020, **12**, 3190–3194.

47 M. Dürrenberger, T. Heinisch, Y. M. Wilson, T. Rossel, E. Nogueira, L. Knörr, A. Mutschler, K. Kersten, M. J. Zimbron, J. Pierron, T. Schirmer and T. R. Ward, *Angew. Chem. Int. Ed.*, 2011, **50**, 3026–3029.

48 K. Mitsukura, M. Suzuki, K. Tada, T. Yoshida and T. Nagasawa, *Org. Biomol. Chem.*, 2010, **8**, 4533–4535.

49 L. M. Jarvis, *Chem. Eng. News*, 2016, **94**, 12–17.

50 J. P. C. Coverdale, C. Sanchez-Cano, G. J. Clarkson, R. Soni, M. Wills and P. J. Sadler, *Chem. Eur. J.*, 2015, **21**, 8043–8046.

51 D. J. C. Constable, P. J. Dunn, J. D. Hayler, G. R. Humphrey, J. L. Leazer, R. J. Linderman, K. Lorenz, J. Manley, B. A. Pearlman, A. Wells and T. Y. Zhang, *Green Chem.*, 2007, **9**, 411–420.

52 A. Ruff, C. Kirby, B. C. Chan and A. R. O'Connor, *Organometallics*, 2016, **35**, 327–335.

53 J. W. Faller and A. R. Lavoie, *Organometallics*, 2010, **21**, 3493–3495.

54 T. Ikariya, K. Murata and R. Noyori, *Org. Biomol. Chem.*, 2006, **4**, 393–406.

55 S. E. Clapham, A. Hadzovic and R. H. Morris, *Coord. Chem. Rev.*, 2004, **248**, 2201–2237.

56 P. A. Dub and J. C. Gordon, *Dalton Trans.*, 2016, **45**, 6756–6781.

57 R. Noyori, M. Yamakawa and S. Hashiguchi, *J. Org. Chem.*, 2001, **66**, 7931–7944.

58 M. Yamakawa, H. Ito and R. Noyori, *J. Am. Chem. Soc.*, 2000, **122**, 1466–1478.

59 E. D. Martins, G. J. Clarkson and M. Wills, *Org. Lett.*, 2009, **11**, 847–850.

60 M. D. Patil, G. Grogan, A. Bommarius and H. Yun, *ACS Catal.*, 2018, **8**, 10985–11015.

61 S. Hashiguchi, A. Fujii, J. Takehara, T. Ikariya and R. Noyori, *J. Am. Chem. Soc.*, 1995, **117**, 7562–7563.

62 A. Fujii, S. Hashiguchi, N. Uematsu, T. Ikariya and R. Noyori, *J. Am. Chem. Soc.*, 1996, **118**, 2521–2522.

63 J. Barrios-Rivera, Y. Xu, G. J. Clarkson and M. Wills, *Tetrahedron*, 2022, **103**, 132562.

64 F. Foubelo and M. Yus, *Chem. Rec.*, 2015, **15**, 907–924.

65 K. E. Jolley, A. Zanotti-Gerosa, F. Hancock, A. Dyke, D. M. Grainger, J. A. Medlock, H. G. Nedden, J. J. M. Le Paih, S. J. Roseblade, A. Seger, V. Sivakumar, I. Prokes, D. J. Morris and M. Wills, *Adv. Synth. Catal.*, 2012, **354**, 2545–2555.

66 K.-J. Haack, S. Hashiguchi, A. Fujii, T. Ikariya and R. Noyori, *Angew. Chem. Int. Ed. Engl.*, 1997, **36**, 285–288.

67 K. Murata, T. Ikariya and R. Noyori, *J. Org. Chem.*, 1999, **64**, 2186–2187.

68 A. Fujii, S. Hashiguchi, N. Uematsu, T. Ikariya and R. Noyori, *J. Am. Chem. Soc.*, 1996, **118**, 2521–2522.

69 A. M. Hayes, D. J. Morris, G. J. Clarkson and M. Wills, *J. Am. Chem. Soc.*, 2005, **127**, 7318–7319.

70 M. Yamakawa, I. Yamada and R. Noyori, *Angew. Chem. Int. Ed.*, 2001, **40**, 2818–2821.

71 M. R. Ringenberg and T. R. Ward, *Chem. Commun.*, 2011, **47**, 8470–8476.

72 P. A. Dub, N. V Tkachenko, V. K. Vyas, M. Wills, J. S. Smith and S. Tretiak, *Organometallics*, 2021, **40**, 1402–1410.

73 A. M. R. Hall, D. B. G. Berry, J. N. Crossley, A. Codina, I. Clegg, J. P. Lowe, A.

Buchard and U. Hintermair, *ACS Catal.*, 2021, **11**, 13649–13659.

74 J. Vácalavík, P. Kačer, M. Kuzma and Č. L, *Molecules*, 2011, **16**, 5460–5495.

75 J. Vácalavík, M. Kuzma, J. Přech and P. Kačer, *Organometallics*, 2011, **30**, 4822–4829.

76 M. Hestericovà, T. Heinisch, L. Alonso-Cotchico, J.-D. Maréchal, P. Vidossich and T. R. Ward, *Angew. Chem. Int. Ed.*, 2018, **57**, 1863–1868.

77 D. Ghislieri and N. J. Turner, *Top. Catal.*, 2014, **57**, 284–300.

78 J. H. Schrittwieser, S. Velikogne and W. Kroutil, *Adv. Synth. Catal.*, 2015, **357**, 1655–1685.

79 J. Mangas-Sanchez, S. P. France, S. L. Montgomery, G. A. Aleku, H. Man, M. Sharma, J. I. Ramsden, G. Grogan and N. J. Turner, *Curr. Opin. Chem. Biol.*, 2017, **37**, 19–25.

80 G. Grogan, *Curr. Opin. Chem. Biol.*, 2018, **43**, 15–22.

81 M. Hestericová, M. R. Correro, M. Lenz, P. F. Corvini, P. Shahgaldian and T. R. Ward, *Chem. Commun.*, 2016, **52**, 9462–9465.

82 Y. Okamoto, V. Köhler, C. E. Paul, F. Hollmann and T. R. Ward, *ACS Catal.*, 2016, **6**, 3553–3557.

83 X. Wu, X. Li, A. Zanotti-Gerosa, A. Pettman, J. Liu, A. J. Mills and J. Xiao, *Chem. Eur. J.*, 2008, **14**, 2209–2222.

84 X. Wu and J. Xiao, *Chem. Commun.*, 2007, 2449–2466.

85 T. Thorpe, J. Blacker, S. M. Brown, C. Bubert, J. Crosby, S. Fitzjohn, J. P. Muxworthy, J. M. J. Williams, H. Works, P. O. B. A, L. Road and H. H. D. Ff, 2001, **42**, 4041–4043.

86 X. Sun, G. Manos, J. Blacker, J. Martin, A. Gavriilidis, C. Engineering, V. Uni, C. London and T. Place, 2004, **8**, 909–914.

87 Z. M. Heiden and T. B. Rauchfuss, *J. Am. Chem. Soc.*, 2009, **131**, 3593–3600.

88 C. Li and J. Xiao, *J. Am. Chem. Soc.*, 2008, **130**, 13208–13209.

89 C. Li, B. Villa-Marcos and J. Xiao, *J. Am. Chem. Soc.*, 2009, **131**, 6967–6969.

90 R. L. Booth, G. Grogan, K. S. Wilson and A.-K. Duhme-Klair, *RSC Chem. Biol.*, 2020, **1**, 369–378.

91 J. M. Zimbron, T. Heinisch, M. Schmid, D. Hamels, E. S. Nogueira, T. Schirmer and T. R. Ward, *J. Am. Chem. Soc.*, 2013, **135**, 5384–5388.

92 T. Quinto, F. Schwizer, J. M. Zimbron, A. Morina, V. Köhler and T. R. Ward, *ChemCatChem*, 2014, **6**, 1010–1014.

93 S. Wu, Y. Zhou, J. G. Rebelein, M. Kuhn, H. Mallin, J. Zhao, N. V Igareta and T. R. Ward, *J. Am. Chem. Soc.*, 2019, **141**, 15869–15878.

94 A. Stein, D. Chen, N. V Igareta, Y. Cotelle, J. G. Rebelein and T. R. Ward, *ACS Cent. Sci.*, 2021, **7**, 1874–1884.

95 M. Genz, D. Singer, E. Hey-Hawkins, R. Hoffmann and N. Sträter, *Z. Anorg. Allg. Chem.*, 2013, **639**, 2395–2400.

96 R. S. Roy and B. Imperiali, *Protein Eng.*, 1997, **10**, 691–698.

97 M. Genz, V. Köhler, M. Krauss, D. Singer, R. Hoffmann, T. R. Ward and N. Sträter, *ChemCatChem*, 2014, **6**, 736–740.

98 G. S. Biggs, O. J. Klein, S. L. Maslen, J. M. Skehel, T. J. Rutherford, S. M. V Freund, F. Hollfelder, S. R. Boss and P. D. Barker, *Angew. Chem. Int. Ed.*, 2021, **60**, 10919–10927.

99 F. L. Martins, A. Pordea and C. M. Jäger, *Faraday Discuss.*, 2022, **234**, 315–335.

100 D. J. Raines, J. E. Clarke, E. V. Blagova, E. J. Dodson, K. S. Wilson and A.-K. Duhme-Klair, *Nat. Catal.*, 2018, **1**, 680–688.

101 I. J. Schalk and L. Guillon, *Amino Acids*, 2013, **44**, 1267–1277.

102 R. C. Hider and X. Kong, *Nat. Prod. Rep.*, 2010, **27**, 637–657.

103 A. L. Crumbliss and J. M. Harrington, *Iron sequestration by small molecules: thermodynamic and kinetic studies of natural siderophores and synthetic model compounds*, Elsevier, 2009, vol. 61.

104 M. Miethke and M. A. Marahiel, *Microbiol. Mol. Biol. Rev.*, 2007, **71**, 413–451.

105 D. J. Raines, O. V. Moroz, K. S. Wilson and A. K. Duhme-Klair, *Angew. Chem. Int. Ed.*, 2013, **52**, 4595–4598.

106 T. Heinisch, M. Pellizzoni, M. Dürrenberger, C. E. Tinberg, V. Köhler, J. Klehr, D. Häussinger, D. Baker and T. R. Ward, *J. Am. Chem. Soc.*, 2015, **137**, 10414–10419.

107 G. Klein, N. Humbert, J. Gradinaru, A. Ivanova, F. Gilardoni, U. E. Rusbandi and T.

R. Ward, *Angew. Chem. Int. Ed.*, 2005, **44**, 7764–7767.

108 N. Tokuriki and D. S. Tawfik, *Curr. Opin. Struct. Biol.*, 2009, **19**, 596–604.

109 D. J. Diprimio and P. L. Holland, *J. Inorg. Biochem.*, 2021, **219**, 111430.

110 X. Ren and R. Fasan, *Curr. Opin. Green Sustain. Chem.*, 2021, **31**, 100494.

111 S. Chordia, S. Narasimhan, A. L. Paioni, M. Baldus and G. Roelfes, *Angew. Chem. Int. Ed.*, 2021, **60**, 5913–5920.

112 J. Huang, Z. Liu, B. J. Bloomer, D. S. Clark, A. Mukhopadhyay, J. D. Keasling and J. F. Hartwig, *Nat. Chem.*, 2021, **13**, 1186–1191.

113 E. T. Kaiser, *Angew. Chem. Int. Ed.*, 1988, **27**, 913–922.

114 M. Creus, A. Pordea, T. Rossel, A. Sardo, C. Letondor, A. Ivanova, I. LeTrong, R. E. Stenkamp and T. R. Ward, *Angew. Chem. Int. Ed.*, 2008, **47**, 1400–1404.

115 M. M. Pellizzoni, F. Schwizer, C. W. Wood, V. Sabatino, Y. Cotelle, S. Matile, D. N. Woolfson and T. R. Ward, *ACS Catal.*, 2018, **8**, 1476–1484.

116 G. Facchetti and I. Rimoldi, *New J. Chem.*, 2018, **42**, 18773–18776.

117 G. Kiss, N. Çelebi-Ölçüm, R. Moretti, D. Baker and K. N. Houk, *Angew. Chem. Int. Ed.*, 2013, **52**, 5700–5725.

118 V. Muñoz Robles, E. Ortega-Carrasco, L. Alonso-Cotchico, J. Rodriguez-Guerra, A. Lledós and J.-D. Maréchal, *ACS Catal.*, 2015, **5**, 2469–2480.

119 V. Muñoz Robles, P. Vidossich, A. Lledós, T. R. Ward and J. D. Maréchal, *ACS Catal.*, 2014, **4**, 833–842.

120 M. T. Reetz, J. J.-P. Peyralans, A. Maichele, Y. Fu and M. Maywald, *Chem. Commun.*, 2006, 4318–4320.

121 Y. M. Wilson, M. Dürrenberger, E. S. Nogueira and T. R. Ward, *J. Am. Chem. Soc.*, 2014, **136**, 8928–8932.

122 M. Hestericová, T. Heinisch, M. Lenz and T. R. Ward, *Dalton Trans.*, 2018, **47**, 10837–10841.

123 T. Heinisch, K. Langowska, P. Tanner, J.-L. Reymond, W. Meier, C. Palivan and T. R. Ward, *ChemCatChem*, 2013, **5**, 720–723.

124 J. Zhao, J. G. Rebelein, H. Mallin, C. Trindler, M. M. Pellizzoni and T. R. Ward, *J. Am. Chem. Soc.*, 2018, **140**, 13171–13175.

125 V. Köhler, Y. M. Wilson, M. Du, D. Ghislieri, E. Churakova, T. Quinto, L. Kno, F. Hollmann, N. J. Turner and T. R. Ward, *Nat. Chem.*, 2013, **5**, 93–99.

126 Y. Okamoto, V. Köhler and T. R. Ward, *J. Am. Chem. Soc.*, 2016, **138**, 5781–5784.

127 F. Schwizer, V. Köhler, M. Dürrenberger, L. Knörr and T. R. Ward, *ACS Catal.*, 2013, **3**, 1752–1755.

128 H. Li, P. Tian, J. Xu and G.-W. Zheng, *Org. Lett.*, 2017, **19**, 3151–3154.

129 D. Wetzl, M. Berrera, N. Sandon, D. Fishlock, M. Ebeling, M. Müller, S. Hanlon, B. Wirz and H. Iding, *ChemBioChem*, 2015, **16**, 1749–1756.

130 S. Hussain, F. Leipold, H. Man, E. Wells, S. P. France, K. R. Mulholland, G. Grogan and N. J. Turner, *ChemCatChem*, 2015, **7**, 579–583.

131 J. Zhu, H. Tan, L. Yang, Z. Dai, L. Zhu, H. Ma, Z. Deng, Z. Tian and X. Qu, *ACS Catal.*, 2017, **7**, 7003–7007.

132 T. Reiner, D. Jantke, A. N. Marziale, A. Raba and J. Eppinger, *ChemistryOpen*, 2013, **2**, 50–54.

133 C. Daguenet, R. Scopelliti and P. J. Dyson, *Organometallics*, 2004, **23**, 4849–4857.

134 S. Gladiali and E. Alberico, *Chem. Soc. Rev.*, 2006, **35**, 226–236.

135 K. M. Steward, M. T. Corbett, C. G. Goodman and J. S. Johnson, *J. Am. Chem. Soc.*, 2012, **134**, 20197–20206.

136 F. K. Cheung, M. A. Graham, F. Minissi and M. Wills, *Organometallics*, 2007, **26**, 5346–5351.

137 D. S. Matharu, D. J. Morris, J. Clarkson and M. Wills, *Chem. Commun.*, 2006, 3232–3234.

138 D. J. Morris, A. M. Hayes and M. Wills, *J. Org. Chem.*, 2006, **71**, 7035–7044.

139 W. Baratta, W. A. Herrmann, R. M. Kratzer and P. Rigo, *Organometallics*, 2000, **19**, 3664–3669.

140 L. Ackermann, A. Althammer and R. Born, *Angew. Chem. Int. Ed.*, 2006, **45**, 2619–2622.

141 A. Fürstner and L. Ackermann, *Chem. Commun.*, 1999, 95–96.

142 S. Movassaghi, M. Hanif, H. U. Holtkamp, T. Söhnel, S. M. F. Jamieson and C. G. Hartinger, *Dalton Trans.*, 2018, **47**, 2192–2201.

143 T. Reiner, D. Jantke, X.-H. Miao, A. N. Marziale, F. J. Kiefer and J. Eppinger, *Dalton Trans.*, 2013, **42**, 8692–8703.

144 A. M. R. Hall, P. Dong, A. Codina, J. P. Lowe and U. Hintermair, *ACS Catal.*, 2019, **9**, 2079–2090.

145 C. Wang, B. Villa-Marcos and J. Xiao, *Chem. Commun.*, 2011, **47**, 9773–9785.

146 B. R. Wilson, A. R. Bogdan, M. Miyazawa, K. Hashimoto and Y. Tsuji, *Trends Mol. Med.*, 2016, **22**, 1077–1090.

147 P. G. M. Wuts and T. W. Greene, *Greene's Protective Groups in Organic Synthesis, Fourth Edition*, 2006.

148 S. Wittmann, M. Schnabelrauch, I. Scherlitz-Hofmann, U. Möllmann, D. Ankel-Fuchs and L. Heinisch, *Bioorg. Med. Chem.*, 2002, **10**, 1659–1670.

149 R. J. Bergeron, K. A. Mcgovern, M. A. Channing and P. S. Burton, *J. Org. Chem.*, 1980, **45**, 1589–1592.

150 A. O. Obaseki, J. E. Steffen and W. R. Porter, *J. Heterocycl. Chem.*, 1985, **22**, 529–533.

151 D. B. Bryan, R. F. Hall, K. G. Holden, W. F. Huffman and J. G. Gleason, *J. Am. Chem. Soc.*, 1977, **99**, 2353–2355.

152 J.-F. Morizur, D. J. Irvine, J. J. Rawlins and L. J. Mathias, *Macromolecules*, 2007, **40**, 8938–8946.

153 J. A. Greenberg and T. Sammakia, *J. Org. Chem.*, 2017, **82**, 3245–3251.

154 K. Uehata, N. Kimura, K. Hasegawa, S. Arai, M. Nishida, T. Hosoe, K. Kawai and A. Nishida, *J. Nat. Prod.*, 2013, **76**, 2034–2039.

155 A. Tarapdar, J. K. S. Norris, O. Sampson, G. Mukamolova and J. T. Hodgkinson, *Beilstein J. Org. Chem.*, 2018, **14**, 2646–2650.

156 D. Bhattarai, J. Lee and G. Keum, in *Encyclopedia of Reagents for Organic Synthesis*, 2013.

157 H. Dialer, P. Mayer, K. Polborn and W. Beck, *Eur. J. Inorg. Chem.*, 2001, 1051–1055.

158 J. Kovacs, L. Kisfaludy and M. Q. Ceprini, *J. Am. Chem. Soc.*, 1967, **89**, 183–184.

159 D. H. Rich and F. G. Salituro, *J. Med. Chem.*, 1983, **26**, 904–910.

160 O. Soltani, M. A. Ariger, H. Vázquez-Villa and E. M. Carreira, *Org. Lett.*, 2010, **12**,

2893–2895.

161 V. S. Shende, S. K. Shingote, S. H. Deshpande, N. Kuriakose, K. Vanka and A. A. Kelkar, *RSC Adv.*, 2014, **4**, 46351–46356.

162 C. P. Casey, S. W. Singer, D. R. Powell, R. K. Hayashi and M. Kavana, *J. Am. Chem. Soc.*, 2001, **123**, 1090–1100.

163 C. P. Casey and J. B. Johnson, *J. Org. Chem.*, 2003, **68**, 1998–2001.

164 R. Soni, F. K. Cheung, G. C. Clarkson, J. E. D. Martins, M. A. Graham and M. Wills, *Org. Biomol. Chem.*, 2011, **9**, 3290–3294.

165 E. J. Corey and C. J. Helal, *Tetrahedron Lett.*, 1995, **36**, 9153–9156.

166 Y. Fu, C. Sanchez-Cano, R. Soni, I. Romero-Canelon, J. M. Hearn, Z. Liu, M. Wills and P. J. Sadler, *Dalton Trans.*, 2016, **45**, 8367–8378.

167 A. H. Ngo, M. Ibañez and L. H. Do, *ACS Catal.*, 2016, **6**, 2637–2641.

168 A. H. Ngo, S. Bose and L. H. Do, *Chem. Eur. J.*, 2018, **24**, 10584–10594.

169 R. Kanega, N. Onishi, L. Wang, K. Murata, J. T. Muckerman, E. Fujita and Y. Himeda, *Chem. Eur. J.*, 2018, **24**, 18389–18392.

170 C. L. Pitman, K. R. Brereton and A. J. M. Miller, *J. Am. Chem. Soc.*, 2016, **138**, 2252–2260.

171 K. M. Waldie, A. L. Ostericher, M. H. Reineke, A. F. Sasayama and P. Kubiak, *ACS Catal.*, 2018, **8**, 1313–1324.

172 M. Li, S. Zhang, X. Zhang, Y. Wang, J. Chen, Y. Tao and X. Wang, *Angew. Chem. Int. Ed.*, 2021, **60**, 6003–6012.

173 R. G. Ball, W. A. G. Graham, D. M. Heinekey, J. K. Hoyano, A. D. McMaster, B. M. Mattson and S. T. Michel, *Inorg. Chem.*, 1990, **29**, 2023–2025.

174 F. P. Gasparro and N. H. Kolodny, *J. Chem. Educ.*, 1977, **54**, 258–261.

175 F. Bloch, *Phys. Rev.*, 1946, **70**, 460–474.

176 G. S. Remya and C. H. Suresh, *Phys. Chem. Chem. Phys.*, 2016, **18**, 20615–20626.

177 A. Chimiak and J. B. Neilands, in *Structure and Bonding*, Springer, 1984, pp. 89–96.

178 E. J. Wilde, A. Hughes, E. V Blagova, O. V Moroz, R. P. Thomas, J. P. Turkenburg, D. J. Raines, A.-K. Duhme-Klair and K. S. Wilson, *Sci. Rep.*, 2017, **7**, 45941.

179 K. Palyada, D. Threadgill and A. Stintzi, *J. Bacteriol.*, 2004, **186**, 4714–4729.

180 H. Naikare, J. Butcher, A. Flint, J. Xu, K. N. Raymond and A. Stintzi, *Metallomics*, 2013, **5**, 988–996.

181 D. J. Raines, O. V. Moroz, E. V. Blagova, J. P. Turkenburg, K. S. Wilson and A.-K. Duhme-Klair, *PNAS*, 2016, **113**, 5850–5855.

182 A. Miller, *Unpublished work*, 2021.

183 W. Besenmatter, P. Kast and D. Hilvert, *Proteins Struct. Funct. Bioinforma.*, 2007, **66**, 500–506.

184 J. D. Bloom, S. T. Labthavikul, C. R. Otey and F. H. Arnold, *PNAS*, 2006, **103**, 5869–5874.

185 M. Jeschek, S. Panke and T. R. Ward, *Trends Biotechnol.*, 2018, **36**, 60–72.

186 O. Mayol, S. David, E. Darii, A. Debard, A. Mariage, V. Pellouin, J. Petit, M. Salanoubat, V. De Berardinis, A. Zaparucha and C. Vergne-Vaxelaire, *Catal. Sci. Technol.*, 2016, **6**, 7421–7428.

187 M. T. Reetz, P. Soni, L. Fernández, Y. Gumulya and J. D. Carballeira, *Chem. Commun.*, 2010, **46**, 8657–8658.

188 S. Chatterjeet and A. J. Russell, *Biotechnol. Prog.*, 1992, **8**, 256–258.

189 T. Satoh, S. Suzuki, Y. Suzuki, Y. Miyaji and Z. Imai, *Tetrahedron Lett.*, 1969, **52**, 4555–4558.

190 B. Large, *Unpublished work*, 2020.

191 J. Reid Mooring, SuazetteLiu, Z. Liang, J. Ahn, S. Hong, Y. Yoon, J. P. Snyder and H. Shim, *ChemMedChem*, 2013, **8**, 622–632.

192 E. V Blagova, *Unpublished work*, 2021.

193 M. Persson, D. Costes, E. Wehtje and P. Adlercreutz, *Enzyme Microb. Technol.*, 2002, **30**, 916–923.

194 R. S. Phillips, *Trends Biotechnol.*, 1996, **14**, 13–16.

195 B. H. Pogostin, A. Malmendal, C. H. Londergan and K. S. Åkerfeldt, *Molecules*, 2019, **24**, 405.

196 H. Gokcan and O. Isayev, *Chem. Sci.*, 2022, **13**, 2462–2474.

197 E. Gasteiger, C. Hoogland, A. Gattiker, S. Duvaud, M. R. Wilkins, R. D. Appel and A. Bairoch, in *The Proteomics Protocols Handbook*, 2005, pp. 571–607.

198 J. A. Cabeza and P. M. Maitlis, *J. Chem. Soc. Dalton Trans.*, 1985, 573–578.

199 D. Carta, P. Brun, M. Dal Pra, G. Bernabé, I. Castagliuolo and M. G. Ferlin, *Med. Chem. Commun.*, 2018, **9**, 1017–1032.

200 T. Senthamarai, K. Murugesan, J. Schneidewind, N. V Kalevaru, W. Baumann, H. Neumann, P. C. J. Kamer, M. Beller and R. V Jagadeesh, *Nat. Commun.*, 2018, **9**, 4123–4135.

201 A. Tarapdar, J. K. S. Norris, O. Sampson, G. Mukamolova and J. T. Hodgkinson, *Beilstein J. Org. Chem.*, 2018, **14**, 2646–2650.

202 M. A. Bennet and A. K. Smith, *J. Chem. Soc., Dalton Trans.*, 1974, 233–241.

203 S. B. Jensen, S. J. Rodger and M. D. Spicer, *J. Organomet. Chem.*, 1998, **556**, 151–158.

204 J. C. Sheehan and W. A. Bolhofer, *J. Am. Chem. Soc.*, 1950, **72**, 2786–2788.

205 A. A. Shaik, S. Nishat and P. R. Andreana, *Organ. Lett.*, 2015, **17**, 2582–2585.

206 W. H. Rastetter, T. J. Erickson and M. C. Venuti, *J. Org. Chem.*, 1981, **46**, 3579–3590.

207 A. Müller, A. J. Wilkinson, K. S. Wilson and A. K. Duhme-Klair, *Angew. Chem. Int. Ed.*, 2006, **45**, 5132–5136.